Aspects of Charge Exchange in Ion-atom Collisions

Christine Forster, B.Sc.

A thesis submitted to the University of Durham
for the Degree of Doctor of Philosophy

May 8, 1990

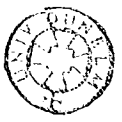

Abstract

The straight line semi-classical Impact Parameter method has been modified for use with classical trajectories. Ion-atom collisions have been modelled using wavefunctions expanded in terms of atomic basis states which were centred on either the target or projectile ions.

Total and differential charge exchange cross-sections are presented for $^4He^{++}$ and $^4He^+$ collisions within the centre of mass energy range 0.21 kev $< E_{cm} <$ 2.5 keV. Results using curved and straight line paths are compared with data from other authors. Significant trajectory effects were found at the lower energies in the range. The curved trajectory results were lower than those from the straight line model and also lower than previous calculations carried out. At higher energies in the range there was good agreement between straight line and curved trajectory models and previous work. Differential cross-sections were found to be sensitive to the trajectories employed, and comparisons have been made with previous work.

Total, state specific and differential cross- sections for charge exchange are presented for Be^{++} and H collisions using a five state basis, within the centre of mass energy range 0.111 keV $< E_{cm} <$ 0.4444 keV. There was reasonable agreement between the straight line results and previous work. There were significant trajectory effects for all the final charge transfer states.

Results are presented for low-energy collisions between positively charged muons and atomic hydrogen. An eight state basis has been used. Direct excitation cross sections for n = 2 atomic states and charge transfer cross sections to 1s and n = 2 have been calculated. The effect on the cross sections of using different internuclear potentials has been examined. Trajectory effects were small for charge transfer to 1s but were more pronounced in the direct excitation and charge exchange cross-sections to n = 2. These results have been compared to those obtained for curved trajectory H^+ and H collisions at the same relative velocity, to assess the validity of velocity scaling. It was found that velocity scaling was reliable for charge transfer to 1s and for total electron capture cross-sections. However, it was progressively inaccurate for direct excitation and for electron capture into excited states for μ^+ impact energies of less than 300 eV.

These results are discussed and suggestions for further work are made.

Dedication

For Don and the Boys

Acknowledgements

I would like to thank my supervisor Dr. D. R. Flower for all his help and encouragement during the work carried out for, and the writing of, this thesis. I am grateful also to Professor B.H. Bransden for his guidance and assistance, and to Dr. R. Shingal who gave me unstinting support during the work carried out on his original computer programs. I have benefitted from many discussions with Drs. H. Slim and L. Heck during the writing of the thesis, and would like to thank them both. I am grateful to Dr. A. S. Dickinson for all his help and his cooperation in allowing me to use the computer programs associated with his previous work. I wish to acknowledge the help and advice given by Dr. C. Courbin and Dr. R. Allan on specific problems that arose during the course of the work.

I would like to thank the Durham and Newcastle Computing departments and also the computing laboratory at Daresbury for access to their main frame computers. I also thank the University of Durham Physics Department for the use of their facilities and I acknowledge the receipt of a Science and Engineering Research Council research studentship.

My grateful thanks go to Margaret Norman for typing this thesis, and also to Dorothy Cooper for drawing the diagrams.

Finally I would like to express my profound gratitude to my husband and sons who have been a great source of strength and support, in spite of being frequently inconvenienced.

Contents

Abstract

Dedication i

Acknowledgements ii

1 Ion-Atom and Ion-Ion Collisions 1

1.1 Introductory remarks 1

1.1.1 Classical Scattering 2

1.1.2 Rutherford Scattering Differential cross-sections 3

1.2 Partial Wave Scattering 3

1.3 Semi-Classical Methods 4

1.3.1 The Semi-Classical Impact Parameter Method 4

1.3.2 Electronic Wave Functions 5

1.3.3 The Perturbed Stationary State Model 6

1.4 Electronic Translation Factors 8

1.5 Semi-Classical Cross-sections 10

1.5.1 The Eikonal Approximation 11

1.5.2 The Common Trajectory Method 13

1.6 Semi-Classical Differential Cross-sections 17

1.7 Semi-Classical Total Cross-sections 19

1.8 Curved Trajectories 19

1.8.1 Total Cross Sections Using Curved Trajectories 20

1.8.2 Differential Cross Sections using Curved Trajectories 22

2 The atomic orbital impact parameter method with non-linear trajectories 24

2.1 Classical Trajectories 24

2.2 The Eikonal Phase Transformation 28

2.3 The Impact Parameter Method for calculation of the Probability Amplitudes 30
2.3.1 Explicit Form of the Matrix elements 32
2.3.2 Integration of the Matrix Elements 34
2.3.3 Transformation of the Space Fixed Velocity Components to the Body Fixed frame 34
2.3.4 Transformation of the Origin in the Body Fixed Frame of Reference 37
2.3.5 Explicit Form of the Wave Functions 39
2.3.6 Integration in Prolate Spheroidal Coordinates 40
2.3.7 Rotation of the Body Fixed Integrals to the Space Fixed Frame 42
2.3.8 Symmetries and Time Reversal 43
2.4 Total Cross Sections 44
2.5 Differential Cross Sections 44
2.5.1 Electronic Phase Factors 45
2.5.2 Internuclear Phase Shifts 46

3 Computation **51**
3.1 Probability Amplitudes 51
3.2 Trajectories 52
3.2.1 Data input to the Trajectory Programs 52
3.3 Computation of the Integrals Comprising the Matrix Elements . . 53
3.3.1 Body Fixed Integration of the Matrix Elements in Subroutine Entgin 54
3.3.2 Rotation of the Integrals into the Space Fixed Frame 56
3.3.3 Combination of the Space Fixed integrals into Matrix Elements 56
3.3.4 Integration of the Time-Dependent Coupled Equations . . . 56
3.3.5 Total Cross-sections 58
3.3.6 Differential Cross-sections 58

4 Charge exchange in $^4He^{++}$ and $^4He^{+}$ collisions : symmetric resonance **62**
4.1 Symmetric Resonance 62
4.2 Previous work 62
4.3 Results 64

4.4 Total Cross-Sections 64
4.5 Differential Cross Sections 66
4.5.1 Full Semi-Classical Results 66
4.5.2 Differential Cross Sections- First Order Approximation . . 68
4.6 Integrated Partial cross-sections 69

5 Low Energy Charge Exchange between Doubly Ionised Beryllium and Atomic Hydrogen 73
5.1 Introduction 73
5.2 Model Potentials and Pseudopotentials 74
5.3 Previous work 75
5.4 Total and partial cross-sections 76
5.5 Differential Cross-section Results 78
5.5.1 Angular Distributions for Charge Transfer to 2s 79
5.5.2 Angular Distributions for Charge Transfer to 2p States . . 80
5.6 Discussion 80

6 Direct excitation and charge exchange in low energy muon$^+$ and hydrogen collisions 86
6.1 Muon$^+$ Production and Muon$^+$ - hydrogen collisions 86
6.2 Internuclear Potentials for Muon$^+$ and hydrogen Collisions 87
6.3 Results 88
6.4 Two state basis calculations 88
6.5 Eight state basis calculations 89
6.5.1 Charge exchange to 1s 89
6.5.2 Charge exchange and direct excitation to 2s states 89
6.5.3 Charge exchange and Excitation to 2p States 90
6.6 Total Cross sections 91
6.7 Velocity Scaling 91
6.8 Discussion 93

7 Final Discussion and Conclusions 103
7.1 Straight line results 103
7.2 Curved Trajectories 103
7.3 Velocity Scaling 105
7.4 Differential Cross sections 105
7.5 Conclusion and Possibilities for Further Work 105

Appendix A **A Derivation of the Eikonal Scattering Amplitude** **107**

Appendix B **The Stationary Phase approximation** **111**

Appendix C **An Expression for the Internuclear Phase.** **113**

Appendix D **Derivation of the Relationships 2.67, 2.68 and 2.69** **116**

Bibliography **118**

Chapter 1

Ion-Atom and Ion-Ion Collisions

1.1 Introductory remarks

Theoretical studies of atomic collisions are useful in several fields of physics. In fusion plasmas, atomic reactions are important, both in the centre of the plasma where the fusion occurs, and at the plasma edge. In the outer regions of the plasma, interactions with the atoms of the vacuum vessels, wall and limiters take place. Impurities are formed, which are an important source of energy losses and theoretical models can be used to study the effects of impurities on the plasma. Collision theory can also help explain the charge transfer processes, by which diagnostic neutral particle analyzers provide details of the ion temperatures within the plasma (Post,1983). Atomic collision models are also used to help interpret astronomical data in terms of the processes taking place in the interstellar medium (Flower,1983). Theoretical calculations are also often a valuable check on the results of collision experiments in the laboratory, and vice versa.

The work in this thesis is concerned with low energy collisions between ions and atoms. Quasi or actual one- electron systems are considered, consisting of an atom B with one active electron, and an ion A. A is either a fully stripped nucleus or a nucleus surrounded by an inert core of electrons. Several processes can occur during ion- atom collisions. Firstly, a fully elastic collision can take place in which the electron stays bound to B in its original ground state. Secondly, excitation of the electron to a more energetic bound state can occur. Thirdly, the electron may be 'captured' by ion A. This process is called charge exchange or charge transfer and the captured electron may be in either the ground state or an excited state of A. Lastly, if the collision is sufficiently energetic, B is ionized and the electron is free, leaving both A and B positively charged. These processes are summarised below.

$$A^+ + B(1s) - - - - - A^+ + B(1s) \text{ elastic collision} \tag{1.1}$$

$$A^+ + B(1s) - - - - - A^+ + B^*(n,l) \text{ excitation} \tag{1.2}$$

$$A^+ + B(1s) - - - - - A^*(n,l) + B^+ \text{ charge transfer} \tag{1.3}$$

$$A^+ + B(1s) - - - - - A^+ + B^+ + e^- \text{ ionization} \tag{1.4}$$

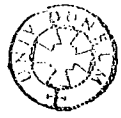

Most of the results to be presented are concerned with the third of these processes, namely charge transfer, although some results for direct excitation will appear in Chapter six. Low collision energies have been employed at which ionization cross-sections are negligible. Because of the low energies involved, a curved trajectory model has been used. Comparisons have been made between straight line and curved trajectory results for the atomic systems under consideration.

This chapter will consider the development of semi-classical methods for ion-atom collisions. The Impact Parameter method, using atomic wavefunctions, upon which the present work is based will be dealt with comprehensively in Chapter 2. Therefore, the basic model will only be briefly described in this chapter. As some of this work is compared with results obtained using the Perturbed Stationary State (PSS) method, a description of the PSS method will be given. The development of the use of electronic translation factors for both the Impact Parameter and Perturbed Stationary State methods will be outlined. The techniques for obtaining total and differential cross-sections by semi-classical or other methods will also be discussed. The final section in this chapter will consider the use of curved trajectories to model the internuclear motion. Particular reference will be made to some of the work which has been carried out using non-linear trajectories.

1.1.1 Classical Scattering

The results of scattering experiments in the laboratory are usually presented in terms of cross-sections. Figure 1.1. shows a uniform beam of particles which are assumed not to interact. These particles are incident on a target composed of n scattering centres. The target is assumed to be sufficiently thin that multiple scattering of an incident particle can be discounted. If N is the number of particles per unit area of target passing per unit time, then the number of particles scattered in a solid angle $d\Omega$ from this area is dN'. b is the impact parameter. dN' is expressed as (see Bransden, 1983)

$$dN' = Nn\sigma(\theta,\phi)d\Omega \tag{1.5}$$

$$\text{where } \sigma(\theta,\phi) = \frac{d\sigma}{d\Omega}(\theta,\phi)$$

is the classical differential cross-section which has dimensions of area. The total cross-section σ_{tot} is obtained by integrating $\sigma(\theta,\phi)$, over all possible angles of scattering.

$$\sigma_{tot} = \int_o^{2\pi} d\phi \int_o^{\pi} d\theta sin\theta \frac{d\sigma}{d\Omega}(\theta,\phi) \tag{1.6}$$

The classical differential cross-section is

$$\frac{d\sigma}{d\Omega} = \frac{1}{\mu^2 V^2} \frac{L}{sin\theta} \left| \frac{dL}{d\theta} \right| \tag{1.7}$$

where V is the relative velocity and L is the classical angular momentum.

1.1.2 Rutherford Scattering Differential cross-sections

When the interaction between the scattering particles is that due to a coulomb potential, an exact expression for the differential cross section may be obtained. This was used by Rutherford in his original scattering experiment, hence the name. The exact relationship between the scattering angle θ and b, the impact parameter, for a coulomb potential, may be obtained from the classical scattering equation

$$b = \frac{Z_A Z_B cot\frac{\theta}{2}}{(4\pi\epsilon_o)2E_{cm}} \tag{1.8}$$

where E_{cm} is the centre of mass energy and Z_A, Z_B are the nuclear charges of A and B respectively. The Rutherford formula for the differential cross- section is therefore

$$\frac{d\sigma}{d\Omega} \mid_{Ruth} = \frac{(Z_A Z_B)^2}{(4\pi\epsilon_o)^2} \frac{1}{16E_{cm}^2 sin^4\frac{\theta}{2}} \tag{1.9}$$

For forward scattering ($\theta = 0$), 1.9 is singular, and when used in 1.6 the integral becomes infinite for coulomb scattering. The coulomb potential is unique in that the differential cross section obtained by classical means is identical to that found using quantum theory.

1.2 Partial Wave Scattering

The partial wave theory of scattering is discussed in many standard texts, for example Mott and Massey (1965). For this reason it will not be discussed in detail and the partial wave expressions for cross-sections are simply quoted to clarify the semi-classical approximations used later.

The partial wave scattering amplitude $f(\theta)$ is

$$f(\theta) = \frac{1}{2ik} \sum_{\ell=0}^{\infty} (2l+1)(S_\ell - 1) P_\ell(cos\theta) \tag{1.10}$$

where S_ℓ is the scattering matrix, $S_\ell = \exp(2i\eta_\ell)$. The η_ℓ are partial wave phase shifts. The differential cross-section is $I(\theta)$ where

$$I(\theta) = \mid f(\theta) \mid^2 \tag{1.11}$$

and the total cross section is obtained from

$$Q = 2\pi \int_o^\pi \mid f(\theta) \mid^2 sin\theta d\theta \tag{1.12}$$

1.3 Semi-Classical Methods

1.3.1 The Semi-Classical Impact Parameter Method

For ion-atom collisions, the nuclei are very massive compared to electrons. Partial wave analysis can therefore become impractical in computing terms because of the large number of partial waves in the summation of 1.10. As a consequence, semi-classical methods have been developed which simplify this problem. The semi-classical Impact Parameter method developed by Mott (1931) assumed that the two nuclei followed strictly classical paths. At the same time, the electronic transition and exchange probabilities were calculated using quantal perturbation theory. Classical path assumptions are regarded as being valid when the wavelength of the relative motion of the ions is small compared to atomic dimensions, and if the uncertainty, $d\theta$ in the scattering angle θ is small compared to θ (Bransden, 1972). Other criteria for the validity of the classical trajectory equations have been discussed by Delos et al (1972). These are firstly, that there are negligible differences between trajectories associated with different internal states of the colliding system. This means that a common trajectory can be used for all final states. Secondly, that close to the classical turning points, the coupling between states should be very small.

In the coordinate system shown below,

Fig. 1.2

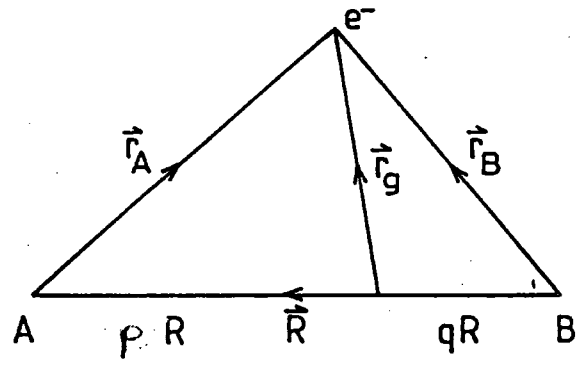

$\vec{R}$ is the separation between the heavy particles, A, with mass M_A, and B with mass M_B, and $\vec{r}_g$ is the vector coordinate of the electron with respect to the centre of mass of A and B. p and q are the ratios

$$p = \frac{M_B}{M_A + M_B} \; q = \frac{M_A}{M_A + M_B} \tag{1.13}$$

and $p + q = 1$.

The Hamiltonian for the three body system can be written

$$H = \frac{-\hbar^2}{2\mu}\nabla_R^2 - \frac{\hbar^2 \nabla^2 r_g}{2m_e} + V_B(\vec{r}_B) + V_A(\vec{r}_A) \tag{1.14}$$

where $V_B(\vec{r}_B)$ is the interaction between e and B and $V_A(\vec{r}_A)$ that between e and A. $\mu = \frac{M_A M_B}{M_A + M_B}$ is the reduced mass. The Schrödinger equation is

$$[H + U(R)]\Psi = E\Psi \tag{1.15}$$

where U(R) is the internuclear potential, and Ψ is the wavefunction associated with the electronic and nuclear motion. The basis of the Impact Parameter method is that the energy $\Delta\epsilon$ required by an electron to make a transition from state i to state j is much less than the relative energy of the ions. The assumption is made that $\Delta\epsilon$ is acquired from the total energy of the system without affecting the internuclear motion (Briggs, 1976). The internuclear potential is a function of $\vec{R}$(t) and the relative motion can be associated with a particular impact parameter b and angular momentum L.

1.3.2 Electronic Wave Functions

The type of electronic wave functions used in ion- atom collisions is primarily determined by the collision energy. At intermediate to high energies, with relative velocities greater than 0.25 a.u., it is often assumed that the electron will be attached to one or other of the nuclei for most of the collision and that a good approximation to the wave function is an expansion in atomic orbitals of the type:-

$$\Psi = \sum_n a_n^B(b,t)\phi_n^B(\vec{r}_B) + \sum_m c_m^A(b,t)\phi_m^A(\vec{r}_A) \tag{1.16}$$

where $\phi_n^B(\vec{r}_B)$ and $\phi_m^A(\vec{r}_A)$ are eigen-functions of the electronic Hamiltonian.

$$\left(\frac{\hbar^2}{2m_e}\nabla_{r_A}^2 + V_A(\vec{r}_A) - \epsilon_A\right)\phi_m^A = 0 \tag{1.17}$$

$$\left(\frac{\hbar^2}{2m_e}\nabla_{r_B}^2 + V_B(\vec{r}_B) - \epsilon_B\right)\phi_n^B = 0 \tag{1.18}$$

This is the assumption made in the Atomic Orbital Impact Parameter model upon which the present work is based, and a full description is given in Chapter two.

For slower collisions, v < 1 a.u. and for smaller internuclear separations, the atomic wavefunction approximation may no longer be adequate. At lower relative velocities the electron spends a considerable time in the field of the two nuclei and the system can be considered to behave as a quasi-molecule. Under such circumstances, the molecular orbital basis is often felt to be a better approximation. Using such a basis, the molecular wave functions ideally satisfy two conditions. At R→0 when A and B are in close proximity (the united atom limit), the wavefunction represents the molecule formed by the two nuclei and the electron. As R→ ∞, the electron must be attached to either A or B and the wavefunction tends

to the appropriate atomic eigenfunction (separated atom limit). The PSS method described below is an example of the molecular approach.

1.3.3 The Perturbed Stationary State Model

This was originally developed as a quantal method by Massey and Smith (1933) and was adapted by Bates, Massey and Stewart (1953). In the PSS method, the wave functions are represented by products of electronic and nuclear wave functions. The model of Bates et al included distortions in the nuclear wave function due to the relative motion of the ions. The authors were able to show that when these effects were ignored the expressions for the cross- sections reduced to the original Impact Parameter form of Mott. A detailed description of the method is given in Mott and Massey (1965). The total wave function which satisfies 1.15 above is assumed to be of the form

$$\Psi = F_n^A(R)\chi_n(\vec{r}_g) + \sum_m F_m^B(R)\chi_m(\vec{r}_g) \tag{1.19}$$

where $\chi(\vec{r}_g)$ are the electronic molecular wave functions and the F(R) are related to the nuclear motion. The simplest molecular wave functions are those which are expressed as linear combinations of atomic orbitals (the LCAO method). One of the most successful applications of the PSS method using LCAOs is in the case of collisions between two identical nuclei (symmetric resonance), for example proton-hydrogen collisions. The linear combinations of orbitals in H^+ - H collisions may be

$$\chi_g(R:\vec{r}_g) = \frac{1}{\sqrt{2}}[\psi_{1s}(\vec{r}_A) + \psi_{1s}(\vec{r}_B)] \tag{1.20}$$

or

$$\chi_u(R:\vec{r}_g) = \frac{1}{\sqrt{2}}[\psi_{1s}(\vec{r}_A) - \psi_{1s}(\vec{r}_B)] \tag{1.21}$$

where the g or gerade functions are even under reflection about the midpoint of A and B, and the u or ungerade, are odd. The wave functions with the correct asymptotic values for charge exchange are therefore

$$\chi^+(\vec{r}_g) = \frac{1}{\sqrt{2}}[\chi_g + \chi_u] \rightarrow_{R\rightarrow\infty} \psi_{1s}(\vec{r}_A) \tag{1.22}$$

and

$$\chi^-(\vec{r}_g) = \frac{1}{\sqrt{2}}[\chi_g - \chi_u] \rightarrow_{R\rightarrow\infty} \psi_{1s}(\vec{r}_B) \tag{1.23}$$

From 1.19 Ψ is expressed as

$$\Psi = F^+(R)\chi^+(\vec{r}_g) + F^-(R)\chi^-(\vec{r}_g) \tag{1.24}$$

The asymptotic values for $F^+(R)$ and $F^-(R)$ are

$$F^+(R) \sim \frac{1}{2}\{e^{ikz} + \vec{r}_g^{-1}\, f^+(\theta,\phi)e^{ikR}\} \tag{1.25}$$

$$F^-(R) \sim \frac{1}{2}\{e^{ikz} + \vec{r}_g^{-1}\, f^-(\theta,\phi)e^{ikR}\} \tag{1.26}$$

and thus

$$\Psi \sim_{R\to\infty} e^{ikz}\psi_{ls}(\vec{r}_A) + \frac{1}{2R}e^{ikR}\{\psi_{ls}(\vec{r}_B)[f^+ - f^-] \tag{1.27}$$

$$+\psi_{ls}(\vec{r}_A)[f^+ + f^-]\} \tag{1.28}$$

where the scattering amplitudes $f^{\pm}$ are determined from the solution of 1.15. The molecular wave functions satisfy

$$\left[-\frac{\hbar^2\nabla_r^2}{2m_e} + V_A(\vec{r}_A) + V_B(\vec{r}_B) + \epsilon^{\pm}(R)\right]\chi^{\pm}(\vec{r}_g) = 0 \tag{1.29}$$

and from the symmetry of the system

$$\int \chi^{\pm}\chi^{\pm} d\,\vec{r} = 0 \tag{1.30}$$

$$\int \chi^{\pm}\,\vec{\nabla}_R\,\chi^{\pm} d\,\vec{r} = 0 \tag{1.31}$$

$$\int \chi^{\pm}\nabla_R^2\chi^{\pm} d\,\vec{r} = 0 \tag{1.32}$$

Using these relationships the coupled equations for $F^{\pm}$ (R) are

$$[\nabla_R^2 + k^2 - \frac{2\mu}{\hbar^2}\{U(R) + \epsilon^{\pm}(R)\}]F^{\pm}(R) = 0 \tag{1.33}$$

In ion-atom collisions the functions $F^{\pm}$ may be regarded as classical and in the form

$$F(R) = \frac{2\mu}{\hbar^2}\{[E_{cm} - V_{AB}] - \frac{(l+\frac{1}{2})^2}{R^2}\} \tag{1.34}$$

satisfy 1.33.

The semi-classical form of the phase shifts $\eta^{\pm}$ is (Mott and Massey, 1965)

$$\eta_c^{\pm} = \frac{1\pi}{4} + \frac{l\pi}{2} - kR_o + \int_{R_o}^{\infty} F^{\pm}(\vec{R})^{\frac{1}{2}} - kdR \tag{1.35}$$

where k is the momentum of the classical motion, k = μv, and R_o is the classical turning point. The cross-section for charge transfer then becomes, from 1.12.

$$Q = \frac{2\pi}{k^2} \int_o^{\infty} (l + \frac{1}{2}) sin^2(\eta_c^+ - \eta_c^-) dl \tag{1.36}$$

1.4 Electronic Translation Factors

Although the model of Bates et al (1953) took account of distortions due to the nuclear motion, it was realised that the PSS and Impact Parameter methods both had serious defects. One was that the wave function failed to take into account the momentum and energy acquired by the electron due to the relative motion of the ions. Bates and McCarroll (1958) pointed out that as a result of this, the semi-classical Schrödinger equation in atomic units where $\hbar = 1$ $m_e = 1$

$$H\Psi(\vec{r}_g, t) = \frac{i\partial}{\partial t}\Psi(\vec{r}_g, t) \tag{1.37}$$

was not satisfied at infinite nuclear separations by an electronic time-dependent wave function of the form

$$\Phi(\vec{r}_g) = \sum c_n(t)\phi_n(\vec{r}_g, t);\ \phi_n = \chi_n(\vec{r}_g) exp(-i \int \varepsilon_n dt) \tag{1.38}$$

where $\chi_n(\vec{r}_g)$ represents the atomic or molecular wavefunction and ε_n is the corresponding eigen-energy. They found that when allowance was made for the translational motion by using

$$\phi_n^A(\vec{r}_g, t) = \chi_n^A(\vec{r}_g) exp(ip\ \vec{v}\ .\ \vec{r}\ - i \int \varepsilon_n(t) + \frac{1}{2}p^2v^2 dt \tag{1.39}$$

$$\phi_m^B(\vec{r}_g, t) = \chi_m^B(\vec{r}_g) exp(-iq\ \vec{v}\ .\ \vec{r}\ - i \int \varepsilon_m(t) + \frac{1}{2}q^2v^2 dt \tag{1.40}$$

then 1.37 was satisfied in the separated atom limit. The addition of Electronic Translation Factors (ETFs) ensured that the matrix elements were translationally invariant and that the probability amplitudes were independent of the choice of coordinate origin.

The effect of ETFs on the total cross-sections for resonant charge exchange in H(1s) - H^+ collisions was investigated by Ferguson (1961) using a molecular PSS approach, and at the same time, McCarroll (1961) carried out atomic orbital calculations for the same system. Ferguson found the cross- sections were much reduced by the inclusion of ETFs. When the atomic and molecular results were compared, they were found to be very similar for 5 keV < E <15 keV. Above

15 keV the cross- sections computed by McCarroll showed a more rapid decrease with increasing collision energy. McCarroll concluded that the effect of momentum transfer is important for proton energies greater than 1 keV, corresponding to a relative velocity of 0.2 a.u.

However, a disadvantage of using ETFs of the form 1.39 and 1.40 in the PSS method was that the electron was constrained to one or other of the nuclei, which was inconsistent with the molecular picture as R$\rightarrow$ 0. In addition, the molecular orbitals with ETFs were not orthogonal, owing to the phase factor $\exp(\pm\ \vec{v}\ .\ \vec{r})$. Thorson (1965) examined the behaviour of the velocity dependent factors in the united atom limit. Physically, these should have vanished but, in fact, gave rise to sine and cosine terms due to the non-orthogonality of the basis set. To try to overcome these problems, Schneiderman and Russek (1969) introduced velocity dependent factors of the form

$$exp(\frac{i\mu}{2}\ \vec{v}\ .\ \vec{r}\ f(\vec{r},\vec{R})) \tag{1.41}$$

and proposed certain criteria for the determination of $f(\vec{r},\vec{R})$. The most important of these were, first, that the switching function $f(\vec{r},\vec{R})$ should be state independent, ensuring orthonormality of the full wavefunction. Secondly, that $f(\vec{r},\vec{R}) \rightarrow \pm\ 1$ as R$\rightarrow\ \infty$, depending on the nucleus to which the electron was attached, ensuring the correct asymptotic behaviour. Lastly that $f(\vec{r},\vec{R}) \rightarrow 0$ as R$\rightarrow$ 0. Schneiderman and Russek proposed that $f(\vec{r},\vec{R})$ should be

$$f(\vec{r},\vec{R}) = \frac{cos\theta}{1+(a/R)^2} = \frac{R^2 cos\theta}{R^2+a^2} \tag{1.42}$$

which has the correct asymptotic value. θ is the angle between the internuclear axis and the electron, and a is a distance parameter below which the system may be regarded as a quasi-molecule. The method was applied to proton-hydrogen collisions for comparison with the experiments of Lockwood and Everhart (1962) and Helbig and Everhart (1965). It was found that at higher energies in the experimental range, the cross sections tended towards the experimental values. Other forms of $f(\vec{r},\vec{R})$ have been proposed by Levy and Thorson (1969), Riley and Green (1971), Rankin and Thorson (1978), Crothers and Hughes (1978), Crothers and Todd (1981a) and Riera (1984) amongst others.

Although problems such as the origin dependence of the amplitudes and lack of unitarity have been solved by the use of translation factors, some difficulties are still associated with the molecular PSS method (Riera and Salin, 1976). Some of these are due to the finiteness of the molecular bases used in these calculations. McCarroll (1980) has also pointed out that the results obtained could be sensitive to the form of switching function used, due to the difficulties of optimising these translation factors.

Newby (1985) used an atomic basis set within the Impact Parameter formalism, employing switching functions in the ETFs. He looked at charge transfer in He^+

- H^+ and He^{++} - H collisions over an energy range of 0.25 keV/amu to 200.0 keV/amu using straight line paths. Newby tried four forms of switching functions, including those of Schneiderman and Russek and compared these with the results obtained using plane wave translation factors (PWTF) by Hatton et al (1979), Bransden and Noble (1981b) and Bransden et al (1983). He found that the cross-sections agreed fairly well at energies below 2.5 keV/amu. At higher energies, however, the use of switching functions resulted in cross-sections at 200 keV/amu, which were greater, by an order of magnitude than those obtained using PWTFs. It was concluded that at lower energies, there was no advantage in using switching functions rather than PWTFs in atomic orbital calculations.

Fritsch (1984) and Shingal et al (1986) have used PWTFs in the atomic orbital Impact Parameter method to calculate cross-sections for charge transfer in H^+ and Na^o collisions. Shingal et al compared their results with those obtained by Allan (1986) using a molecular orbital method with switching function translation factors. There was good agreement at energies of less than 5 keV/amu, but at energies above the maximum in the cross-sections, the molecular cross-sections were larger than both the atomic orbital results of Shingal et al and Fritsch, and the experimental measurements of Anderson et al (1979).

1.5 Semi-Classical Cross-sections

In the quantal approach, the total and partial cross-sections are expressed in terms of the S matrix given by 1.10. When using semi-classical methods, a corresponding semi-classical expression for the S matrix is utilised, which takes account of the electronic transition and exchange probabilities and also allows for the heavy particle motion. The relationship

$$\mathbf{S}_{ab} = \sum_{ab} P_{ab}^{\frac{1}{2}} exp(i\nabla_{ab}) \tag{1.43}$$

where the P_{ab} are the probabilities for transition from state a to state b and ∇_{ab} depends on the trajectory, has been derived by Marcus (1970, 1972a, 1972b) and Connor and Marcus(1971), who considered the semi-classical relationship between the Schrödinger equation and the classical Hamilton-Jacobi equations. The same result was obtained by Pechukas (1979a, 1979b) and Miller (1970a,b) using a path integral approach originating with Feynman and Hibbs (1965). The text by Child (1974) discusses the former method in detail. The semi-classical R matrix describing charge exchange is thus

$$\mathbf{R}_{ab} = \sum_{ab} P_{ab}^{\frac{1}{2}} exp(i\Delta_{ab}) \tag{1.44}$$

where

$$\mathbf{R} = \frac{i[\mathbf{I} - \mathbf{S}]}{[\mathbf{I} + \mathbf{S}]}$$

and P_{ab} is now the probability for charge exchange.

The following section will describe some of the methods employed to find total and differential cross-sections using the semi-classical approach. Section 1.5.1 describes an essentially straight line approach (the Eikonal approximation), and Section 1.5.2 considers some models where the trajectories of the heavy particles are not assumed to be rectilinear, with special reference to the Common Trajectory equations.

1.5.1 The Eikonal Approximation

For a more detailed discussion of this approximation, the reader is referred to the review by McCarroll (1974) and the text by Nikitin and Umanskii (1984). This approximation is used at high energies, where the internuclear potential is much less than the relative kinetic energy (E) of the nuclei, and the electronic transitional energy $\Delta\epsilon$ is also much less than E. Under such conditions the trajectories of the two nuclei can be assumed to be rectilinear.

The method assumes that the initial wave function is

$$\Psi_i(\vec{r},\vec{R}) = exp(i\ \vec{k}_i\ .\ \vec{R})\phi_{nlm} \tag{1.45}$$

ϕ_{nlm} represents the initial state of the atom. The z axis is taken to be parallel to the initial momentum k_i and so 1.45 can also be expressed as

$$\Psi_i = exp(i\ \vec{k}_i\ .\ \vec{z})\phi_{nlm} \tag{1.46}$$

The final wave function is of the form

$$\Psi = exp(i\ \vec{k}\ .\ \vec{z})\Phi \tag{1.47}$$

where exp $(i\ \vec{k}\ .\ \vec{z})$ represents the rapidly oscillating plane wave nuclear motion and Φ is a more slowly varying electronic wave function. Ψ is substituted into the Schrödinger equation

$$H\Psi = E_T\Psi \tag{1.48}$$

H is the total Hamiltonian of the system and E_T is the total energy. Due to the slowly varying nature of Φ the term in $\nabla^2_R\Phi$ which results from the action of H on the wavefunction is neglected and the Schrödinger equation

$$\frac{ik}{\mu}\frac{\partial\Phi}{\partial z} = H_{el}\Phi \tag{1.49}$$

is obtained. At high energies only scattering through small angles is expected to occur and at Z$\rightarrow$ - ∞

$$\Phi \rightarrow_{z\rightarrow-\infty} exp(i\,\vec{k}_n - \vec{k}_i)\,\vec{z}\,\phi_{nlm} \tag{1.50}$$

In the straight line approximation the internuclear vector R is expressed as

$$\vec{R}\,(t) = \vec{b} + \vec{v}\,t,\ \vec{Z} = \vec{v}\,t \tag{1.51}$$

the impact parameter $\vec{b}$ is in the $\vec{X},\vec{Y}$ plane, normal to $\vec{v}$. For high energies

$$k_i - k_n \simeq \frac{\varepsilon_n}{v} \tag{1.52}$$

ε_n corresponds to the eigen-energy of state n. Using 1.51 expression 1.50 becomes

$$\Phi \rightarrow_{z\rightarrow-\infty} exp(-i\varepsilon_n t)\phi_{nlm} \tag{1.53}$$

using 1.51 the Schrödinger equation is then

$$i\frac{\partial\Phi}{\partial t} = H_{el}\Phi \tag{1.54}$$

For a multichannel collision, Φ is an expansion of the form

$$\Phi(\vec{R},\vec{r}) = \sum_{n'l'm'} c_{n'l'm'} exp(-i\varepsilon_{n'}t)\phi_{n'l'm'} \tag{1.55}$$

where the $c_{n'l'm'}$ are eikonal expansion coefficients, or probability amplitudes, which are subject to the boundary conditions

$$c_{n'l'm'} \rightarrow_{t=-\infty} \delta_{nn'}\delta_{ll'}\delta_{mm'} \tag{1.56}$$

and which are found by solving the differential equations resulting from using 1.55 in 1.54

$$\frac{i\partial}{\partial t}c_{n'l'm'} = \sum_{n''l''m''} < \phi_{n'l'm'} \mid V_{AB} \mid \phi_{n''l''m''} > * \\ exp(i[\varepsilon_{n'} - \varepsilon_{n''}]t)c_{n''l''m''} \tag{1.57}$$

In the integral representation (Messiah, 1962), the scattering amplitude corresponding to 1.10 is

$$f_{jk}(\theta,\phi) = -\frac{\mu}{2\pi}\int d^3\,\vec{R}\,exp(i[k_i - k]\,\vec{R}) < \phi_j \mid V_{AB} \mid \Psi > \tag{1.58}$$

where j represents the state n'l'm' and k represents n"l"m". After some algebra 1.58 reduces to

$$f_{jk}(\theta,\phi) = i\mu v exp(i[m-m']\phi)\int_o^\infty bdb(\delta_{jk}-S)$$
$$J_{m'-m}(kb\theta) \qquad (1.59)$$

S is the space fixed semi-classical scattering matrix which is found from the eikonal probability amplitudes. Expression 1.59 is derived in Appendix A.

The advantage of using the Eikonal approximation for calculating differential cross-sections is that anisotropic potentials can be used. Its main drawback is that rectilinear trajectories are a condition for its validity. At low collision energies, this condition will not be fulfilled and other methods have been developed, which are valid for non- linear trajectories. One of the most successful of these has been the Common Trajectory method.

1.5.2 The Common Trajectory Method

This method is discussed by Gaussorgues et al (1975a), Nikitin and Umanskii (1984), and Bransden (1988). The basis of the method is that for all the final states in a collision, there is a common potential W(R) which defines a single classical trajectory with a common total energy E and angular momentum L. One important condition for the assumption of a common trajectory for all the final states, is that the turning points for all the channels must be close, another is that conditions for assuming classical motion, such as those in Section 1.3.1 are fulfilled for all R beyond the turning points. The general case where the trajectories for each channel are distinct will be discussed first.

Using the Langer approximation for the angular momentum L

$$L^2 = l(l+\frac{1}{2}) \approx (l+\frac{1}{2})^2 \qquad (1.60)$$

the radial function of the motion in the nth channel, $F_n(R)$ satisfies the radial equation below

$$(\frac{d^2}{dR^2} + k_n^2 - (\frac{(l+\frac{1}{2})^2}{R^2}))F_n(R) = 2\mu\sum_{n'} V_{nn'}F_{n'}(R) \qquad (1.61)$$

$V_{nn'}$ represents the interaction between the electron and ion in the final state and the term also includes the internuclear potential which goes to zero at large R . If W_n (R) is the internuclear potential for the nth channel,then including this in 1.61 results in

$$\{\frac{d^2}{dR^2} + \kappa_n^2(R)\}F_n(R) = \sum_{n'}[V_{nn'} - W_n(R)\delta_{nn'}]2\mu F_{n'}(R) \qquad (1.62)$$

$$\kappa_n(R) = \{k_n^2 - 2\mu W_n(R) - \frac{(l+\frac{1}{2})^2}{R^2}\}^{\frac{1}{2}} \qquad (1.63)$$

$\kappa_n(R)$ is therefore the radial part of the classical action along the trajectory. From Mott and Massey (1965) $F_n(R)$ can be represented asymptotically by

$$F(R) = \frac{1}{k^{\frac{1}{2}}}[exp(-i(kR - l\pi/2))\delta_{nn'} - S_{nn'}exp(i(kR - l\pi/2)) \tag{1.64}$$

where $S_{nn'}$ is the scattering matrix and the phases are the JWKB solutions for 1.61 with the right side set to zero. The motion takes place between t= $\pm\infty$ and the radial wavefunctions are constructed to represent solutions for both the inward and outward part of the motion (to and from the turning point R_n). A suitable trial function for $F_n(R)$ is

$$F_n(R) = b^+v^+ + b^-v^- \tag{1.65}$$

b^+v^+ and b^-v^- represent the outward and inward motions respectively. $v^\pm$ are the primitive JWKB solutions for the motion, away from the turning point R_n.

$$v^\pm = \frac{1}{(\kappa_n(R))^{\frac{1}{2}}}exp(\pm iS_n) \tag{1.66}$$

$$S_n = \int_{R_n}^{R} \kappa_n(R')dR' \tag{1.67}$$

At the classical turning point, expression 1.63 is zero, and $F_n(R)$ in terms of 1.66 and 1.67 is

$$F_n(R) = \frac{1}{(\kappa_n(R))^{\frac{1}{2}}}[b^+exp(iS_n) + b^-exp(-iS_n)] \tag{1.68}$$

In the asymptotic region the condition

$$\frac{db^+}{dR}exp(iS_n) + \frac{db^-}{dR}exp(-iS_n) = 0 \tag{1.69}$$

is met (Froman and Froman, 1965). Substituting 1.67 into the radial equation 1.62 and using 1.69, the coupled equations for $b^\pm$ are recovered.

$$\frac{\partial^2}{\partial R^2}\frac{1}{(\kappa_n(R))^{\frac{1}{2}}}(b^+ + b^-exp(-2iS_n)) + 2i(\kappa_n(R))^{\frac{1}{2}}\left[\frac{\partial b^+}{\partial R}\right]$$
$$= \sum 2\mu[V_{nn'} - W_n(R)\delta_{nn'}]$$
$$\times\frac{1}{(\kappa_n(R))^{\frac{1}{2}}}(b^+exp(i(S_{n'} - S_n)) + b^-exp(-i(S_{n'} + S_n))) \tag{1.70}$$

$$\frac{\partial^2}{\partial R^2}\frac{1}{(\kappa_n(R))^{\frac{1}{2}}}(b^+exp(2iS_n)+b^-)-2i(\kappa_n(R))^{\frac{1}{2}}\left[\frac{\partial b^-}{\partial R}\right]$$
$$=\sum 2\mu[V_{nn'}-W_n(R)\delta_{nn'}]$$
$$\times\frac{1}{(\kappa_n(R))^{\frac{1}{2}}}(b^+exp(i(S_{n'}+S_n))+b^-exp(-i(S_{n'}-S_n))) \quad (1.71)$$

Using the semi-classical inequality

$$(\kappa_n(R))^{-\frac{3}{2}}\frac{\partial^2\kappa_n(R)^{-\frac{1}{2}}}{\partial R^2}<<1 \quad (1.72)$$

the terms including second order derivatives of κ_n(R) may be neglected. As the $b^{\pm}$ vary slowly compared to exp(iS_n) the term in i2S_n $\approx|$ S_n + $S_{n'}$ $|$ is also neglected. The equations then uncouple giving separate expressions for b^+ and b^-.

$$2i\kappa_n(R)^{\frac{1}{2}}\frac{\partial b^+}{\partial R}=\sum_{n'}2\mu[V_{nn'}-W_n(R)\delta_{nn'}]*$$
$$\frac{1}{(\kappa_{n'}(R))^{\frac{1}{2}}}b^+exp(i[S_{n'}-S_n]) \quad (1.73)$$

and

$$-2i\kappa_n(R)^{\frac{1}{2}}\frac{\partial b^-}{\partial R}=\sum_{n'}2\mu[V_{nn'}-W_n(R)\delta_{nn'}]*$$
$$\frac{1}{(\kappa_{n'}(R))^{\frac{1}{2}}}b^-exp(-i[S_{n'}-S_n]) \quad (1.74)$$

The boundary conditions for $b^{\pm}$ are 1.64 as R $\rightarrow \infty$, $\kappa_n(R)\rightarrow k_n$

$$b^-\rightarrow\delta_{nn'}exp[i(S_n-\frac{\pi}{4})] \quad (1.75)$$

$$b^+\rightarrow S_{nn'}exp[-i(S_n-\frac{\pi}{4})] \quad (1.76)$$

The amplitudes b^+ and b^- are assumed to match at the turning point R if the coupling between states is small, giving the further condition on $b^{\pm}$ that

$$b^+=-b^- \text{ at } R_n \quad (1.77)$$

The Common Trajectory equations can be recovered by assuming a common potential W(R) for all channels, and a common classical action $\overline{\kappa}$(R)

$$\overline{\kappa}(R) = (\overline{k}^2 - 2\mu W(R) - \frac{(l+\frac{1}{2})^2}{R^2})^{\frac{1}{2}}$$
$$\overline{k}^2 = (2\mu E)^{\frac{1}{2}} \tag{1.78}$$

It is assumed that the turning points R_n are close enough for a single turning point R_T to be used for all states.

$R_n \approx R_T$ for all n.

This can be expressed in terms of time by using

$$\frac{dR}{dt} = \pm\frac{1}{\mu}\overline{\kappa}(R) \tag{1.79}$$

Writing $\kappa_n(R)$ as

$$\kappa_n(R) = [\overline{k}^2 - 2\mu W(R) + (k_n^2 - \overline{k}^2) + 2\mu[W_n(R) - W(R)]]^{\frac{1}{2}} \tag{1.80}$$

$$= \overline{\kappa}(R)[1 + \frac{(k_n^2 - \overline{k}^2)}{\overline{\kappa}(R)} + 2\frac{[W_n(R) - W(R)]}{\overline{\kappa}(R)}]^{\frac{1}{2}} \tag{1.81}$$

the condition for a common trajectory is that k $\approx$ k_n and $W_n(R) \approx$ W(R), so that the second term in the bracket of 1.81 is small, allowing the expression to be expanded,

$$\kappa_n(R) \approx \overline{\kappa}(R)[1 + \frac{1}{2}\frac{(k_n^2 - \overline{k}^2)}{\overline{\kappa}(R)} + \frac{(W_n(R) - W(R)}{\overline{\kappa}(R)}] \tag{1.82}$$

leading to the approximation that

$$\kappa_n(R) \approx \overline{\kappa}(R) \text{for all n} \tag{1.83}$$

Using 1.79, 1.73 and 1.74 become

$$i\frac{d}{dt}b_n^{\pm}(t) = \sum[V_{nn'}(t) - W_n(R)\delta_{nn'}] *$$
$$exp(i\int_o^t \frac{1}{2\mu}[k_n^2 - k_{n'}^2] + [W_n(R) - W_{n'}(R)]dt \; b_{n'}^{\pm} \tag{1.84}$$

where the approximation

$$S_{n'} - S_n \approx \frac{1}{2}\frac{(k_{n'}^2 - k_n^2) + 2\mu(W_n(R) - W_{n'}(R))}{\overline{K}(R)} \tag{1.85}$$

has been used. To integrate from t = - ∞ to t = +∞ , the amplitude $c_n(t)$ can be introduced, where

$$c_n(t) = b_n^-(t)exp(-i(\eta^- - \frac{\pi}{4}) \text{ for } t < 0 \quad (1.86)$$

$$c_n(t) = -b_n^+(t)exp(i(\eta^+ - \frac{\pi}{4}) \text{ for } t > 0 \quad (1.87)$$

where $\eta^{\pm}$ are the JWKB semi-classical phase shifts 1.35.

The $c_n(t)$ satisfy 1.84 with the initial condition that

$$c_n(-\infty) = \delta_{nn'} \quad (1.88)$$

The probablity amplitudes are found by integrating over the range of t, and the relationship

$$S_{nn'} = c_n(\infty)exp(\eta^+ + \eta^-) \quad (1.89)$$

corresponding to 1.43 is used to obtain the semi-classical S matrix. Total and differential cross-sections can then be calculated from the probability amplitudes and associated phase factors.

1.6 Semi-Classical Differential Cross-sections

The general expression for the scattering amplitude 1.10, is adapted for semi-classical cross-sections, firstly by using the classical relationship between the impact parameter and the angular momentum

$$kb = l + \frac{1}{2} \quad (1.90)$$

The number of l values in the summation in 1.10 means that the Legendre polynomials $P_\ell(\cos\theta)$ may be approximated in the limit of large R. For small angled scattering where $\theta << 1$, the approximation

$$P_l(cos\theta) \approx J_o(kb\theta) \quad (1.91)$$

can be used. The summation in $f(\theta, \phi)$ is then expressed in integral form, and the semi-classical scattering amplitude becomes, for direct excitation

$$f(\theta, \phi) = -ik \int_o^\infty bdbJ_o(kb\theta)[I - S] \quad (1.92)$$

For charge exchange

$$f(\theta, \phi) = -ik \int_o^\infty bdbJ_o(kb\theta)S \quad (1.93)$$

For large angle scattering, the asymptotic form for $P_\ell(\cos\theta)$ is (Abramowitz and Stegun, 1975):

$$P_\ell(cos\theta) \approx \left[\frac{2}{l\pi sin\theta}\right]^{\frac{1}{2}} cos[(l+\frac{1}{2})\theta - \frac{\pi}{4}] \tag{1.94}$$

which is valid for lsin $\theta >> 1$. In the two state approximation, 1.94 is substituted into the partial wave scattering equation and the summation is changed to an integral to give

$$f(\theta,\phi) \simeq \int_o^\infty \frac{1}{k[2\pi \sin\theta]^{\frac{1}{2}}} l^{\frac{1}{2}} dl[exp(i\phi_l^+) + exp(i\phi_l^-)] \tag{1.95}$$

where

$$\phi^\pm \simeq 2\eta^\pm - \frac{\pi}{2} \pm (l\theta - \frac{\pi}{4}) \tag{1.96}$$

The main contribution to $f(\theta,\phi)$ above, occurs when either ϕ^+ or ϕ^- is stationary. If the internuclear potential is purely repulsive there is only one point of stationary phase, which occurs in the ϕ^- branch of the phases. This corresponds to an angular momentum $l = l_s$. The stationary phase is found by expanding ϕ^- about the point $l = l_s$.

$$\phi_\ell^- \simeq \phi^-(l_s) + \frac{1}{2}\frac{\partial^2\phi^-}{\partial\ell^2}\,|_{(l-l_s)} \tag{1.97}$$

Using the JWKB semi-classical phase shift, 1.35, which rearranged is (McCarroll, 1974)

$$\delta_\ell^{(JWKB)} = \int_{R_T}^\infty \overline{\kappa}_\ell(R)dR - \int_{R_T}^\infty \tilde{\kappa}_\ell(R)dR \tag{1.98}$$

where

$$\tilde{\kappa}_l(R) = \left(k^2 - \frac{(l+\frac{1}{2})^2}{R^2}\right) \tag{1.99}$$

and $\overline{\kappa}_l$ (R) is from 1.78, then

$$2\frac{\partial\delta}{\partial R} = \pi - 2b\int_{R_T}^\infty \frac{1}{R^2[1 - \frac{W(R)}{E} - \frac{b^2}{R^2}]^{\frac{1}{2}}} dR \tag{1.100}$$

which is identical to the classical scattering angle . This clear correspondence between the deflection angle and the semi-classical phase shifts at $l = l_s$ means that at the point of stationary phase, a classical impact parameter b can be associated with l . The integral in 1.95 is then evaluated at this point, using the classical relationship 1.90. In the Primitive Semi- classical approximation (Connor, 1979), $f(\theta,\phi)$ is therefore

$$f(\theta,\phi) = [I(\theta)]^{\frac{1}{2}} exp(i\gamma) \tag{1.101}$$

where I(θ) is $\frac{b}{sin\theta} \mid \frac{d\theta}{db} \mid$, the classical cross section 1.7, and

$$\gamma = \phi^{-}(ls) - \frac{\pi}{4} \tag{1.102}$$

Expression 1.101 is derived in Appendix B. The validity of this approximation, within the limits set by using the asymptotic form 1.94 for $P_l(\cos\theta)$, is that

$$\Delta l \approx \left(\frac{(d\theta)}{dl}\right)^{-\frac{1}{2}} >> l \text{ (Child, 1974)} \tag{1.103}$$

Although the Stationary Phase Approximation in the two state collision establishes the correspondence between l and b, some authors feel that the method does not always give accurate results (Gaussorgues et al, 1975, Broglia et al, 1974).

1.7 Semi-Classical Total Cross-sections

Total cross-sections are found from

$$Q = 2\pi \int_o^\infty \mid f(\theta,\phi) \mid^2 sin\theta d\theta \tag{1.104}$$

Because the modulus of the scattering amplitude is taken, the phase factors which have modulus 1 can be neglected and in the Impact Parameter approximation 1.104 becomes

$$Q = 2\pi \int_o^\infty bdbP(b) \tag{1.105}$$

where the integration is over the range of impact parameters. The probabilities P(b) are obtained from the probability amplitudes

$$P(b) = \mid c_n(b,t) \mid^2 \tag{1.106}$$

1.8 Curved Trajectories

In high energy ion-atom or atom-atom collisions, the interaction time is short and any deviation of the collision partners from straight line paths is often assumed to be negligible. Excellent results at higher energies have been obtained, using straight line path approximations with both atomic and molecular orbital methods.

At low energies, however, the colliding ions move more slowly and the effect of the internuclear potential is more pronounced. In such circumstances it may be more physically correct to employ curved trajectories.

The effects, on the direct and exchange matrix elements, of using velocity components which vary with time, are two fold. Firstly, the action of the operators H -i$\frac{\partial}{\partial t}$ on the wave function, results in acceleration factors being introduced into the matrix elements. Secondly, any velocity terms in the ETFs will vary with changes in the internuclear separation. However, the main effect of including the internuclear potential in the determination of the trajectory, is to change the distance of closest approach of the two ions, from b in the straight line case, to the root of the classical energy equation

$$2\mu(E - W(R)) - \frac{(l+\frac{1}{2})^2}{2\mu R^2} = 0 \tag{1.107}$$

The use of the classical turning point results in probability amplitudes for excitation and charge exchange which differ from those obtained using straight lines, both in magnitude and phase.

1.8.1 Total Cross Sections Using Curved Trajectories

Bates and Boyd (1962a,b) noted that when coulomb trajectories were used in H^+ + H and He^{++} + He^+ collisions at low energies, that the total cross sections were lower than those where straight line paths were used. This was due to the internuclear repulsion keeping the ions apart and lessening the probabilities for excitation and charge exchange. They derived a simple scaling law for use with symmetric resonance collision, which corrected total cross sections, calculated using straight line trajectories, for the effect of coulomb repulsion. For a coulomb potential of the form C/R experienced by a projectile of reduced mass μ , and an initial relative velocity V(∞), the corrected cross section is

$$Q \simeq Q_o - \frac{C}{\mu V(\infty)^2}(2\pi Q_o)^{\frac{1}{2}} \tag{1.108}$$

where Q_o is the total cross-section calculated on straight line paths. An approximate expression for the total cross section using a coulomb trajectory was found to be

$$Q \simeq \{[\frac{X}{Z^2} - \frac{19.0(Z-1)}{E}]X\}\pi a_o^2$$
$$X = 7.45 - log_{10}E/MZ \tag{1.109}$$

E is the centre of mass energy in eV, M is the reduced mass and Z is the atomic number.

Most low energy work with curved trajectories, has, until recently been undertaken using molecular methods. The determination of which type of trajectory is

best suited to ion-atom collisions has been of interest to some authors. Knudson and Thorson (1970) compared a quantal method with a classical trajectory model when considering both excitation and charge exchange in low energy $H^+ + H$ collisions. Separate trajectories for the molecular gerade and ungerade states were used in the latter method. These trajectories were determined by the initial state elastic scattering potential. The results, while not in complete agreement with quantal results were much improved on straight line Impact Parameter results obtained at the same time.

Corrigall and Wallace (1971) also used classical trajectories determined by a mean quantum mechanical potential energy

$$\overline{E}(R,t) = < \Psi(R,t) \mid H \mid \Psi(R,t) > \tag{1.110}$$

and found that although the proton-hydrogen collision cross-sections were not sensitive to trajectory effects, with the scattering angle being less than 1 at all energies, the charge exchange probabilities showed marked disagreement with the straight line probabilities of Gallaher and Wilets (1968) and were in good agreement with experiment. Bates and Crothers (1970) forced a common turning point for the trajectories in different channels, for $H^+ + H$ collisions, and this method was also used by Bates and Sprevak (1970), Perrot (1970) and Burns and Crothers (1976). The latter authors studied low velocity proton-helium collision and their results were in good agreement with the measurements of Helbig and Everhart (1964). Delos et al (1972) compared two methods of finding transition probabilities using classical trajectories, firstly by treating the nuclear wave function as a narrow wave packet and secondly by using semi-classical WKB methods. Ryufuku and Watanabe (1976) carried out a semi-classical Impact parameter calculation, using coulomb trajectories for the reaction

$$X^{z+} + X^{(z-1)+}(1s) \rightarrow X^{(z-1)+}(1s) + X^{z+} \tag{1.111}$$

using a scaled cross-section $\overline{\sigma} = Z^2\sigma_{z,M}$ and laboratory energy $\overline{E} = E/Z^2M(eV/amu)$ of the projectile. When the internuclear potential was ignored, the relationship of $\overline{\sigma}$ to $\overline{E}$ for all Z became the same as that for proton hydrogen collisions. Ryufuku and Watanabe also established that the cross-sections were affected by the internuclear potential for E_{lab} (keV) $< 0.1\ Z^2\ (Z\text{-}1)$. Green et al (1981), using a PSS method similar to that of Piacentini and Salin (1974), found that trajectory effects, in C^{6+} and H collisions, occured when there was strong rotational coupling between the molecular states, at small internuclear separations.

More recently, van Hemert et al (1985) have compared charge exchange cross sections obtained using quantal methods with those from a semi-classical Impact Parameter method using a molecular basis. The quantal results were only comparable with the semi-classical when coulomb rather than straight line trajectories were employed in the latter.

The atomic orbital Impact Parameter method using straight line paths has been regarded, until recently, as valid only for high energy collisions, but Fritsch and Lin (1982a,b) and Bransden and Noble (1982) have shown that the method

can be used successfully at intermediate and low energies. Curved trajectories have also been used by Fritsch (1982), in a study of C^{6+} – H collisions, and the cross sections were significantly lower than when straight line paths were used.

The sensitivity of total and partial cross-sections to the trajectory employed has been found to be more marked, if the maximum probabilities for any particular reaction occur at smaller impact parameters. If a molecular basis has been used, greater trajectory effects are seen if the coupling between states occurs at small internuclear separations. The phase of the probability amplitudes does not affect the total cross sections as the moduli of the $c_n(b,t)$ are used, but these phases are much more important when differential cross sections are to be considered.

1.8.2 Differential Cross Sections using Curved Trajectories

The straight line Eikonal approximation has been used to calculate differential cross-sections by McCarroll and Salin (1968), McCarroll et al. (1970), Piacentini and Salin (1974), Chen and Watson (1969) and more recently by Crothers and Todd (1981b), Winter et al (1987) and Winter (1988). Piacentini and Salin (1974) used the method of McCarroll et al (1970) to calculate differential cross sections in He^{++} and H collisions. This method was employed in subroutine EIKON (Piacentini and Salin, 1977), which calculates expression 1.59. This subroutine has been adapted for use with a curved trajectory in the present work (Forster et al, 1988) and a full description will be given in Chapters two and three. He^{++} + H differential cross-sections were also calculated using a straight line trajectory PSS model by Winter et al (1987). These cross sections were compared to a first order approximation to the differential cross sections, an approach also used by Greenland (1981). The method was similar to that employed in the stationary phase approximation, in that the phase factors associated with both the electronic and nuclear motions

$$\eta = exp(-\frac{1}{V}\{\int_{-\infty}^{z_o} \epsilon_i dz + \int_{z_o}^{\infty} \epsilon_j dz + 2\int_{o}^{\infty} \frac{dz}{R}\}) \tag{1.112}$$

were separated into coulombic and non-coulombic terms. The non-coulombic phases (excluding exp(-4i(lnb)/v)) were expanded about the classical impact parameter b

$$b = \frac{1}{Esin\frac{\theta}{2}} \tag{1.113}$$

and then to lowest order,

$$\frac{d\sigma}{d\Omega} \simeq \mid c_n(b,t) \mid^2 \left[\frac{d\sigma}{d\Omega}\right]_{Ruth} \tag{1.114}$$

where

$$\left[\frac{d\sigma}{d\Omega}\right]_{Ruth} = \frac{1}{4E^2 sin^4\frac{\theta}{2}}$$

Winter et al found that at larger scattering angles (μbv $\sin\theta > 10$) there was good qualitative agreement between the semi-classical and the first order differential cross-sections from 1.114, showing the strong dependence of the cross-sections on Rutherford classical scattering at larger angles. Probability amplitudes calculated using both straight line and curved trajectories were used in expression 1.114 to assess the effect of the trajectory. For all $\theta < 90^o$ the effect of the trajectory was less than 2% at 3 keV. Further three centre calculations were carried out on the same system by Winter (1989), and although there was good agreement at lower energies, at impact energies of 70 keV there was poor agreement, attributed to the lack of translation factors in the earlier calculation.

Various methods have been used to calculate curved trajectory cross sections using semi-classical methods. Gaussorgues et al (1975a,b) derived the Common Trajectory equations by the method already described and applied then to proton-hydrogen collisions. The differential cross-sections were found accurately by summing the semi-classical partial wave expression for the scattering amplitude. The results were in good agreement with the experiment of Houver et al (1974), but were in qualitative agreement only with cross-sections obtained using the Stationary Phase approximation. Dickinson and Hardy (1979) and Hardy (1981) used the primitive semi-classical approximation to calculate differential cross-sections using coulomb trajectories for $^3He^{++}$ and $^4He^+$ collisions. These results have been compared with the present calculations in Chapter four. Dickinson (1981) used an adaptation of the method of Broglia et al (1974), to derive an expression for curved trajectory differential cross sections using the Sudden Approximation within the Impact Parameter method. The Stationary Phase approximation was used, but when comparisons were made with results obtained using the classical perturbation theory of Richards (1981), this approximation did not appear to select the classical paths accurately.

There appears to have been little, if any, work done on differential cross sections using atomic orbital methods, with curved trajectories. In view of this it was felt that a comparison of straight line and curved trajectory differential cross-sections over a range of small angles would be useful. The methods used will be described in Chapter 2.

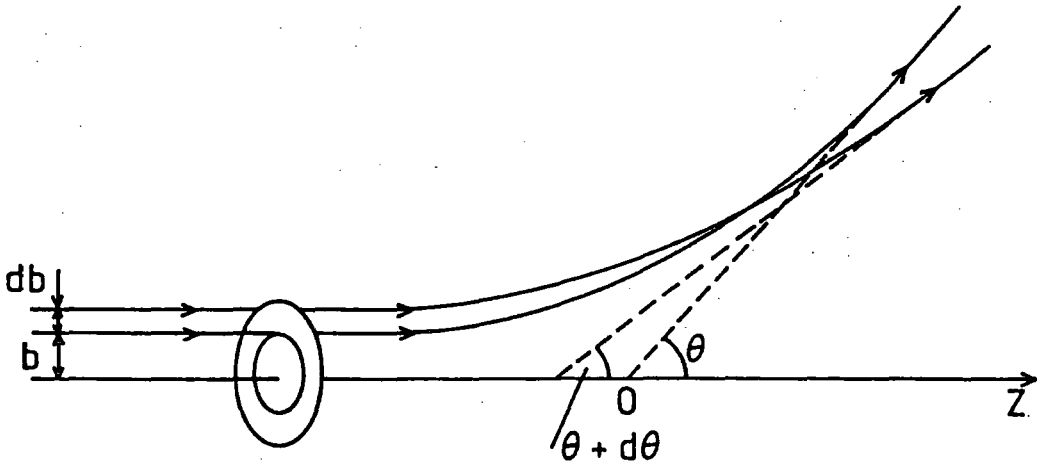

Figure 1.1 The Classical Scattering of a Particle by a Centre of Force.

Chapter 2

The atomic orbital impact parameter method with non-linear trajectories

This chapter will describe the specific methods and approximations used to calculate the results presented in Chapters four, five and six for the charge exchange reaction

$$A^+ + B(1s) \rightarrow A(n,l) + B^+ \qquad (2.1)$$

A classical trajectory has been assumed for the nuclei of A and B in 2.1 , and Section 2.1 will describe the formulae used to model the motion. Section 2.2 describes the Eikonal phase transformation made to the wavefunction (Bransden, 1983). The straight line path Impact Parameter model, using atomic orbital basis functions, from which this work was developed, has been employed by Bransden et al (1984), Shingal et al (1986,1987) and Allan et al (1986b) for higher energies. This method has been modified for use with curved trajectories and the specific changes necessary are detailed in Section 2.3. Sections 2.4 and 2.5 are concerned with the calculation of total and differential cross-sections obtained using non-linear paths.

2.1 Classical Trajectories

The classical trajectories produced by a centre of force have been discussed at length by numerous authors, including for example, Landau and Lifshitz (1976) and Goldstein (1980). The classical motion of two positively charged particles, ion B with mass M_B, energy E^B_{lab} and ion A, mass M_A and energy E^A_{lab}, are shown in the laboratory frame in Figure 2.1. The problem of the mutual motion is much simplified if a transformation is made to the centre of mass frame. Then it is only necessary to consider a single particle A of reduced mass μ moving in the field of a central potential W(R) at a distance R from A. The centre of mass energy is found by using the transformation

$$E_{cm} = \frac{M_B}{M_A + M_B} E^A_{lab} \tag{2.2}$$

and the reduced mass is

$$\mu = \frac{M_A M_B}{M_A + M_B} \tag{2.3}$$

Figure 2.2 shows the resulting centre of mass motion. The parameter b is the impact parameter, $\vec{R}_o$ is the distance of closest approach and δ is the angle $\vec{R}$ makes with the space fixed z axis. A has an initial relative velocity V_i at $\vec{R} = \infty$. The interaction potential W(R) is taken to be spherically symmetric, and the angular momentum of the motion

$$L = \mu R^2 \delta = \mu v_i b \tag{2.4}$$

is a constant, the motion taking place in the x,z plane. The total energy of the system, E_{cm} is conserved and is described by

$$E_{cm} = T + W(R) \tag{2.5}$$

$T = [\dot{R}^2 + R\dot{\delta}^2]$ is the kinetic energy and therefore

$$E_{cm} = \frac{\mu}{2}[\dot{R}^2 + \frac{L^2}{\mu R^2}] + W(R) \tag{2.6}$$

The $\cdot$ notation is used for differentiation with respect to time. At $R = \infty$ where the potential is assumed to be zero, the total energy is equal to the initial kinetic energy of the projectile A

$$E_{cm} = \frac{1}{2}\mu v_i^2 R \to \infty \tag{2.7}$$

The radial velocity $\frac{dR}{dt}$ at time t, from 2.6, is

$$\frac{dR}{dt} = (\frac{2}{\mu}(E_{cm} - W(R)) - \frac{L^2}{\mu R^2})^{\frac{1}{2}} \tag{2.8}$$

The classical turning point or the distance of closest approach, R_o, is found by setting the LHS of 2.8 to zero and finding the largest positive root of the equation. Using the relation $L = \sqrt{2\mu E}\, b$, the time is given by

$$t - t_o = \left(\frac{\mu}{2E_{cm}}\right)^{\frac{1}{2}} \int_{R_o}^{R} \frac{dR}{\left(1 - \frac{W(R)}{E_{cm}} - \frac{b^2}{R^2}\right)^{\frac{1}{2}}} \tag{2.9}$$

and the angle δ by

$$\delta - \delta_o = \int_{R_o}^{R} \frac{b\,dR}{R^2\left(1 - \frac{W(R)}{E_{cm}} - \frac{b^2}{R^2}\right)^{\frac{1}{2}}} \tag{2.10}$$

If the time t_o at the distance of closest approach is taken to be zero, the trajectory is then symmetric under time reversal. At $t \rightarrow \infty$, the trajectory will approach a straight line, the direction of which will be changed from that of the initial ($t \rightarrow -\infty$) path, due to the action of the potential. Denoting the angle between the asymptotes of the locus as α, the deflection function Θ is

$$\Theta = \pi - \alpha \tag{2.11}$$

and

$$\alpha = 2\int_{R_o}^{\infty} \frac{bdR}{R^2\left(1 - \frac{W(R)}{E_{cm}} - \frac{b^2}{R^2}\right)^{\frac{1}{2}}} \tag{2.12}$$

The classical scattering angle θ where $0 < \theta < \pi$ is dependent on the value of the deflection function and takes the values

$$\theta \quad = \Theta \qquad \text{if } 0 < |\,\Theta\,| \leq \pi \tag{2.13}$$

$$\theta \quad = 2\pi - \Theta \qquad \text{if } \pi < |\,\Theta\,| < 2\pi \tag{2.14}$$

For a trajectory which is symmetric about the space fixed x axis, δ_o can be taken to be $\frac{\pi}{2}$ at the turning point. If a less explicitly symmetric trajectory is required, as in Figure 2.2, then δ_o can be found from (Bransden and Joachain 1983).

$$\delta_o = \Theta + \frac{\alpha}{2} \tag{2.15}$$

and from expressions 2.11, 2.12 for α and Θ

$$\delta_o = \pi - \int_{R_o}^{\infty} \frac{bdR}{R^2\left(1 - \frac{W(R)}{E_{cm}} - \frac{b^2}{R^2}\right)^{\frac{1}{2}}} \tag{2.16}$$

An expression for the distance, s, along the classical trajectory can be derived from consideration of a small element of the classical path , δs, shown below.

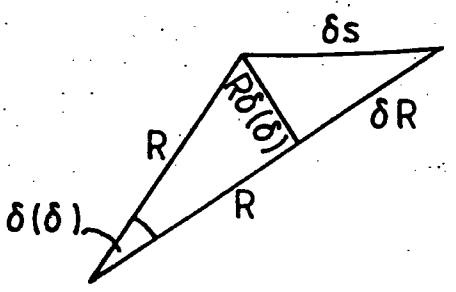

For $\delta(\delta)$ sufficiently small, δs may be regarded as a straight line element, and

$$\delta s^2 = R^2[(\delta(\delta))^2 + (\delta R)^2] \tag{2.17}$$

which in the limit as $\delta \rightarrow 0$ becomes

$$\frac{ds}{dR} = \left(R^2\left(\frac{d\delta}{dR}\right)^2 + 1\right)^{\frac{1}{2}} \tag{2.18}$$

and using 2.10

$$\frac{ds}{dR} = \frac{[E_{cm} - W(R)]^{\frac{1}{2}}}{E_{cm}^{\frac{1}{2}}\left[1 - \frac{W(R)}{E_{cm}} - \frac{b^2}{R^2}\right]^{\frac{1}{2}}} \tag{2.19}$$

and the change in trajectory with respect to time can be written

$$\frac{ds}{dt} = \left[\frac{2}{\mu}[E_{cm} - W(R)]\right]^{\frac{1}{2}} \tag{2.20}$$

At higher energies, which in the case of proton-hydrogen collisions, may be a few hundred eV, the straight line approximation is often considered to be adequate. The straight line case may be recovered from the classical trajectory equations by setting the internuclear potential to zero.

Coulomb Trajectories

Assuming a coulomb interaction between the two colliding nuclei, of the form $W(R) = \alpha/R$, where $\alpha = Z_A Z_B$, simplifies the integration of the equations which define the trajectory parameters. Expression 2.10 becomes, on using a coulomb potential,

$$\delta - \delta_o = \int_{R_o}^{R} \frac{b dR}{R^2\left(1 - \frac{\alpha}{RE_{cm}} - \frac{b^2}{R^2}\right)^{\frac{1}{2}}} \tag{2.21}$$

which is then integrated analytically. The expression

$$\delta = \cos^{-1}\left[\frac{(L/R + \mu\alpha/L)}{(2\mu E_{cm} + \mu^2\alpha^2/L)^{\frac{1}{2}}}\right] + c \tag{2.22}$$

from Landau and Lifshitz (1976) for δ has been used in the present work. The value of the square bracket is 1 at the turning point and the inverse cos term is zero. The constant C is therefore equal to δ_o and the full expression is

$$\delta = \cos^{-1}\left[\frac{[L/R + \mu\alpha/L]}{[2\mu E_{cm} + \mu^2\alpha^2/L]^{\frac{1}{2}}}\right] + \delta_o \tag{2.23}$$

The analytic expression for the time t is, from Gradshteyn and Ryzhik (1980)

$$t = \left(\frac{\mu}{2E_{cm}}\right)[R^2 - \alpha R/E_{cm} - b^2]^{\frac{1}{2}} + \tag{2.24}$$

$$+ \frac{\alpha}{2E_{cm}} ln[2(R^2 - \alpha R/E_{cm} - b^2)^{\frac{1}{2}} + 2R - \alpha/E_{cm}] + c \tag{2.25}$$

When evaluated at the turning point, t = 0, the terms in $[R^2 - \alpha R/E_{cm} - b^2]$ are zero and C = $-(\alpha/2E_{cm})\ln(2R_o - (\alpha/E_{cm}))$.

2.25 becomes

$$t = \left(\frac{\mu}{2E_{cm}}\right)^{\frac{1}{2}}[R^2 - \alpha R/E_{cm} - b^2]^{\frac{1}{2}} +$$
$$ln[2(R^2 - \alpha R/E_{cm} - b^2)^{\frac{1}{2}} + 2R - \alpha/E_{cm}] -$$
$$- \frac{\alpha}{2E_{cm}} ln(2R_o - \alpha/E_{cm}) \tag{2.26}$$

2.2 The Eikonal Phase Transformation

In the coordinate system shown in Figure 1.2, the Schrödinger equation for the three body system in the centre of mass frame, is expressed as

$$(-\frac{\hbar^2\nabla_R^2}{2\mu} - \frac{\hbar^2\nabla_{rg}^2}{2m_e} + V_{AB} + V_{Ae} + V_{Be} - E)\Psi(\vec{R}, \vec{r}_g) = 0 \tag{2.27}$$

It is assumed that the mass of the electron is negligible compared to that of the ions. $\vec{r}_A$ and $\vec{r}_B$ are the position vectors of the electron with respect to A and B and the internuclear vector is $\vec{R}$. $\vec{r}_g$ is the position of e^- with respect to the centre of mass of A and B. In equation 2.27 V_{AB} is the coulomb reaction between the two ions, V_{Ae} is that between the electron and A, and similarly V_{Be} is the potential between e^- and B.

If W(R) is some common potential which defines the trajectories of the nuclei, then 2.27 can be written

$$[-\frac{\hbar^2\nabla_R^2}{2\mu} - \frac{\hbar^2\nabla_{rg}^2}{2m_e} + (V_{AB} - W(R) + V_{Ae} + V_{Be} + W(R) - E]\Psi'(\vec{R}, \vec{r}_g) = 0 \tag{2.28}$$

where E is the total energy of the motion, $E = E_{cm} + \varepsilon$. ε is the eigen-energy of the electron. In order to simplify the above equation a phase transformation is made to $\Psi'(\vec{R}, \vec{r}_g)$ where

$$\Psi'(\vec{R}, \vec{r}_g) = \exp(iS(\vec{R}/\hbar)\Psi(\vec{R}, \vec{r}_g) \tag{2.29}$$

In the classical limits as h→ 0, then $S(\vec{R})$ is the classical action along the trajectory (Goldstein, 1980, Landau and Lifshitz, 1976). $S(\vec{R})$ must satisfy conservation of energy, expressed as the condition

$$[-\frac{\hbar^2\nabla_R^2}{2\mu} + W(R) - E_{cm}]\exp(iS(\vec{R})) = 0 \tag{2.30}$$

Figure 2.3 shows the relationship of the trajectory to $S(\vec{R})$. $S(\vec{R})$ is parallel to the normal to the surface on which S is constant. Operating with ∇_R^2 on exp(iS($\vec{R}$))

$$\nabla_R^2 \exp(iS(\vec{R})) = [i\nabla_R^2 S(\vec{R}) + (i\,\vec{\nabla}_R\, S(\vec{R}))^2]\exp(iS(\vec{R})) \tag{2.31}$$

and making the classical assumption that $\nabla_R^2 S(\vec{R})$ is very small compared to $(\vec{\nabla}_R S(\vec{R}))^2$, the RHS of 2.31 is substituted in 2.30 to obtain the classical Hamilton-Jacobi equation

$$\vec{\nabla}_R\,(S(\vec{R})) = \{2\mu[E_{cm} - W(R)]\}^{\frac{1}{2}} \tag{2.32}$$

From Figure 2.3, $S(\vec{R})$ is parallel to the velocity $\vec{v}$ along the trajectory and so the solution of 2.32 is

$$S(\vec{R}) = \int \vec{\nabla}_R\, S(\vec{R}).d\,\vec{s} = \int |\vec{\nabla}_R\, S(\vec{R})\,|\,\hat{v}.d\,\vec{s}$$

from which it can be shown that

$$S(\vec{R}) = \int_{-\infty}^{\infty}\{2\mu E_{cm}(1 - \frac{W(R)}{E_{cm}})\}^{\frac{1}{2}}ds \tag{2.33}$$

which is derived in Appendix C. Returning to the Schrödinger equation 2.27 and using atomic units, so that $\hbar$ =1 and m_e = 1, the operation of ∇_R^2 on $\Psi I(\vec{R}, \vec{r}_g)$ results in

$$\begin{aligned}\nabla_R^2\Psi I,(\vec{R},\vec{r}_g) = {} & i\nabla_R^2 S(\vec{R})\exp(iS(\vec{R}))\Psi(\vec{R},\vec{r}_g) \\ & -(\vec{\nabla}_R\, S(\vec{R}))\exp(iS(\vec{R}))\Psi(\vec{R},\vec{r}_g) \\ & +exp(iS(\vec{R})\nabla_R^2\Psi(\vec{R},\vec{r}_g) \\ & +\frac{2i}{\mu}\,\vec{\nabla}_R\, S(\vec{R}).\,\vec{\nabla}_R\,\Psi(\vec{R},\vec{r}_g)\exp(iS(\vec{R}))\end{aligned} \tag{2.34}$$

$\frac{i}{\mu}\,\vec{\nabla}_R\, S(\vec{R}).\,\vec{\nabla}_R\,\Psi(\vec{R},\vec{r}_g)$ becomes, on taking the scalar product and using $|\,\nabla_R\Psi(\vec{R},\vec{r}_g)\,| = \frac{\partial}{\partial s}\Psi(\vec{R},\vec{r}_g)$along the trajectory,

$$\frac{i}{\mu}(2\mu[E_{cm} - W(R)])^{\frac{1}{2}}\frac{\partial}{\partial s}\Psi(\vec{R},\vec{r}_g)\,|_{rg} \tag{2.35}$$

From equation 2.20 and using $\frac{\partial}{\partial s}|_{r_g} = \frac{\partial_t \partial}{\partial_s \partial_t}|_{r_g}$; $\frac{\partial_s}{\partial_t}|_{r_g} = \frac{ds}{dt} = [\frac{2}{\mu}(E_{cm} - W(R)]^{\frac{1}{2}}$ and

$$\frac{i}{\mu}\vec{\nabla}_R \Psi(\vec{R},\vec{r}_g)S(\vec{R}).\vec{\nabla}_R \Psi(\vec{R},\vec{r}_g) = \frac{i\partial}{\partial t}|_{r_g} \Psi(\vec{R},\vec{r}_g) \tag{2.36}$$

Substituting 2.32 and 2.35 into 2.27, the Schrödinger equation becomes

$$[-\frac{\nabla^2 r_g}{2} + (V_{AB} - W(R) + V_{Ae} + V_{Be} - \frac{i\partial}{\partial t}|_{r_g}] \times \Psi(\vec{R},\vec{r}_g) = 0 \tag{2.37}$$

2.3 The Impact Parameter Method for calculation of the Probability Amplitudes

Following the method of Bransden (1972), the wavefunction $\Psi(R,r_g)$ is expressed as an expansion of atomic orbital functions of the form

$$\Psi(R,r_g) = \sum_{n=1}^{N} a_n(b,t)\phi_n{}'(\vec{r}_g,t) + \sum_{m=N+1}^{M} c_m(b,t)\chi'(\vec{r}_g,t) \tag{2.38}$$

In the expansion, the $a_n(b,t)$ are probability amplitudes for elastic or direct excitation channels for the target ion B, and the $c_m(b,t)$ are for charge exchange channels for the projectile A. The quantities $|\, a_n(b,t)\,|^2$ and $|\, c_m(b,t)\,|^2$ represent the probabilities for the final channel n or m. At $t = -\infty$ the boundary conditions require that the electron be attached to the target ion in initial state 1, and therefore $|a_1(b,t)|^2 = 1$ at $t = -\infty$. Unitarity considerations also require that at $t = +\infty$

$$|\, a_n(b,t)\,|^2 + |\, c_m(b,t)\,|^2 = 1 \tag{2.39}$$

The $\phi'_n(\vec{r}_g,t)$ and $\chi'_m(\vec{r}_g,t)$ are orthonormal electronic basis functions which asymptotically satisfy

$$[-\frac{1}{2}\nabla^2 r_B + V_{Be} - \frac{i\partial}{\partial t}|_{r_g}]\phi'_n(\vec{r}_g,t) = 0 \tag{2.40}$$

$$[-\frac{1}{2}\nabla^2 r_A + V_{Ae} - \frac{i\partial}{\partial t}|_{r_g}]\chi'_m(\vec{r}_g,t) = 0 \tag{2.41}$$

and are of the form

$$\phi'_n(\vec{r}_g,t) = \phi_n(\vec{r}_B)\exp(i\gamma_n^B) \tag{2.42}$$

$$\chi'_m(\vec{r}_g,t) = \chi_m(\vec{r}_A)\exp(i\gamma_m^A) \tag{2.43}$$

From the discussion in Chapter one, the electron attached to either of the collision partners will have, in addition to its bound state energy, momentum and kinetic energy due to the relative motion of the ions. The terms γ_n^B and γ_m^A are electronic translational factors of the form (Bates and McCarroll, 1958)

$$\gamma^c = \vec{v}_c \cdot \vec{r}_g - \int_o^t dt(\varepsilon_c + \frac{v_c^2}{2})$$

where c = A or B, $\varepsilon_c = \varepsilon_A$ or ε_B

$\vec{v}_A$ is the velocity of A and $\vec{v}_B$ is that of B, relative to the centre of mass of the motion.

The amplitudes $a_n(b,t)$ and $c_m(b,t)$ are recovered by solving equation 2.37. For convenience the operators

$-\frac{\nabla^2 r_g}{2} + (V_{AB} - W(R) + V_{Ae} + V_{Be})$ are denoted by H_{el}.

Expression 2.37 then becomes:-

$$[H_{el} - \frac{i\partial}{\partial t}|_{rg}]\Psi(\vec{R}, \vec{r}_g) = 0 \tag{2.44}$$

where the time differential $\frac{\partial}{\partial t}$ is for fixed $\vec{r}_g$. The integral

$$\int_{-\infty}^{\infty} dt \int d\vec{r}^3 \, \Psi^*[H_{el} - \frac{i\partial}{\partial t}|_{rg}]\Psi \tag{2.45}$$

is reduced by the variational method to a set of coupled equations (Bransden, 1972),

$$i[I\dot{\mathbf{a}}(t) + \mathbf{S}\dot{\mathbf{c}}(t)] = \mathbf{H}\mathbf{a}(t) + \mathbf{K}\mathbf{c}(t) \tag{2.46}$$

$$i[\overline{\mathbf{S}}\dot{\mathbf{a}}(t) + \mathbf{I}\dot{\mathbf{c}}(t)] = \overline{\mathbf{K}}\mathbf{a}(t) + \overline{\mathbf{H}}\mathbf{c}(t) \tag{2.47}$$

and

$$I'_{nn} = < \phi l_n(\vec{r}_g, t) \mid \phi l_n l(\vec{r}_g, t > = \delta_{nn}l, \tag{2.48}$$

$$I_{mm'} = < \chi l_m(\vec{r}_g, t) \mid \chi l_m l(\vec{r}_g, t) > = \delta_{mm}l, \tag{2.49}$$

$$S_{nm} = < \phi l_n(\vec{r}_g, t) \mid \chi l_m(\vec{r}_g, t) > \tag{2.50}$$

$$\overline{S}_{mn} = < \chi l_m(\vec{r}_g, t) \mid \phi l_n(\vec{r}_g, t) > \tag{2.51}$$

$$H_{nn'} = < \phi l_n(\vec{r}_g, t) \mid H_{el} - \frac{i\partial}{\partial t} \mid \phi l_n, (\vec{r}, t) > \tag{2.52}$$

$$K_{nm} = < \phi l_n(\vec{r}_g, t) \mid H_{el} - \frac{i\partial}{\partial t} \mid \chi l_m(\vec{r}_g, t) > \tag{2.53}$$

$$\overline{H}_{mm'} < \chi l_m(\vec{r}_g, t) \mid H_{el} - \frac{i\partial}{\partial t} \mid \chi l_m l \, \vec{r}_g, t) > \tag{2.54}$$

$$\overline{K}_{mn} = < \chi l_m(\vec{r}_g, t) \mid H_{el} - \frac{i\partial}{\partial t} \mid \phi l_n(\vec{r}_g, t) > \tag{2.55}$$

2.3.1 Explicit Form of the Matrix elements

When the substitutions 2.42 and 2.43 are made in expressions 2.48 - 2.55, they become

$$I_{nn'} = \delta_{nn'} \tag{2.56}$$

$$I_{mm'} = \delta_{mm'} \tag{2.57}$$

$$S_{nm} = < \phi_n(\vec{r}_B)e(i\gamma_n^B) \mid \chi_m(\vec{r}_A)e(i\gamma_m^A) > \tag{2.58}$$

$$\overline{S}_{mn} = < \chi_m(\vec{r}_A)e(i\gamma_m^A) \mid \phi_n\ \vec{r}_B)e(i\gamma_n^B > \tag{2.59}$$

$$H_{nn'} = < \phi_n(\vec{r}_B)e(i\gamma_n^B) \mid H_{el} - \frac{i\partial}{\partial t} \mid \phi_{n'}(\vec{r}_B)e(i\gamma_{n'}^B) > \tag{2.60}$$

$$\overline{H}_{mm'} = < \chi_m(\vec{r}_A)e(i\gamma_m^A) \mid H_{el} - \frac{i\partial}{\partial t} \mid \chi_{m'}(\vec{r}_A)e(i\gamma_{m'}^A) > \tag{2.61}$$

$$K_{nm} = < \phi_n(\vec{r}_B)e(i\gamma_n^B) \mid H_{el} - \frac{i\partial}{\partial t} \mid \chi_m(\vec{r}_A)e(i\gamma_m^A) > \tag{2.62}$$

$$\overline{K}_{mn} = < \chi_m(\vec{r}_A)e(i\gamma_m^A) \mid H_{el} - \frac{i\partial}{\partial t} \mid \phi_n(\vec{r}_B)e(i\gamma_n^B) > \tag{2.63}$$

where e( ) represents exp( )

The action of H_{el} on the individual states

are with respect to the centre of mass of the two heavy particles. From Figure 2.5

$$\vec{r}_B = \vec{r}_g - q\,\vec{R} \tag{2.64}$$

$$\vec{r}_A = \vec{r}_g + p\,\vec{R} \tag{2.65}$$

and $\nabla^2_{r_g} = \nabla^2_{rB} = \nabla^2_{rA}$. Operating on the wavefunction $\phi(\vec{r}_B)e(i\gamma_n^B)$ and using the abbreviation $\phi = \phi(\vec{r}_B)$.

$$[H_{el} - \frac{i\partial}{\partial t}]exp(i\gamma_n^B)\phi = e(i\gamma_n^B)[H_{el} - i(\vec{\nabla}_{r_g}\,\gamma_n^B.\,\vec{\nabla}_{r_g} - \\ -\frac{1}{2}\nabla^2_{r_g}(i\gamma) - \frac{i\partial}{\partial t} + \dot{\gamma}_n^B]\phi \tag{2.66}$$

This expression is simplified by using the relations

$$\vec{\nabla}_{r_g}\,\gamma_n^B = \vec{v}_B;\ \nabla^2_{r_g}(i\gamma) = 0; \tag{2.67}$$

$$\frac{\partial}{\partial t}\mid_{r_g} \phi = -\,\vec{v}_B\,.\,\vec{\nabla}_{r_g}\,\phi \tag{2.68}$$

$$\dot{\gamma}_n^B = \vec{v}_B\,.\,\vec{r}_g - \epsilon_n - \frac{V_B^2}{2} \tag{2.69}$$

These expressions are derived in Appendix D. The kets in 2.25 + 2.55 become, with respect to the target wavefunction

$$exp(i\gamma_n^B)[H_{el} - \epsilon_{nl} + \dot{\vec{v}}_B . \vec{r}_g]\phi_{nl} > \tag{2.70}$$

and similarly with respect to the projectile functions $\chi = \chi(\vec{r}_A))$

$$exp(i\gamma_m^A[H_{el} - \epsilon_{ml} + \dot{\vec{v}}_A . \vec{r}_g]\chi_{ml} > \tag{2.71}$$

The matrix elements H,$\overline{\text{H}}$,K,$\overline{\text{K}}$ therefore contain acceleration terms due to the non-uniformity of the relative velocity. These terms are zero for the straight line trajectory model.

Denoting

$$\gamma_n^B - \gamma_{nl}^B = B_n B_{nl} \tag{2.72}$$

$$\gamma_m^A - \gamma_{ml}^A = A_m A_{ml} \tag{2.73}$$

$$\gamma_n^B - \gamma_m^A = B_n A_m \tag{2.74}$$

$$\gamma_m^A - \gamma_n^B = A_m B_n \tag{2.75}$$

$$H_{nnl} =< \phi_n e^{(iB_n B_{nl})} \mid H_{el} - \epsilon_n l + \dot{\vec{v}}_B . \vec{r}_g \mid \phi_{nl} > \tag{2.76}$$

$$\overline{H}_{mml} =< \chi_m e^{(iA_m A_{ml})} \mid H_{el} - \epsilon_n l + \dot{\vec{v}}_A . \vec{r}_g \mid \chi_{ml} > \tag{2.77}$$

$$K_{nml} =< \phi_n e^{(iB_n A_{ml})} \mid H_{el} - \epsilon_m + \dot{\vec{v}}_A . \vec{r}_g \mid \chi_m > \tag{2.78}$$

$$\overline{K}_{mn} = \chi_m e^{(iA_m B_{nl})} \mid H_{el} - \epsilon_n + \dot{\vec{v}}_B . \vec{r}_g \mid \phi_n > \tag{2.79}$$

The Direct Matrix elements H_{nnl} and $\overline{H}_{mml}$ can be further simplified by using

$$[-\frac{1}{2}\nabla_{r_g}^2 + V_{Be} - \epsilon_n]\phi_n(r_B) = 0 \tag{2.80}$$

and therefore

$$H_{nn'} =< \phi_n e^{iB_n B_{nl}} \mid V_{AB} + v_{Ae} - W(R) + \dot{\vec{v}}_B . \vec{r}_g \mid \phi_{nl} > \tag{2.81}$$

and

$$\overline{H}_{mm'} =< \chi_m e^{iA_m A_{ml}} \mid V_{AB} - W(R) + V_{Be} + \dot{\vec{v}}_A . \vec{r}_g \mid \chi_{ml} > \tag{2.82}$$

2.3.2 Integration of the Matrix Elements

The matrix elements above are calculated for each value of the nuclear vector $\vec{R}$ in the body fixed frame of reference, and subroutine ENTGIN has been developed by Shingal (1985) to carry out the body fixed integration for the straight line trajectory model. The electronic translation factors in the matrix elements must be transformed to body fixed coordinates before the integration can take place. This is described in 2.3.3. In the straight line case for which subroutine ENTGIN was written, the position of the origin of coordinates in the body fixed frame is arbitrary as will be shown. The electron is usually chosen for convenience, to be at position $\vec{r}$ with respect to the midpoint of $\vec{R}$. This simplifies the later transformation of the matrix elements to prolate spheroidal coordinates. However in the case of curved trajectories, where the relative velocity is not constant, the origin of coordinates must be at the centre of mass of the two nuclei, to coincide with the origin in the space fixed frame. ENTGIN has been changed in the present work for use with a curved trajectory, and in order to keep the alterations to a minimum, a transformation has been made from the centre of mass, to the midpoint of $\vec{R}$ which will be described in section 2.3.4.

2.3.3 Transformation of the Space Fixed Velocity Components to the Body Fixed frame

In the body fixed frame of reference, the body fixed z direction is along the internuclear axis. Figure 2.4 shows the relationship of the body fixed to the space fixed frame. The body fixed coordinates are denoted by x", y" and z" and the space fixed coordinates are unprimed. the y" axis coincides with the y axis for all positions of x" and z" and is in the direction outwardly perpendicular to the plane of the paper. Because of the assumption that the classical angular momentum remains constant there is no y component to the space fixed velocity and the motion takes place in the x,z frame.

The transformation of the electronic translation factors was made by first expressing the space fixed z coordinates in terms of the body fixed (Bransden (1972), Briggs (1976)).

$$x = z" \sin\delta + x" \cos\delta \tag{2.83}$$

$$z = z" \cos\delta - x" \sin\delta \tag{2.84}$$

$$y = y" \tag{2.85}$$

In the space fixed frame

$$\vec{v} \,.\, \vec{r}_{\,g} = v_x x + v_z z \tag{2.86}$$

Taking the space fixed coordinates as

$$x = R\sin\delta \tag{2.87}$$

$$z = R\cos\delta \tag{2.88}$$

then the velocity components in the x and z directions are

$$\frac{dx}{dt} = \dot{R}\sin\delta + R\cos\delta\dot{\delta} \tag{2.89}$$

$$\frac{dz}{dt} = \dot{R}\cos\delta - R\sin\delta\dot{\delta} \tag{2.90}$$

When x and z from 2.83, 2.84 are used with the above, 2.86 becomes

$$\vec{v} \,.\, \vec{r}_g \text{ (space fixed)} = R\dot{\delta}x'' + \dot{R}z'' \tag{2.91}$$

Because $\vec{v} \,.\, \vec{r}_g$ is a scalar then

$$\vec{v} \,.\, \vec{r}_g \text{ (body fixed)} = \vec{v} \,.\, \vec{r}_g \text{ (space fixed)} \tag{2.92}$$

and so

$$V_{x''}x'' + V_{z''}z'' = R\dot{\delta}x'' + \dot{R}z'' \tag{2.93}$$

from which it can be seen that $v_{x''} = R\dot{\delta}$ and $v_{z''} = \dot{R}$. $\dot{R}$ and $R\dot{\delta}$ are defined by the classical trajectory of the centre of mass motion, $\dot{R}$ from 2.8 and $R\delta = \frac{-L}{\mu R}$ from 2.4.

From Figure 2.5, using the notation of Bates and McCarroll (1958), the vector from the centre of mass to A is $p\vec{R}$ and to B is $-q\vec{R}$. The space fixed velocities of A and b in terms of the relative velocity v are

$$\vec{v}_A = p\,\vec{v} \tag{2.94}$$

$$\vec{v}_B = -q\,\vec{v} \tag{2.95}$$

Therefore the velocity components of A and B in the body fixed frame are respectively

$$\begin{gathered} v_{x''A} = pv_{x''} = p\dot{R}\ ;\ v_{z''A} = pv_{z''} = pR\dot{\delta}\ ; \\ v_{x''B} = -qv_{x''} = -q\dot{R}\ ;\ v_{z''B} = -qv_{z''} = -qR\dot{\delta} \end{gathered} \tag{2.96}$$

The acceleration terms $\dot{\vec{v}}_B . \vec{r}_g$ and $\dot{\vec{v}}_A . \vec{r}_g$ contained in the matrix elements 2.76 - 2.79, are similarly transformed to the body fixed frame. The acceleration in the space fixed x and z directions in the centre of mass motion is

$$\frac{d^2x}{dt^2} = (\ddot{R}\sin\delta + 2R\cos\delta\dot{\delta} - R\sin\delta(\dot{\delta})^2 + R\cos\delta\ddot{\delta}) \tag{2.97}$$

$$\frac{d^2z}{dt^2} = (\ddot{R}\cos\delta - 2R\sin\delta\dot{\delta} - R\cos\delta(\dot{\delta})^2 + (R\sin\delta\ddot{\delta}) \tag{2.98}$$

$$\dot{\vec{v}} . \vec{r}_g = \frac{d^2x}{dt^2}x + \frac{d^2z}{dt^2}z \text{ in the space fixed frame,} \tag{2.99}$$

and using the fact that

$\dot{\vec{v}} . \vec{r}_g$ (space fixed) $= \dot{\vec{v}} . \vec{r}_g$ (body fixed),

substituting,

$$\frac{d^2x^{\alpha}}{dt^2}x^{\alpha} + \frac{d^2z^{\alpha}}{dt^2}z^{\alpha} = (\ddot{R} - R(\dot{\delta})^2)z^{\alpha} + (2\dot{R}\dot{\delta} + R\ddot{\delta})x^{\alpha} \tag{2.100}$$

Comparing the two sides of 2.100

$$\frac{d^2x^{\alpha}}{dt^2} = (2\dot{R}\dot{\delta} + R\ddot{\delta}) = A_{x^{\alpha}} \tag{2.101}$$

$$\frac{d^2z^{\alpha}}{dt^2} = (\ddot{R} - R(\dot{\delta})^2 = A_{z^{\alpha}} \tag{2.102}$$

using $R\ddot{\delta} = \frac{Rd\delta}{dR}\frac{dR}{dt}$ in 2.102

$$A_{x^{\alpha}} = \dot{R}(2\dot{\delta} + \frac{Rd\dot{\delta}}{dR})$$

If the trajectory is classical, then $\frac{d\delta}{dt} = \frac{L}{\mu R^2}$;

$$\frac{d\dot{\delta}}{dR} = \frac{-2L}{\mu R^3};\ \frac{Rd\dot{\delta}}{dR} = \frac{-2L}{\mu R^2}$$

$\dot{R}\frac{(2L}{\mu R^2} - \frac{2L}{\mu R^2}) = 0$. There is no contribution from $A_{x^{\alpha}}$ and for a spherically symmetric potential, the body fixed acceleration is along the z^{α} axis only. From the classical trajectory equations

$$\frac{d^2z^{\alpha}}{dt^2} = (\ddot{R} - R(\dot{\delta})^2) = -\frac{1}{\mu}\frac{\partial W(R)}{\partial R} \tag{2.103}$$

which is the central force acceleration .

2.3.4 Transformation of the Origin in the Body Fixed Frame of Reference

From Figure 2.5, the midpoint of $\vec{R}$ is at the origin o' and the electron is at position $\vec{r}$(x',z') with respect to o'. The relationship of $\vec{r}_g$ to $\vec{r}$ is

$$\vec{r}_g = \vec{r} - \vec{R}\,\frac{(q-p)}{2} \tag{2.104}$$

The doubled primed coordinates are related to the single primed by

$$z'' = z' - \frac{R(q-p)}{2} \tag{2.105}$$

$$x'' = x' \tag{2.106}$$

and for the purposes of integration, the ETFs in the body fixed frame become

$$\gamma^c = v_{cz''}z' - v_{cz''}\frac{R(q-p)}{2} + v_{cz''}x' - \int_o^t dt(\epsilon_c + \frac{v_c^2}{2}) \tag{2.107}$$

c = A or B, $\epsilon_c = \epsilon_A$ or ϵ_B.

The acceleration terms in the curved trajectory matrix elements become

$$\vec{v}_c \,.\, \vec{r}_g = A_{cz''}z' - A_{cz''}\frac{R(q-p)}{2} \tag{2.108}$$

Using all these transformations, the combination of ETFs for $H_{nn'}$ become

$$\gamma_n^B - \gamma_{n'}^B = -\int_o^t (\epsilon_n - \epsilon_{n'})dt \tag{2.109}$$

$$\gamma_m^A - \gamma_{m'}^A = -\int_o^t (\epsilon_m - \epsilon_{m'})dt \tag{2.110}$$

The expression for the ETFs for the exchange matrix elements K_{nm} is derived below:-

$\gamma_n^B - \gamma_m^A$ in the body fixed frame is

$$\begin{aligned}&(\vec{v}_B^{\,BF} - \vec{v}_A^{\,BF}).\,\vec{r} - (\vec{v}_B^{\,BF} - \vec{v}_A^{\,BF}).\,\vec{R}\,\frac{(q-p)}{2} \\ &- \int_o^t (\epsilon_n - \epsilon_m)dt - \int_o^t \frac{1}{2}[(\vec{v}_B^{\,BF})^2 - (\vec{v}_A^{\,BF})^2]dt\end{aligned} \tag{2.111}$$

$$\vec{v}^{\,BF} = (v_{x''}, v_{z''}), \tag{2.112}$$

$$\vec{v}_A^{BF} = p\,\vec{v}^{BF} \tag{2.113}$$

$$\vec{v}_B^{BF} = -q\,\vec{v}_{BF} \tag{2.114}$$

Using these relationships, 2.112 becomes

$$-(p+q)\,\vec{v}^{BF}\,.\,\vec{r} + (p+q)\,\vec{v}^{BF}\,.\,\vec{R}\,\frac{(q-p)}{2} - \int_o^t (\epsilon_n - \epsilon_m)dt + \int_o^t \frac{(p^2-q^2)}{2}(v^{BF})^2 dt \tag{2.115}$$

p+q =1 and the second term in 2.115 is

$$v_{x''}R\frac{(q-p)}{2}\cos 0 + v_{x''}R\frac{(q-p)}{2}\cos\frac{\pi}{2} = v_{x''}R\frac{(q-p)}{2} = R\dot{R}\frac{(q-p)}{2}$$

Using

$$R\dot{R} = \frac{RdR}{dt} = \int_o^t \frac{d}{dt}R\frac{dR}{dt}dt = \int_o^t ((\dot{R})^2 + R\ddot{R})dt \tag{2.116}$$

and $v^{BF^2} = (R^2\dot{\delta}^2 + \dot{R}^2)$
the combined terms in 2.115 are

$$-\vec{v}^{BF}\,.\,\vec{r} - \int_o^t (\epsilon_n - \epsilon_m)dt + \frac{(q-p)}{2}\int_o^t R(\ddot{R} - R\dot{\delta}^2)dt$$

From 2.103, the final term is

$$\frac{(q-p)}{2}\int_o^t RAz''dt$$

$$\gamma_n^B - \gamma_m^A = -(q+p)v_{x''}z' + V_{x''}\frac{R(q-p)}{2} - (q+p)v_{x''}x' - \int_o^t (\epsilon_n - \epsilon_m) - \frac{(q-p)v}{2}dt = v_{x''}z' + v_{x''}x' - \int_o^t (\epsilon_n - \epsilon_m) - \frac{(q-p)RA_{z''}}{2} \tag{2.117}$$

and for $\overline{K}_{mn}$

$$\gamma_m^A - \gamma_n^B = (v_{x^n} z^i + v_{x^n} x^n) - \\ - \int_o^t (\epsilon_m - \epsilon_n) - \frac{R(q-p)A_{x^n}}{2} dt \qquad (2.118)$$

For a straight line trajectory, the velocity is constant and the central force acceleration is zero. As a result, the acceleration terms in the matrix elements and in the exponential factors disappear. The matrix elements are independent of p and q and the position of o on the internuclear axis is arbitrary. On the other hand, where the internuclear potential is included in the classical motion, the origin of coordinates of the ETFs must be at the centre of mass of the two nuclei. In the case of two identical nuclei, such as He^{++} and He^{+} collisions, results for which are in Chapter four, p = q = and r_g = r, resulting in the terms in p-q being eliminated.

The ETFs are divided into those parts which are dependent on the electronic coordinates, and those which are independent. The r independent terms which together are

$$exp(i \int_o^t (\epsilon_n - \epsilon_m) + (\frac{q-p}{2}) R A_{x^n} dt) \qquad (2.119)$$

are later multiplied with the integrals over the electronic coordinates.

2.3.5 Explicit Form of the Wave Functions

The eigen functions $\phi_i(\vec{r}_B), \chi_j(\vec{r}_A)$ have the same structure and the description which follows for $\phi_i(\vec{r}_B)$ is also appropriate for $\chi_j(\vec{r}_A)$. The electronic eigenfunctions are of the form

$$C_i r_B^n \exp(-\alpha_B r_{Bi}) \overline{Y}_{\ell m}(\theta_B, \phi_B) \qquad (2.120)$$

The radial components of 2.113 are hydrogentic slater orbitals (Slater, 1963), and the $\overline{Y}_{\ell m}(\theta_B, \phi_B)$ are real spherical harmonics defined by

$$\overline{Y}_{\ell m}(\theta, \phi) = N_m [Y_{\ell m}(\theta, \phi) + Y^*_{\ell m}(\theta, \phi)] \quad m > 0 \qquad (2.121)$$

$N_m = \frac{1}{2}$ for m = 0, and $N_m = \frac{1}{\sqrt{2}}$ when m > 0 and

$$Y_{\ell m}(\theta, \phi) = (-1)^m \left[\frac{(2l+1)(l-m)!}{4\pi(l+m)!} \right] P_{\ell m}(\cos\theta) \exp(im\phi) \qquad (2.122)$$

The $P_{\ell m}(\cos\theta)$ are associated Legendre functions.

The use of real spherical harmonics ensures that the real part of exp(imϕ) is used, i.e. cos mϕ in the expressions for $\phi(\vec{r}_B), \chi(\vec{r}_A)$, and the analysis is simplified. Taking

$$(-1)^m \left[\frac{(2l+1)(1-m)!}{2(l+m)!}\right]^{\frac{1}{2}} = F_{lm}$$

$$\overline{Y}_{lm}(\theta,\phi) = 2\left(\frac{1}{2\pi}\right)^{\frac{1}{2}} N_m F_{lm} P_e(\cos\theta)\cos m\phi \tag{2.123}$$

The effect of using the ∇^2 operator on the wavefunction above can be determined analytically. Operating on the radial part of 2.120 and using the relationships

$$\nabla_r^2 = \nabla^2 r_g = \nabla^2 r_A = \nabla^2 r_B$$

$$-\nabla^2 r_B \phi_i = -\frac{1}{2}\nabla^2 r_B [C_i r_B^n \exp(-\alpha_B r_{Bi})]\overline{Y}_{lm}(\theta_B,\phi_B) \tag{2.124}$$

where

$$\nabla^2 r_B = \frac{d^2}{dr_B^2} + \frac{2d}{r_B dr_B} - \frac{l_B(l_B+1)}{r_B^2}$$

The RHS of 2.124 becomes

$$(\frac{P}{r_B} + \frac{Q}{r_B} + R')\phi_i \tag{2.125}$$

where

$$P = -\frac{1}{2}(n(n+1) - l(l+1)) \tag{2.126}$$

$$Q = \alpha(n+1) \tag{2.127}$$

$$R' = \frac{-1}{2}\alpha^2 \tag{2.128}$$

The same operation is carried out for the projectile functions χ_j.

2.3.6 Integration in Prolate Spheroidal Coordinates

Prolate spheroidal coordinates are used to carry out the two centre integrations. Figure 2.6 from Slater (1963) shows the spheroidal coordinates ξ,η, with the two nuclei at the foci. ξ,η,ϕ satisfy

$$\xi = \frac{1}{R}(r_A + r_B) \;\; 1 < \xi \leq \infty \tag{2.129}$$

$$\eta = \frac{1}{R}(r_A - r_B) \quad -1 \leq \eta \leq 1 \tag{2.130}$$

$$0 < \phi < 2\pi \tag{2.131}$$

from which the various identities required in the integration can be obtained :

$$r_A = \frac{R}{2}(\xi + \eta), \quad r_B = \frac{R}{2}(\xi - \eta) \tag{2.132}$$

$$r = \frac{R^2}{4}(\xi^2 + \eta^2 - 1) \tag{2.133}$$

$$\cos\theta = \frac{\xi\eta}{(\xi^2 + \eta^2 - 1)^{\frac{1}{2}}} \tag{2.134}$$

$$\sin\theta = \frac{(\xi^2 - 1)^{\frac{1}{2}}(1 - \eta^2)^{\frac{1}{2}}}{(\xi^2 + \eta^2 - 1)^{\frac{1}{2}}} \tag{2.135}$$

and from the definition of θ_A, θ_B given in Figure 2.6.

$$\begin{aligned} \sin\theta_A &= \frac{(1-\eta)^{\frac{1}{2}}(\xi^2-1)^{\frac{1}{2}}}{(\xi-\eta)} \quad \cos\theta_A = \frac{\xi\eta - 1}{\xi - \eta} \\ \sin\theta_B &= \frac{(1-\eta^2)^{\frac{1}{2}}(\xi^2-1)^{\frac{1}{2}}}{(\xi+\eta)} \quad \cos\theta_B = \frac{\xi\eta + 1}{\xi + \eta} \end{aligned} \tag{2.136}$$

The volume element $d\tau$ becomes in spheroidal coordinates:-

$$d\tau = \frac{R^2}{8}(\xi^2 - \eta^2)d\xi d\eta d\phi \tag{2.137}$$

The electronic coordinates x',z', which in spherical polars are

x' = r sin θ cosϕ , z' = r cosθ become :-

$$x' = \frac{R}{2}(1 - \eta^2)^{\frac{1}{2}}(\xi^2 - 1)^{\frac{1}{2}}\cos\theta = \lambda\cos\phi \tag{2.138}$$

$$z' = \frac{R}{2}(\xi\eta) \tag{2.139}$$

The Legendre polynomials are constructed in spheroidal coordinates by using the above expressions for cosθ_A etc. The transformation of the element S_{nm} is shown below.

$$S_{nm} = \int \phi_n(\vec{r}_B)\chi_m(\vec{r}_A)\exp(i\,\vec{v}\,.\,\vec{r})d\tau \tag{2.140}$$

becomes

$$\frac{R}{2}F_A F_B N_A N_B \int_1^{\infty} d\xi \int_{-1}^{+1} d\eta C_n(\xi\eta) C_m(\xi\eta)(\frac{R}{2}(\eta+\xi))^{n_A}$$
$$\frac{R}{2}(\xi-\eta)^{n_B} \exp(\frac{iRA}{2})(\xi^2-\eta^2) P_{\ell_{mB}}(\cos\theta_B) P_{\ell_{mA}}(\cos\theta_A)\mathbf{J} \qquad (2.141)$$

where

$$\mathbf{A} = \alpha_A(\xi+\eta) + \alpha_B(\xi-\eta) + v_{s'}\xi\eta \qquad (2.142)$$

and J is the integral

$$\begin{aligned}\mathbf{J} &= \frac{1}{2\pi}\int_o^{2\pi} d\phi \cos m_A\phi \cos m_B\phi \exp(i\lambda\cos\phi) \\ &= \frac{1}{4\pi}\int_o^{2\pi} d\phi \cos(m_A+m_B)\exp(i\lambda\cos\phi) + \\ &\quad + \frac{1}{4\pi}\int_o^{2\pi} d\phi \cos(m_A-m_B)\exp(i\lambda\cos\phi) \qquad (2.143)\end{aligned}$$

which are Bessel functions from the identity (Watson 1966)

$$J_n(\lambda) = \frac{1}{2\pi i^m}\int_o^{2\pi} d\phi \cos n\phi \exp(i\lambda\cos\theta) \qquad (2.144)$$

leading to

$$J = \frac{1}{2}i^{(m_A+m_B)} J_{(m_A+m_B)}(\lambda) + \frac{1}{2}i^{(m_A-m_B)} J_{(m_A-m_B)}(\lambda) \qquad (2.145)$$

H, $\overline{\mathrm{H}}$ K, $\overline{\mathrm{K}}$ are transformed in the same manner and integration is carried out in subroutine ENTGIN by gaussian quadrature methods. these are discussed in Chapter three.

2.3.7 Rotation of the Body Fixed Integrals to the Space Fixed Frame

Because the probability amplitudes are recovered by solving the coupled differential equations 2.46, 2.47 in the space fixed frame, the body fixed integrals are rotated back into this frame of reference. Figure 2.4 shows the sense of the rotation. Using the convention of Rose (1957), the space fixed spherical harmonics $Y^{SF}_{\ell m}(\theta,\phi)$ are expressed in terms of the body fixed $Y^{BF}_{\ell m}(\theta,\phi)$ by using

$$Y^{SF}_{\ell m}(\theta,\phi) = D^{\ell}_{mlm}(\alpha,\beta,\gamma) Y^{BF}_{\ell m}(\theta l,\phi l) \qquad (2.146)$$

The $D^{\ell}_{m'm}(\alpha,\beta,\gamma)$ are rotation matrices (Rose, 1957) which in terms of the Euler angles α,β,γ are

$$D^{\ell}_{m'm} = \exp(im'\alpha)d_{m'm}(\beta)\exp(-im\gamma) \tag{2.147}$$

For the work in this thesis $\gamma = 0$, $\alpha = 0$,$\beta = \pi$ - δ, and 2.147 is modified to

$$Y^{SF}_{\ell m}(\theta,\phi) = \sum_{m'=-1}^{m'=1} d^{\ell}_{m'm}(\beta)Y^{BF}_{\ell m'}(\theta',\phi'). \tag{2.148}$$

2.3.8 Symmetries and Time Reversal

The integration of the matrix elements, is the most expensive and time consuming part of the calculations. However, considerable savings may be made by integrating only the elements of S, H, K, and $\overline{H}$ and finding $\overline{S}$ and $\overline{K}$ by using the relationships

$$\overline{S} = (-1)^{L}(S)^{*} \quad L = l_A + l_B \tag{2.149}$$

$$K = (-1)^{L}(K)^{*} \tag{2.150}$$

The coupled equations 2.46 and 2.47 may be expressed in matrix form as

$$i\mathbf{N}\dot{A} = \mathbf{M}A \tag{2.151}$$

$$\mathbf{N} = \begin{bmatrix} I & S \\ \overline{S} & I \end{bmatrix} \quad , \quad \mathbf{M} = \begin{bmatrix} H & K \\ \overline{K} & \overline{H} \end{bmatrix}$$

where A is the column of vectors including both a_n(b,t) and c_m(b,t). Green (1965) has shown that N and M are related by

$$i\frac{d}{dt}\mathbf{N} = \mathbf{M} - \mathbf{M}^{*} \tag{2.152}$$

when N is hermitian and M is hermitian only at zero velocity, and that

$$\frac{id}{dt}(A_i(b,t)^{\dagger}\,\mathbf{N}\,A_j(b,t)) = 0 \tag{2.153}$$

when A_i and A_j are any two solutions of the above. He has also shown that the above relationships do not depend on the choice of the basis states or on the type of nuclear trajectory employed. 2.152 can provide a useful check of the matrix elements during the course of the calculation if required.

Green (1965) has shown that the impact parameter method is consistent with detailed balancing, even with a finite basis set. The matrices M and N therefore

need only be computed for negative times and those elements for positive times are recovered by using

$$M(+t) = (-1)^{L+M'}M(-t);$$
$$N(+t) = (-1)^{L+M'}N(-t);$$
$$M' = m_A + m_B \qquad (2.154)$$

The coupled equations 2.151 are integrated between the limits t = -t_f to t = t_f to find the probability amplitudes corresponding to each centre of mass energy and impact parameter.

2.4 Total Cross Sections

The total cross-sections are calculated using the Impact Parameter integral 1.105. Any phase factors associated with the internuclear motion or residual coulombic interactions between the electron and the ion, can be ignored when total cross-sections are calculated, as the moduli of these quantities will be one.

2.5 Differential Cross Sections

Differential cross-sections are calculated by using

$$\frac{d\sigma_{nm}}{d\Omega} = k^2 \mid \int_o^\infty bdb \exp(i\Delta)(c_m(b,t) - \delta_{nm})J_{\Delta M}(\rho b) \mid^2 \qquad (2.155)$$

where the c_m(b,t) are the probability amplitudes for the final state m. $J_{\Delta M}$ (ρ b) is the Bessel function of order $\Delta M = m_n - m_m$.

The same expression is used for both straight line and curved trajectories, but the Bessel function is derived differently in the two methods. In the straight line Eikonal Approximation, the argument of ρb is 2μ Vb sin (θ /2), which for small angles can be approximated by μbVθ . When using curved trajectories, the Bessel function originates from the small angle approximation to the Legendre polynomials, 1.91, where $\rho b \simeq \mu V b\theta$.

When ΔM is not equal to zero, the relationship

$$lim_{l\to\infty} l^{\Delta M} P_l^{-\Delta M}(\cos\frac{x}{l}) = J_{\Delta M}(x) \qquad (2.156)$$

is used.

In the next sections the phases shifts Δ for an assumed coulomb trajectory will be described, and then the straight line approximation will be discussed. The general approach is that used by Piacentini and Salin (1977) for straight line differential cross-sections. Δ contains terms to represent, firstly the effect of the

classical action along the trajectory, and secondly, the effect of the long range coulomb attraction between the electron and either A or B.

2.5.1 Electronic Phase Factors

The probability amplitudes $c_n(b,t)$ have been recovered by integration of the coupled equations over the range $-t_f < t < t_f$. From $-\infty$ to $-t_f$ and t_f to∞ , because of the long range nature of the coulomb attraction, the electron attached to either A or B will still interact with the distant nuclear charge of the other ion. In the case of electron exchange, this long range potential can be represented in the phase shift Δ by the integrals

$$\int_{-\infty}^{-t_f} V_{Ae}dt - \int_{t_f}^{\infty} V_{Be}dt \tag{2.157}$$

For a coulomb potential

$$V_{Ae} = \frac{-Z_A}{r_A} \simeq \frac{-Z_A}{R} \quad t \to \infty$$
$$V_{Be} = \frac{-Z_B}{r_B} \simeq \frac{-Z_B}{R} \quad t \to -\infty$$

and 2.157 becomes

$$\int_{t_f}^{\infty} (Z_A + Z_B)\frac{1}{R}dt \tag{2.158}$$

This is transformed to an integral with respect to R by using the relationship

$$dt = (\frac{\mu}{2E})^{\frac{1}{2}} \frac{1}{(1 - \frac{W(R)}{E_{cm}} - \frac{2^2}{R^2})^{\frac{1}{2}}} dR \tag{2.159}$$

For a coulombic internuclear potential, $W(R) = \frac{\alpha}{R}$ and

$$dt = (\frac{\mu}{2E_{cm}})^{\frac{1}{2}} \frac{R}{(R - \frac{\alpha R}{E_{cm}} - b^2)^{\frac{1}{2}}} dR \text{ for positive times} \tag{2.160}$$

Substituting into 2.158 and integrating, the analytic expression for the electronic part of the phase shifts is

$$(\frac{\mu}{2E_{cm}})^{\frac{1}{2}}(Z_A + Z_B)\left[ln\{2(R^2 - \frac{\alpha R}{E_{cm}} - b^2)^{\frac{1}{2}} + 2R - \frac{\alpha}{E_{cm}}\}\right]_{R_f}^{\infty} \tag{2.161}$$

If it is assumed that the only important phases are b dependent (Piacentini and Salin, 1977 and Winter et al, 1987), then the contribution to 2.161 as $t \to +\infty$,

R→ ∞, is effectively b independent and the infinite part of the integral can be neglected. The electronic phase shifts for a coulomb trajectory are therefore

$$-(\frac{\mu}{2E_{cm}})^{\frac{1}{2}}(Z_A+Z_B)ln\{2(R_f^2-\frac{R_f}{E_{cm}}-b^2)^{\frac{1}{2}}+2R_f-\frac{\alpha}{E_{cm}}\} \tag{2.162}$$

In the straight line approximation, the substitutions

$Z = vt$; $R^2 = b^2 + Z^2$, are used in 2.158, which becomes

$$\frac{1}{v}\int_{z_f}^{o}(Z_A+Z_B)\frac{1}{(Z^2+b^2)^{\frac{1}{2}}}dZ$$

$$=\frac{1}{v}(Z_A+Z_B)ln\{\mid Z\mid+(b^2+Z_f^2)^{\frac{1}{2}}\} \tag{2.163}$$

Once more neglecting the phase as $Z \rightarrow \infty$ the b dependent part of 2.163 is

$$\frac{-1}{v}(Z_A+Z_B)ln\{\mid Z_f\mid^2+(b^2+Z_f^2)^{\frac{1}{2}}\} \tag{2.164}$$

$$=\frac{-1}{v}(Z_A+Z_B)ln\{Z_f(1+(1+\frac{b^2}{Z_f^2})^{\frac{1}{2}})\} \tag{2.165}$$

$$=\frac{-1}{v}(Z_A+Z_B)\{lnZ_f+ln(1+(1+\frac{b^2}{Z_f^2})^{\frac{1}{2}})\} \tag{2.166}$$

Z_f is the maximum Z value corresponding to t_f. The $\ln Z_f$ term in 2.166 is also neglected, and for straightline paths, the electronic phase is

$$\frac{-1}{v}(Z_A+Z_B)ln\{1+(1+\frac{b^2}{Z_f^2})^{\frac{1}{2}}\} \tag{2.167}$$

2.5.2 Internuclear Phase Shifts

The internuclear phase was defined in 2.33 as the classical action along the trajectory. When slightly rearranged, the expression is that below :

$$S(R)=\int_{-\infty}^{\infty}(2\mu E_{cm})^{\frac{1}{2}}(1-\frac{W(R)}{E_{cm}})^{\frac{1}{2}})ds \tag{2.168}$$

The classical action to be expected if the internuclear potential were zero, would be

$$S_o(R)=\int_{-\infty}^{\infty}(2\mu E_{cm})^{\frac{1}{2}}ds' \tag{2.169}$$

A method similar to that used by Nikitin and Umanskii (1984) has been employed to express the effect of the potential on the nuclear motion in terms of the phase shift Δ S.

$$\Delta S = S(R) - S_o(R)$$

$$\Delta S = \int_{-\infty}^{\infty} (2\mu E_{cm})^{\frac{1}{2}} (1 - \frac{W(R)}{E_{cm}})^{\frac{1}{2}} ds - \int_{-\infty}^{\infty} (2\mu E_{cm})^{\frac{1}{2}} ds' \qquad (2.170)$$

S(R) is changed to an integral with respect to R by using

$$ds = \frac{(1 - W(R)/E_{cm})^{\frac{1}{2}}}{(1 - \frac{W(R)}{E_{cm}} - \frac{b^2}{R^2})^{\frac{1}{2}}} dR \qquad (2.171)$$

so that S(R) becomes

$$2\int_{R_o}^{\infty} \frac{(2\mu E_{cm})^2 (1 - \frac{W(R)}{E_{cm}})^{\frac{1}{2}}}{(1 - \frac{W(R)}{E_{cm}} - \frac{b^2}{R^2})^{\frac{1}{2}}} dR$$

$$= 2\int_{R_o}^{\infty} (2\mu E_{cm})^{\frac{1}{2}} [(1 - \frac{W(R)}{E_{cm}} - \frac{b^2}{R^2})^{\frac{1}{2}} + \frac{b^2}{R^2 (1 - \frac{W(R)}{E_{cm}} - \frac{b^2}{R^2})^{\frac{1}{2}}}] dR \qquad (2.172)$$

Using $\frac{d\delta}{dR}$ from 2.10, S(R) becomes in terms of radial and angular integrals:-

$$2\int_{R_o}^{\infty} (2\mu E_{cm})^{\frac{1}{2}} (1 - \frac{W(R)}{E_{cm}} - \frac{b^2}{R^2})^{\frac{1}{2}} dR + 2\int_{\theta_{R_o}}^{\theta_\infty} (2\mu E_{cm})^{\frac{1}{2}} b d\delta \qquad (2.173)$$

Similarly

$$S_o(R) = 2\int_{R_o'}^{\infty} (2\mu E_{cm})^{\frac{1}{2}} (1 - \frac{b^2}{R^2})^{\frac{1}{2}} dR + \int_o^{\pi} (2\mu E_{cm})^{\frac{1}{2}} b d\delta \qquad (2.174)$$

The radial part of Δ S is therefore

$$2\int_{R_o}^{\infty} (2\mu E_{cm})^{\frac{1}{2}} (1 - \frac{W(R)}{E_{cm}} - \frac{b^2}{R^2})^{\frac{1}{2}} dR - 2\int_{R_o}^{\infty} (2\mu E_{cm})^{\frac{1}{2}} (1 - \frac{b^2}{R^2})^{\frac{1}{2}} dR \qquad (2.175)$$

which is the same as the radial integrals obtained in 1.98 and 1.99. The angular terms, from 2.173 and 2.174, when integrated are

$$2(2\mu E_{cm}) b[\theta_\infty - \theta_{R_o}] + (2\mu E_{cm})^{\frac{1}{2}} b\pi \qquad (2.176)$$

$2[\theta_\infty - \theta_{R_o}]$ is the angle between the asymptotes of the trajectory. If equation 2.12 is used, the angular phase shift in terms of the classical deflection function is recovered. The full expression for ΔS is

$$2\delta_e^{JWKB} - (2\mu E_{cm})^{\frac{1}{2}} b\Theta \tag{2.177}$$

The phase shift is not necessarily limited to small angles, but as the work in this thesis has been limited to small angled scattering, where the inequality $\frac{W(R)}{E_{cm}} << 1$ is assumed to hold, a small angle approximation has been made to 2.170 where the expression $(1 - \frac{W(R)}{E_{cm}})^{\frac{1}{2}}$ is expanded to second order so that

$$\Delta S \simeq \int_{-\infty}^{\infty} (2\mu E_{cm})^{\frac{1}{2}} - \frac{1}{2}(2\mu E_{cm})^{\frac{1}{2}} \frac{W(R)}{E_{cm}} ds - \int_{-\infty}^{\infty} (2\mu E_{cm})^{\frac{1}{2}} ds' \tag{2.178}$$

For small angles, ds $\simeq$ ds' and the classical phase shift is approximately

$$\Delta S \approx -\frac{1}{2}\left(\frac{2\mu}{E_{cm}}\right)^{\frac{1}{2}} \int_{-\infty}^{\infty} W(R) ds \tag{2.179}$$

$$\simeq -\left(\frac{2\mu}{E_{cm}}\right)^{\frac{1}{2}} \int_{R_o}^{\infty} \frac{W(R)[1 - (W(R)/E_{cm})]^{\frac{1}{2}}}{\left(1 - \frac{W(R)}{E_{cm}} - \frac{b^2}{R^2}\right)^{\frac{1}{2}}} dR \tag{2.180}$$

which to first order is

$$\Delta s \simeq -(\frac{(2\mu)}{E_{cm}})^{\frac{1}{2}} \int_{R_o}^{\infty} \frac{W(R)}{\left(1 - \frac{W(R)}{E_{cm}} - \frac{b^2}{R^2}\right)^{\frac{1}{2}}} dR \tag{2.181}$$

When a coulomb potential is employed

$$\Delta S \simeq -\alpha \left(\frac{2\mu}{E_{cm}}\right)^{\frac{1}{2}} \int_{R_o}^{\infty} \frac{1}{R\left(1 - \frac{\alpha}{RE_{cm}} - \frac{b^2}{R^2}\right)^{\frac{1}{2}}} dR \tag{2.182}$$

$$\simeq -\left(\frac{2\mu}{E_{cm}}\right)^{\frac{1}{2}} \alpha \int_{R_o}^{\infty} \frac{1}{\left(R^2 - \frac{\alpha R}{E_{cm}} - \frac{b^2}{R^2}\right)^{\frac{1}{2}}} dR \tag{2.183}$$

where $\alpha = Z_A Z_B$.

Using standard integrals

$$\Delta \simeq -\left(\frac{2\mu}{E_{cm}}\right)^{\frac{1}{2}} \alpha [ln(2(R^2 - \frac{\alpha R}{E_{cm}} - b^2)^{\frac{1}{2}} + 2R - \frac{\alpha}{E_{cm}})]_{R_o}^{\infty} \tag{2.184}$$

Following the procedure adopted for the electronic phase shifts, the infinite phase is neglected. At R_o, the expression $R^2 - \frac{\alpha R}{E_{cm}} - b^2$ is zero and

$$\Delta S \simeq \left(\frac{2\mu}{E_{cm}}\right)^{\frac{1}{2}} \alpha ln(2R_o - \frac{\alpha}{E_{cm}}) \tag{2.185}$$

Using the fact that $R_o = \frac{\alpha}{2E_{cm}} + (\frac{\alpha^2}{4E_{cm}^2} + b^2)^{\frac{1}{2}}$ expression 2.185 can be further simplified to

$$\left(\frac{2\mu}{E_{cm}}\right)^{\frac{1}{2}} \alpha ln2 \left(\frac{\alpha^2}{4E_{cm}^2} + b^2\right)^{\frac{1}{2}}$$

and the internuclear phase shift for a coulomb trajectory is

$$\Delta S \simeq \left(\frac{2\mu}{E_{cm}}\right)^{\frac{1}{2}} \alpha \frac{1}{2} ln\left(\frac{\alpha^2}{4E_{cm}^2} + b^2\right) \tag{2.186}$$

where ln2 has been included in the infinate phase and neglected.

For the straight line model, ds = dz and $R^2 = b^2 + z^2$, and for a coulomb potential

$$\Delta S \approx -\left(\frac{2\mu}{E_{cm}}\right)^{\frac{1}{2}} \alpha \int_o^\infty \frac{1}{(z^2 + b^2)^{\frac{1}{2}}} dz \tag{2.187}$$

Integrating analytically, the internuclear phase shift in the straight line case is

$$\Delta S = \left(\frac{2\mu}{E_{cm}}\right)^{\frac{1}{2}} \alpha [ln(|Z| + (Z^2 + b^2)^{\frac{1}{2}}] \tag{2.188}$$

The b dependant phase, consisting of expression 2.188 evaluated at Z = O is

$$\Delta S \approx \alpha \left(\frac{2\mu}{E_{cm}}\right)^{\frac{1}{2}} lnb \tag{2.189}$$

(Piacentini and Salin 1977).

The combined phase shifts for electronic and nuclear motion, for a coulomb trajectory are therefore

$$\Delta = -\frac{1}{2}\left(\frac{2\mu}{E_{cm}}\right)^{\frac{1}{2}} (Z_A + Z_B)[ln\{2(R_f^2 - \frac{\alpha R_f}{E_{cm}} - b^2)^{\frac{1}{2}} + 2R_f - \frac{\alpha}{E_{cm}}\}] + \frac{1}{2}\left(\frac{2\mu}{E_{cm}}\right)^{\frac{1}{2}} \alpha ln(\frac{\alpha^2}{4E_{cm}^2} + b^2] \tag{2.190}$$

and for rectilinear paths, using $v = \left(\frac{2E_{cm}}{\mu}\right)^{\frac{1}{2}}$ the phase shifts are

$$\Delta = -\left(\frac{\mu}{2E_{cm}}\right)^{\frac{1}{2}} (Z_A + Z_B)]ln^{\frac{1}{2}}[1 + (1 + \frac{b^2}{Z_f^2})^{\frac{1}{2}}] + \left(\frac{2\mu}{E_{cm}}\right)^{\frac{1}{2}} \alpha lnb \tag{2.191}$$

Expression 2.155 is then evaluated with the above phases using the method described in Chapter three.

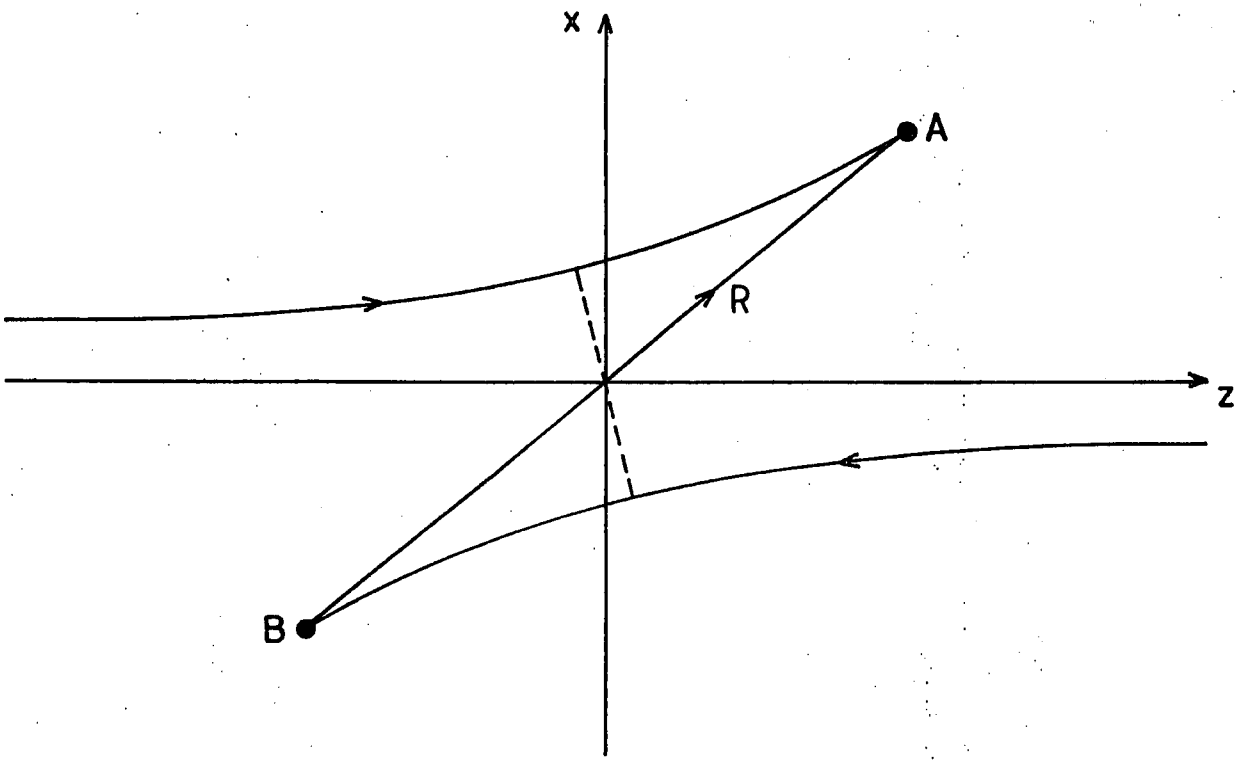

Fig. 2.1. The Classical Motion of Two Charged Particles in the Laboratory Frame.

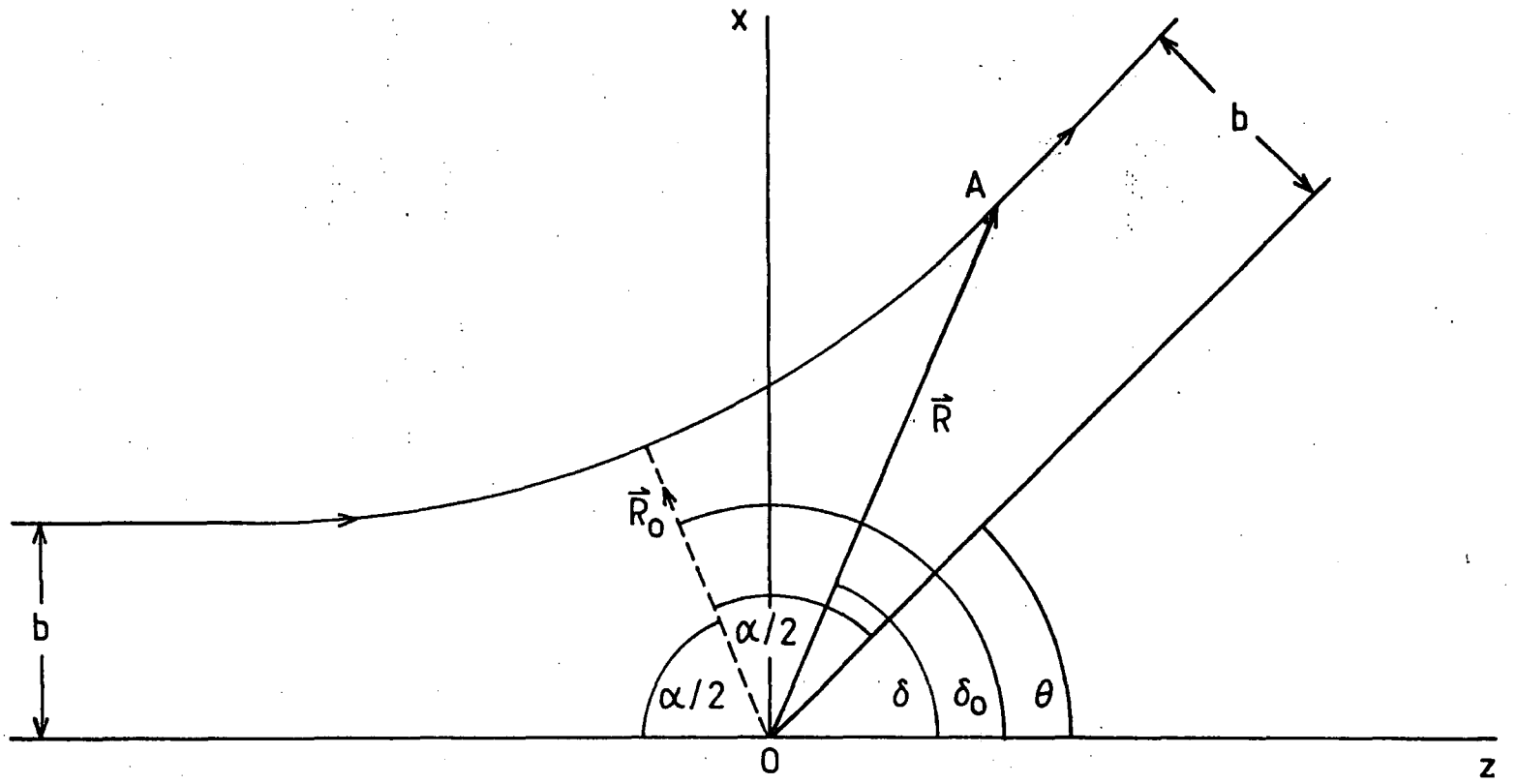

Figure 2.2 Classical Centre of Mass Motion.

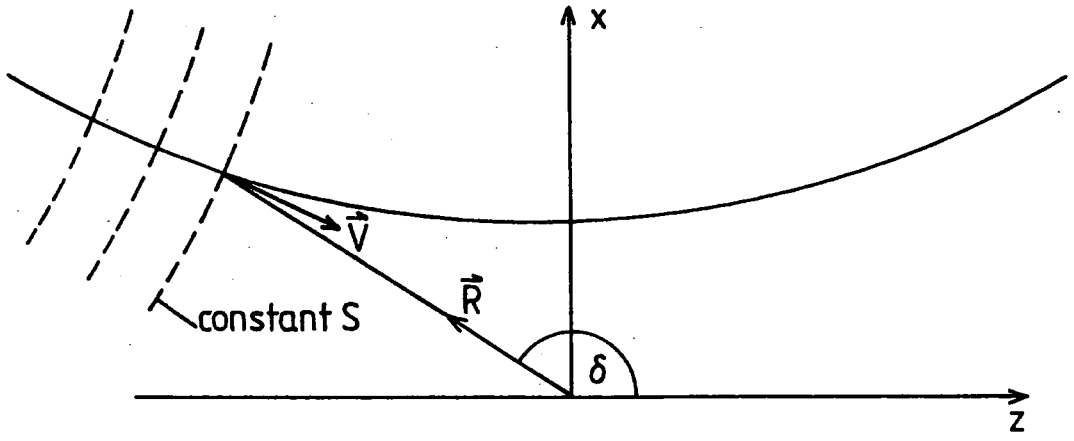

Figure 2.3 The Classical Action along the Trajectory.

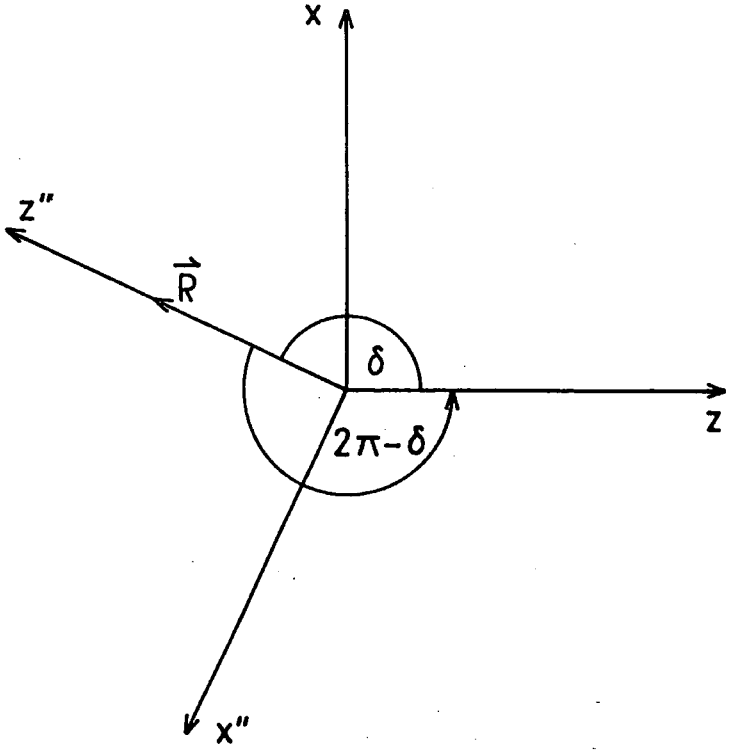

Figure 2.4 The Relationship of the Body-Fixed to the Space-Fixed Frame of Reference.

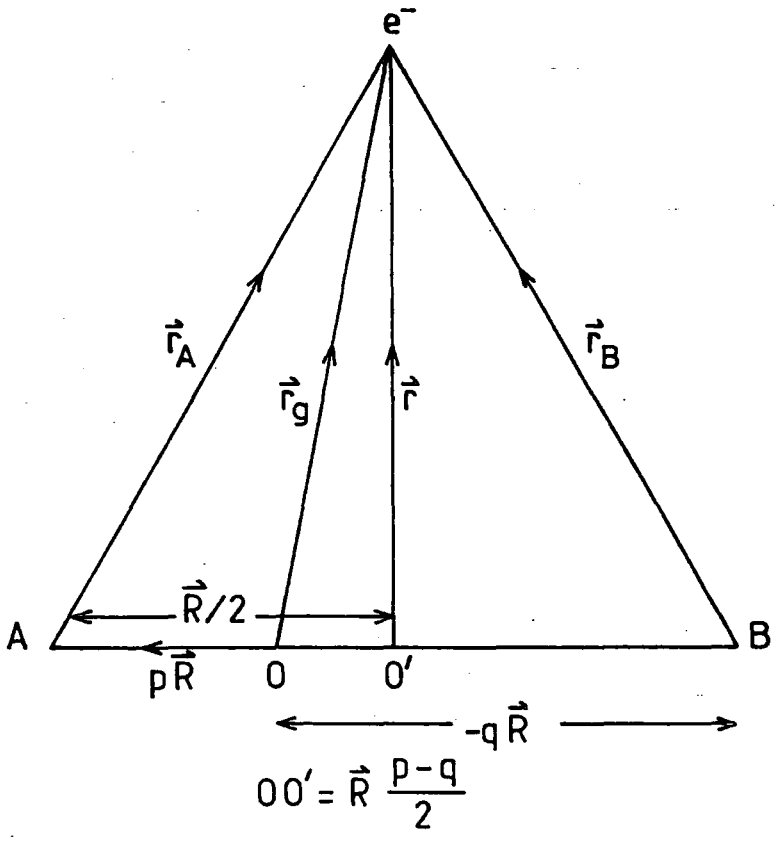

Figure 2.5 The Co-ordinate System in the Body-Fixed Frame of Reference.

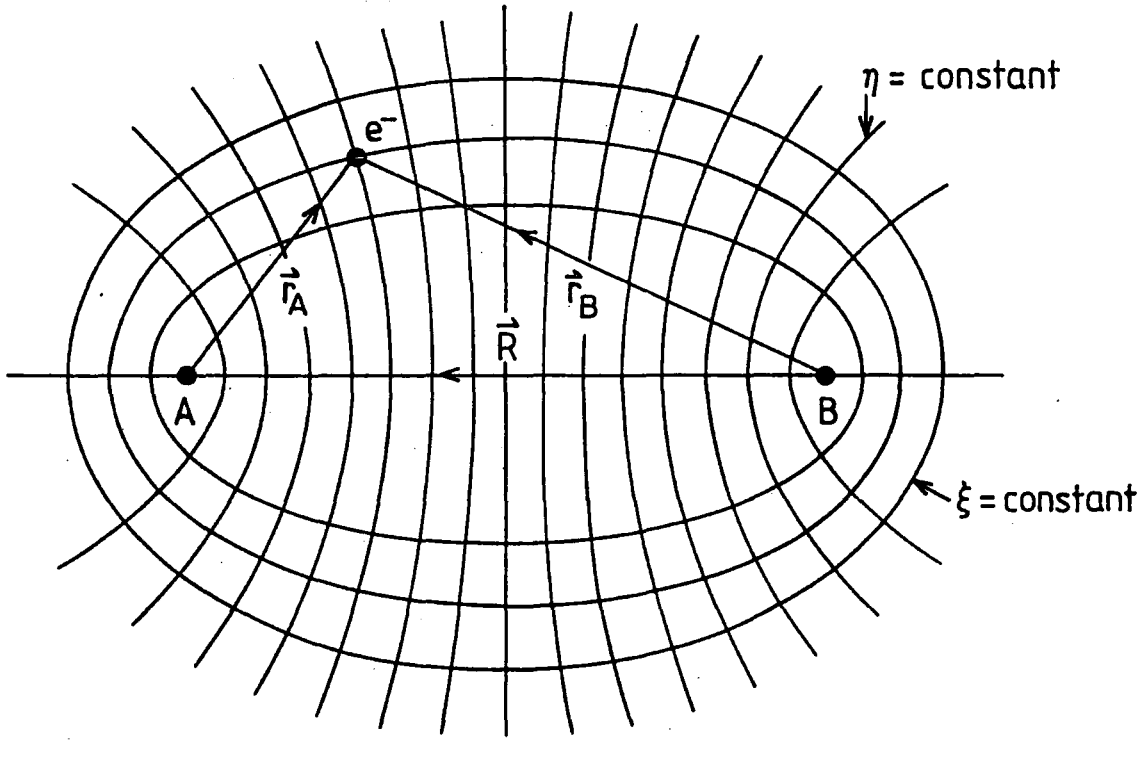

Figure 2.6 Prolate Spheroidal Co-ordinates.

Chapter 3

Computation

The computation for the present work was carried out on three machines:-

(a) The Amdahl 5860 main frame computer on Newcastle MTS.

(b) The Amdahl 5860 main frame computer on Durham MTS.

(c) The NAS IBM main frame computer at Daresbury Laboratory.

The programs used were written in FORTRAN77 and double precision was used throughout. The results obtained from the two MTS machines were identical. Those obtained using the NAS agreed with the Amdahl machines to within 0.1^{-10}.

Total and differential cross sections, obtained using the methods of Chapter 2, were both calculated from the same probability amplitudes. The computation of these are described in Sections 3.1 and 3.2. Section 3.3 will be concerned with the cross-sections themselves.

3.1 Probability Amplitudes

For each impact energy selected, matrix elements and probability amplitudes were calculated at given values of the impact parameter b. The total cross sections were obtained by integration of the probability amplitudes over the range of b values, using Gaussian quadrature. For this reason the impact parameters were taken to be those from the three point Gauss Legendre rule

$$b_i = (B - A)X_i/2 + (B + A)/2. \; i = 1, 2, 3 \tag{3.1}$$

where X_i is the abscissa and A,B are the lower and upper limits of each interval. The number and size of the intervals were decided by the number of impact parameters needed.

The probability amplitudes for each impact parameter were found by running three programmes sequentially in the same job batch. This meant that information could be passed from one program to the next, using temporary files. For example, the matrix elements, calculated in the second of the programs and transferred to the third, were not as a routine permanently stored. Large amounts of permanent

storage space were therefore not required. The use of direct access files ensured that the probability amplitudes for each impact parameter were stored in the correct position for retrieval by the cross-section routines. This was in ascending order of b, irrespective of the order in which the impact parameters were used. The programs are described below.

3.2 Trajectories

In order to provide input for the matrix element program, parameters for the centre of mass motion were calculated first. This had the advantage that the matrix element code was independent of the trajectory and a common program could be used to calculate matrix elements for either straight line, coulomb or other trajectories. Two trajectory programs were written in the course of the work. For a coulomb trajectory, the integrals occurring in Section 2.1 were treated analytically. This program was also used for straight line paths, by setting the internuclear potential to zero. For the non-coulombic potentials, employed in the treatment of μ^+ and H collisions in Chapter six, analytic solutions of the trajectory equations were not possible and numerical integration was carried out.

3.2.1 Data input to the Trajectory Programs

The input to the program consisted of the complete array of impact parameters to be used in the calculation. A further file provided information on nuclear charges, atomic masses and impact energy of the projectile. The index of the impact parameter to be used and the number of values of R, at which the trajectory parameters were to be calculated, were also supplied. After input of the data, the distance of closest approach was found. In the straight line case this corresponded to the impact parameter b. For a coulomb trajectory, R was found using the positive root of

$$R^2 - \frac{W(R)}{E_{cm}} R - b^2 = 0 \qquad (3.2)$$

When the form of the internuclear potential precluded an analytic solution of 3.2 the NAG routine C05ADF was used to find the root. This procedure employed a combination of linear interpolation, extrapolation and bisection to locate the zero of a continuous function within a given interval [A,B]. The error tolerance was set to $0.1*10^{-7}$. To check that a correct root had been found, the value given by C05ADF was replaced in expression 3.2 to see if the function was zero at that point. In general, the positive root of 3.2 occurred within the interval [b - 0.3, b + 2.0]a.u. However, at very low energies, it was sometimes necessary to adjust A to a smaller value, when using a potential with an attractive component.

The grid of R values was selected within the range $R_o < R < R_f$ by incrementing the value of R by dR. Generally any curvature of the trajectory is at a maximum at values of R close to R_o. It is therefore important to have sufficient

numbers of R values close to the turning point, in order to define the internuclear motion precisely. The largest value of R was the same for all the impact parameters and energies used. This allowed a comparison of all asymptotic values including time and velocity components. Using the analytic program, the values of the integrals 2.23 and 2.26 for the angle and time respectively, were calculated at each value of R. The arguments of the exponential factors 1.

$$exp\left(i\int_{t_o}^{t}\frac{(q-p)}{2}RA_{z'}dt\right) \tag{3.3}$$

were also integrated in the trajectory program at every value of R. These were passed to the matrix element program for later multiplication with the integrals forming the matrix elements.

When a non-coulomb potential was assumed, as in the μ^+ - H collisions in Chapter six, the integrals were evaluated using Subroutine DE written by Shampine and Gordon (1970). This uses an Adams' method, variable step, variable length integration. As input, DE requires the lower limit of the integration. If the exact turning point is given to the subroutine, it returns an error , as 2.9 and 2.10 are undefined at R_o. This difficulty was overcome by adding $0.1*10^{-12}$ to the value of R_o and supplying this as the lower limit of the integral. The accuracy of the integration was checked by running the program for a coulomb trajectory and comparing the numerical results with the exact analytic values. The accuracy was found to be greater than $0.1*10^{-6}$.

The trajectory parameters calculated at each value of R for use in the matrix element program included time, velocities in the body fixed x and z directions and acceleration in the body fixed z direction. The angle which the internuclear vector made with the space fixed z direction was also required for the rotation of the matrix elements from the body fixed to the space fixed frame. The trajectory information was then read to a machine code file for use in the matrix element program. The CPU time used in running the analytic program was approximately 7 seconds. The numerical program used about 16 seconds of CPU time.

3.3 Computation of the Integrals Comprising the Matrix Elements

The Matrix element program was adapted from a code written and developed by Shingal (1985) for use with straight line trajectories. The program has six main parts:-

(i) Input of atomic data and determination of the Slater orbitals to be used for the wave functions. Data was input to the main program by means of two data files. The first of these contained the trajectory parameters for the range of R values calculated in the previous program. These were for negative times. The second file supplied data relating to the orbitals used in the wavefunctions. For a Slater orbital of the form

$$C_i r_{B_i}^n exp(\alpha_i r_{B_i}) \tag{3.4}$$

The parameters C_i, α_i and the eigenenergies ϵ_n were pre-determined by diagonalisation of the atomic Hamiltonian. These numerical values were input by means of the data file. This second data file also contained information about the number of states to be included in the calculation, together with the number of integrals, the number of Gaussian integration points, the shell structure of any core electrons and the form of any model or effective potential. Parameters for the direct access files were also supplied. In the following section, ion A is referred to as the projectile, and atom B as the target.

Normalisation factors for associated Legendre functions for target-target, projectile-projectile and target-projectile combinations of l and m were calculated in Subroutine AFACT. These were placed into arrays, for later use in the integration routine ENTGIN.

The main program contained a DO loop, over the 120 R values. In the original straight line program, the index of the DO loop selected the z value to be used. The value of R and the body fixed velocity components were then calculated from the straight line expressions. In the curved trajectory version of the program, the index of the DO loop selected the appropriate R and R dependent values from the trajectory data. Subroutine ENTGIN was then called.

3.3.1 Body Fixed Integration of the Matrix Elements in Subroutine Entgin

Integration of the body fixed integrals was carried out by means of Gaussian integration. For η where -1 < η < -1 Gauss Legendre quadrature points were used, and for X_i where 1 < ξ < ∞ Gauss Laguerre points were used. As the lower limit of the integration is 1 not 0 for the Gauss Laguerre integration, a transformation was made, so that for the Gauss Laguerre point XL(I) with weight WL(I)

$$\xi = \frac{1}{XMAX}[\frac{2}{R}RMAX - 1]XL(I) + 1 \tag{3.5}$$

$$W_g = \frac{1}{XMAX}[\frac{2}{R}RMAX - 1]WL(I) \tag{3.6}$$

where XMAX is the largest Gauss Laguerre node and RMAX is 1 a.u. larger than the largest R value included in the integration. The number of quadrature points was preselected, being any of 4,8,16,32,64 for the Gauss Legendre integration and 12,18,24,30,64 for the Gauss Laguerre integration. The present calculations were carried out using 32 Gauss Legendre and 30 Gauss Laguerre points. These were read from the block data included in the program and placed into arrays for use in the integration subroutine.

A double DO loop, over the integration range, was executed in ENTGIN. The values of the radial functions were first found in terms of the spheroidal coordinates as described in Chapter 2.

The Bessel functions $J_{(M_A \pm M_B)}(\lambda)$ in expression 2.145 were computed using subroutine AJNU (Coleman,1980). This calculated the regular Bessel function $J_n(x)$ for real non-negative argument x. n was restricted to the range $0 \leq n \leq 10$. In this subroutine, the Bessel functions were constructed from their expansions in terms of Chebyshev polynomials. TSUMP was called which evaluated an m term Chebychev series by the recurrence method of Clenshaw (Clenshaw and Curtis, 1960). The accuracy of $J_n(x)$ depended on the number of terms included in the Chebychev series. In the present calculations 40 terms were used, giving an accuracy of $\approx 1.0*10^{-15}$.

To calculate the associated Legendre functions for all the values of l and m needed for both target and projectile, $\cos\theta_A$ and $\cos\theta_B$ were expressed in terms of η and ξ as described in 2.136. Subroutine PLM then calculated $P_\ell(\cos\theta_A)$ and $P_\ell(\cos\theta_B)$ according to the definition given in Rose (1957).

Once all the above functions have been constructed for a particular R value, the radial parts of the integrands were combined, together with the appropriate Bessel functions, the Legendre polynomials and the normalisation factors from AFACT. Direct and exchange integrals for each combination of states were formed.

To enable a curved trajectory to be used, certain modifications were necessary within ENTGIN. Changes were made to the input routines so that the trajectory data could be read and used by the program. The construction of the extra integrands containing the acceleration terms was also necessary. The contributions these extra integrals made to a particular matrix element varied with both the size of the internuclear vector and the centre of mass energy. Generally, the moduli of the acceleration integrals were some orders of magnitude smaller than the matrix elements themselves. Table 3.1 below shows some typical values of the moduli of the acceleration integrals compared with the relevant matrix elements. These are from Be^{++} - H collisions, at a centre of mass energy of 0.266 keV. The impact parameter was 0.03 a.u.

The program has a complex system of indexing each integral in a one dimensional array, for assembly into the separate matrix elements after rotation. It was therefore necessary to index the new integrals in the correct order and extend the array for this purpose. After the numerical integration over the range of the spheroidal coordinates, the final complex integrals were placed into array SBF in separate real and imaginary parts, for rotation into the space fixed frame.

3.3.2 Rotation of the Integrals into the Space Fixed Frame

Subroutine ROTMAT constructed the reduced rotation matrices $d^l_{m'm}$ from the definition in Rose (1961), and the body fixed integrals were then rotated into the space fixed frame using these. The angular rotation was through 2π - δ where δ has been defined in 2.21. The space fixed integrals were placed in array SMSF, still in the form of separate imaginary and real parts, and returned to the main program.

3.3.3 Combination of the Space Fixed integrals into Matrix Elements

The combination of integrals to form the matrix elements S, $\overline{S}$, H, $\overline{H}$, K and $\overline{K}$ took place in Subroutine MATR. The direct matrix elements H and $\overline{H}$ and the target-projectile matrix elements S and K were constructed from the appropriate integrals and then the elements $\overline{S}$ and $\overline{K}$ were obtained from the conjugates of the former by using 2.149 and 2.150. During this procedure, the matrix elements were also multiplied by the time-dependent exponential factors 3.3. These were changed to sine and cosine terms to represent the real and imaginary parts of the exponential function. TDEX was state-independent and also varied slowly with respect to time. Therefore, the integration of 3.3 was carried out in the trajectory program instead of during the integration of the coupled equations. The variation of sin(TDEX) and cos(TDEX) with R(t) is shown in Figure 3.1. Figure 3.2 shows the real and imaginary parts of the matrix elements H_{11} and K_{11} calculated at each value of R. Both the figures are from Be^{++} and H collisions at a centre of mass energy of 0.355 keV and an impact parameter of 0.06 a.u. The range of the exchange matrix elements did not extend beyond 30 a.u., but H_{11} is significant at much larger values of the internuclear vector, and is still non-zero at R = 100 a.u.

Determination of the time reversed matrix elements took place in Subroutine DERIVA by using the relationships 2.154 discussed in Chapter two. In this subroutine the NAG routine F04ADF was called to invert the matrix N and find the elements of $N^{-1}M$. This routine uses Crout's Factorization method to find the approximate solution to a set of complex linear equations. These were then read, together with the separate elements of N to direct access files for use in the third program which determined the probability amplitudes.

3.3.4 Integration of the Time-Dependent Coupled Equations

The program used to integrate the coupled equations was developed by Shingal (1985) for straight line trajectories. This included subroutines already written by Noble and others as part of a cross section program. Bransden and Noble(1981) and Bransden et al (1983) used this in atomic orbital calculations of He^{++} and H. The amended straight line version was subsequently used for obtaining probability

amplitudes by Shingal et al (1986) and Allan et al (1986) for charge transfer in H^+ - Na^o collisions.

The original form of the straight line program integrated the coupled equations with respect to z, where z = vt. For the curved trajectory calculations, the code was modified to read in the values of time corresponding to the range of R. The initial conditions for the $a_n(b,t)$ and $c_m(b,t)$ were set by calling subroutine START which assigned the value 1 to the initial channel at t = $-t_f$. The probability amplitudes for excitation and charge exchange were initially set to zero. The matrix elements were recovered from the direct access files and integration of the coupled equations with respect to time was performed by the multichannel DE. The matrix elements were interpolated in subroutine SLGINT, using four point Lagrange interpolation. The energy differences in

$$exp(i\int_o^t \varepsilon_n - \varepsilon_m dt) \tag{3.7}$$

were also calculated at each interpolated value of time and the exponential expression was integrated with the matrix elements. The smallest value of t at which the matrix elements were evaluated was not zero, as the time reversal subroutine in the matrix element program would have produced two values at t = 0. This would have resulted in failure of the interpolation routine and incorrect unitarities. The smallest t was therefore set at a time corresponding to R + dR. It was found that the unitarity of the probability amplitudes depended crucially on the value of dR. The optimum values of dR were found to be < 0.0005. The unitarity of the probability amplitudes was tested at intervals during the integration using Green's unitarity law

$$A^+NA = 1 \tag{3.8}$$

where A is the column of vectors $a_n(b,t)$, $c_m(b,t$ and N is from 2.151.

Convergence tests were carried out on the $c_n(b,t)$ with respect to the range and spacing of the R grid used in the calculation. The largest trajectory effects occurred at small values of R and it was necessary to have smaller intervals in the R grid close to Ro than at larger values of R. In straight line calculations performed by Shingal and collaborators (1986), the maximum value of Z had been set at 69 a.u. At the smallest impact parameter of 0.03 a.u., Z was approximately the same as R. in the present coulomb trajectory calculations, the range of R was increased, first to 90 a_o and then to 120 a_o to allow for the effect of possible long range interactions on the probability amplitudes. The changes produced in the values of all the $c_n(b,t)$ by increasing the R range from 90 to 120 a.u. were more than 2% in a 8 state He^{++} - H collisions. The n = 2 states were the most sensitive to the range.

The limits of time integration were set to be the same for all b values at a given energy. This will be discussed further in Chapter four with reference to $^4He^{++}$-$^4He^+$ collisions. The value of t_f was determined by running the trajectory code for the smallest impact parameter and setting the lower limit between the second

and third largest negative times. The upper limit was set at t_f. This ensured that the interpolation procedure was correctly implemented.

After integration, the final $a_n(b,t_f)$ and $c_m(b,t_f)$ were read to direct access files for use in the determination of total or differential cross-sections. For one impact parameter, the CPU time taken for solving the differential equations was 27 secs for a two state calculation. For each impact parameter, the total CPU time used to run the three programs sequentially was 100-200 seconds, depending on the number of states involved in the calculation.

3.3.5 Total Cross-sections

Total cross-sections were obtained from 1.105 by using Gauss Legendre integration. The impact parameters, corresponding to three point Gauss Legendre nodes, and the corresponding probability amplitudes were read into the program from random access files. The cross-sections for each final state were found by integration over the range of impact parameters.

A check was made on the total cross-sections by comparing results obtained using the NAG integration routine D01GAF. This procedure integrated over a range of supplied numerical values of the integrand using third order Finite Difference Formulae. Cross-sections, computed using the D01GAF routine, and those using Gauss Legendre integration agreed to within $0.1*10^{-5}$. Although the Gaussian integration method was the preferred method, it had the limitation that only probability amplitudes calculated from impact parameters selected using 3.1 could be integrated. However, when the integrand of 1.105 was very oscillatory , as in the symmetric resonance collision described in Chapter four, it was sometimes necessary to add probability amplitudes at intermediate values of the impact parameter. When this occurred, the NAG procedure could be used instead for the determination of total and state selected cross-sections.

3.3.6 Differential Cross-sections

Differential cross-sections were obtained using a double precision adaptation of subroutine EIKON (Piacentini and Salin, 1977). In the subroutine the straight line Eikonal differential cross-section obtained from 1.59 was transformed into a partial wave expansion. The expression was then summed using five point Lagrange interpolation of the impact parameters and the probability amplitudes. The Bessel function $J_n(kb\sin\frac{\theta}{2})$ was approximated by a polynomial expansion (Abramowitz and Stegun, 1964). If desired a small angle approximation

$$J_n((2l+1)sin\frac{\theta}{2}) \approx J_n(\ell sin\theta) \tag{3.9}$$

could be used.

In EIKON, the expression actually evaluated was not from 1.59 but

$$\frac{d\sigma}{d\Omega} = \mid ik \int_o^{b_{max}} bdbJ_n(\mu v b sin\frac{\theta}{2})(a_n(b) - a_n(b_{max})) \mid^2 \qquad (3.10)$$

where

$$a_n(b) = c_n(b)exp(i\chi\ell) \qquad (3.11)$$

and χ_ℓ contained the phase contribution 2.184. The term

$$(a_n(b) - a_n(b_{max})) \qquad (3.12)$$

depended on the nature of $a_n(b_{max})$. The probability amplitudes for charge exchange at b_{max} were effectively zero and 3.12 was just $c_n(b,t)exp(i\chi)$. This corresponded to the charge exchange expression 1.93 exactly. However, difficulties were experienced when the elastic differential cross-sections were calculated, due to the complex nature of the amplitudes. The real and imaginary parts were subtracted separately during the course of the integration, and the modulus was taken later. This meant that, although the modulus of a_n (b_{max}) was effectively 1, anomalous numerical effects could occur in the elastic differential cross-sections, if the amplitudes were still oscillating at large b. Small irregularities in the angular distributions could then result. Similar effects have been found by Allan (1988), and may be due to the neglect of the infinite phase. The importance of including b independent phases in the calculation of elastic differential cross sections has been pointed out by Winter et al (1987). The elastic cross-sections were therefore only used for comparisons with charge exchange angular distributions in a qualitative way. Figure 3.3 shows the variation with b of the modulus of the integrand in 3.10 for elastic scattering and charge exchange in $^4He^{++}$ and $^4He^{+}$. Further work on evaluating the elastic differential cross sections over a much larger range of b values would be valuable to establish the range of impact parameters necessary for elastic differential cross-sections.

The only modifications made to EIKON for the straight line cross sections, other than alterations to the input and output routines, were changes to the electronic phase expressions. In the original molecular form

$$\chi_e = \frac{-1}{v}[v_j(\infty) + v_i(\infty)] + 2Z_AZ_B\int_o^\infty \frac{1}{R}dz \qquad (3.13)$$

$$v_j(\infty) = v_j(\mid z_m \mid) - Z_j\int_o^\infty \frac{1}{R}dz \qquad (3.14)$$

$$v_j(\infty) = v_j(\mid z_m \mid) - Z_i\int_o^\infty \frac{1}{R}dz \qquad (3.15)$$

where $v_j(\mid z_m \mid)$ and $v_j(\mid z_m \mid)$ were terms representing the molecular nature of the electronic energies at z values less than z_m. For the atomic basis model, the expressions for $v_j(\mid zm \mid)$ and $v_i(\mid zm \mid)$ were set to zero and the straight line electronic phase was reduced to expression 2.166.

An additional subroutine was written for the curved trajectory cross-sections which calculated the curved trajectory phases 2.190 for each interpolated b in the integration. Differential cross-sections were found for each energy at 270 values of the centre of mass scattering angle θ , where $0^o < \theta < 13^O$. These cross-sections could be read to data files for plotting the angular distributions.

Using the methods described in Chapters two and three, total and partial cross sections have been calculated for three ion-atom or ion-ion systems. Differential cross-sections have also been calculated for the first two systems. The results of these are presented in Chapters four, five and six.

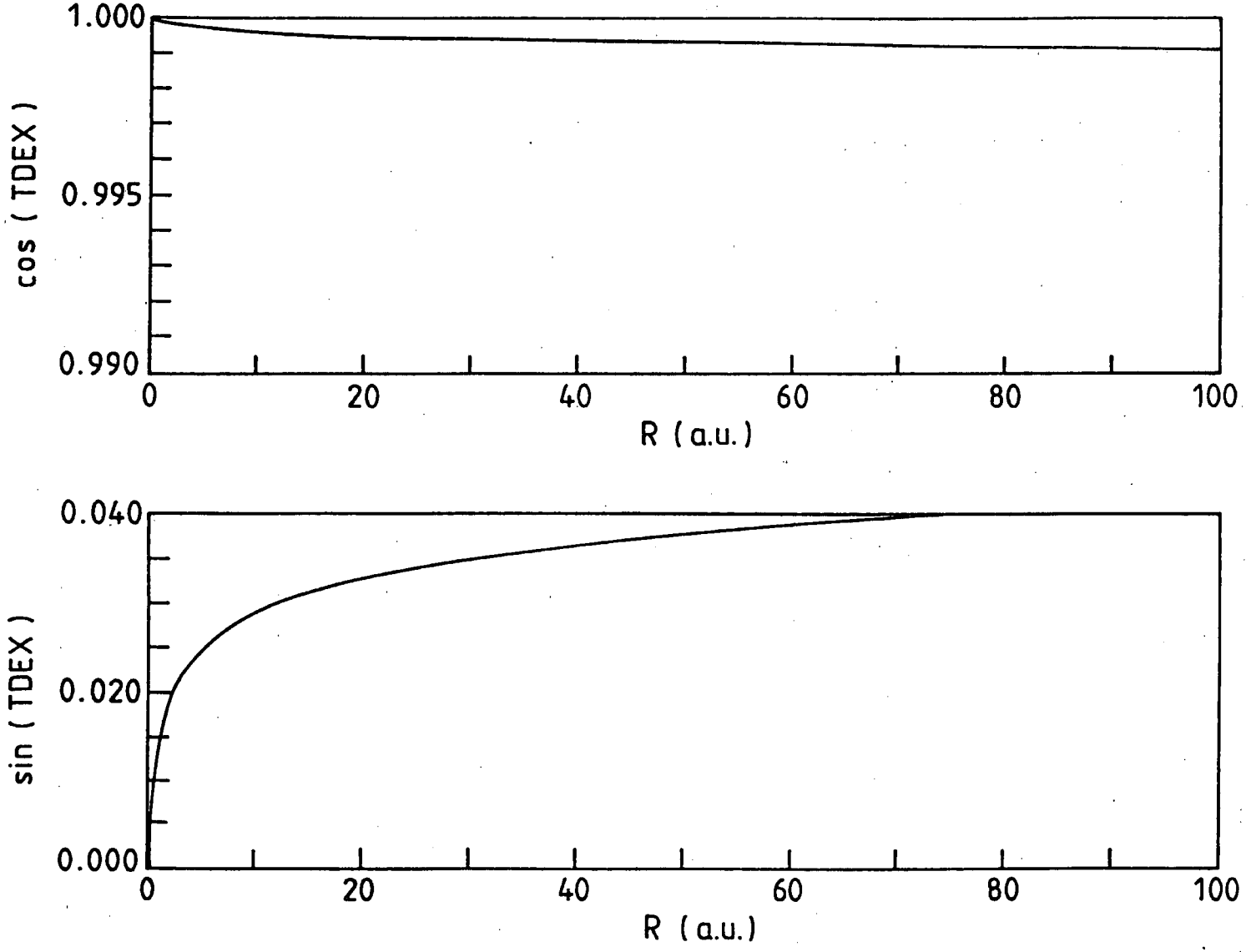

Figure 3.1 The Variation of sin(TDEX) and cos(TDEX) with R(t).

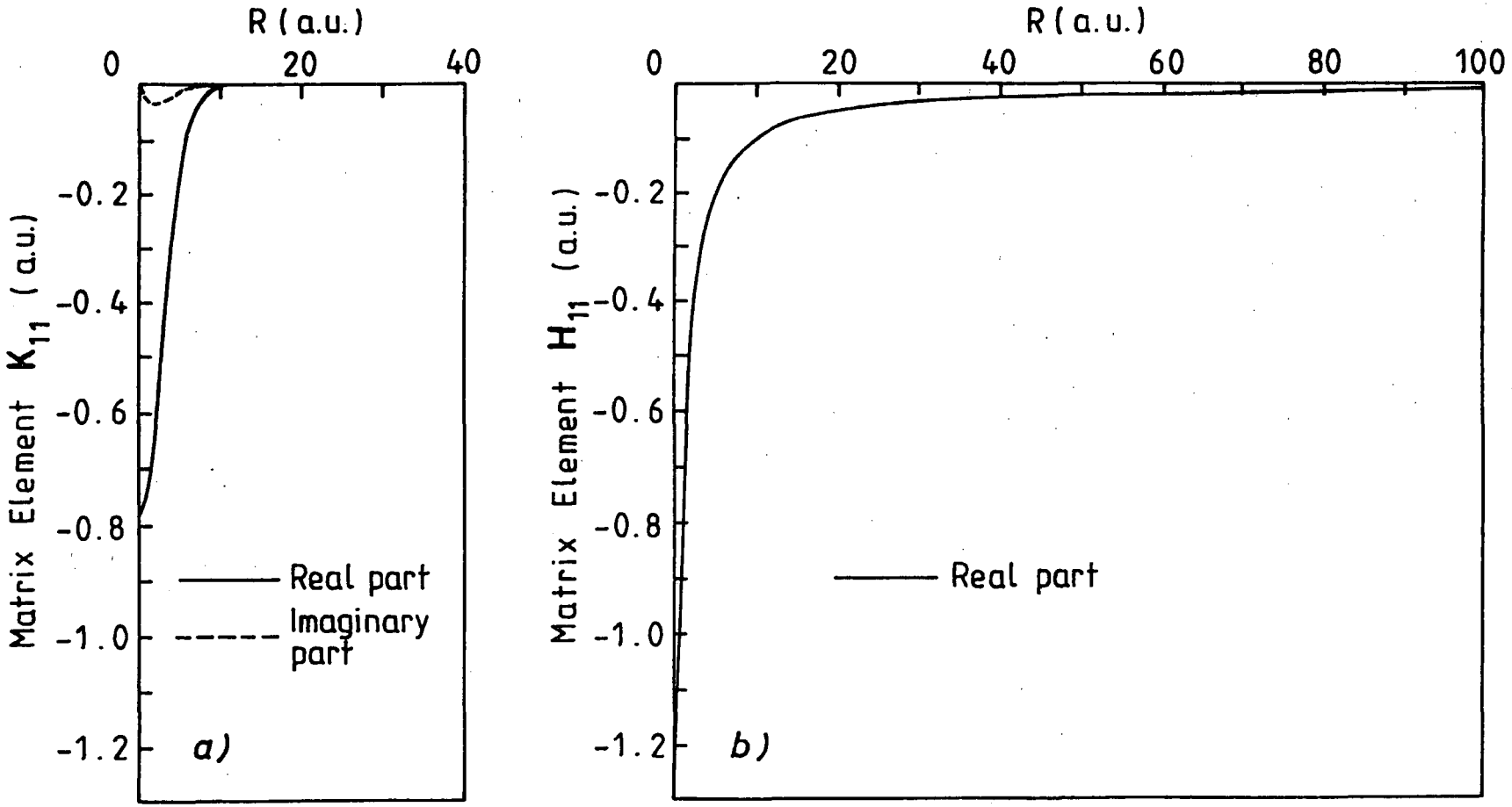

Figure 3.2 The Variation of the Matrix Elements H_{11} and K_{11} with R(t).

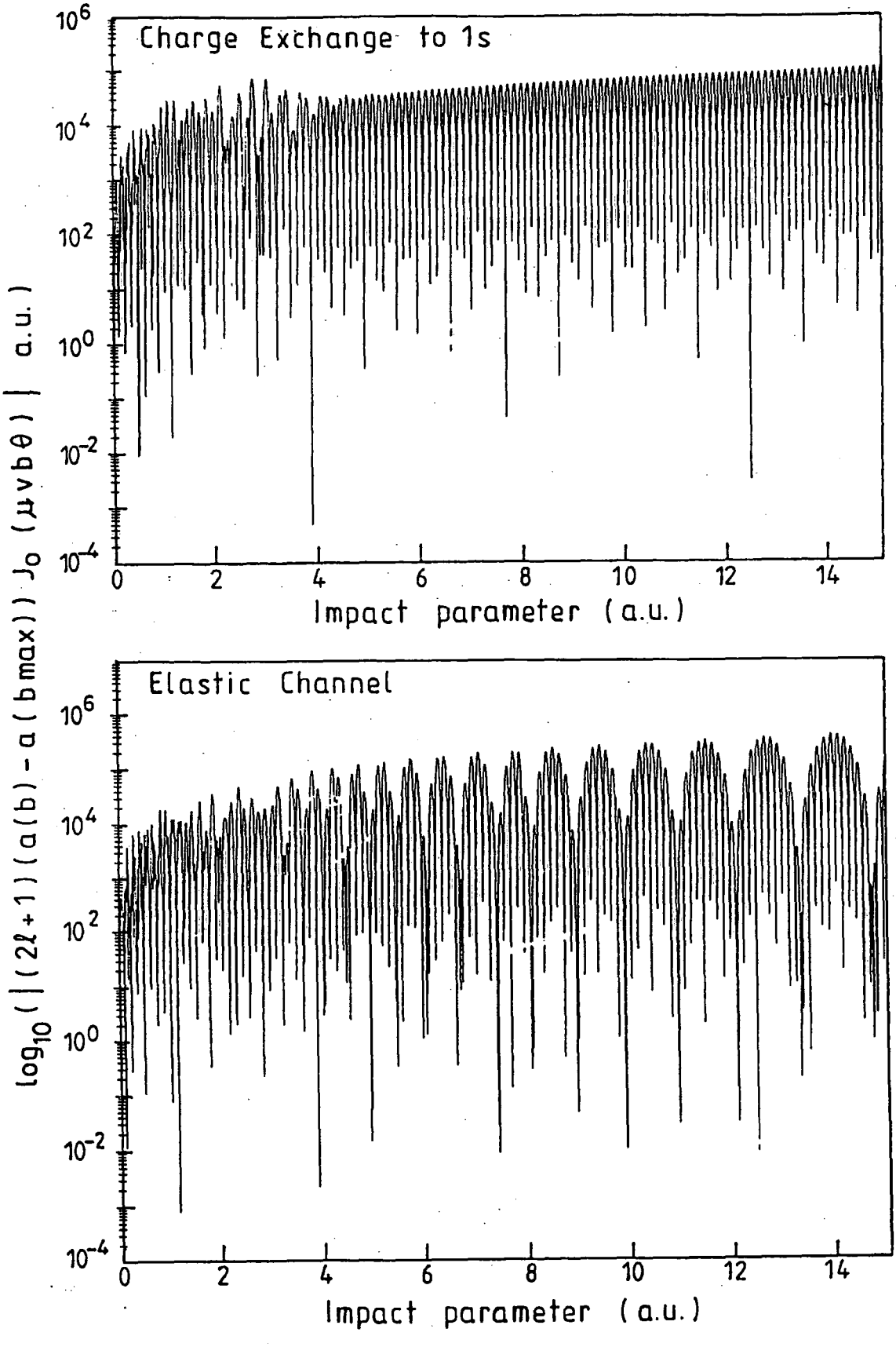

Figure 3.3 $^4He^{++}$ - $^4He^+$ Collisions. Comparison of Elastic and Charge Exchange Differential Cross Sections. The variation of $|(2l+1)(a(b,t) - a(b_{max}))J_0(\mu v b\theta)|^2$ with b.

R	Element K_{11} Matrix Element	Acceleration term of K_{11}	K_{11} Matrix Element
98.1	0.218^{10-12}	0.172^{10-15}	0.332^{10-11}
58.4	0.353^{10-7}	0.263^{10-10}	0.293^{10-6}
21.0	0.444^{10-4}	0.269^{10-7}	0.115^{10-3}
6.3	0.017	0.105^{10-5}	0.415^{10-2}

Table 3.1: Comparison of Acceleration terms with exchange matrix elements for Be^{++} and H collisions

Chapter 4

Charge exchange in $^4He^{++}$ and $^4He^{+}$ collisions : symmetric resonance

4.1 Symmetric Resonance

Charge exchange in symmetric resonance collisions is of particular interest when looking at the processes taking place in fusion plasmas and at collision processes in the interstellar medium. Because the electron in the ground state is captured by a nucleus of the same charge, charge exchange takes place resonantly to the ground state of that ion. He^{++} and He^{+} collisions are dominated by the coulomb repulsion between the two nuclei, and this precludes close approach of the ions. The probabilities for electron capture are reduced when coulomb repulsion is taken into account by using curved trajectories in the calculation. A comparison has therefore been made between results obtained using straight line and coulomb trajectories for low energy collisions between doubly and singly ionized helium ions. Total and differential cross-sections for the symmetric reaction

$$^4He^{++} + ^4He^{+}(1s) \rightarrow ^4He^{+}(1s) + ^4He^{++} \qquad (4.1)$$

have been calculated for a range of centre of mass energies from 0.075 keV to 2.5 keV.

4.2 Previous work

Previous work on this system has been carried out by several authors. Bates and Boyd (1962b) have used coulomb trajectories to carry out a two state PSS calculation for reaction 4.1 in which ETFs were not employed. The total charge exchange cross-sections were found to increase for decreasing relative energy until a maximum of 8.9 πa_o^2 (7.83 x 10^{-16} cms^2) in the cross section was reached at

a relative energy of 100 eV. Below this, the cross-sections decreased for decreasing energy. There was good agreement between these cross sections and those they obtained using 1.108 and 1.109. Results were also obtained by Ryufuku and Watanabe (1976) for reaction 1.8.5 with Z = 2. Their calculations showed that the cross-sections were affected by the internuclear potential, for Elab(keV) less than 0.1 Z^2 (Z-1), which for reaction 4.1 is 0.4 keV.

Experimentally it is easier to measure the isotopically distinct reaction

$$^3He^{++} + ^4He^+ \rightarrow ^3He^+ + ^4He^{++} \tag{4.2}$$

and Peart and Dolder (1979) have measured cross-sections for this reaction at centre of mass energies from 0.1 keV to 20.0 keV, using an intersecting beam apparatus. They experienced difficulties, due in part to the strong coulomb repulsion between the two isotopes. This caused deflection of some $^4He^{++}$ ions, which were then not detected. Dickinson and Hardie (1979), and Hardie (1981) calculated total charge exchange cross-sections, Q_T, using a 2 state PSS model without ETFs and confirmed that the theoretical results were higher than the experimental cross-sections, This discrepancy was 50% at the lowest energy, namely 106 eV, and 10% at 20 keV. They then performed a further calculation integrating the differential cross-sections for charge transfer, obtained using the Primitive Semi-Classical approximation, over the acceptance angle of the apparatus of Peart and Dolder.

The centre of mass differential cross-section is related to the laboratory differential cross-section by

$$\frac{d\sigma}{d\Omega} lab(\theta_L, \phi_L) = \frac{d\sigma}{d\Omega_{cm}}(\theta, \phi)\frac{d\Omega}{d\omega} \tag{4.3}$$

where θ_L, ϕ_L are the laboratory scattering angles and , θ, ϕ are the centre of mass angles. $d\Omega/d\omega$ is the centre of mass to laboratory transformation Jacobian. The expression for a merged beam apparatus, used by Dickinson and Hardy is from Morse and Bernstein (1962).

The results for the partial cross-sections (Q_p), agreed with the experimental results to within 18% for the whole energy range. From this they concluded that the large discrepancies in the measured cross-sections and the calculated Q_T were due to the angular acceptance of the apparatus.

Concurrently, Jognaux et al (1978) measured reaction 4.2 using a merged beam apparatus for centre of mass energies from 16 eV to 1700 eV. These measured total cross-sections were also found to be less than current theoretical results. Jognaux carried out his own semiclassical calculation over the acceptance angle of the apparatus and found the cross-sections were still significantly higher than the experimental values. Subsequently, Falcon (1983) used a quantal PSS model to compare with the results of the Jognaux experiment. The total cross-sections showed good agreement with the Q_T obtained by Dickinson and Hardie. The partial cross sections, again obtained by integration of $\frac{d\sigma}{d\Omega}$ over the acceptance angle of the apparatus, confirmed the discrepancy with the results of Jognaux et

al. They exceeded the measured values by a factor of two in the higher energy range, and although the differences were less at the lower energies, they were still significant. Falcon therefore suggested that the estimate of the acceptance angle given by Jognaux should be re-examined.

4.3 Results

The present calculations for reaction 4.1 were carried out using both straight line and curved trajectories for most energies considered. The curved paths were produced by a coulomb potential of the form

$$W(R) = \frac{Z_A Z_B}{R} \tag{4.4}$$

For reaction 4.1 the centre of mass of the two ions is at the midpoint of the internuclear vector and p = q = $\frac{1}{2}$ from 1.13. Matrix elements were computed using a grid of 240 R values for each impact parameter, and the maximum value of R was 120 a.u. to allow for the long range coulomb interaction.

4.4 Total Cross-Sections

Probability amplitudes for each energy were calculated for 78 impact parameters over the range 0.0 a.u. < b < 8.0 a.u. The energy range for the total cross sections (Q_T) was 0.075 keV < E_{cm} < 2.5 keV. Q_T was found by integration of expression 1.105. Figure 4.1 shows the variation of b | c(b,t) |^2 with b for curved and straight line trajectories. At 0.21 kev there are considerable differences due to the trajectory and the maximum value of the function occurs at smaller impact parameters in the coulomb trajectory calculation.At 2.5 keV the two curves are virtually indistinguishable to the accuracy of the plot. The b value for which the function was a maximum is shown below

	Impact Parameter (a.u.)	
E_{cm}(keV)	Straight Line Model	Coulomb Trajectory Model
0.21	3.23	3.00
0.50	2.97	2.89
2.50	2.41	2.41

As stated previously, the system is strongly resonant to 1s charge exchange because of the nuclear symmetry. A two state basis was thus felt to be adequate,

with n = 1, l = 0, on each centre. In order to assess the possible contributions from higher states to the 1s partial cross sections, a twenty state calculation was carried out with 1s, 2s, 2p , 2p , 3s, 3p ,3d ,3d , 3d on each atomic centre. For the twenty state basis, curved trajectories only were used, for three energies, 0.21, 0.5, and 2.5 keV.

Total cross-sections for two and twenty state calculations are shown in Table 4.1. Comparisons between straight line and coulomb trajectory results have been made for the former, for 0.21 keV $< E_{cm} <$ 2.5 keV. The curved path cross-sections are lower than the straight line for all these energies, the trajectory effect being much more marked at lower energies, as expected (Fritsch, 1982, van Hemert et al.1985). The difference is 11% at the lowest energy and 0.7% at the highest. These results also confirm that, for energies in excess of those considered here, the straight line approximation is satisfactory for the calculation of total cross-sections. Calculations at the lower energies 0.1 keV and 0.075 keV, carried out for curved trajectories only, confirm the existence of the maximum in the cross-section (Bates and Boyd, 1962b and Hardie, 1981). Increasing the basis set to twenty states resulted in increases in the total cross-sections of less than 3.3% for all three energies, almost all of which was due to increases in the 1s charge transfer cross sections, with other states contributing less than 0.004% to the total cross-sections.

The adequacy of using seventy eight impact parameters for the calculation of the total cross sections was tested by comparing with the cross-section obtained using 330 impact parameters at a centre of mass energy of 0.21 keV. The cross-sections obtained using 330 impact parameters were less than 0.15% higher than the 78 impact parameter results for both straight line and curved trajectory models. The comparison is shown below.

No. of Impact Parameters	Total Cross Sections (10^{-16} cms^2)	
78	7.843	6.640
330	7.854	6.943

It was not possible to compare the Bates and Boyd PSS results directly with the present work, due to lack of their numerical data. However, comparison was possible with their approximate expression 1.108. The present straight line total cross-sections were used in 1.108 and the approximate cross-sections were then compared with those obtained using curved trajectories. The cross-sections agreed to within 0.7% for all energies and are shown in Table 4.2. Approximate total cross sections using expression 1.109 were also calculated and these are compared with the present coulomb trajectory cross-sections in Table 4.4(3). These cross-sections are plotted in Figure 4.2 together with the results of Ryufuku and Watanabe (1976) for reaction 1.111 (Z=2). The approximate cross-sections obtained using

1.109 lie between the present straight line and curved trajectory cross-sections. The curved trajectory results are consistently lower than the approximate cross-sections, by 15% at 0.075 keV and 4.0% at 2.5 keV, and the straight line results are less than 4% above the approximate values at all energies. The fact that good agreement was achieved using 1.108, indicates that the estimate of the effect of the coulomb potential on the cross-sections is correct. Therefore it would seem that because expression 1.109 was derived from the two state PSS approximation, it is not a suitable approximation for results obtained using an atomic orbital basis.

The straight line results are 4.4% higher than those of Ryufuku and Watanabe at 75 eV. At the highest energy the two sets of results agree to within 0.8%. The curved trajectory results are consistently lower, the disagreement being about 13% at 0.1 keV and 3% at 0.75 keV. These discrepancies in the curved trajectory results are unlikely to be due to their neglect of the acceleration matrix elements, as these are very small in this calculation. All three curved trajectory results have a maximum in the total cross-section in the region of 100 eV.

The total cross-sections obtained by Hardie for the isotopic reaction 4.2 are compared with straight line and coulomb total cross-sections for reaction 4.1 in Figure 4.3. Because of the different reduced masses of the system, the results are again presented in terms of centre of mass energies. The straight line results lie above both sets of curved trajectory cross-sections. The present curved trajectory results are lower than the molecular model especially at the very lowest energies, where the disagreement at 0.1 keV is 10%. The three results are in closer agreement at 2.5 keV, where the lack of ETFs in the PSS model probably accounts for the fact that these cross-sections lie above both sets of the present results at this energy.

4.5 Differential Cross Sections

4.5.1 Full Semi-Classical Results

Differential cross-sections for reaction 4.1 have been calculated for three centre of mass energies, 0.21, 0.5 and 2.5 keV. Probability amplitudes for charge exchange were calculated at these three energies, using the methods described in Chapters two and three, for both straight line and coulomb trajectories. For the two state resonant charge exchange reaction, it has been shown, see Bransden (1983), that

$$| c_m(b,t) |^2 = sin^2 \int_{-\infty}^{\infty} M(t)dt \tag{4.5}$$

where

$$M = (1 - | S |^2)^{-1}(K - S\overline{H}) \tag{4.6}$$

and the values of the probabilities $| c_m(b,t)|^2$ oscillate between 0 and 1 with respect to b. In the PSS method employed by Dickinson and Hardie (1979), the probability amplitudes are represented by $\sin^2\xi$ (b), where ξ (b) is the difference between the

non-coulombic phase shifts from 1.102. This is caused by the potentials $V^{\pm}$ (R) corresponding to ungerade and gerade molecular states.

$$\xi(b) = k\int_{R+}^{R^-} F^+(R)dR + \frac{k}{E}\int_{R-}^{\infty} \frac{V^-(R) - V^+(R)}{F^+(R) + F^-(R)} \tag{4.7}$$

$$F^{\pm}(R) = \left(1 - \frac{V^{\pm}(R)}{E} - \frac{b^2}{R^2}\right);\ F^{\pm}(R^{\pm}) = 0 \tag{4.8}$$

These probabilities therefore oscillate in an analagous manner to the $|\ c_m(b,t)|^2$ in the present work.

Within the range of energies used for the total cross-sections, the number of oscillations occurring in the range of impact parameters was found to increase as the energy decreased. A maximum was reached at the energy which produced the largest total cross-section. At energies lower than this, the number of oscillations again decreased. The present cross-sections have been calculated at centre of mass energies above this maximum, and the number of oscillations found decreased with increasing energy.

In order to define the rapidly changing probability amplitudes with respect to b, large numbers of impact parameters were necessary. This is expensive in terms of computing time and is the reason why the investigation of the differential cross-sections was limited to three centre of mass energies. The number of impact parameters used for the calculations at 0 21 kev was 369,and 328 and 240 were used at 2.5 and 0.5 keV respectively. The maximum value of b was taken to be that at which the amplitudes for charge exchange were effectively zero, and beyond which the addition of further impact parameters made no significant difference to $d\sigma$ /de . This was found to range from b = 12 a.u. at 2.5 keV to b=14 a.u. at 0.21 keV. The $c_m(b,t)$ were found by integration of the coupled equations 2.3.8 and 2.3.9 from $-t_f$ to t_f. The importance of using the same value of t_f for all impact parameters at one energy has been stressed by Piacentini and Salin (1977) and by Winter et al (1987), to ensure consistent phase in the differential cross-sections. To verify this, two calculations were carried out at 0.21 keV. The first used the same value of t_f for all impact parameters. The second had limits which were the positive and negative times, corresponding to the largest value of R used to calculate the matrix elements, for each impact parameter. These values of t were therefore dependent on the distance of closest approach at each impact parameter. The angular distributions for the two calculations had the same shape and magnitudes of oscillation but the phases of the two distributions differed by a constant angle of 0.15^o.

Semiclassical differential cross-sections were calculated using 3.10. For the straight line approximation, 2.191 was used for the phase, and the curved trajectory phases were those from 2.190. Charge exchange differential cross-sections were first obtained using straight line probability amplitudes and straight line phases (SLTD) . The angular distributions obtained were then compared with those obtained using curved trajectory amplitudes and phases (CTD). To try to

assess the effect of the curved trajectory phase factors alone, differential cross-sections for charge exchange using curved trajectory amplitudes and straight line phases (CTSLTD) were calculated. This latter approximation has been employed by Winter et al (1987) in their calculation of differential cross-sections in alpha particle collisions with atomic hydrogen, on the grounds that this might be a satisfactory approximation for small angle scattering.The forward scattering in all the models is into the elastic channel, whereas for angles close to zero, the charge exchange cross-sections are negligible for angles close to zero. As theta increases, charge exchange processes become more important. The oscillatory behaviour, manifested by the probability amplitudes because of the symmetry, also occurs in the angular distributions. The elastic and charge exchange distributions shown in Figure 4.4 for a centre of mass energy of 2.5 kev are typically in anti-phase.

Figures 4.5 and 4.6 show angular distributions for the three sets of results at 0.21 and 2.5 keV. At 0.21 keV, the two curved trajectory distributions are displaced to larger angles as expected. There is a difference in angular phase of $\simeq 0.7^o$ between the SLTD and the CTSLTD first minima which is entirely due to the differences in the variation of $\mid c_m\ (b,t) \mid^2$ with b in the straight line and coulomb trajectory models. The phase difference between the SLTD and CTD angular distributions is less, 0.5^o , and so the effect of using the curved trajectory phase shifts is to displace the angular distributions to slightly smaller angles. At larger angles the SLTD and CTD models are in antiphase, due in part to the increased frequency of the oscillations in the distributions. At 2.5 keV, the differences between the CTD and the CTSLTD angular distributions are negligible at all $\theta < 13^o$. Between the SLTD and the CTD results, differences at the first minima are small. However, at the larger angles $7^o < \theta < 13^o$ the differences are more pronounced. This is due to the effect of the trajectory on the amplitudes obtained for small impact parameters.

4.5.2 Differential Cross Sections- First Order Approximation

Differential cross-sections were found to first order by using 1.114, where each $c_m(b,t)$ was calculated assuming a coulomb trajectory at impact parameter b, and the Rutherford cross-section was also obtained from 1.114. The classical relationship

$$b = \frac{Z_A Z_B}{2E_{cm}} cot\frac{\theta}{2} \tag{4.9}$$

was used to find theta for each impact parameter. The angular distributions for charge exchange and elastic scattering, found using the first order approximation, are shown for each energy in Figures 4.7 and 4.8 respectively. The elastic and charge exchange angular distributions are compared at a centre of mass energy of 2.5 keV in Figure 4.9. The positions of the first minima occurred at progressively smaller angles as the centre of mass energy increased, reflecting the greater trajectory effect at the lower energies. The comparison between elastic and charge

exchange distributions again shows the correct anti-phase relationship for a two state resonant system.

Figure 4.10 compares the charge exchange differential cross-sections obtained using the full semiclassical formulae with those using the first order approximation. The same curved trajectory probability amplitudes were used for both models. At 0.21 and 0.5 keV the first order distributions are displaced to much larger angles than the semiclassical model, reflecting the classical nature of the assumed relationship between b and θ , and there is only qualitative agreement between the two methods. At 2.5 keV, there is fairly good agreement between the two distributions especially for $5^o < \theta^o < 13^o$. This suggests that expression 4.114 may be a good approximation at higher collision energies than those in the present work (Winter et al, 1987).

The angular distributions calculated using 3.10 have been compared with those computed using the method of Hardie (1981), described in Chapter three, for reaction 4.1. The comparisons of CTD SLTD and PSS for all three energies are shown in Figures 4.11, 4.12 and 4.13. At all energies there are differences of angular phase, which are more pronounced at larger angles, resulting in $d\sigma/d\Omega$ being different by an order of magnitude or more at certain angles. The basic forms of the angular distributions are very similar. At 0.21 keV the PSS angular distribution is in closer agreement with the SLTD model than the CTD. From the present SLTD and CTSLTD results, differences in the behaviour of the probability amplitudes with respect to b, in the straight line and curved trajectory models, result in phase differences in the angular distributions. It seems likely that the different arguments of the sin functions in 4.5.1 and 4.5.3, produced respectively by the molecular model and the atomic basis impact parameter method, are the major contribution to the disparities between the differential cross-sections for a particular angle.

4.6 Integrated Partial cross-sections

As discussed in Section 4.2, the partial cross-sections Qp calculated by Dickinson and Hardie, to compare with experiment, were found by integrating the differential cross-sections over the acceptance angle of the apparatus. In view of the differences found between the PSS and the present work, it was decided to carry out a comparison of partial cross-sections, to establish whether the phase differences in the angular distributions were significant in the calculation of Qp (Forster et al, 1988).

It was possible to use the method of Dickinson and Hardie to integrate the present coulomb trajectory differential cross-sections, transformed to the laboratory frame, over the acceptance angle of the apparatus.

These were computed using the program originally written by them. For the present work, the differential cross-sections were obtained by calling EIKON at each value of the centre of mass angle . This was transformed to the laboratory frame and integrated over the laboratory angles θ_L and ϕ_L.

	Partial Cross-sections (10^{-16}cms^2)	
E_{cm}(keV)	Method of Dickinson and Hardie	Present Curved Trajectory
0.21	7.67	6.85
0.50	6.92	6.69
2.50	5.66	5.62

The integration over θ_L was performed by the NAG procedure D01AG using an automatic Clenshaw Curtis algorithm (Oliver, 1972). The NAG procedure D01ACF (Patterson, 1968) employing a modified Gaussian method carried out the integration over L. The overall numerical accuracy of the partial cross sections was estimated to be 2%.

The comparisons with the molecular method are shown above for $^4He^{++}$ and $^4He^+$.

When partial cross-sections are considered, it appears that the differences between the two methods are less significant. The ageement at 2.5 keV is very good (1%), and although the results at lower energies agree less well, the cross-sections are within 10% of the molecular values. These results confirm the earlier work of Dickinson and Hardie, and their conclusion that further experimental work with more precisely defined effective apertures would be of value.

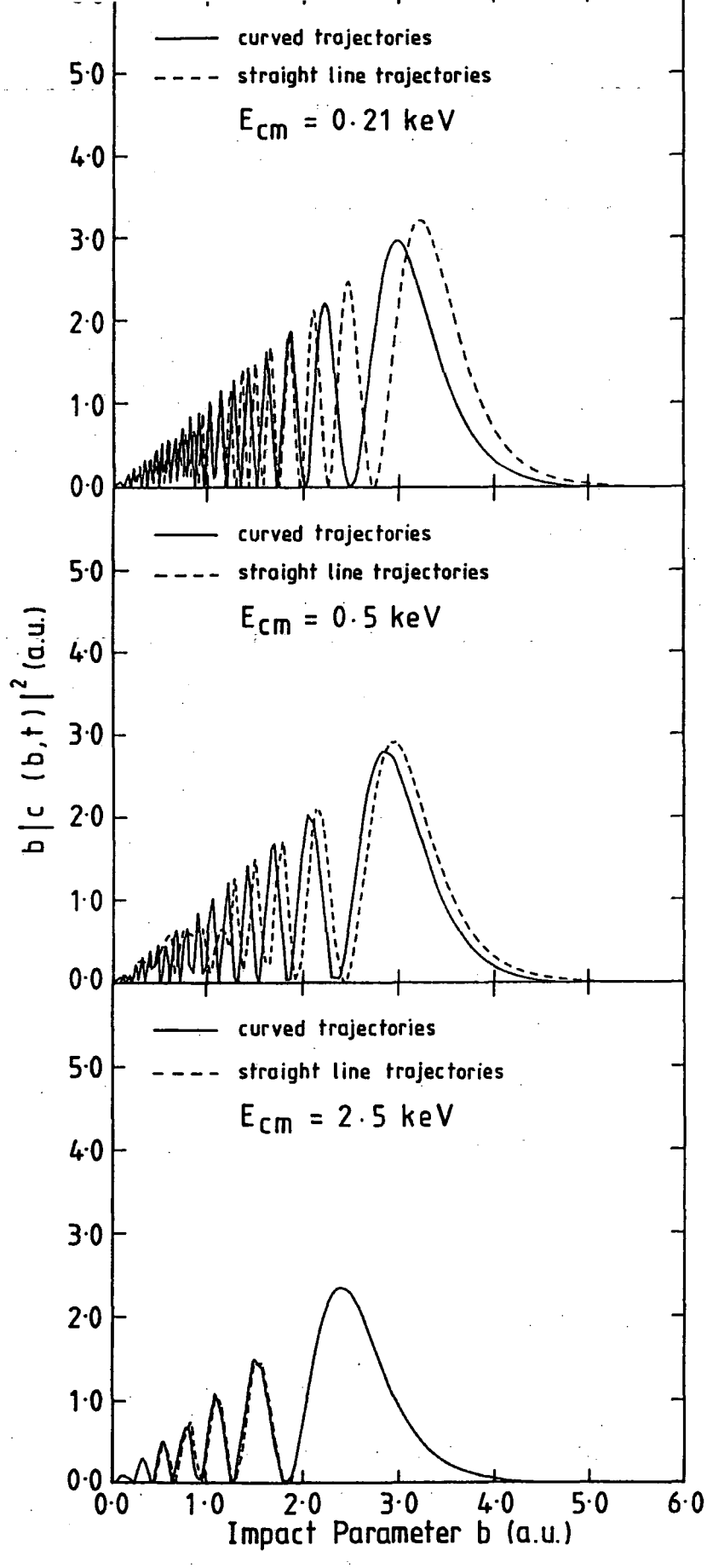

Figure 4.1 $^4He^{++}$ and $^4He^+$ Collisions: The Variation of b | c(b,t)|² with b for Straight Line and Coulomb Trajectories.

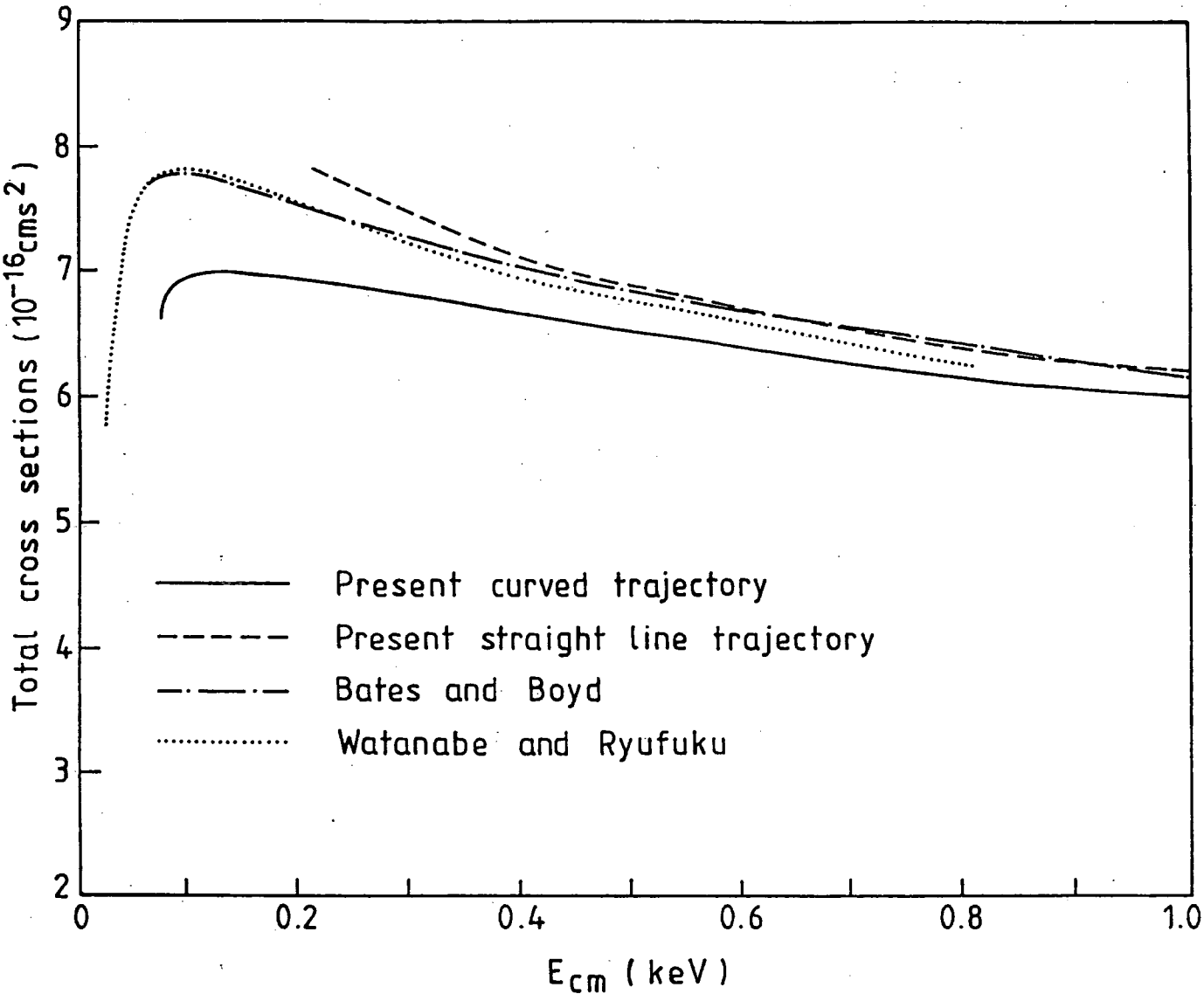

Figure 4.2 $^4He^{++}$ and $^4He^{+}$ Collisions: Total Charge Exchange Cross-sections.

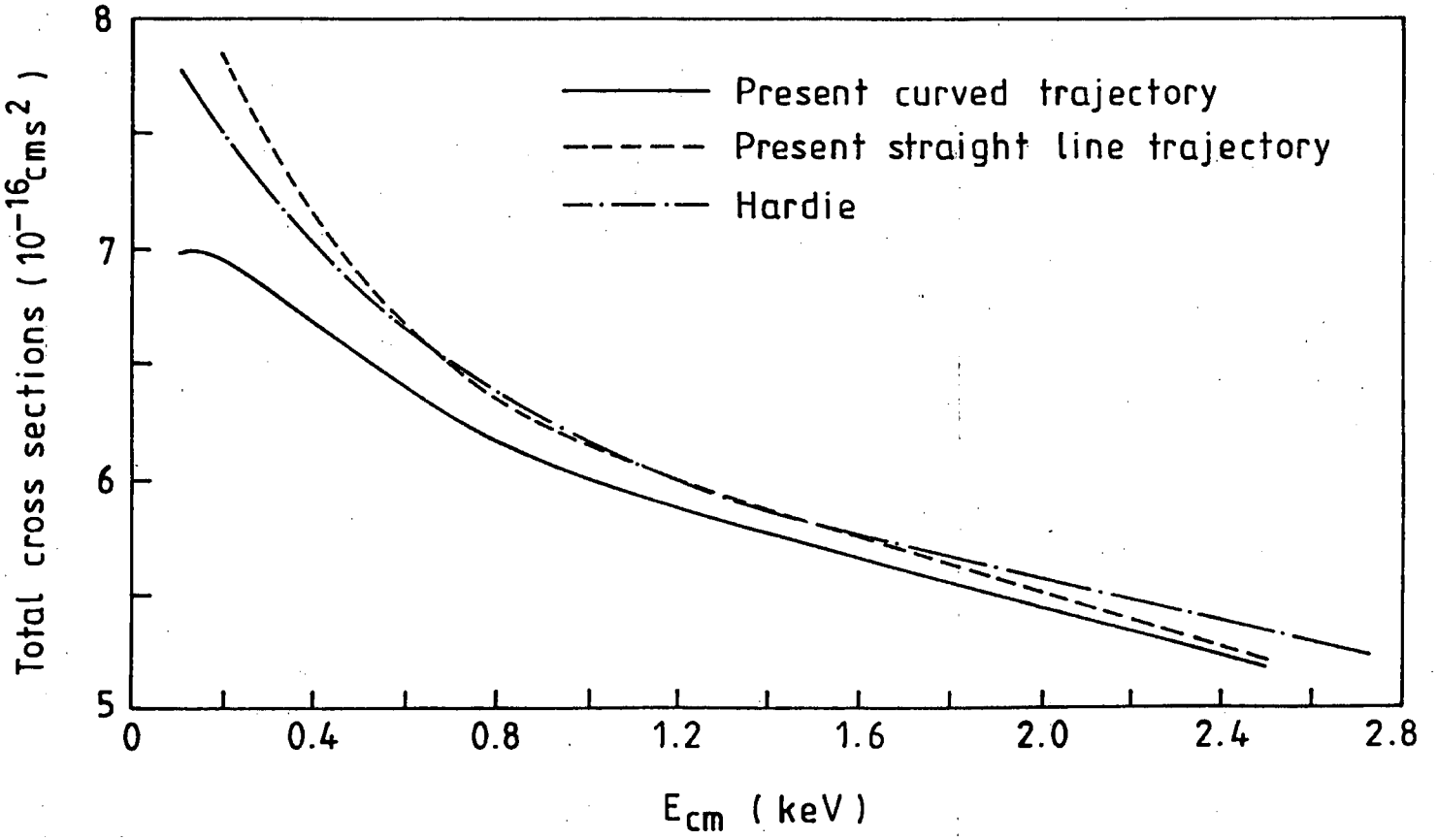

Figure 4.3 $^4He^{++}$ and $^4He^+$ Collisions: Total Charge Exchange Cross-sections. Comparison of the Present $^4He^{++}$ and $^4He^+$ Results with the $^3He^{++}$ and $^4He^+$ Results of Hardie (1981).

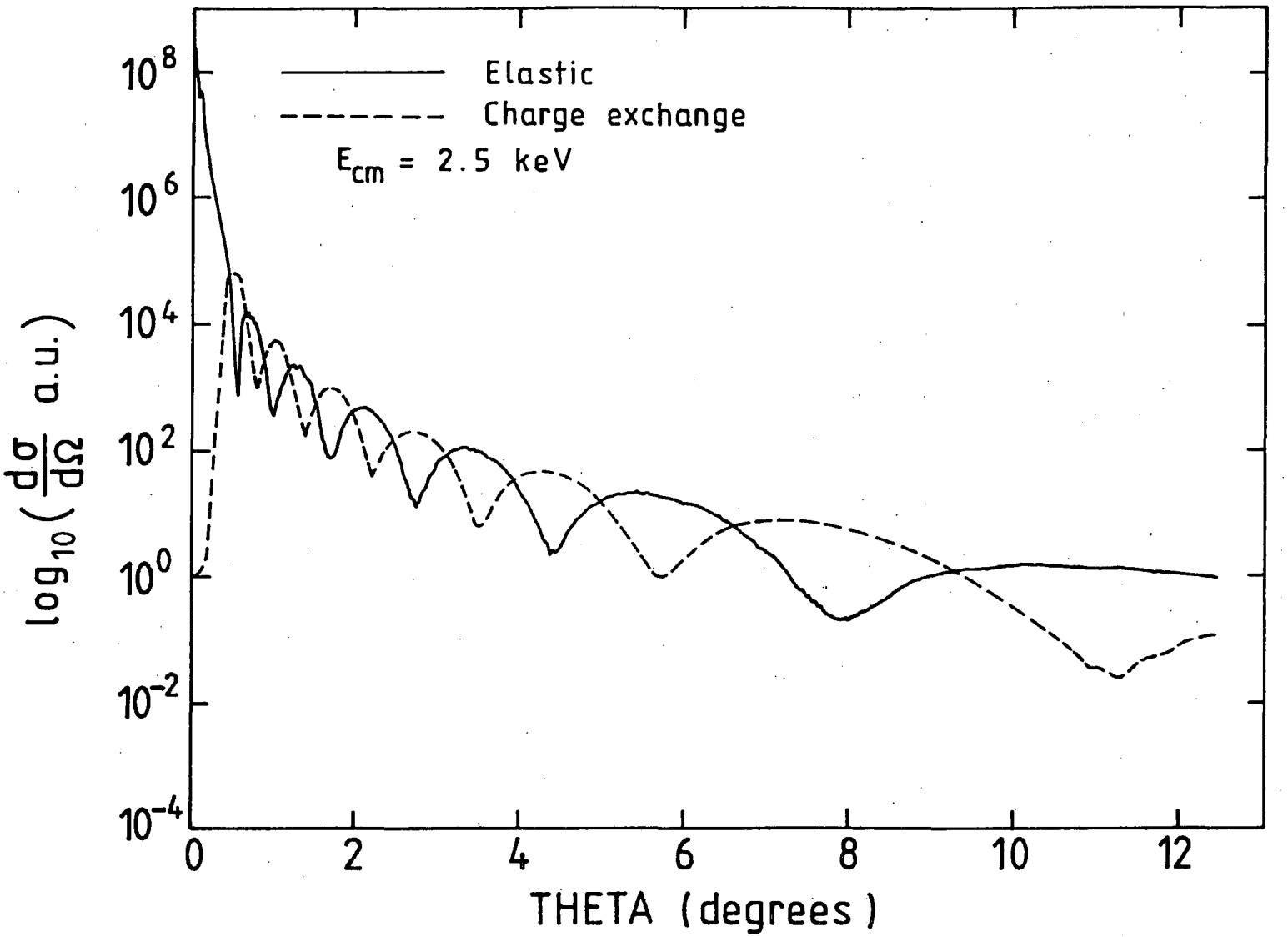

Figure 4.4 $^4He^{++}$ and $^4He^{+}$ Collisions: Comparison of the Elastic and Charge Exchange Differential Cross-sections.

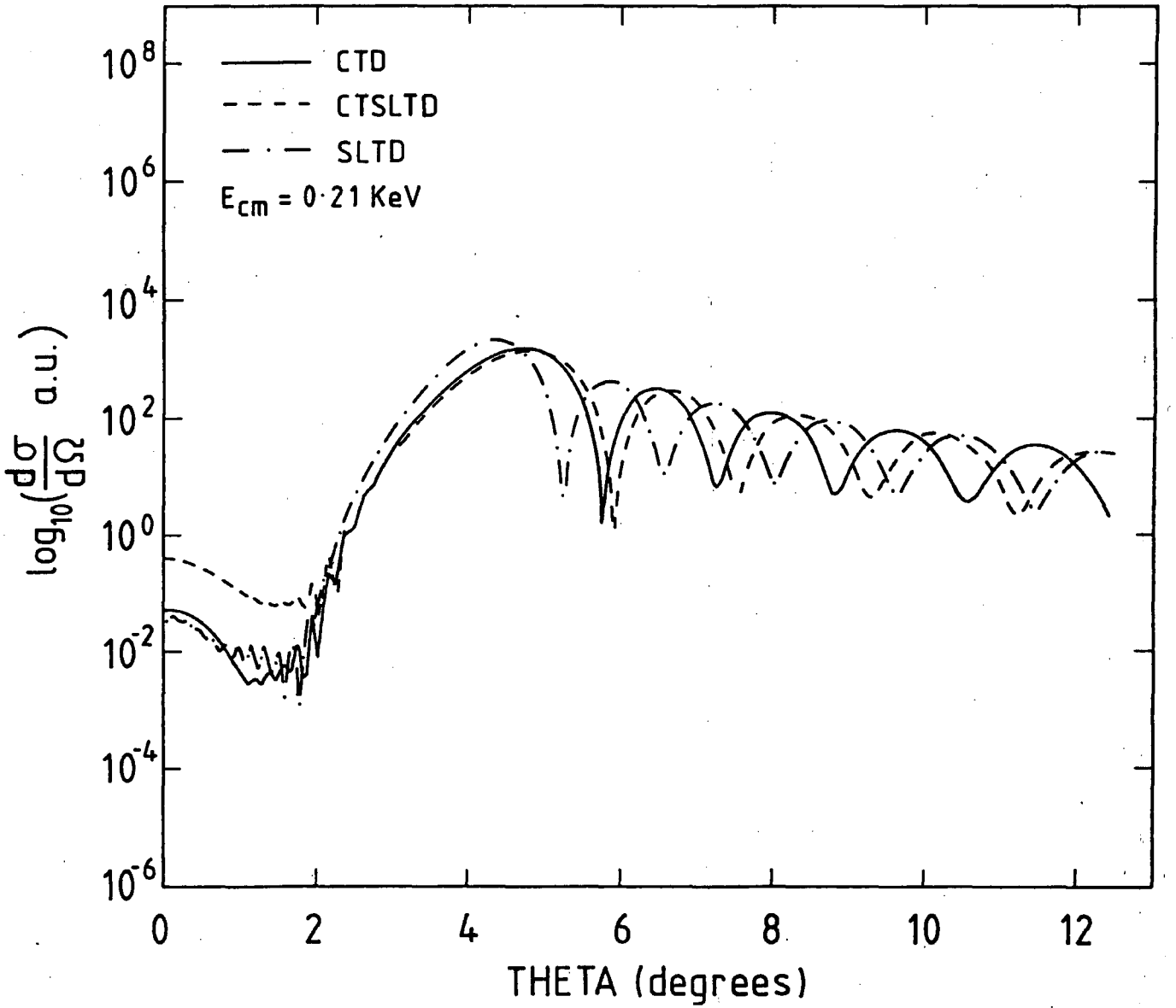

Figure 4.5 $^4He^{++}$ and $^4He^+$ Collisions: Charge Exchange Differential Cross-sections
[illegible] Centre of Mass Energy of 0.21 keV

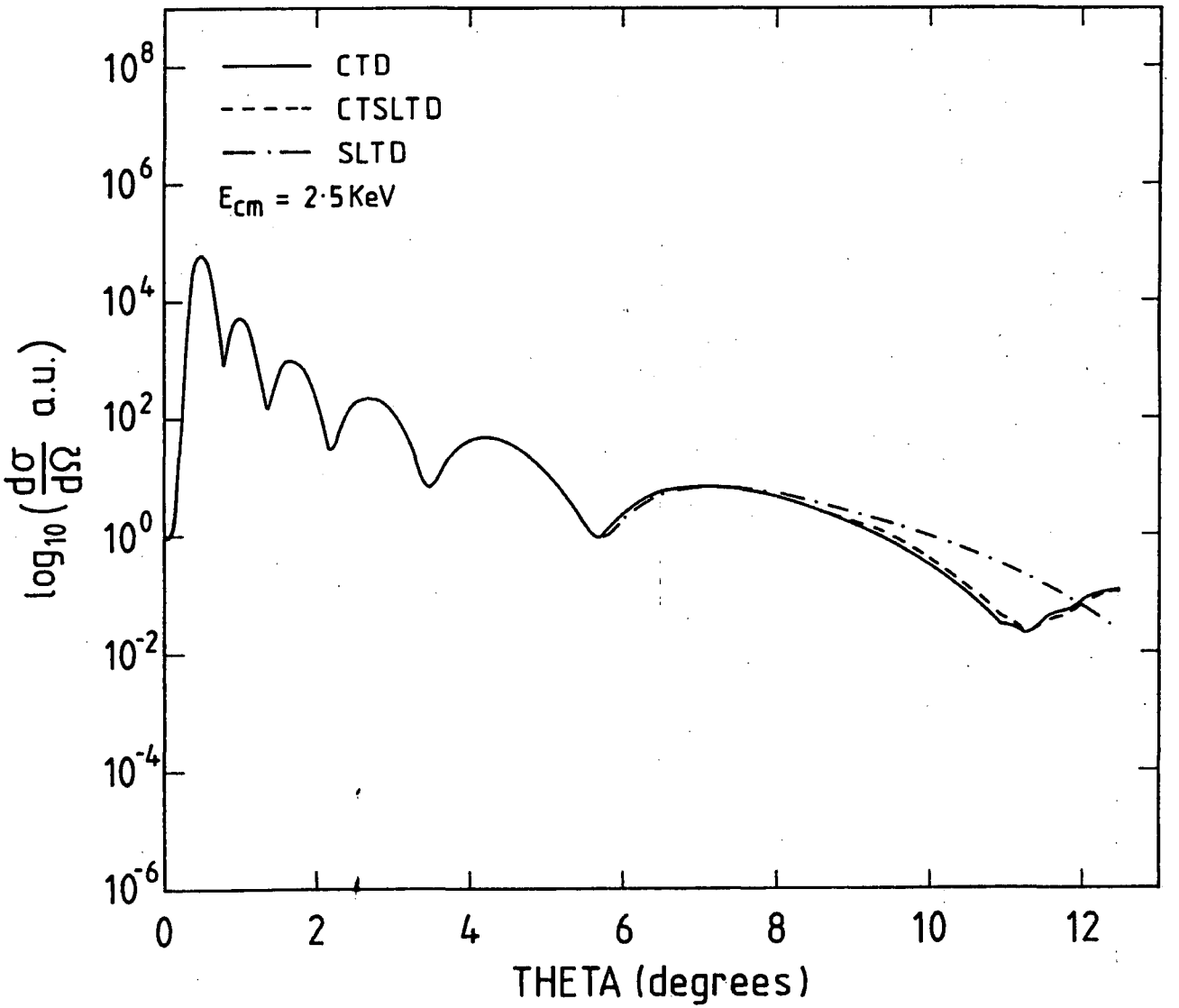

Figure 4.6 $^4He^{++}$ and $^4He^+$ Collisions: Differential Charge Exchange Cross-sections at a centre of Mass Energy of 2.5 keV.

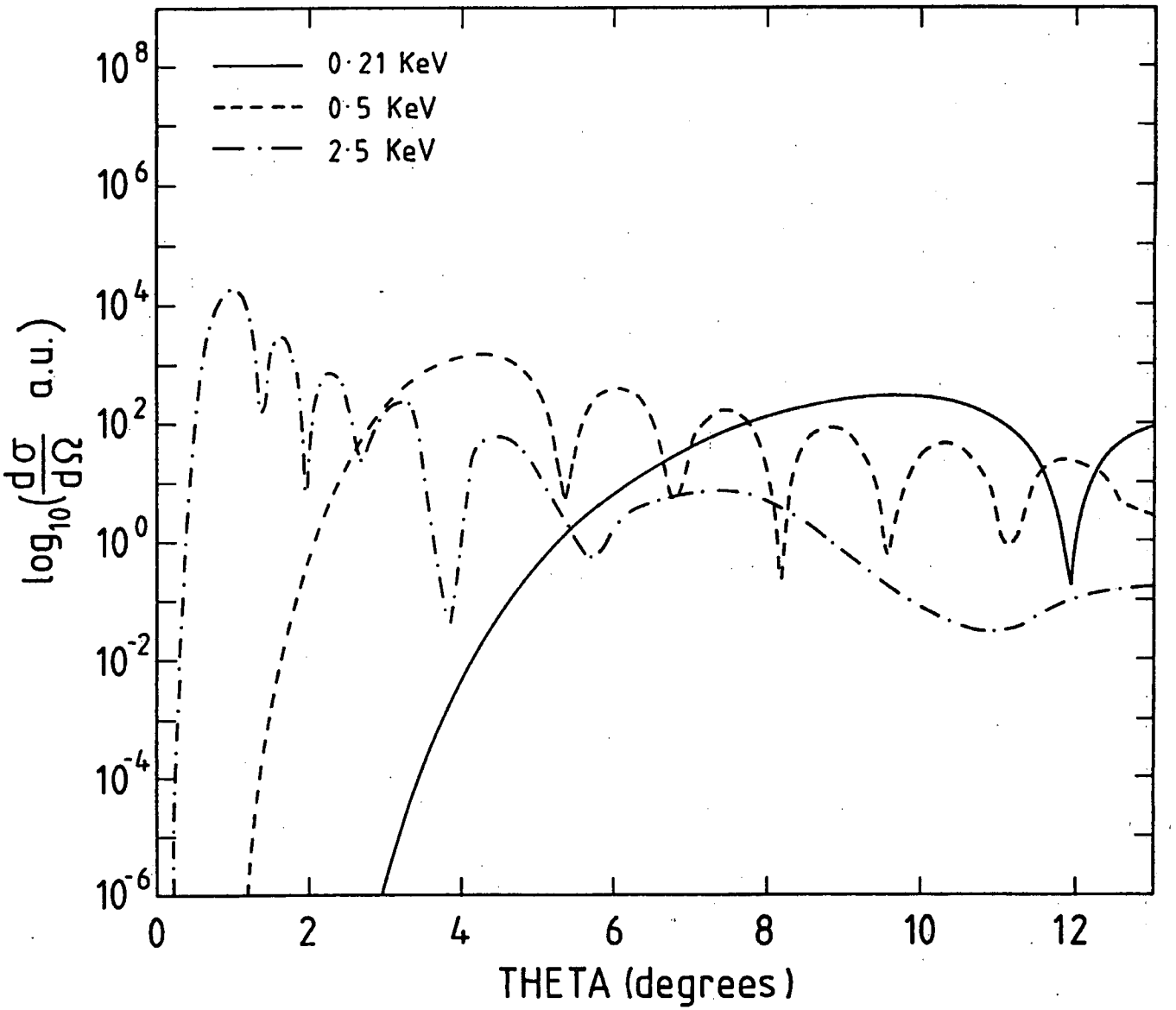

Figure 4.7 $^4He^{++}$ and $^4He^+$ Collisions: Charge exchange Differential Cross-sections

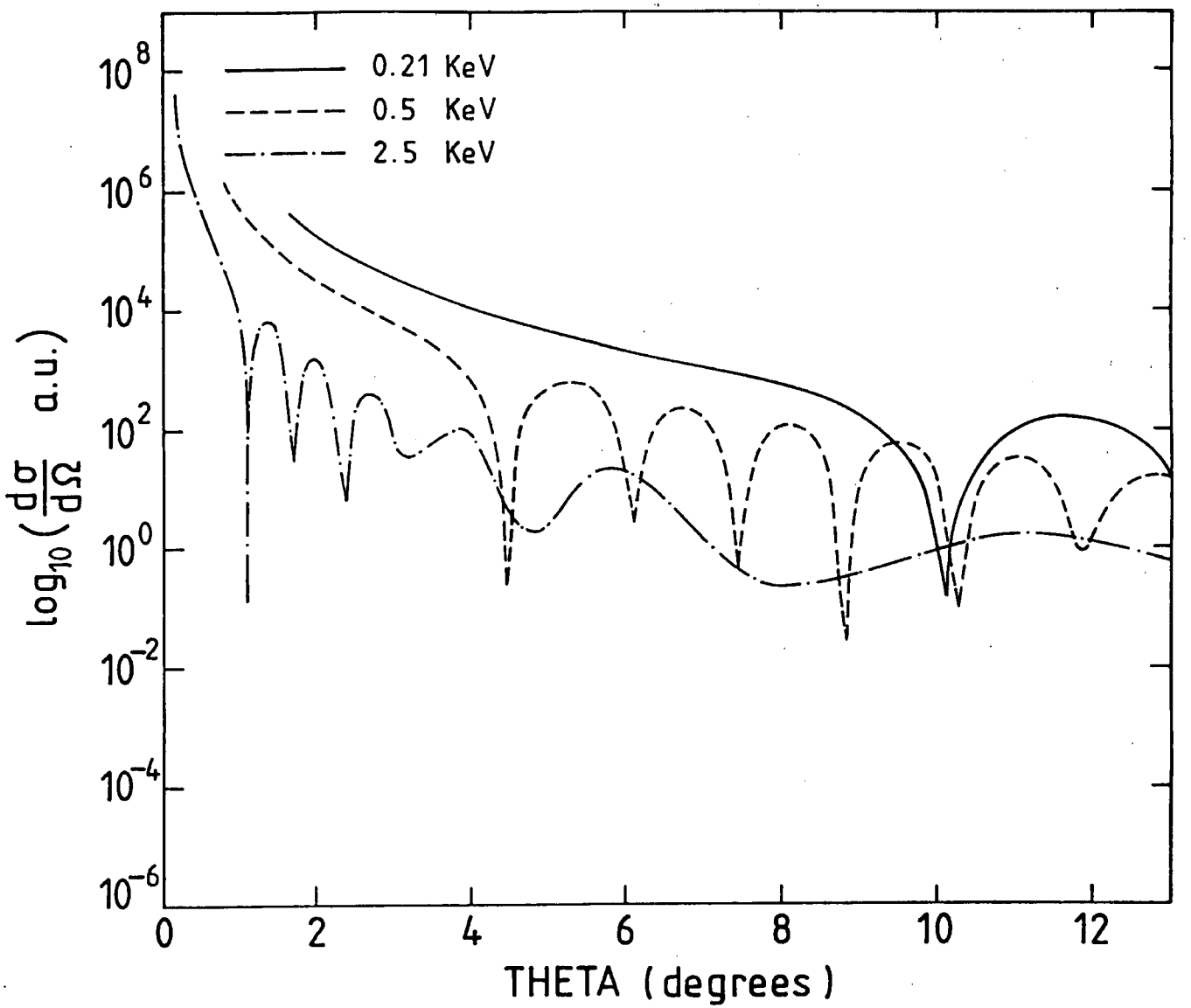

Figure 4.8 $^4He^{++}$ and $^4He^+$ Collisions: Elastic Differential Cross-sections obtained using $\frac{d\sigma}{d\Omega} |_{Ruth}| c(blt) |^2$.

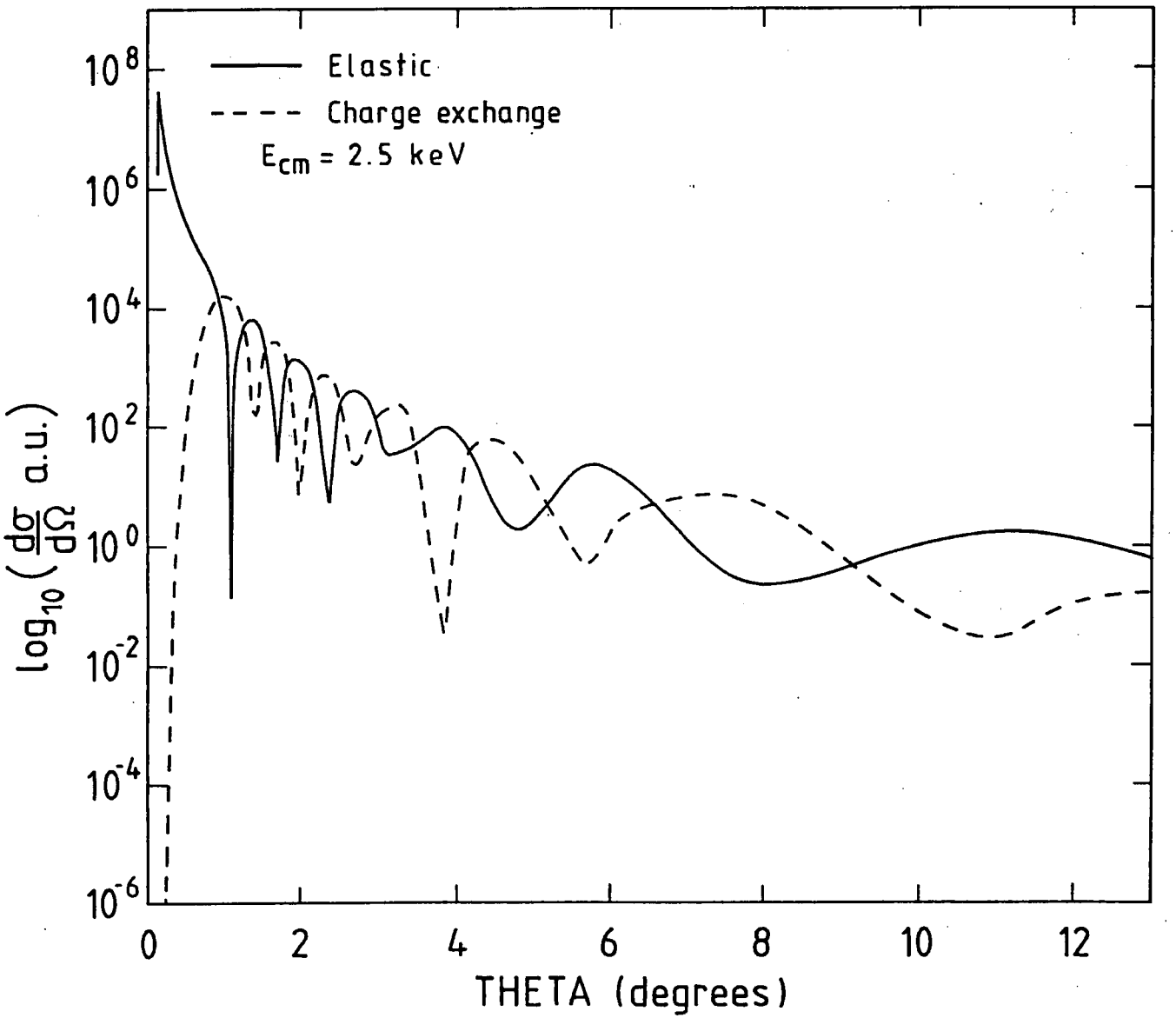

Figure 4.9 $^4He^{++}$ and $^4He^{+}$ Collisions: First Order Approximation. Comparison

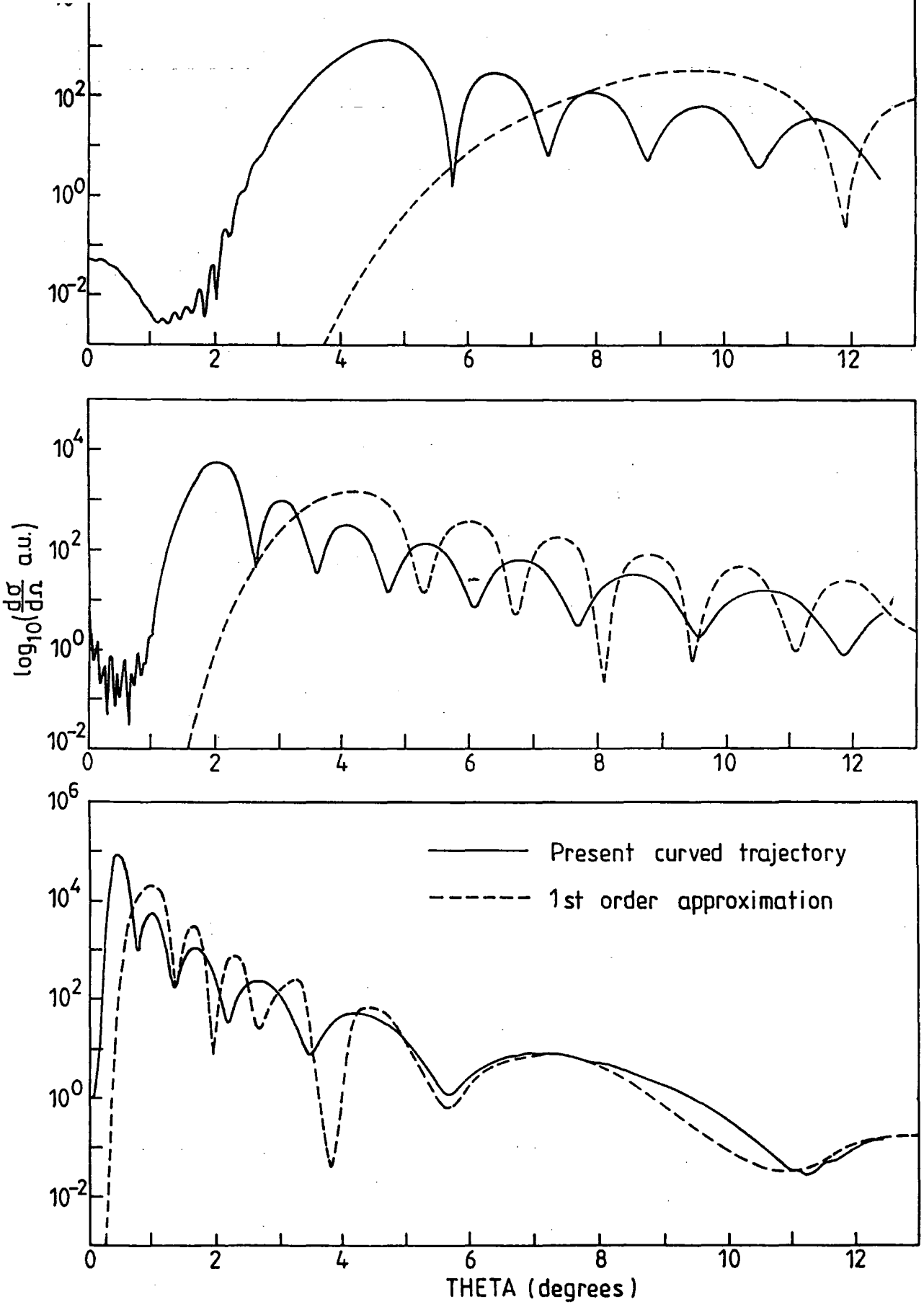

Figure 4.10 $^4He^{++}$ **and** $^4He^+$ **Collisions: Comparison of Charge Exchange Differential Cross-sections for Present Curved Trajectory and First Order Approximation.**

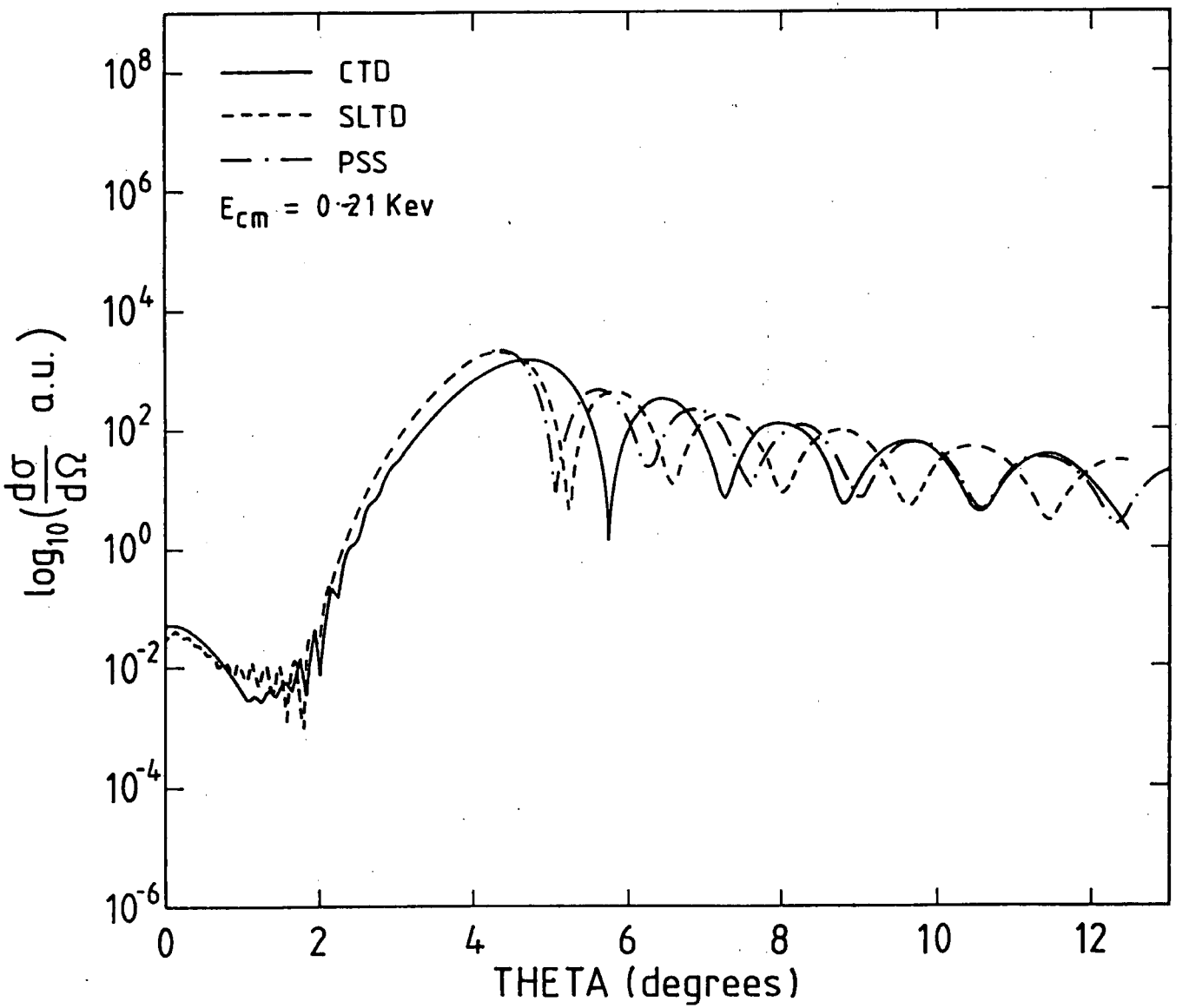

Figure 4.11 $^4He^{++}$ and $^4He^+$ Collisions: Comparison of Present Results with PSS Charge Exchange Differential Cross-sections, at a centre of Mass Energy of 0.21

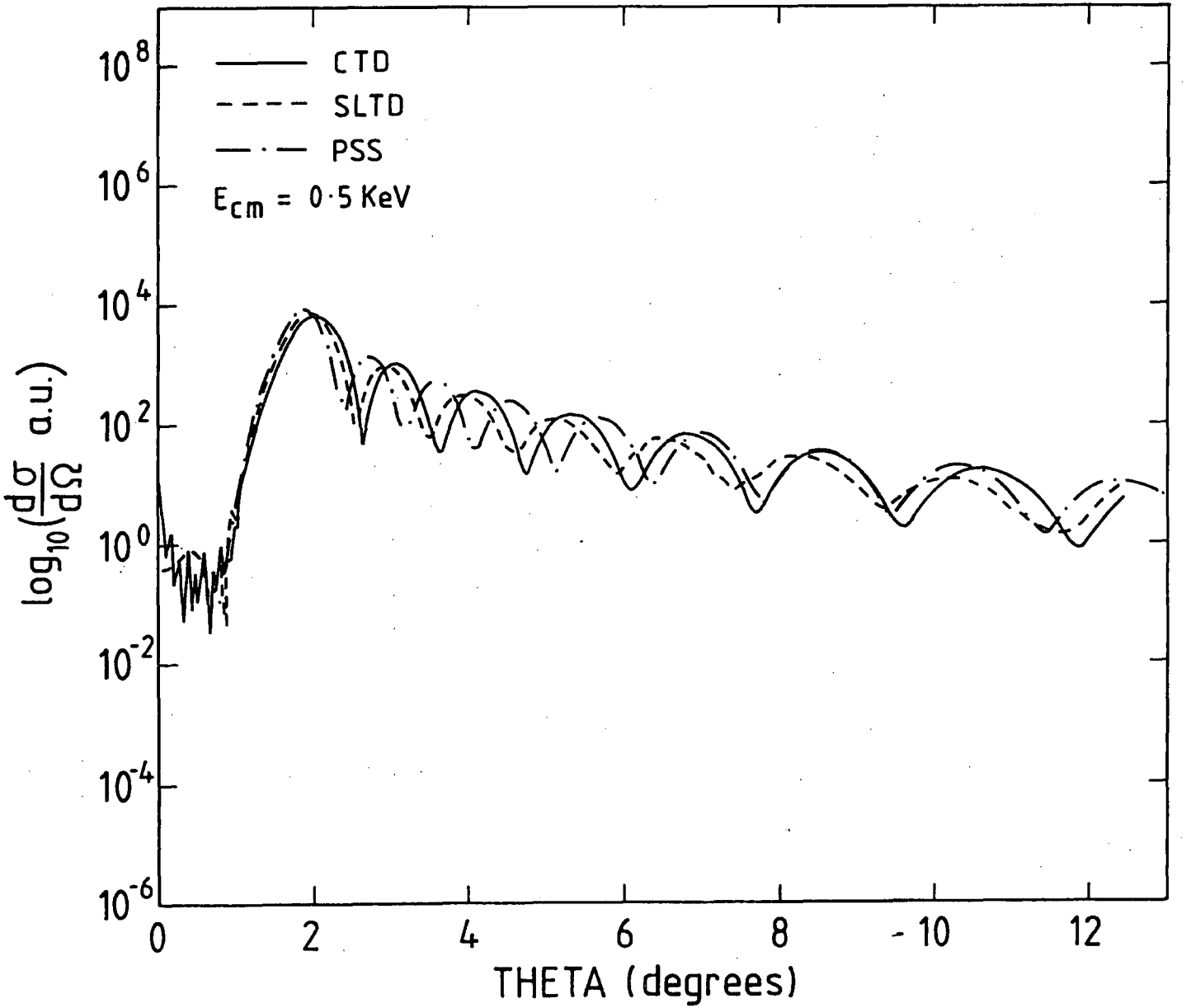

Figure 4.12 $^4He^{++}$ and $^4He^+$ Collisions: Comparison of Present Results with PSS Charge Exchange Differential Cross-sections, at a centre of Mass Energy of 0.50 keV.

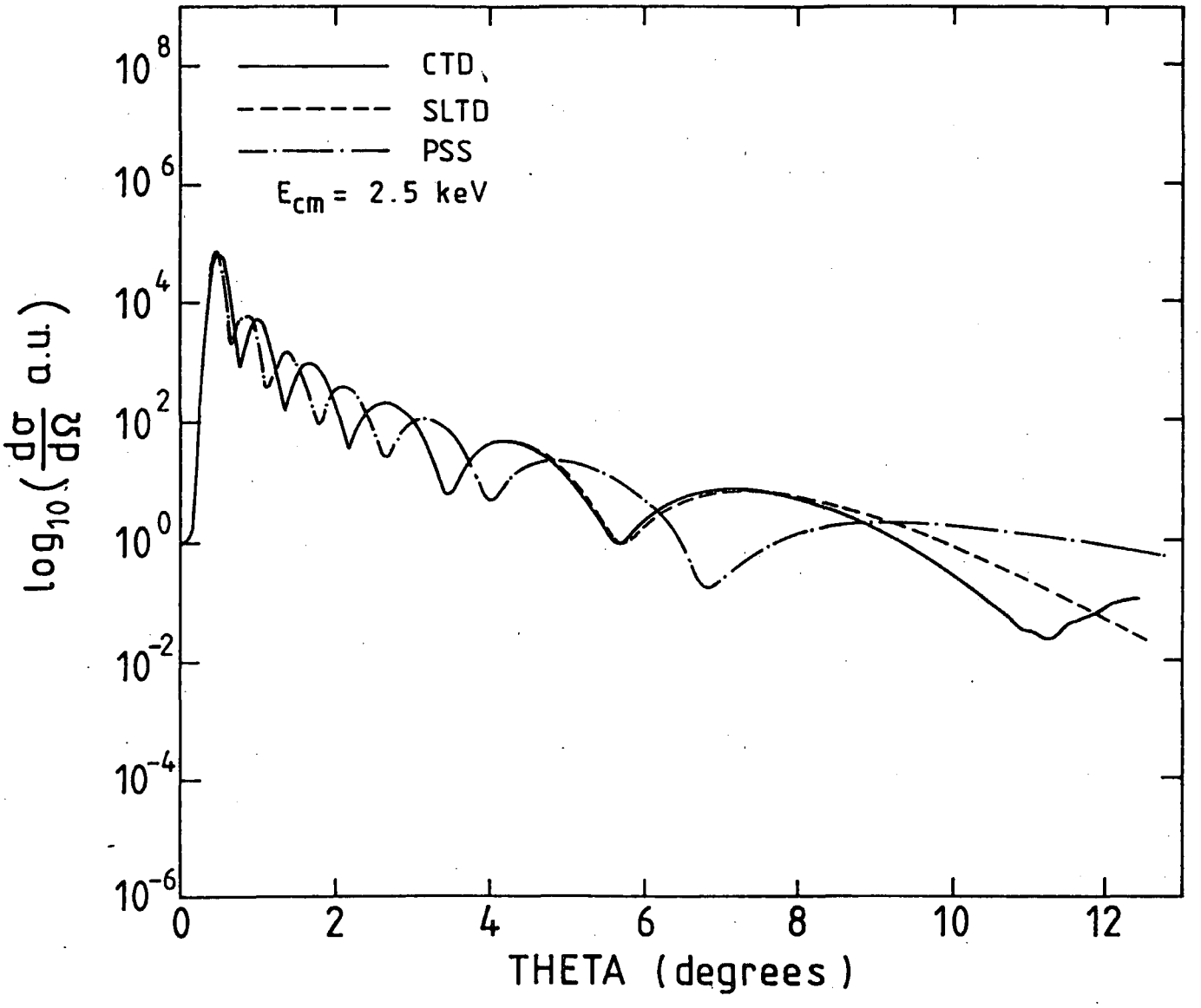

Figure 4.13 $^4He^{++}$ and $^4He^+$ Collisions: Comparison of Present Results with PSS Charge Exchange Differential Cross-Sections, at a Centre of Mass Energy of 2.5 keV

E_{cm}(keV)	Cross Sections (10^{-16}cms^2)		
	Straight line 2 state	Curved trajectory 2 state	Curved trajectory 20 state
0.075		6.599	
0.100		6.991	
0.210	7.843	6.640	7.126
0.223		6.924	
0.235	7.715	6.914	
0.375	7.205	6.719	
0.500	6.899	6.540	6.717
0.750		6.232	
1.000	6.156	5.997	
2.500	5.221	5.176	5.344

Table 4.1: Total cross sections for charge exchange in $^4He^{++}$ and $^4H^+$ collisions

E_{cm}(keV)	Total Cross Sections (10^{-16} cms^2)		
	Straight Line	Curved (Scaled)	Curved (Calculated)
0.210	7.843	6.880	6.940
0.235	7.715	6.861	6.914
0.375	7.205	6.688	6.719
0.500	6.899	6.520	6.540
1.000	6.156	5.976	5.997
2.500	5.221	5.155	5.176

Table 4.2: Cross section for charge exchange in $^4He^{++}$ and $^4He^+$ collisions: comparison with the scaled expression (1.108) of Bates and Boyd

E_{cm}(keV)	Total Cross-sections (10^{-16}cms^2)	
	Curved Trajectory	Bates and Boyd
0.075	6.599	7.786
0.100	6.991	7.816
0.210	6.940	7.520
0.223	6.924	7.481
0.235	6.914	7.445
0.375	6.719	7.088
0.500	6.540	6.843
0.750	6.232	6.478
1.000	5.997	6.213
2.500	5.176	5.367

Table 4.3: $^4He^{++}$ and $^4He^+$ Collisions : Total Cross-sections : Comparison of curved trajectory results with the approximate cross-sections of Bates and Boyd (from 1.109)

Chapter 5

Low Energy Charge Exchange between Doubly Ionised Beryllium and Atomic Hydrogen

5.1 Introduction

The reaction

$$Be^{++} + H(1s) \rightarrow Be^{+}(n,l) + H^{+} \tag{5.1}$$

is an asymmetric reaction whose cross sections cannot be calculated by means of scaling laws such as those used in the symmetric resonance collisions discussed in Chapter four, where the nuclei are identical. Experimental work can be difficult with beryllium, because of its poisonous nature, but Be^{++} and H collisions are theoretically interesting because of their significance to fusion studies. Total and differential cross sections have been calculated for 5.1, employing both straight line and curved trajectories. Lower energies have been used than those previously employed by Shingal (1986) in an atomic orbital calculation with straight line trajectories. The aim was two fold. Firstly, the total cross sections obtained using straight line paths could be compared with molecular calculations already carried out (Bates et al 1964, Crothers and Todd, 1978 and Wetmore et al, 1986). The effectiveness of using atomic orbital expansions, at energies where the molecular model is often felt to be preferable, could then be tested. Secondly, the effect, on the cross sections, of using a curved trajectory could be assessed.

Because the masses of the beryllium and hydrogen nuclei are unequal, the origin of the relative motion is not situated at the mid point of $\vec{R}$. From 1.13, the ratio p:q is 1:9, and those parts of the matrix elements containing terms in p-q are non-zero. Reaction 5.1 therefore provides a test of the full curved trajectory formulae of Chapter two. Be^{++} and H collisions are also complicated by the presence of the two electron ionic core of Be^{++}. However, if it is assumed that the electrons in the 1s closed shell of Be^{++} are closely bound by the nucleus, and are relatively unaffected by charge transfer and excitation effects, the system can be regarded as

having only one valence electron. In these circumstances, either model potentials, pseudopotentials or affective potentials can be used to describe the interaction of the valence electron with the closed shell ionic core (Peach, 1982). The presence of the core electrons means that electron capture is into the 2s and higher excited states of Be^+.

5.2 Model Potentials and Pseudopotentials

The basic theory of model potentials and pseudopotentials has been reviewed by Bottcher and Dalgarno (1974), and also Laughlin and Victor (1988). Pseudopotential methods have been reviewed by Bardsley (1974), and Peach (1982) has discussed both methods. The basis of methods is to reduce the many bodied Schrodinger equation

$$(T + V_{TOT})\Psi = E\Psi, \quad V_{TOT} = V_{Ae} + V_{Be} + V_{AB} \tag{5.2}$$

to a form in which the interaction of the valence electron with the ionic core, is represented by an effective potential. In the case of a model potential, 5.2 becomes

$$(T + V_m)\phi = E\phi \tag{5.3}$$

The form of the model potential V_m can be determined by variation of parameters, so that the eigenvalues of ϕ are the same as the observed values. For systems where there is only one ionic core to be considered, such as in Be^{++} and H collisions, the potential term V_{Be} is merely the coulomb attraction between the hydrogen nucleus and the electron. It is the interaction V_{Ae} which must be modelled. Asymptotically, this depends only on the screened nuclear charge and the polarisability of the core, and here the form of V_m is exact. In the region of the core electrons, V_m has an approximate value. As well as the ground and excited valence states of the ion, the model potential can also produce "virtual states" which have energies lower than those of the valence states above. To ensure that the probabilities for the valence electron being in the core region of the ion are very small, the virtual core states are orthogonal to the valence states. The pseudopotential method, on the other hand, physically prevents the presence of the valence electron in the inner core region by incorporating a short range repulsive potential. The pseudopotential V_p satisfies

$$(T + V_p)\chi = E\chi \tag{5.4}$$

which asymptotically is identical to 5.3 No virtual states of the core region are produced with a pseudopotential and, because of the form of the potential, there is no unique solution to 5.4 although $\chi \rightarrow \phi$ in the asymptotic region. When relatively simple systems such as Be^{++} and H are being considered, the model potential used is local and spherically symmetric, whereas a suitable pseudopotential can be non-local and also l dependant. An alternative method proposed by

Daniele (1979) is the use of an effective potential. The valence electron experiences a combination of the true nuclear potential and a charge distribution created by the closed shell electrons. Effective potentials have been used, for example, in one electron models for He^+ - Li^o collisions by Bransden et al. (1984) and for H^+ - Na^o collisions by Shingal et al. (1986). The many bodies problem is simplified using either of these methods. The effective potential used to represent the Be^{++} core in the present work, was that due to Daniele (1979). The form of the potential used was

$$V_{eff}(r) = -\frac{Z_1}{r} - (\frac{Z_2}{r} + \mu)exp(-\mu)$$
$$Z_1 = 2 \;\; Z_2 = 2 \;\; \mu = 4.12 \qquad (5.5)$$

which has also been used by Shingal (1986) in his straight line calculations and and also in calculations of Be^{2+} + Li collisions (Shingal, 1988). This potential was used to construct the eigenstates of Be^+ shown in Table 5.1. A screened coulomb potential $V_{AB} = (Z_A\text{-}1)Z_B/R$ was also assumed for the internuclear interaction.

5.3 Previous work

Bates and Moiseiwitsch (1954) have used a two state model to investigate 5.1. The transition probabilities, which arose from pseudocrossing of the potential energy curves of the initial and final states were found using Landau Zener methods (Mott and Massey, 1965). Bates et al (1964) repeated the calculation using a two state approximation with electron capture to $Be^+(2s)$. Straight line trajectories were used and momentum translational factors were neglected. The probabilities P(b) for charge transfer were expressed in terms of the solutions of semiclassical equations, similar to those used by Bates (1960). At small impact parameters, where the probabilities oscillated rapidly, an average approximate value was used to facilitate the calculations. These results were compared with those from an adapted Landau-Zener method. The maximum total cross section obtained using the semiclassical method was found to be twice that of the Landau-Zener. This was due to the inclusion of contributions from impact parameters greater than the Landau Zener crossing point R_x in the former method, but not in the latter. It was found that the semiclassical cross sections were much larger in the lower energy range than the Landau Zener results. The authors felt that The neglect of momentum translation factors in the semi-classical model could lead to overestimation of the cross sections. Charge exchange cross sections for the reverse reaction

$$H^+ + Be^+ \rightarrow H + Be^{++} \qquad (5.6)$$

have been calculated by Crothers and Todd (1978) using a Stuecklburg phase integral method developed by Crothers(1978). The two state results obtained were in good agreement with the semi-classical results of Bates et al (1964), both

for the total cross sections and with respect to the variation of the probabilities with b for a fixed energy. The importance of the contributions due to b values larger than those at which curve crossing occurred was also emphasised. These two methods did not explicitly use model potentials or pseudopotentials for describing the ionic core interactions. However Wetmore et al (1986) used pseudopotentials in their investigation of 5.1 for a range of energies 50 eV/amu $< E_{lab} <$ 5 keV /amu using an eight state basis, with 1s,2s, 2p on the hydrogen atom, and 2s, 2p, 3s, 3p, 3d states of Be^+. At low energies, Wetmore et al found that 85% of the total cross section was due to charge exchange to 2s, and the remaining 15% was from charge exchange to 2p states. A PSS method was used, with the switching function ETFs of Kimura and Thorson (1981). The Pseudopotentials were of the form

$$V(R) = a_e \exp(-b_e r^2) - \frac{\alpha_d}{2(r^2+d^2)^2} - \frac{\alpha_q}{2(r^2+d^2)^3} - \frac{q}{r} \qquad (5.7)$$

(Bardsley 1974). Included are the dipole and quadropole polarisabilities α_d and α_q calculated by Dalgarno (1962). The cut-off parameter d limits the range of the polarisation potentials, and is the Hartree Foch expectation value of the core electrons in the 1s state (Froese Fischer, 1977). At large R, q is the ionic charge seen by the valence electron. The Slater orbitals used for the molecular wave functions were determined by variational techniques and straight line trajectories were employed.

The work carried out by Shingal (1986) was at energies in the range 0.266 keV $<$ Ecm $<$ 3.555 keV (0.3 keV/amu $< E_{lab} <$ 4.0 keV/amu). A five state basis was used within the straight line impact parameter method and thirty impact parameters were employed at each energy. Two fifty five state calculations were also carried out to test the convergence of the basis. Shingal found that at E_{cm} = 1.1 keV, the charge transfer cross section obtained using the larger basis was higher by 14%. At the lower energy of 0.44 kev, the difference was only 4.6%. In view of the reasonable convergence of the basis set at low energies, the same five state atomic orbital basis as that employed by Shingal was used in the present work. Cross sections have been calculated over a narrow range of centre of mass energies 0.111 keV $< E_{cm} <$ 0.444 keV (0.125 keV/amu $<$ Elab $<$ 0.5 keV/amu). These energies correspond to cross sections around and below the maximum found by Bates et al, and Wetmore et al.

5.4 Total and partial cross-sections

Probability amplitudes were calculated for six energies within the given range. In the curved trajectory calculations, the extra exponential factors 3.3 were included in the matrix elements. The acceleration matrix elements were also included, for completeness, although they were small.

Two hundred and forty impact parameters were used for all six energies, with a maximum b value of 16.00 a.u. The integrands b$|$ c(b,t)$|^2$ plotted against b, for

charge exchange to 2s, are shown in Figure 5.1 for both straight line (SLT) and curved trajectory (CT) models at centre of mass energies of 0.155 and 0.355 keV. The largest contributions to the partial cross sections to 2s come from b < 10.0 a.u. The integrands are highly oscillatory at 0.155 keV, especially at small impact parameters. Phase differences due to trajectory effects are pronounced, whereas at 0.355 keV the effects are small. The major contributions to the 2p cross sections come from smaller impact parameters, and at lower energies in the range, the cross sections to $2p_1$ dominate charge exchange to 2p. This confirms the results of the molecular model of Wetmore et al (1986), in which the rotational coupling at small R was found to be the principal mechanism for charge exchange to $Be^+(2p)$, with the $Be^+(2p_\pi)$ states dominating, at low energies. The integrands $b|\ c_n(b,t)|^2$ for the two 2p states in the present calculation are shown in Figure 5.2 for curved trajectories only at E_{cm} = 0.155 keV. The total and partial cross sections for both straight line and curved trajectories are in Table 5.2, and are plotted in Figure 5.3. The curved trajectory total cross section is 16% lower than the straight line equivalent at a centre of mass energy of 0.111 keV. This difference is reduced to less than 3% at 0.444 keV which suggests that for the 2s cross section, the straight line approximation would be valid at energies above this. Charge transfer to 2s dominates reaction 5.1 for the whole energy range. The partial cross sections to 2s, account for more than 87% of the total cross sections for the straight line model, and 91% for the CT model, and are an order of magnitude larger than those to 2p. Contributions from 2p to the total cross sections are reduced in both absolute and relative terms when a coulomb trajectory is used. The highest probabilities for the 2p states occur at small impact parameters where the effect of the trajectory is expected to be greatest. The contributions from $2p_o$ and $2p_1$ to the partial cross sections to 2p are shown in Figure 5.4. Significant trajectory effects are still apparent in all the partial cross sections to 2p at the highest energy, 0.44 keV. In view of this, further work would be useful at still higher energies to determine the level at which the differences become insignificant. The cross sections for charge exchange to 3s were negligible in this energy range, contributing less than 0.04% to the total cross sections at all energies.

For easier comparison with the results of other authors, Table 5.3 shows the centre of mass energies used in this work converted to log (E(eV)) and keV/amu.

The present results have been compared with the graphical two state results of Bates et al (1964), in Figure 5.5. Figure 5.5(a) compares the present total cross sections with the semiclassical method (SC) and the Landau Zener method (LZ) used by Bates et al, and Figure 5.5(b) shows charge transfer cross sections to 2s. The SLT total cross sections are in good agreement with the two state model at the lower energies, and are 5% higher at log (E(eV)) = 3.6. The curved trajectory results disagree with Q_{sc} at log (E(eV)) = 3.0 by 15%, and at higher energies are in good agreement. Both sets of partial cross sections to 2s in Figure 5.5(b) are below the results of Bates et al for all energies, the difference being 6% and 9%, in the SLT and CT models respectively, at the maximum cross section at log(E(ev)) = 3.5. The effect, on the total cross sections, of adding 2p and 3s to the beryllium basis is significant at the three highest energies, casting doubt on the adequacy of a two state basis, even for low energies such as these.

Straight line and curved trajectory total and partial cross sections are compared with the results of Wetmore et al (1986) and Shingal (1986) in Figures 5.6 and 5.7. The straight line 2s cross sections were larger than those of Wetmore et al, for all energies, and this was more marked at the maximum, where the disagreement was 5.6%. The CT cross sections were also higher by 2% at this point. Both the CT and SLT partial cross sections to 2p were lower than those of Wetmore et al. This has been attributed to the fact that the 2p states converge more slowly than the total cross sections, and the additional states in the basis of Wetmore et al, may well have resulted in higher cross sections to 2p.

The present straight line total cross sections shown in Figure 5.6 agree with those of Wetmore et al to within 3.5% for all energies. The additional states in the molecular basis set ensure that the total cross sections produced by Wetmore et al are generally larger than the present cross sections. The agreement with the results of Shingal in the overlap region is within 2% for the straight line results. In view of the disparity in the numbers of impact parameters used, and the numerical accuracy of the algorithms used in the programs, this disagreement between the two straight line atomic basis cross sections is not felt to be significant. At energies above 0.444 keV (0.5 keV/amu), the total cross sections obtained by Shingal decrease faster with increase in energy, than those obtained by Wetmore et al. The latter have the characteristic behaviour of molecular calculations where switching functions have been used (Newby, 1985).

The agreement between the SLT cross sections and the results of both Wetmore et al, and Bates et al, show that the atomic orbital method can still give accurate cross sections at these low energies. It was puzzling to note that Wetmore et al describe the position of the maximum of the cross sections obtained by Bates et al as differing considerably from theirs. On examination of Wetmore's graphical results, it was apparent that the results of Bates et al have been plotted incorrectly on the former, an order of magnitude too far to the right. If these results are plotted correctly, the two authors are in close agreement.

5.5 Differential Cross-section Results

Angular distributions were found using differential cross sections calculated at 279 values of θ in the range $0^\circ < \theta < 13^\circ$ (centre of mass), at a spacing of 0.02° . The number of integration points used for each differential cross section after five point Lagrange interpolation is shown below.

E_{cm}(keV)	No. of B Values	No of integration points
0.1111	240	2306
0.1555	240	2728
0.21	240	3170
0.26	240	3572

5.5.1 Angular Distributions for Charge Transfer to 2s

The largest probabilities for charge transfer to 2s occur between 5 a.u. $< b <$ 8 a.u. Figures 5.8 and 5.9 show the angular distributions for 2s at four centre of mass energies, with the differential cross sections plotted on a log scale. The oscillations present are similar to those obtained in symmetric resonance, reflecting the small probabilities for charge transfer to other states at these energies. However, the oscillations tend to become damped at larger angles, especially at higher energies, and there is more structure in the angular distributions at very small angles. This was felt to be due to the presence of other states in the basis set. It was found that, although the main structure of the angular distribution was unaffected by changes in the upper limit to the range of b values for $b > 12$ a.u., the depths of the minima in the distributions and the small angle structure were sensitive to $b <$ 16 a.u.. The main oscillations of the straight line and curved distributions are out of phase, with the CT shifted, as expected, to larger angles. The very small angle structure also differs between the models, and at $\theta < 0.5°$ the SLT differential cross sections are generally larger than those obtained using coulomb trajectories. At $E_{cm} = 0.26$ eV, the CT and SLT distributions are in phase for $0.5 < \theta < 4.0$ degrees. Phase differences are present in the distribution at larger angles, as found in the He^{++}–He^{+} angular distributions. The angular phase differences at the first minimum are shown below for curved and straight line semi-classical models.

E_{cm}(keV)	Angular Phase Difference Ct and SLT
0.11	0.03
0.155	0.15
0.211	0.10
0.266	0.0

The CT angular distribution for charge exchange to 2s at centre of mass energies of 0.11 keV and 0.26 keV are compared with those obtained using the first

order approximation 1.114 in Figures 5.8 and 5.9. The small angle structure seen in the semiclassical model is not present in the first order distributions, and apart from the general oscillatory form, the two distributions are widely divergent in angular phase and frequency.

A comparison of CT differential cross sections for the elastic channel and 2s charge transfer, for $E_{cm} = 0.211$, is shown in Figure 5.10. The same numerical problems, discussed in Chapter three, were experienced with the elastic angular distributions. The comparison shows that the distributions are not in perfect antiphase, as they would be in symmetric resonance, due to the presence of other charge exchange states in the basis set.

5.5.2 Angular Distributions for Charge Transfer to 2p States

Figure 5.2 shows that the largest contributions to the partial cross sections for charge transfer to 2p states occur at small impact parameters. Trajectory effects on the angular distributions for charge transfer were therefore expected to be large. To define the probabilities at small impact parameters as much as possible, fifty extra calculations for 0.0 a.u. $<$ b $<$ 2.0 a.u. were performed.The effect of the extra impact parameters on the angular distributions was not large, although they were included for maximum accuracy. The variation of the probabilities for charge transfer to $2p_o$ and $2p_1$ with b for two centre of mass energies are shown in Figures 5.11, 5.12, 5.13 and 5.14. At impact parameters of less than 1 a.u. there are small oscillations superimposed on the general shape of the probabilities, and these are more pronounced at the higher energy, 0.355 kev, and for charge exchange to $2p_o$ states. The large oscillations of $|\ c(b,\ t)|^2$ with b for the $2p_o$ and $2p_1$ states are in antiphase and trajectory effects are most noticable in the small oscillations in the probabilities at b $<$ 1.0 a.u. The range of impact parameters within which electron capture to 2p states is likely was found to be larger for the $2p_o$ state, although the partial cross sections to $2p_o$ were generally smaller than those to $2p_1$.

The angular distributions have some pronounced small angle structure, but the differential cross sections are largest at angles greater than 5^o . The effect of using a curved trajectory was to move the position of the maximum in the distribution to larger angles. This is illustrated in Figure 5.15 which shows the angular distributions for charge exchange to $2p_o$ on a non-log scale, at an E_{cm} of 0.1555 keV. For comparison with the first order approximation, the angular distributions to 2p states are shown with the differential cross sections plotted on a log scale in Figures 5.16, 5.17, 5.18 and 5.19. There is qualitative agreement between the models at angles less than four degrees, but at angles larger than this, trajectory effects are much more noticable.

5.6 Discussion

The good agreement between the present straight line results and the previous work of other authors confirms that the atomic orbital method can produce cross

sections which are comparable with those from molecular orbital calculations, even at low energies. However, it is evident that neglecting trajectory effects produces significant errors in the cross sections, even in the case of charge exchange to 2s, where the maximum probabilities occur at larger impact parameters. For cross sections such as to 2p states, where contributions from smaller impact parameters dominate, the errors are even greater, and extend to higher energies.

The differential cross sections show that the use of a curved trajectory is significant at larger angles even when trajectory effects at very small angles are negligible. The small angle approximation is valid for angles less than $\simeq 30^o$ from 1.91, and is most appropriate for the calculation of differential cross sections for charge exchange to 2s in this reaction, as the largest contributions to the angular distributions from the differential cross sections comes from angles less than 10.

In view of the fact that scattering generally takes place at larger angles for charge exchange to 2p, a comparison with angular distributions obtained using partial wave expansions might be valuable, to help assess the validity of the present method.

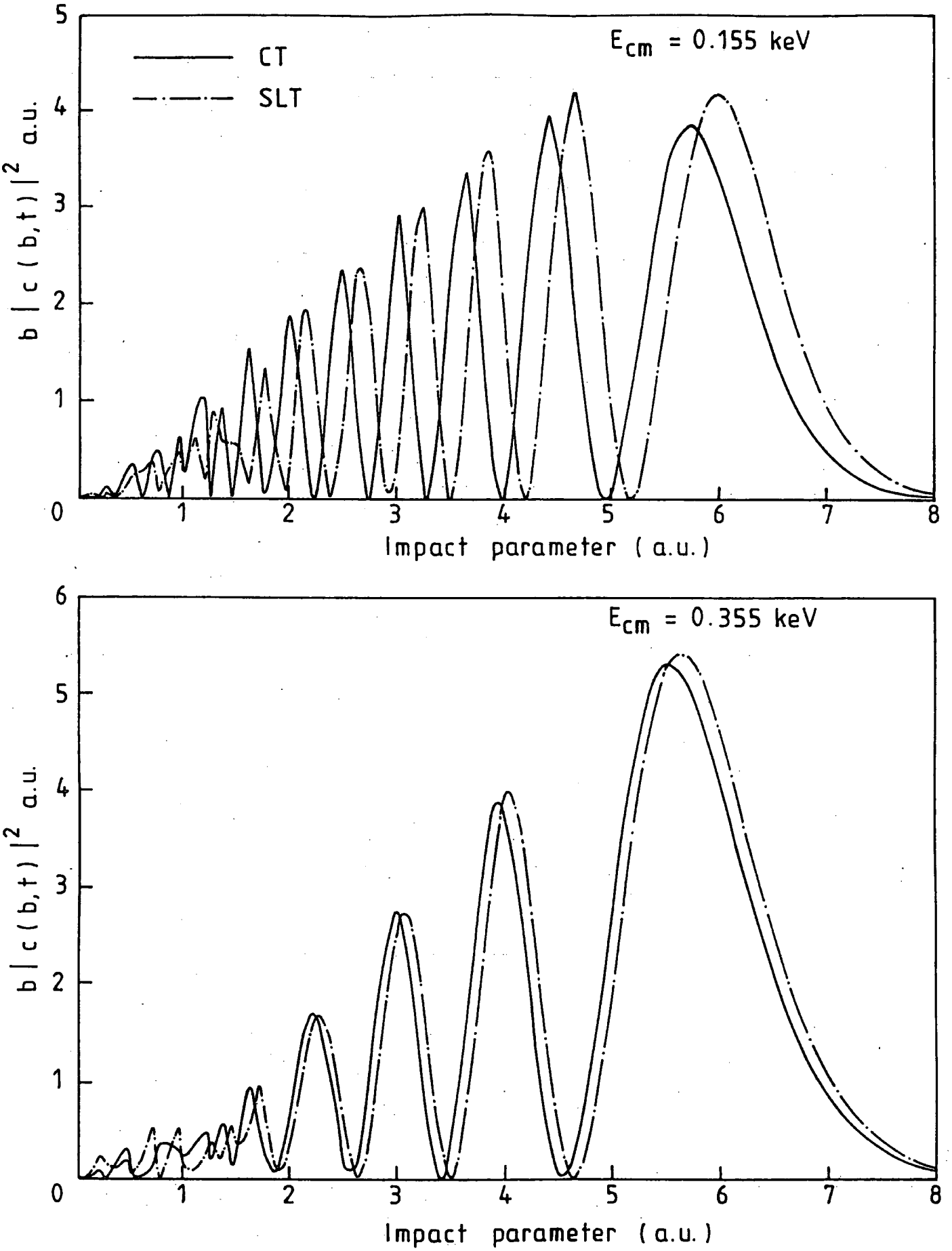

Figure 5.1 Be^{++} and H Collisions: Charge Exchange to Be^{+} (2s) and H^{+}. The Variation of $b|c(b,t)|^2$ with Impact Parameter.

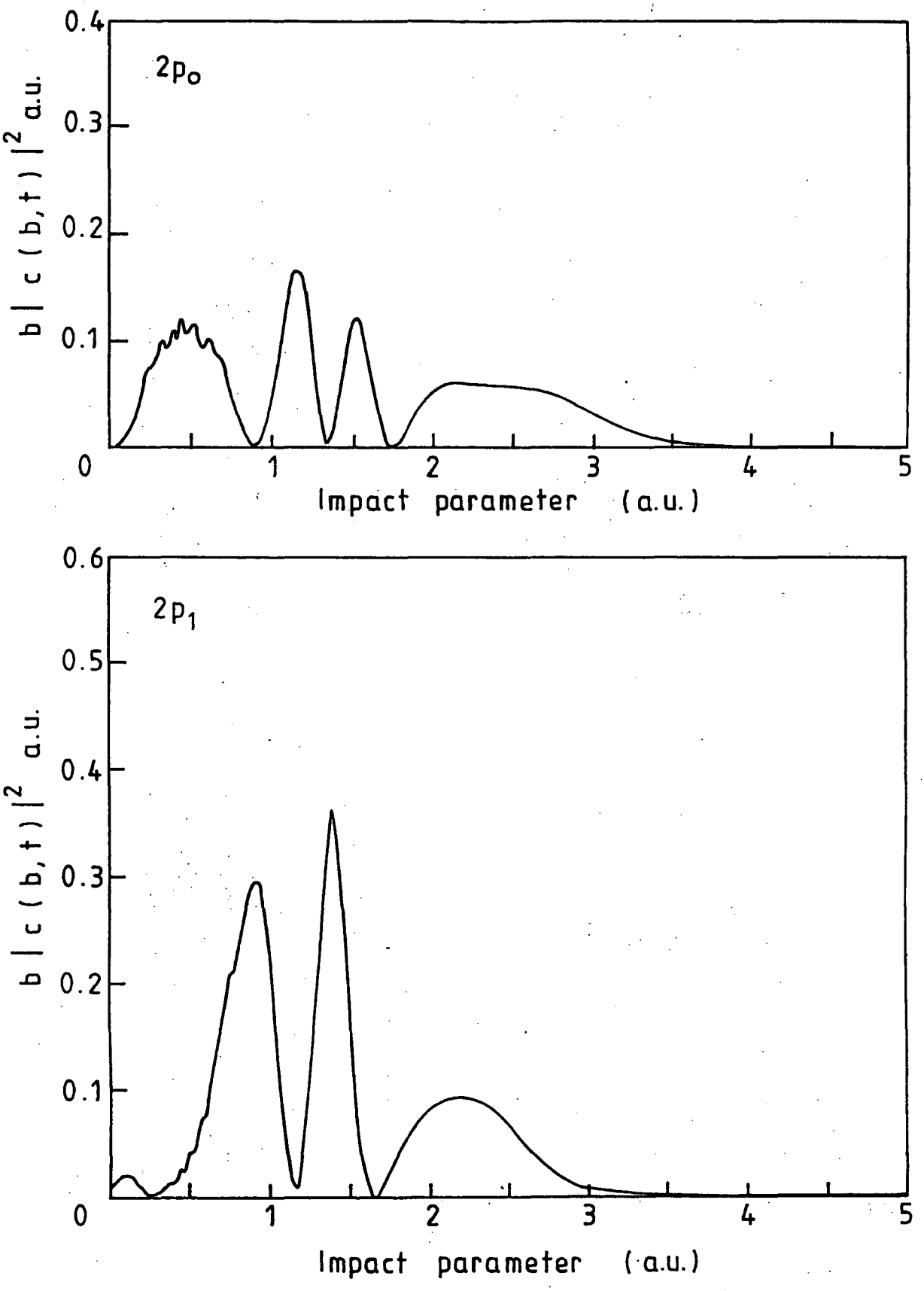

Figure 5.2 Be^{++} and H Collisions: Charge Exchange to Be^{+} $(2p_o)$ - H^{+} and $Be^{+}(2p_1)$ - H^{+}. The Variation of $b|c(b,t)|^2$ with Impact Parameter.

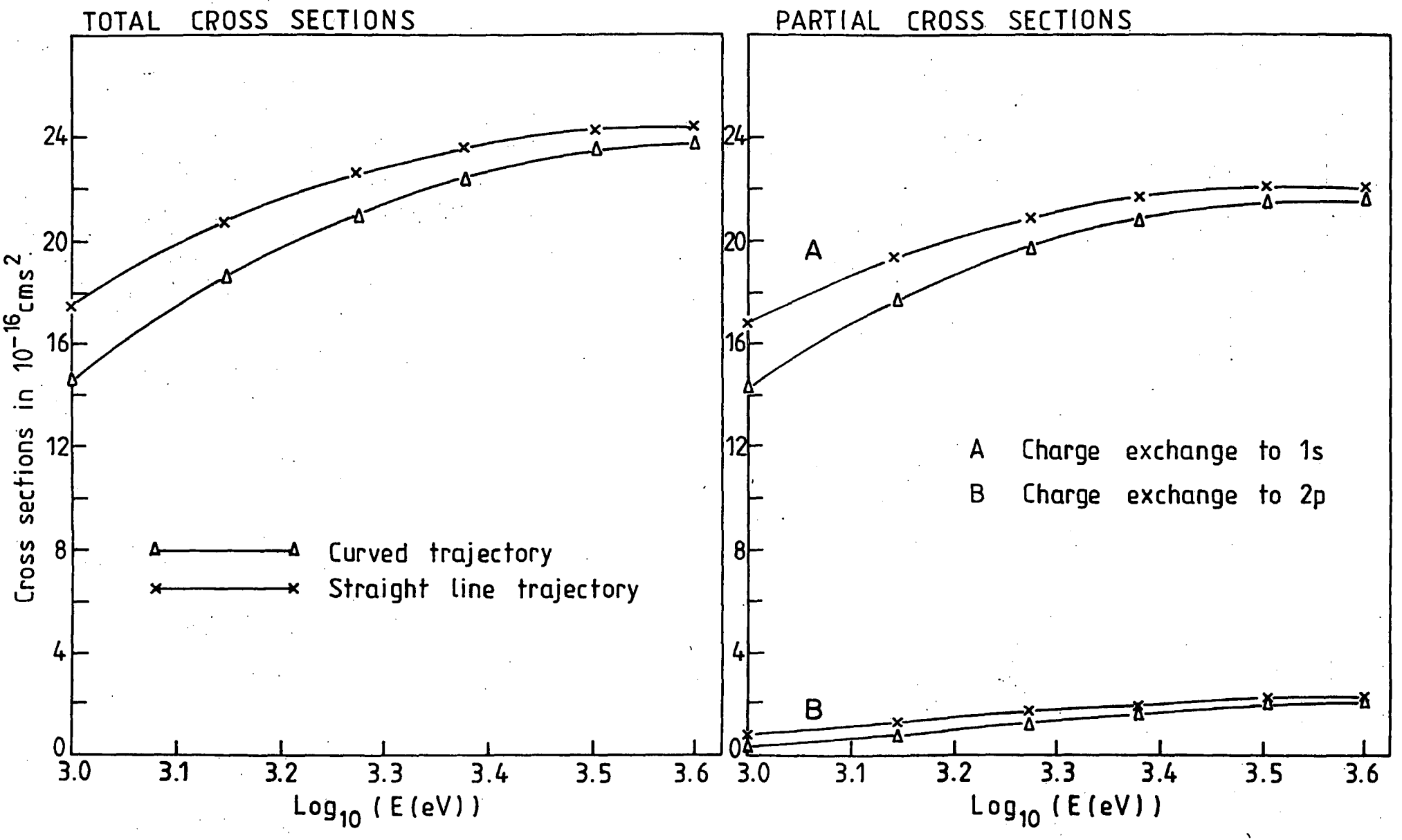

Figure 5.3 Be^{++} and H Collisions: Total and State-selective Charge Exchange Cross-sections.

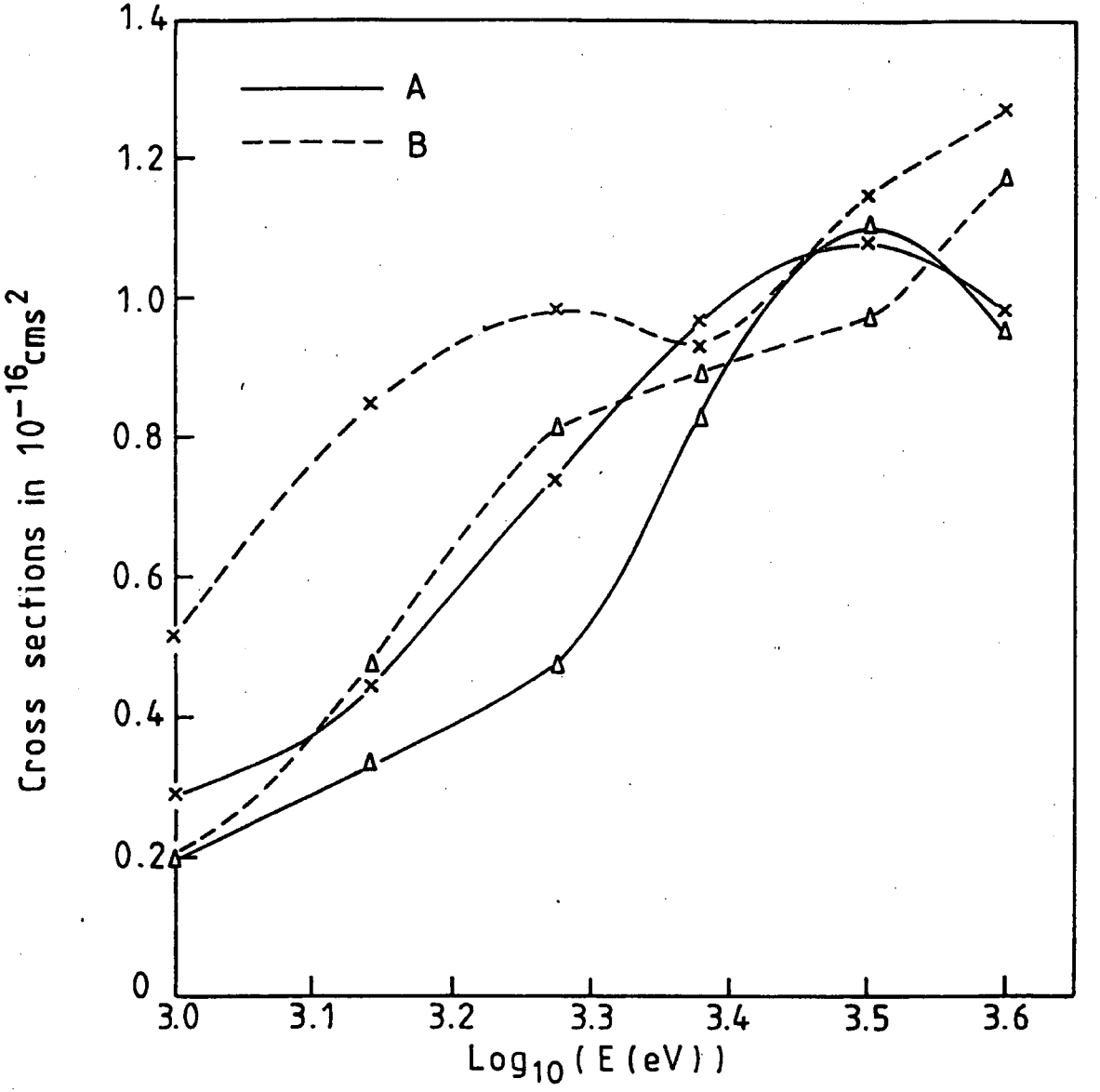

Figure 5.4 Be^{++} and H Collisions: Charge Exchange Cross-sections to:- (A) $Be^{+}(2p_o)$ - H^{+} and (B) $Be^{+}(2p_1)$ - H^{+}. × Present Straight-Line. Δ Present Curved Trajectory.

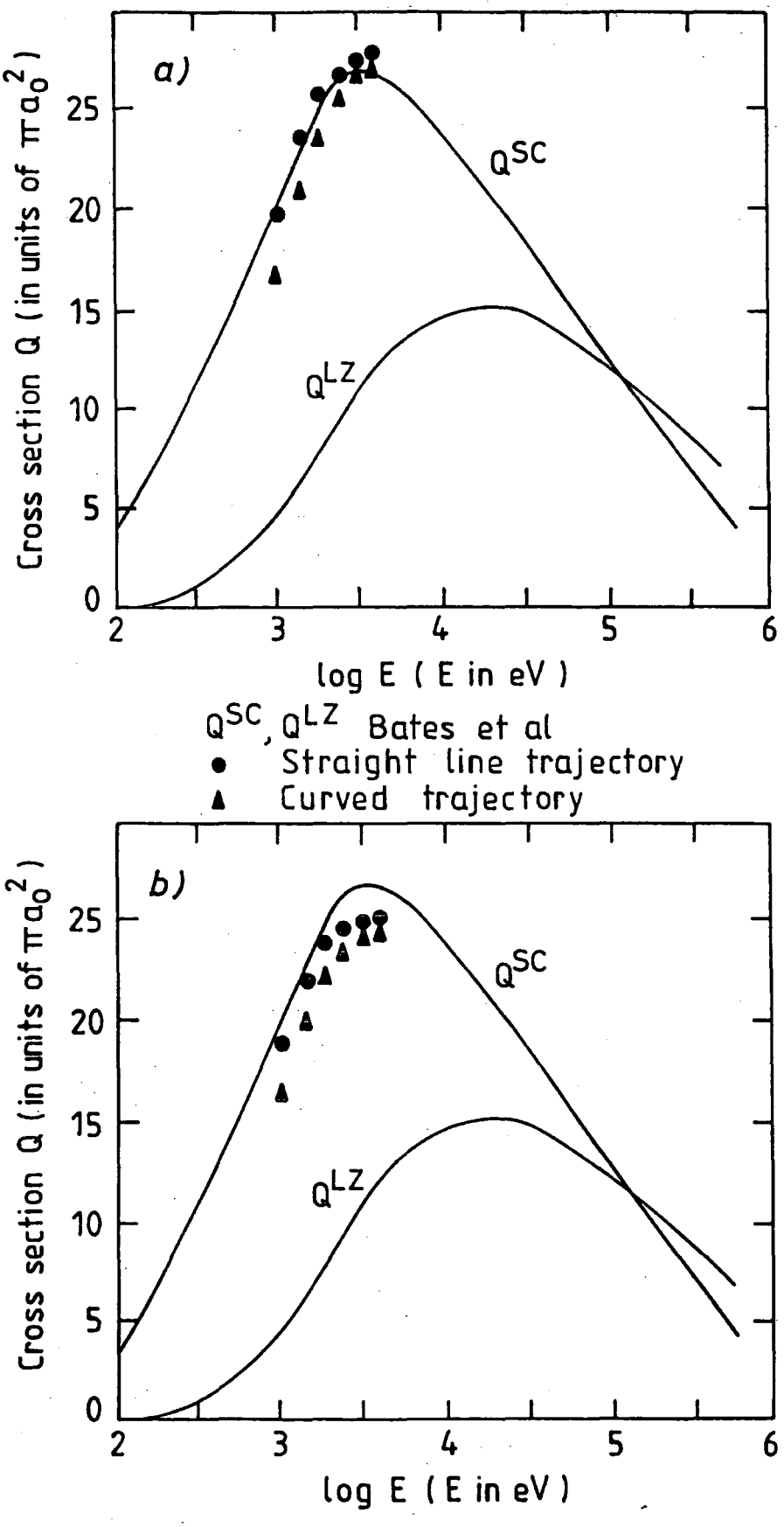

Figure 5.5 Be^{++} and H Collisions: Comparison of the Results of Bates et al. (1964) with (a) Present Total Charge Exchange Cross-sections, 5 state basis. (b) Present Charge Exchange Cross-sections to $Be^{+}(2s)$ - H^{+}.

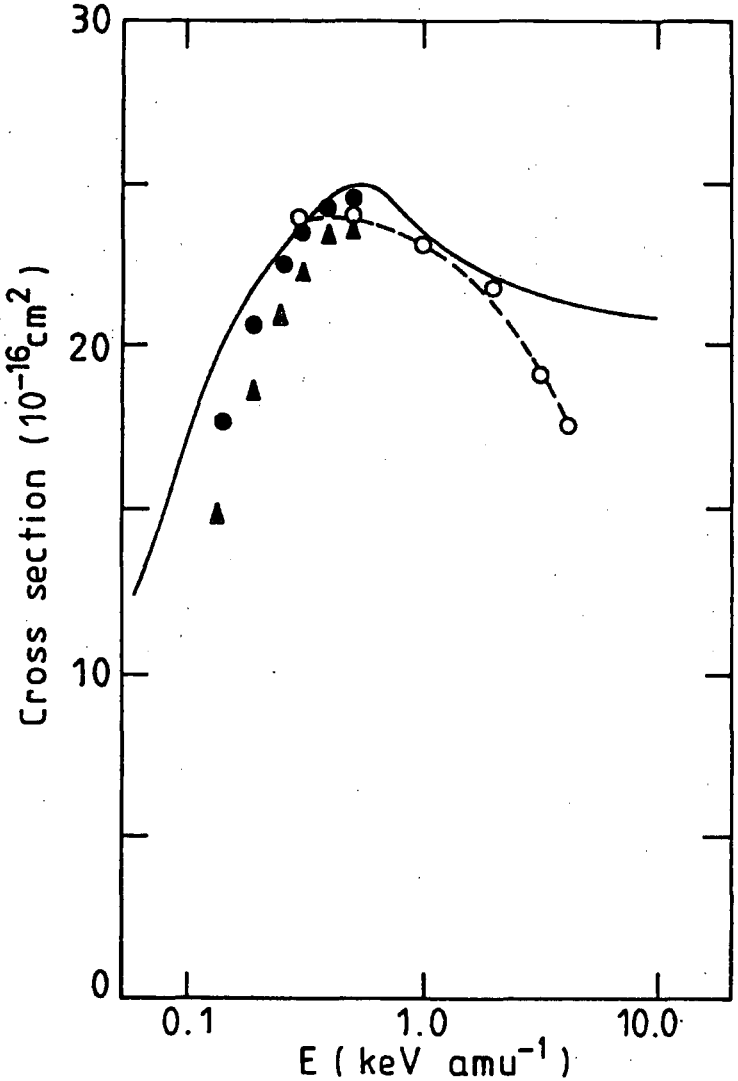

Fig. 5.6 Be^{++} and H Collisions:
Total Charge Exchange Cross Sections.
——— Wetmore et al, o Shingal,
● Present Straight-Line,
▲ Present Curved Trajectory.

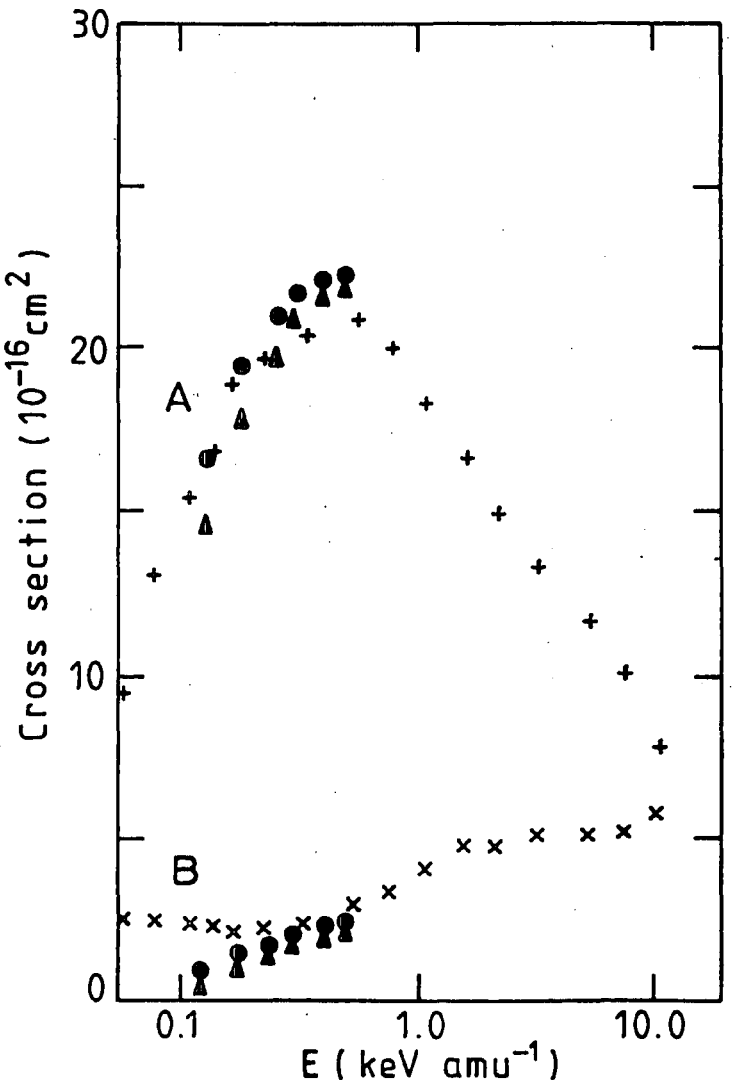

Fig. 5.7 Be^{++} and H Collisions:
A) Charge Exchange Cross-Sections to Be^+ (2s) - H^+.
+ Wetmore et al, • Present Straight-Line.
▲ Present Curved Trajectory.

B) Charge Exchange Cross Sections to Be^+ (2p) - H^+.
x Wetmore et al, ● Present Straight-Lin
▲ Present Curved Trajectory.

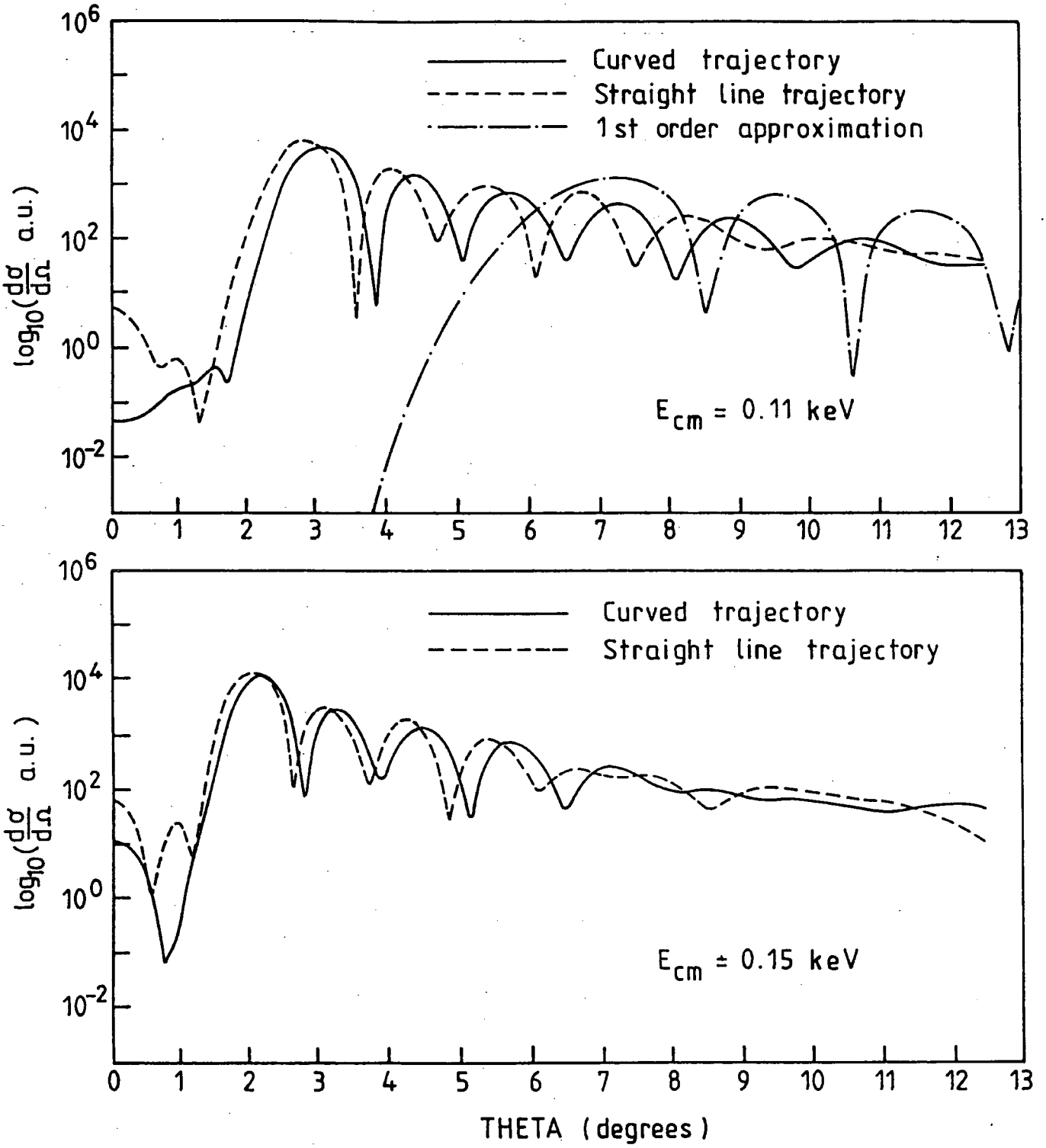

Figure 5.8 Be^{++} and H Collisions: Charge Exchange Differential Cross- sections to $Be^{+}(2s)$ - H^{+} at Centre of Mass Energies of 0.11 and 0.15 keV.

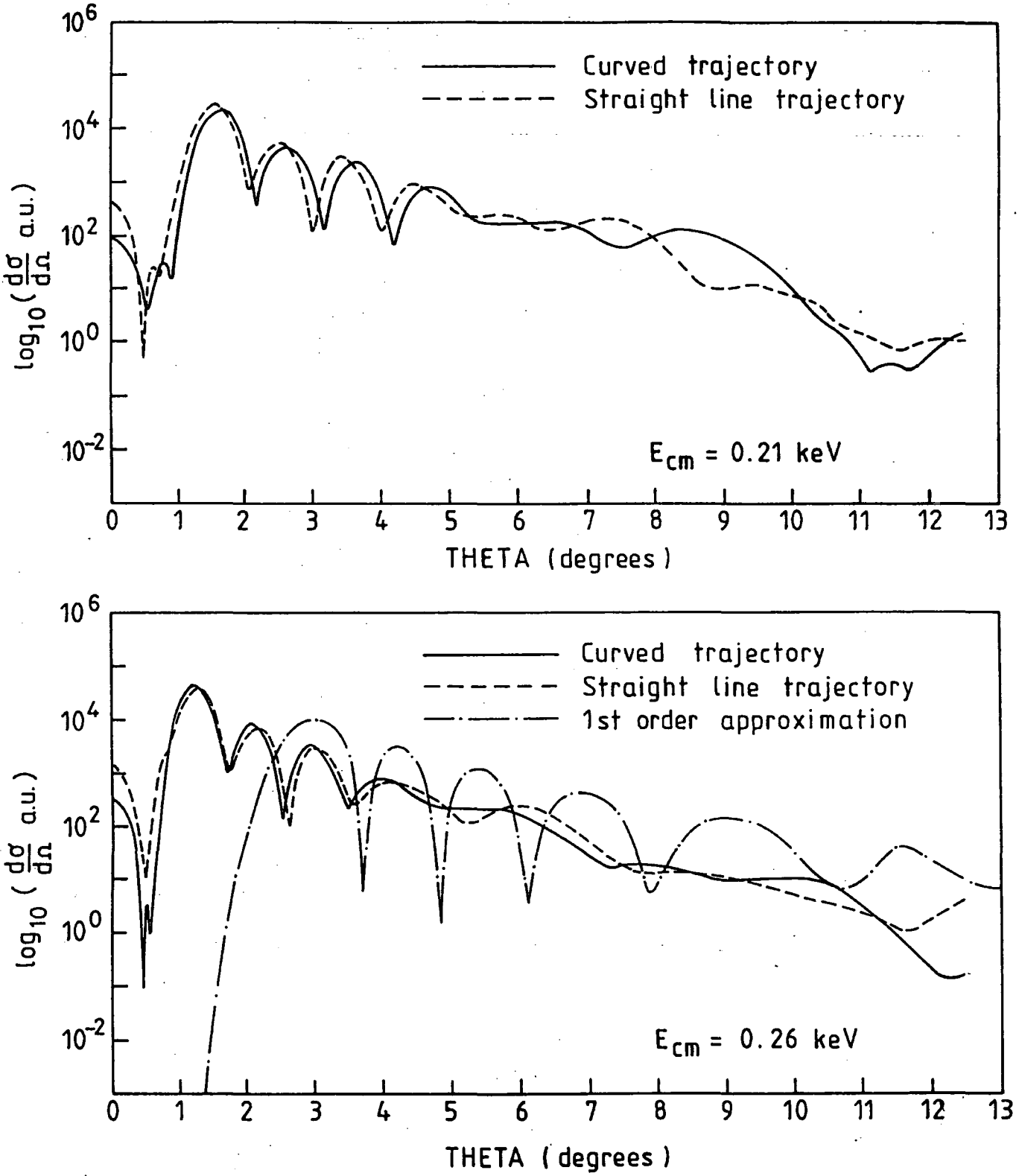

Figure 5.9 Be^{++} and H Collisions: Charge Exchange Differential Cross-sections to $Be^{+}(2s)$ - H^{+} at Centre of Mass Energies of 0.21 and 0.26 keV.

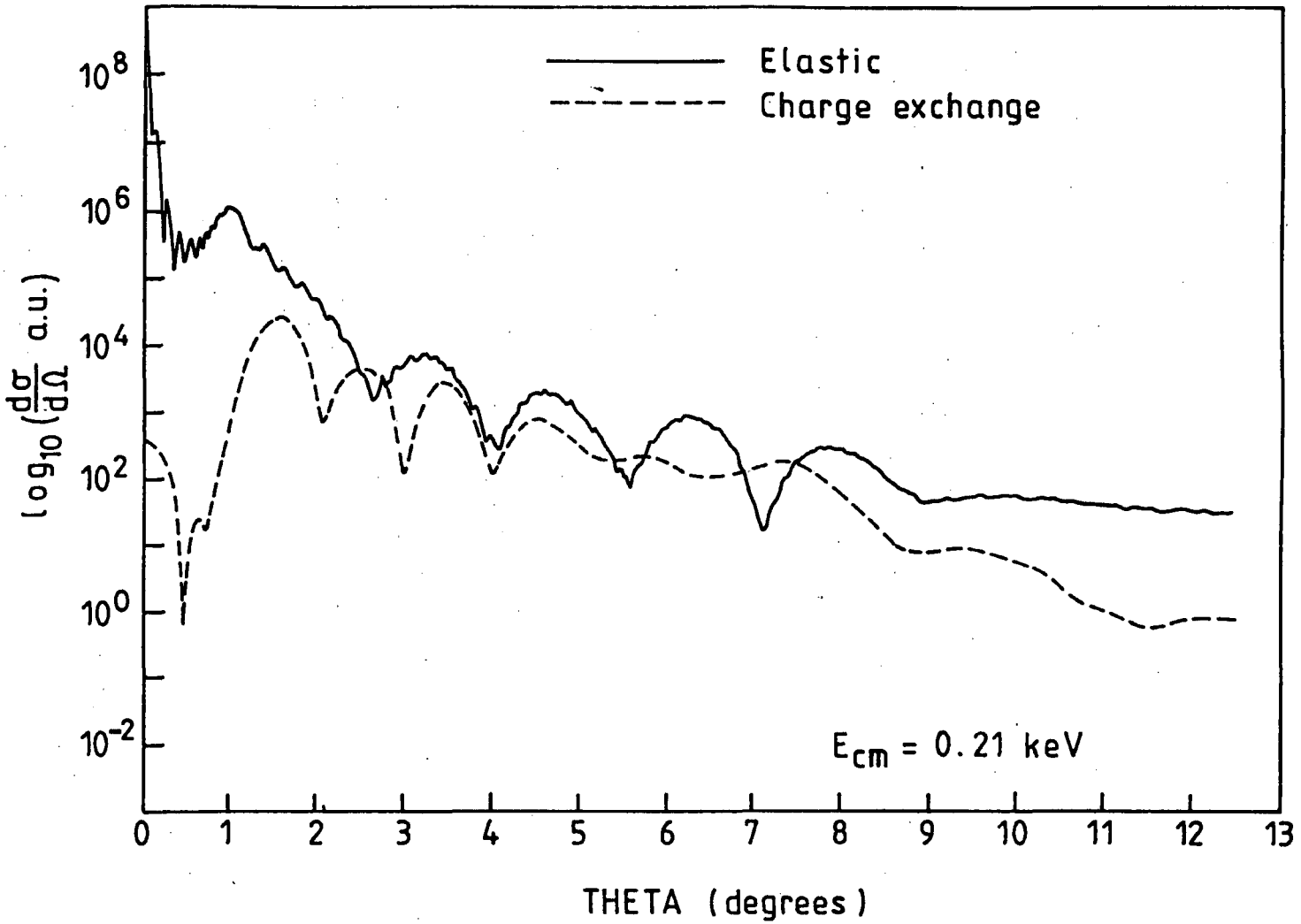

Fig. 5.10 Be^{++} and H Collisions: Differential Cross-Sections - Comparison of Elastic Channel with Charge Transfer to Be^{+} (2s) - H^{+}.

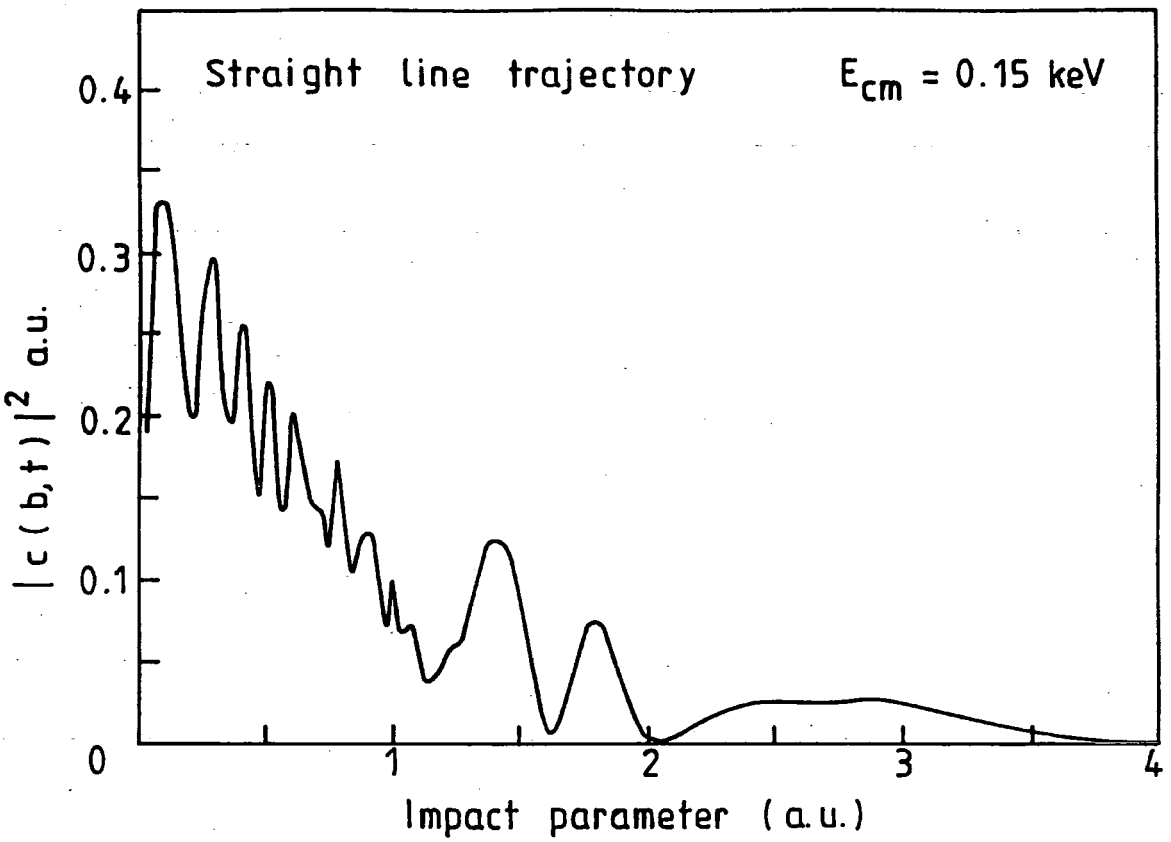

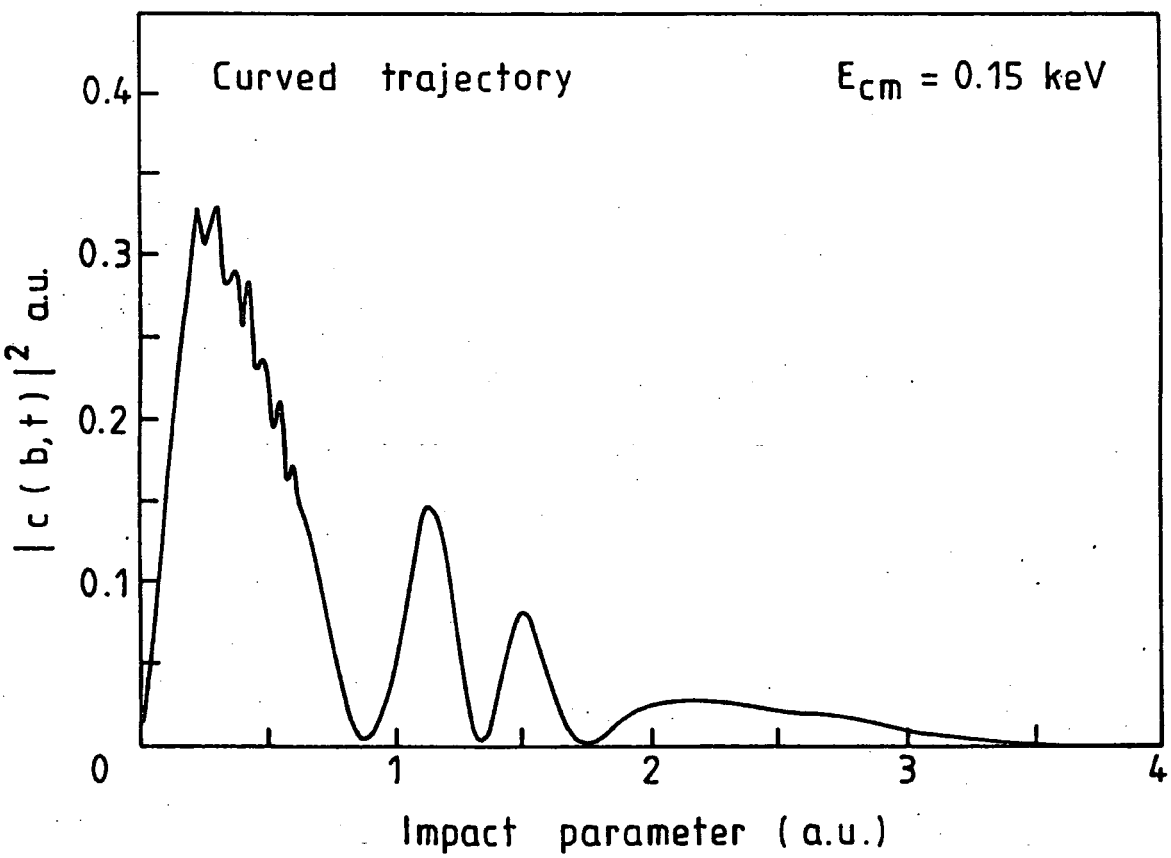

Figure 5.11 Be^{++} **and H Collisions: Probabilities for Charge Exchange to** $Be^{+}(2p_o)$ **-** H^{+} **at** E_{cm} **= 0.15 keV: Trajectory Effects.**

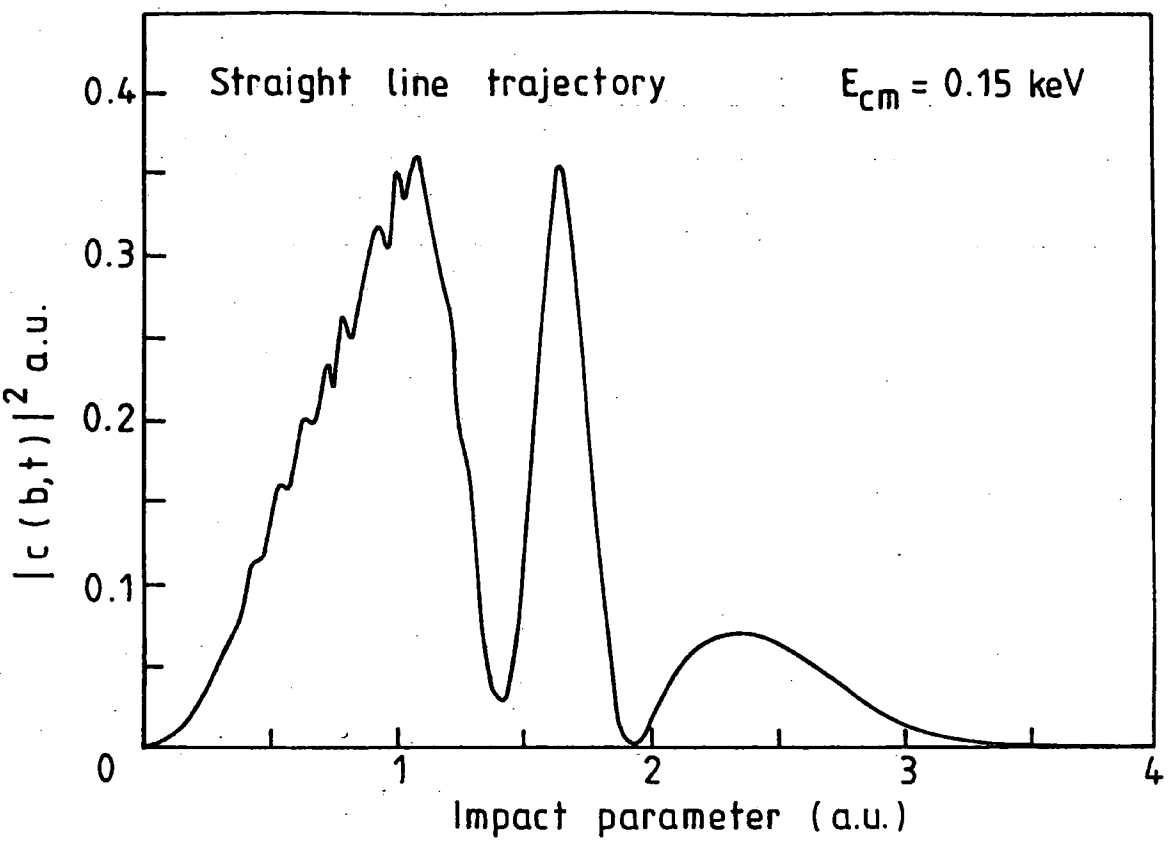

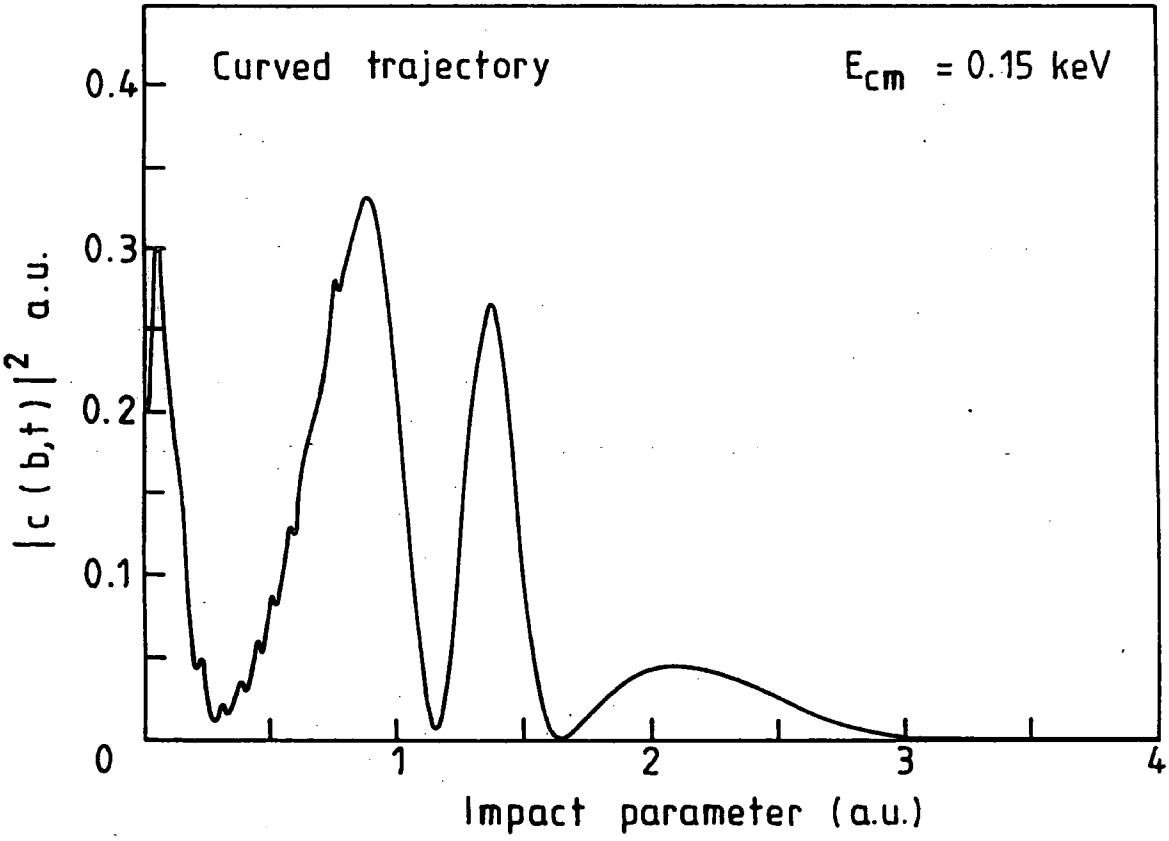

Figure 5.12 Be^{++} **and H Collisions: Probabilities for Charge Exchange to** $Be^{+}(2p_1)$ **-** H^{+} **at** E_{cm} **= 0.15 keV: Trajectory Effects.**

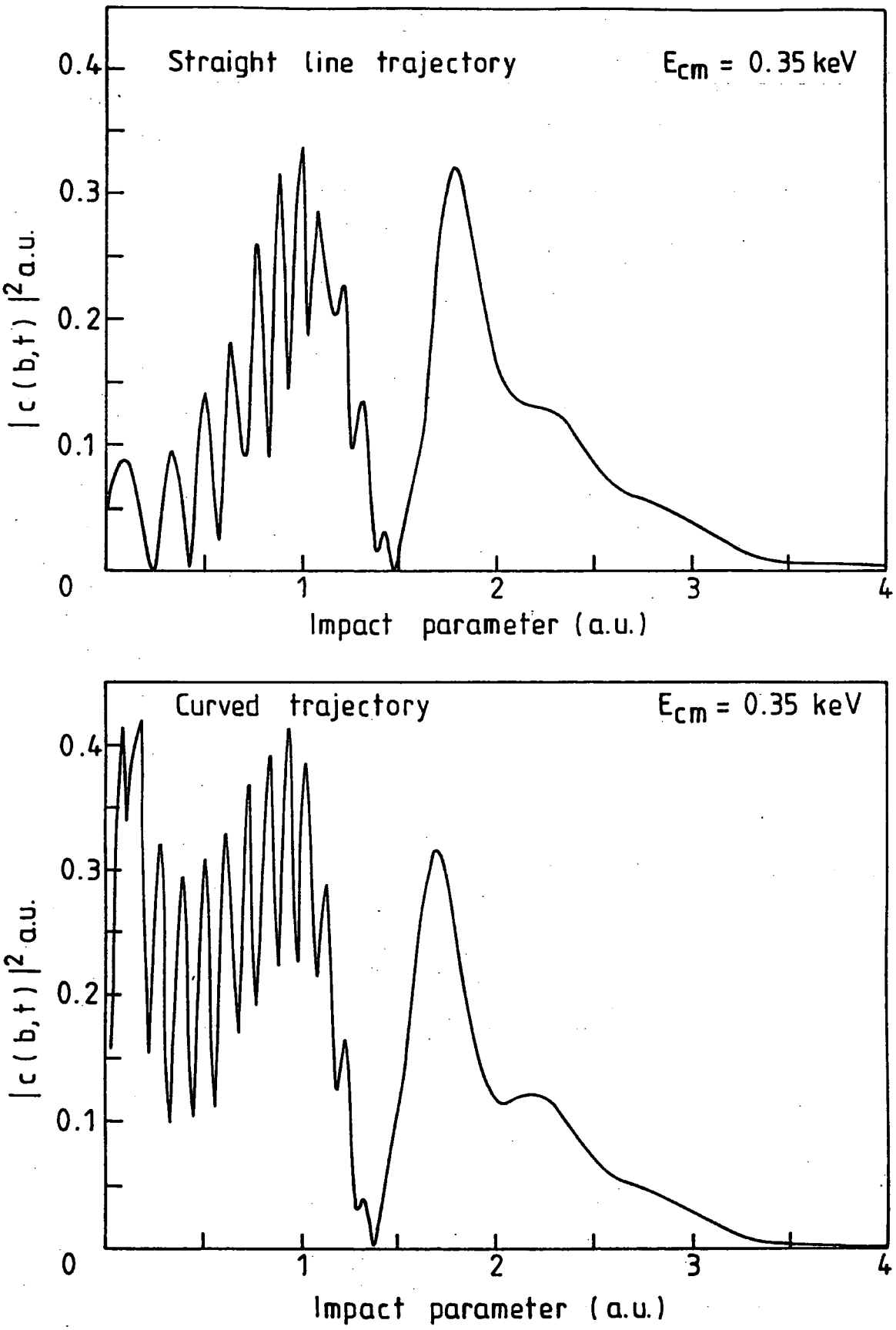

Figure 5.13 Be^{++} and H Collisions: Probabilities for Charge Exchange to $Be^{+}(2p_o)$ - H^{+} at E_{cm} = 0.355 keV: Trajectory Effects.

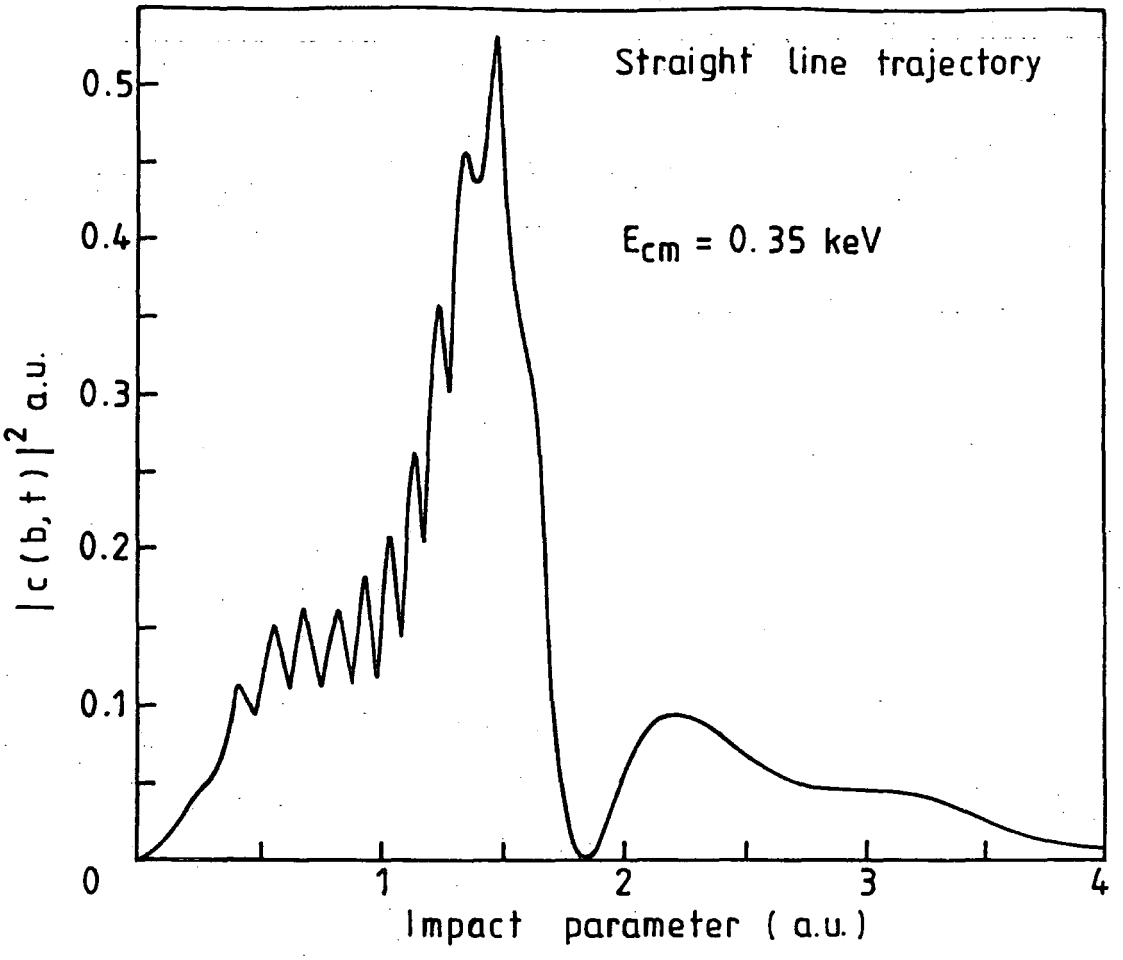

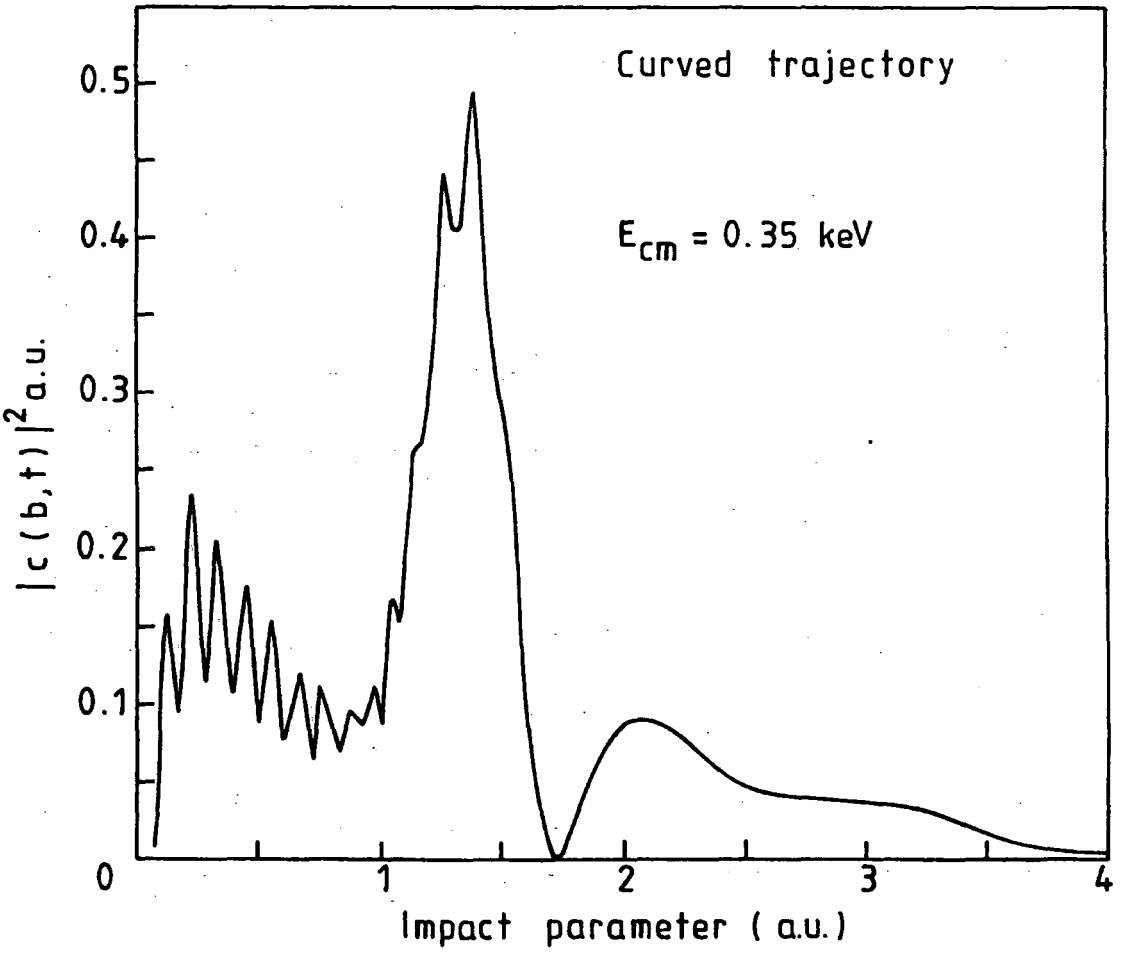

Figure 5.14 Be^{++} **and H Collisions: Probabilities for Charge Exchange; to** $Be^{+}(2p_1)$ **-** H^{+} **at** E_{cm} **= 0.35 keV: Trajectory Effects.**

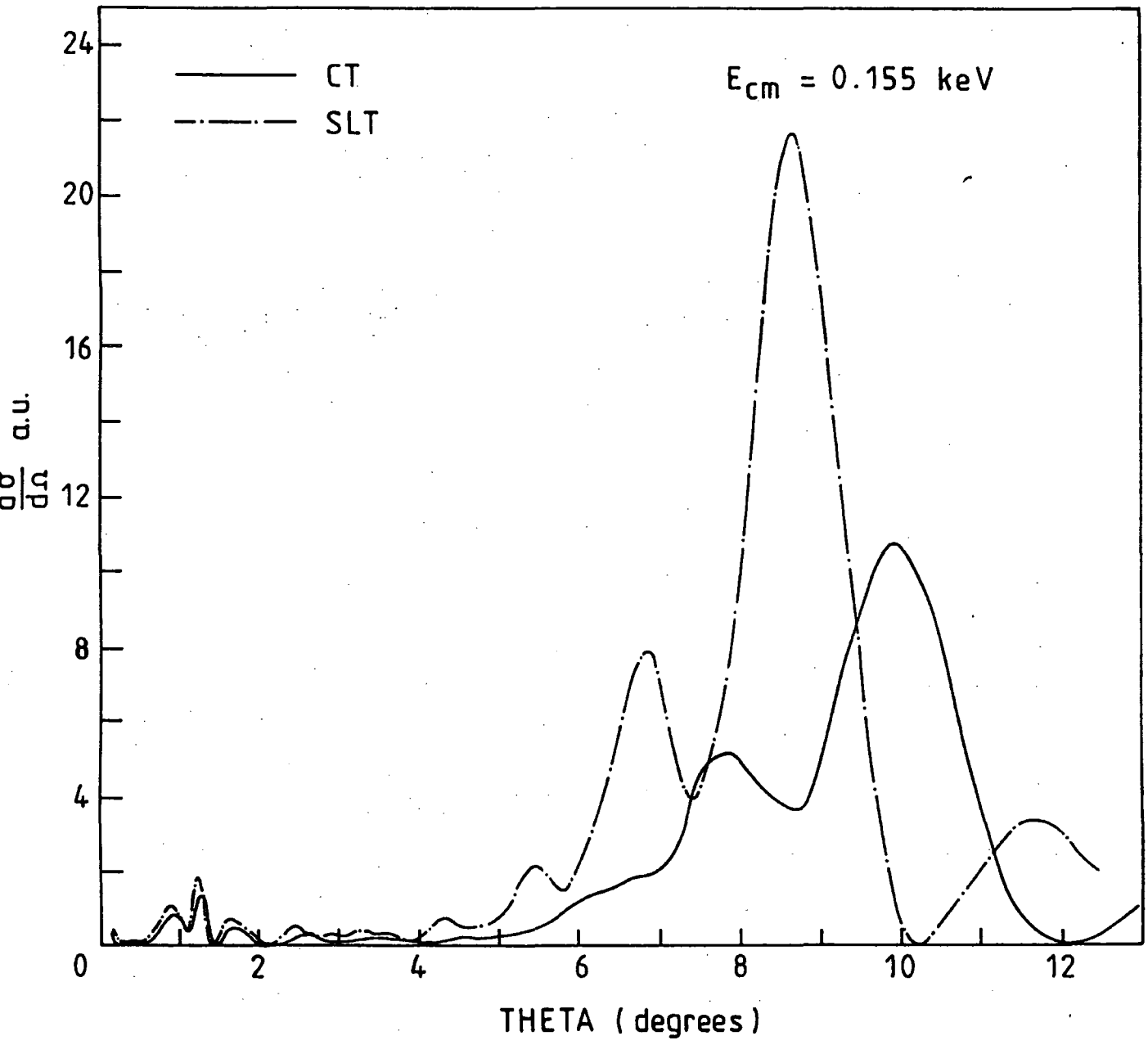

Figure 5.15 Be^{++} and H Collisions: Differential Cross-sections for Charge Exchange to $Be^{+}(2p_o)$ - H^{+} at E_{cm} = 0.15 keV: Trajectory Effects.

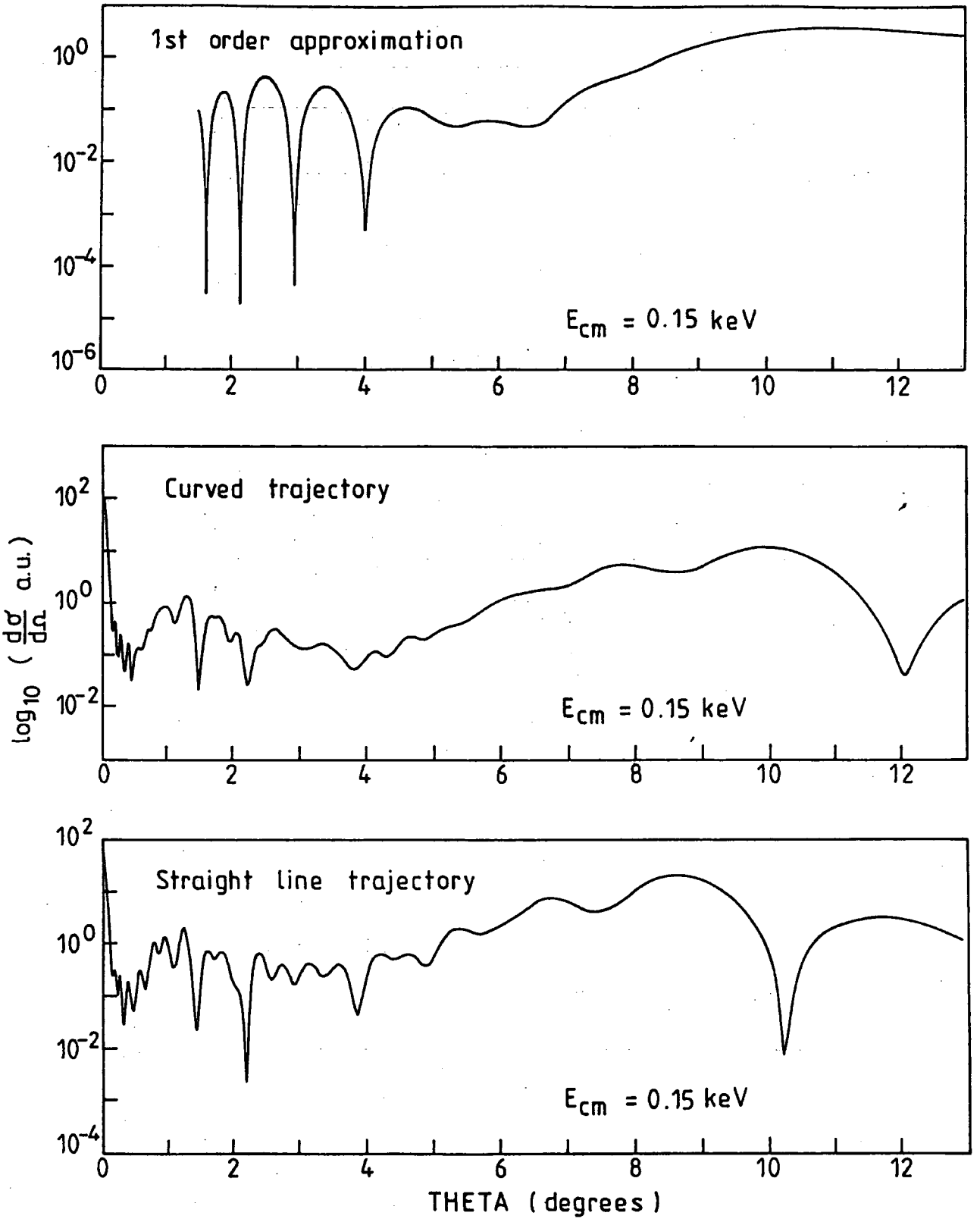

Figure 5.16 Be^{++} and H Collisions: Differential Cross-sections for Charge Exchange to $Be^+(2p_o)$ - H^+ at E_{cm} = 0.15 keV: Trajectory Effects.

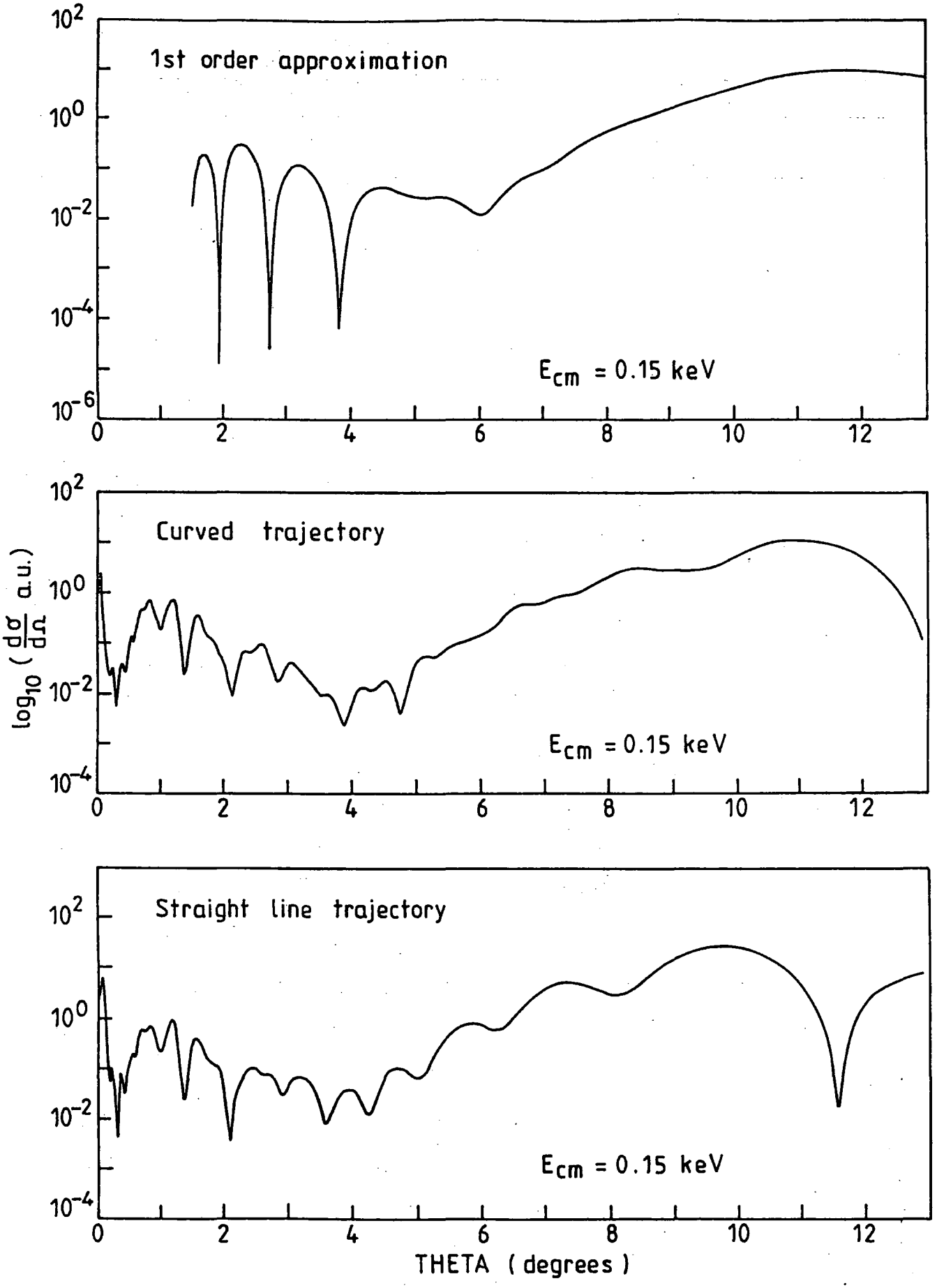

Figure 5.17 Be^{++} and H Collisions: Differential Cross-sections for Charge Exchange to $Be^{+}(2p_1)$ - H^{+} at E_{cm} = 0.15 keV: Trajectory Effects.

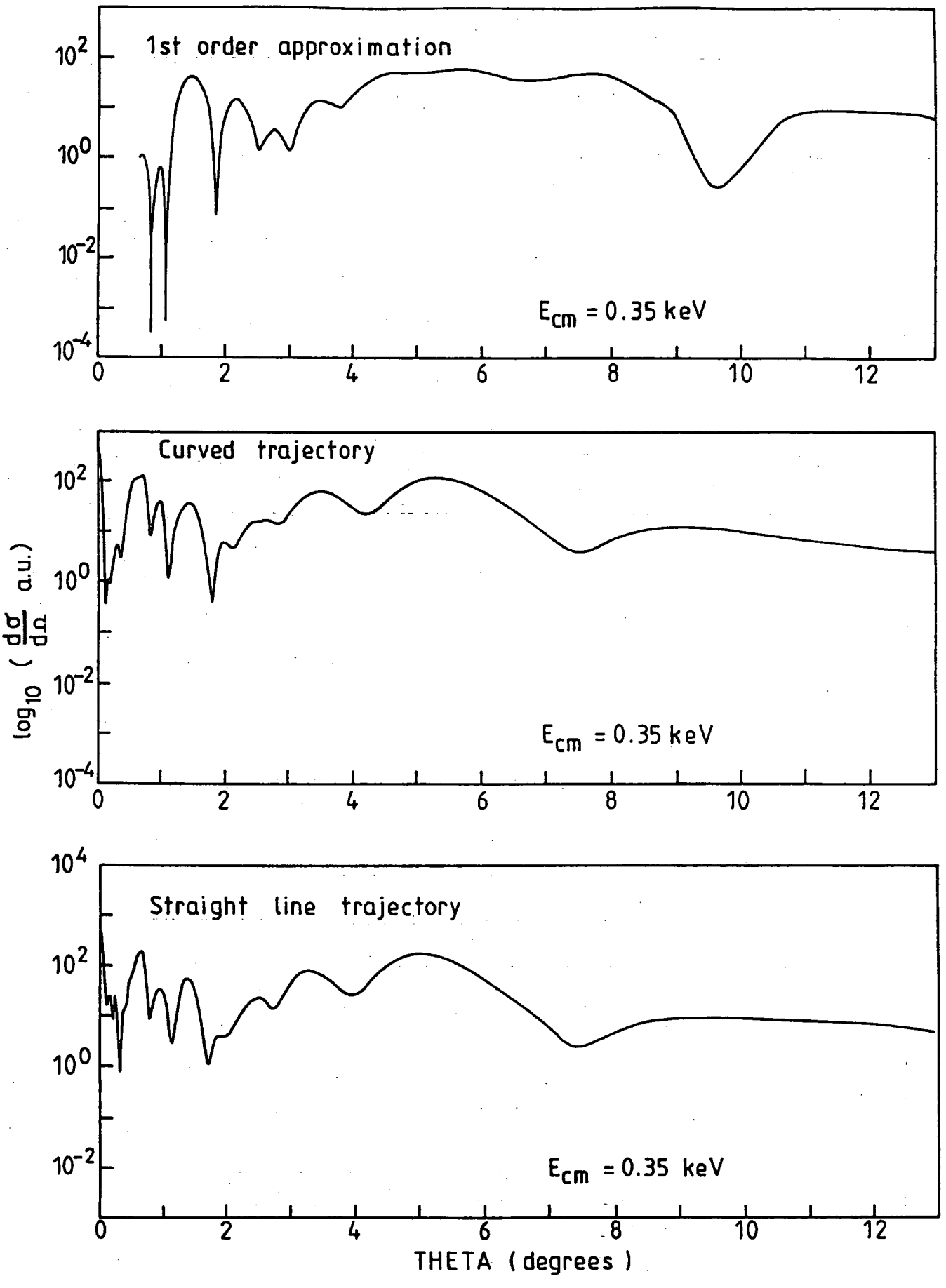

Figure 5.18 Be^{++} **and H Collisions: Differential Cross-sections for Charge Exchange to** $Be^{+}(2p_o)$ **-** H^{+} **at** E_{cm} **= 0.35 keV: Trajectory Effects.**

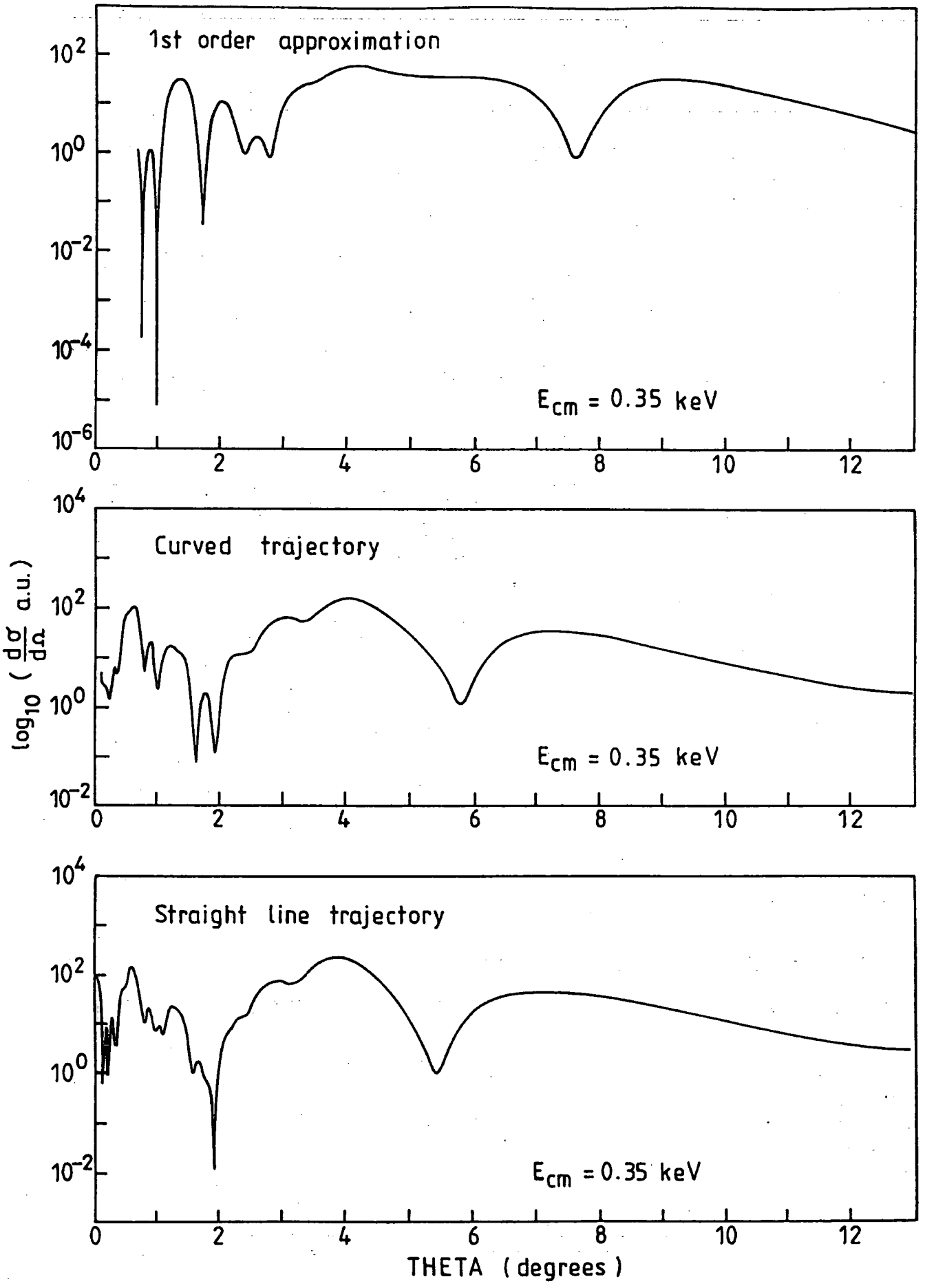

Figure 5.19 Be^{++} and H Collisions: Differential Cross-sections for Charge Exchange to $Be^{+}(2p_o)$ - H^{+} at E_{cm} = 0.35 keV: Trajectory Effects.

Level (ne)	Eigenenergy (a.u.)
n = 2 l = 0	-0.6693
n = 2 l = 1	-0.5241
n = 3 l = 0	-0.2683

Parameters level	i	P_i	α_i
l = 0	1	0	0.5833
	2	1	0.5833
	3	0	0.4464
	4	1	0.4464
	5	2	0.4464
	6	0	1.0304
	7	1	1.0304
	8	0	0.2887
l = 1	1	1	0.6832
	2	1	0.3494
	3	2	0.3494
	4	1	0.2183
	5	2	2.4583
	6	2	4.4583

Table 5.1: Be^+ Wave-functions and Eigenenergies. $\phi_i = \sum_i C_i\, r^{Pi} \exp(-\alpha_i r)$

Table 5.2

E_{cm}(keV)	Cross Sections (10^{-16} cms^2)		
	Straight Line Trajectories	Curved Trajectories	Shingal
	Charge Exchange to 2s		
0.1111	16.76	14.37	
0.1555	19.34	17.77	
0.2111	20.87	19.62	
0.2666	21.66	20.61	21.947
0.3555	21.93	21.47	
0.4444	21.03	21.55	21.644
	Charge Exchange to $2p_o$		
0.1111	0.296	0.204	
0.1555	0.444	0.334	
0.2111	0.740	0.476	
0.2666	0.970	0.829	0.995
0.3555	1.006	1.104	
0.4444	0.981	0.960	1.015
	Charge Exchange to $2p_1$		
0.1111	0.517	0.204	
0.1555	0.847	0.477	
0.2111	0.986	0.815	
0.2666	0.934	0.895	1.047
0.3555	1.165	0.972	
0.4444	1.271	1.174	1.379

Cross-sections for Charge Exchange in Be^{++} - H Collisions - continued overleaf

Table 5.2. (continued

E_{cm}(keV)	SLT	CT	SHINGAL
Charge Exchange to 3s			
0.1111	0.0011	0.0003	
0.1555	0.0035	0.0014	
0.2111	0.0056	0.0020	
0.2666	0.0041	0.0039	0.0053
0.3555	0.0068	0.0060	
0.4444	0.0103	0.0067	0.0078
Total Charge exchange Cross Sections			
0.1111	17.57	14.78	
0.1555	20.64	19.62	
0.2111	22.61	20.91	
0.2666	23.57	22.33	23.99
0.3555	24.17	23.55	
0.4444	24.29	23.69	24.04

Table 5.2: Partial and Total Cross-sections for Charge Exchange in Be^{++} - H Collisions

E_{lab} (keV)	E_{cm} (keV)	V_{rel} 10^7 (cms/sec)	E_{lab} (keV/amu)	log (E_{lab} (eV))
1.00	0.111	7.2	0.125	3
1.40	0.155	10.21	0.175	3.146
1.89	0.211	13.78	0.236	3.276
2.40	0.266	17.50	0.300	3.38
3.2	0.355	23.33	0.400	3.505
4.0	0.444	29.16	0.50	3.602

Table 5.3: Conversion of Energy units for Be^{++} and H collisions

Chapter 6

Direct excitation and charge exchange in low energy muon$^+$ and hydrogen collisions

6.1 Muon$^+$ Production and Muon$^+$ - hydrogen collisions

Negatively or positively charged muons (μ^-, μ^+) are produced at MeV energies from $\pi \rightarrow \mu\nu$ decay.The work in this chapter has been concerned with muons in positive charge states, and further discussion will relate only to μ^+. For the purpose of collision experiments, in which excitation and charge exchange effects are to be measured, such highly energetic muons are of little use, and they must therefore be moderated to keV energies. Single crystal LiF and solid rare gases have been found to be successful moderators (Harshman 1987), and at keV energies, the process takes place mainly by means of ionization. After moderation, the slow muon$^+$ beams produced can be used in experiments similar to those already carried out with positron beams (Humberstone and McDowell, 1983).

At keV energies, charge exchange with the target atoms becomes important. An electron may be captured into a bound state with the μ^+ , forming Muonium (Mu = μ^+e^-). Muons have a mass of 207m$_e$ where m$_e$ is the mass of the electron and the reduced mass of the Muonium is $\frac{207}{208} = 0.995 \approx 1$. This compares with the hydrogen atom reduced mass of $\frac{1836}{1837} = 0.999 \simeq 1$. As the muon$^+$ is singly charged, Muonium can therefore be regarded as an isotope of hydrogen.

A calculation of total and partial cross-sections for muon$^+$ and hydrogen collisions has been carried out (Bransden and Forster, 1989). In addition to looking at trajectory effects, the other main aim of the calculation was to see if the cross-sections produced were the same as those found in proton-hydrogen collisions at the same relative velocity. In the related isotopic system H$^+$ - D, velocity scaling is expected to be correct at higher energies, due to the linearity of the trajectories at these energies (Rille et al, 1982). The merged beam experiments carried out on this system by Newman et al (1982) have shown that velocity scaling appears to

work for centre of mass energies above 4.0 eV. A wider mass difference between isotopes, such as would occur in μ^+ - H collisions, should test velocity scaling further (Fleming and Senba, 1987). The reduced masses of the H^+ -H, H^+-D and μ^+-H systems are shown below

	H^+ - H	H^+ - D	μ^+ - H
Reduced mass (a.u.)	918.2	1224.1	186.0

6.2 Internuclear Potentials for Muon$^+$ and hydrogen Collisions

In the two previous curved trajectory calculations described in Chapters four and five, the internuclear potential employed has been restricted to the simple repulsive coulomb potential. No terms have been included to describe distortion effects due to the polarisation of the target atom, or the electrostatic field due to the electron. It was decided to include some of these effects in the calculations for the processes 6.1.1 and 6.1.2. Cross sections were accordingly calculated for a straight line zero potential model (SLT) and for three other potentials:-

a) Incorporating a repulsive coulomb potential (CT model).

b) Using a shorter range electro- static potential (ST model).

The static potential in a one electron system can be found from the integral

$$V_{ST}^{H}(R) = \pm \int \mid \phi^{H}(r) \mid^2 \left(\frac{1}{R} - \frac{1}{|\vec{R} - \vec{r}|} \right) d\vec{r} \qquad (6.1)$$

where ϕ^H(r) is the ground state hydrogenic wave function, $\phi^H(r) = (\frac{1}{\pi^{\frac{1}{2}}}) \exp(-r)$ 1/R represents the internuclear repulsion and $\frac{1}{|\vec{R}-\vec{r}|}$ is the interaction of the electron with the projectile ion (McDaniel and McDowell,1972).

$$V_{ST}^{H}(R) = \left(1 + \frac{1}{R}\right) exp(-2R) \qquad (6.2)$$

This repulsive potential reduces to 0 exponentially at large R, which accounts for its shorter range than the simple coulomb potential.

c) A model using a combination of static and long range polarisation potentials (PST).

The ST model ignores distortion of the atom during the collision due to polarisation effects. To remedy this, a suitable polarisation potential due to Bethe (Bethe and Salpeter, 1957) has been used in these calculations.

$$V_{pol}^{H} = -\frac{9}{4R^4}\{1 - \frac{1}{3}e^{-2R}(1 + 2R + 6R^2 + \frac{20}{3}R^3 + \frac{4}{3}R^4) - \frac{2}{3}(1+R)^4 e^{-4R}\} \qquad (6.3)$$

In the limit of large R, the polarisation term reduces to the long range dipole interaction which is proportional to $1/R^4$. The combined potential used in the PST model is therefore

$$W(R) = V_{ST}^{H}(R) + V_{pol}^{H}(R) \tag{6.4}$$

Expression 6.5 gives a more realistic potential than a purely repulsive interaction, although V_{pol} can overestimate the long range attraction (Bransden,1969) The variation with R of the potentials used in the curved trajectory models, are shown in Fig 6.1 for a single muon impact energy of 100.0 eV at an impact parameter of 0.48 a.u.. The corresponding trajectories produced are shown in Figure 6.2. The CT and ST potentials are repulsive at all values of R as expected, whereas the combined PST potential is weakly attractive at intermediate nuclear distances.

6.3 Results

Partial and total cross-sections have been calculated for the processes

$$\mu^+ + H(1s) \rightarrow \mu^+ + H^*(n,e) \tag{6.5}$$

Direct excitation

$$\mu^+ + H(1s) \rightarrow Mu(n\ell) + H^+ \tag{6.6}$$

Charge exchange total cross-sections were first calculated using a two state basis with 1s states on both centres, for four μ^+ impact energies, 15, 35, 140, and 2818.4 eV. The basis set was then increased to include 2s and 2p states on each centre, giving an eight state basis. This was used to calculate partial and total cross-sections for 6.6 and 6.7 at a range of impact energies (E_{lab}^{μ}) between 15 eV and 450 eV. 78 impact parameters within the range 0.0 a.u. $<$ b $<$ 8.3 a.u. were used at each energy.

6.4 Two state basis calculations

Total charge exchange cross-sections for a two state basis were calculated using the straight line, CT and PST models for two energies only, and SLT and PST cross sections were obtained for a further two energies. These results are below in Table 6.1. The SLT and PST results for 1s charge transfer agree within 2.5% for all the energy range. There is a much more marked trajectory effect on the cross-sections when coulomb trajectories are used, especially at 35 eV where the disagreement with straight line results is 11%.

6.5 Eight state basis calculations

In view of the relatively small trajectory effects found in the two state model,and the importance of n=2 states in proton hydrogen collisions, even at low collision energies (Bates and Williams, 1964), a larger basis was then employed to look at the effect of using different potentials on cross-sections to excited final channels. Total and partial cross-sections were produced using an eight state basis, with 1s, 2s, $2p_o$, $2p_1$ on each centre, for all four trajectory models. Total and partial cross-sections for the final excitation and charge transfer channels are in Tables 6.2, 6.3, and 6.5 - 6.13. Where graphical results are presented in the next section, the ST model cross-sections are shown only if they differ from the PST results to the accuracy of the graph.

6.5.1 Charge exchange to 1s

A comparison of total charge exchange cross-sections with those for charge transfer to 1s, in Tables 6.2 and 6.3, reveals that the latter is the overwhelmingly dominant reaction in this energy range, with a minimum of 96% of the total charge transfer cross-section being in this channel for all energies. The cross-sections show insignificant trajectory effects except in the CT model, where the 11% difference at 35 eV seen in the two state basis results is confirmed. At 450 eV the differences are less than 1% and are well within the accuracy of the programs. The integrands for charge transfer to 1s are shown in Figure 6.4 for straight line trajectories at impact energies of 70 eV and 450 eV. The maximum contribution to the integral 1.105. comes from impact parameters 2.0 a.u. $< b <$ 6.0 a.u., with the integrand becoming less oscillatory at higher energies.

6.5.2 Charge exchange and direct excitation to 2s states

The cross-sections to 2s are shown in Figure 6.5(a) and (b). The ST and PST cross-sections agree closely (within 2.6%) for all energies, due to the dominance of the short range repulsive static potential in the PST model. The effect of the polarisation potential on the 2s cross-sections is to increase them slightly above those obtained using the ST model. This is assumed to be due to the attractive part of the potential reducing the distance of closest approach and increasing the probability of the reaction taking place. This effect is minor compared to the effect of the repulsion however. The integrands for excitation and charge transfer at 190 eV are shown in Figure 6.6(a) and (b). The maximum contributions are at much smaller impact parameters than for charge exchange to 1s. The CT model has the smallest maximum for both excitation and charge transfer. Differences due to trajectory effects between the SLT and PST models are more pronounced in excitation than they are in charge transfer at this energy. Table 6.4 shows the values of W(R) at the distance of closest approach for the three curved trajectories at an impact parameter of 1.00 a.u. and impact energy of 190.00 eV.

The cross-sections for direct excitation to 2s of the hydrogen atom or charge

exchange to 2s states of μ^+ are shown in Tables 6.5 and 6.6. At 190 eV the CT cross-sections are respectively 23% and 26% lower than the SLT for charge transfer and excitation. The PST cross-sections are also less than the SLT, but by only 2% in charge transfer and 12% for excitation. At 450 eV the disagreement for excitation is less than 4% for all the models. For charge transfer at this energy, the PST and ST cross-sections show few trajectory effects and agree with the SLT results to within 1% whereas the CT cross sections are still 4% lower.

6.5.3 Charge exchange and Excitation to 2p States

Cross sections to 2p are shown plotted in Figure 6.7 and those for separate $2p_o$ and $2p_1$ states are in Figure 6.7. The figures are in Tables 6.7 - 11. For the energy range being considered, the $2p_o$ cross sections are considerable smaller than those to $2p_1$. All the cross-sections to $2p_o$ exhibit small local maxima at the lowest energies, after which the cross-sections increase with increasing energy, and are still rising at 450 eV. The CT model again has the lowest cross sections, which were still 18% below the SLT cross sections at 450 ev. The ST and PST cross-sections show fewer trajectory effects and are 6% lower than the straight line model at this energy.

The $2p_1$ cross-sections have several interesting features. The most significant of these, is that the use of a curved trajectory model leads to higher cross sections than the SLT for both excitation and charge transfer. Gaussorgues et al (1975b) found a similar effect on the probabilities to $2p_\pi$, using a common trajectory method to study proton-hydrogen collisions. The ST and PST cross-sections are consistently higher than the SLT, whereas the CT cross-sections are below those for the SLT model at the lower energies in the range, the curves crossing at 100 ev and 260 eV in excitation and charge exchange respectively. At 450 eV the results of all three curved trajectory models agree to within 2.0% in both excitation and charge transfer. These cross-sections are more than 11% higher than those for the SLT model for excitation, and 6% higher for charge transfer. The graphs of the integrands $b|\ c\ (b,t)|^2$ for excitation to $H(2p_1)$ at an impact energy of 400 ev (Figure 6.9), show that the higher cross-section in the case of the PST and CT models is due to larger contributions to the integral from small impact parameters, than in the straight line case. The effect of including curved trajectories is less obvious when cross-sections to $2p_o$ and $2p_1$ are combined, as in Figure 6.7, because the lower cross-sections to the former counteract the generally higher cross-sections to $2p_1$. The CT model cross-sections are very close to the straight line model at higher energies in the range. Because of the higher contributions from $2p_1$, the ST and PST cross-sections lie above the SLT. The cross-section graphs for excitation or charge exchange to 2p states are very similar, although small differences in detail are apparent in the figures.

6.6 Total Cross sections

Total cross-sections for charge exchange are shown in Figure 6.10 and for excitation in Figure 6.11 and Table 6.13. The charge exchange cross-sections are dominated by the large contributions from 1s and because of this, are more than an order of magnitude larger than the total excitation cross-sections. These charge exchange cross-sections decrease with increasing energy. The differences in the charge transfer cross-sections between the 2 state and the 8 state models were between 2%–3% over the energy range. Only when a coulomb potential was used was there any significant trajectory effect, and this was confined to the lower energies as expected. The direct excitation total cross-sections exhibit more obvious trajectory effects for all the curved trajectory models at lower energies. Both the ST and PST cross-sections lie above the zero potential case, due to the higher contributions from $2p_1$ in these models, whereas the CT cross-sections are lower. At 450 eV the differences are reduced to within the accuracy of the programs.

6.7 Velocity Scaling

For two isotopic systems consisting of ions A and B and A' and B, the laboratory impact energies of the two isotopes A' and A are related by

$$E_{lab}^{A'} = \frac{M_A'}{M_A} E_{lab}^{A} \tag{6.7}$$

using the relations,

$$E_{cm} = \frac{M_B}{M_A + M_B} E_{lab}^{A}, \quad v = \sqrt{\frac{2}{\mu}} E_{cm} \tag{6.8}$$

μ is the reduced mass of the system.

For comparison with proton-hydrogen results, which are presented in terms of proton impact energies, the impact or laboratory energies of the proton in terms of μ laboratory energies are :-

$$E_{lab}^{H} = \frac{M_H}{M\mu} E_{lab}^{\mu} \tag{6.9}$$

The range of muon laboratory energies used in these calculations is 15 eV < E_{lab}^{μ} < 450 eV, which corresponds to a range of proton impact energies 330 eV < E_{lab}^{H} < 3991 eV. The energies and the equvalent proton impact energies are given in Table 6.14.

Proton-hydrogen cross-section calculations for proton laboratory energies greater than one keV, have been carried out by numerous authors, including, Gallaher and Wilets (1968), Cheshire, Gallaher and Taylor (1969), Chidichimo-Frank and Piacentini (1974), Schinke and Kruger (1976), Crothers and Hughes (1978) and Kimura and Thorson (1981). Cross sections have been calculated using a variety

of basis sets and different formulations. For instance, Crothers and Hughes (1978) have used a molecular basis set with atomic type ETFs and Kimura and Thorson (1981) also used a molecular model. Cheshire et al (1969) used atomic bases, one with 1s,2s, and 2p bound states on each centre, and another with pseudostates added to the first basis, in order to model the molecular nature of the collision more closely.

At proton energies of less than five keV, cross-sections for direct excitation and charge exchange to 2s and 2p states have shown themselves to be extremely sensitive to the basis and method used. For comparison with the μ -H results presented above, we have used the results of Cheshire et al (1969), obtained using their basis without pseudostates, as this is the same as that used in the present work. While not giving as good a comparison with other proton-hydrogen collisions as when pseudostates are employed, these straight line cross-sections of Cheshire et al can be compared closely to the present results for proton impact energies greater than one keV. The results of velocity scaling can then be assessed more accurately.

The SLT charge exchange cross-sections obtained using the two state basis are in good agreement with the proton-hydrogen results of McCarroll (1961) for the same relative velocities, and are within 1% for all four energies.

Cross sections for straight line proton-hydrogen collisions were also calculated for the present work, using an eight state basis. The results agreed with μ^+ - H straight line cross-sections at the same relative velocity for all the energy range.

At proton impact energies of less than two keV, the proton-hydrogen cross-sections could be expected to be sensitive to trajectory effects and, to test velocity scaling at these lower energies, cross-sections were obtained for curved trajectory proton hydrogen collisions. The interatomic potential employed was 6.3, for direct comparison with the μ^+ - H PST calculations. Cross sections were calculated for seven energies in the range 133 eV $< E^H_{lab} <$ 3548.00 eV. μ^+ -H cross-sections are compared with H^+-H results in Figures 6.12 and 6.13. The cross-sections are shown plotted at the equivalent proton impact energies for comparison with the results of Cheshire et al at E^H_{lab} of 1, 2 and 4 keV. The cross-sections themselves are in Tables 6.15 - 18 . The agreement between the SLT results and those of Cheshire et al is very good, except for the cross sections for 2s, where the results at 2.0 keV equivalent proton energy disagree for both excitation and charge exchange by about 10%. 2.0 keV is the position of the maximum of the cross-section in this part of the energy range and the reason for the disagreement is not known. The curved trajectory results, also shown in Figures 6.12 and 6.13 disagree for energies below $E^{\mu}_{lab} < 260$ eV ($E^H_{lab} < 2306$ eV). The proton-hydrogen cross-sections are generally closer to the SLT results than are the muon$^+$-hydrogen, reflecting the heavier mass of the proton. However at certain low energies, for example for 2s excitation and charge transfer cross-sections at 15eV/133eV, the position is reversed. When the probabilities for the reactions are examined in Figure 6.14. These differences are found to be due to the behaviour of the probabilities at small impact parameters. The high probabilities at very small impact parameters, appearing in some proton-hydrogen results are not fully understood. When the differences in origin of the two systems are removed by forcing p = q = 0.5 in the muon-hydrogen system, the

μ^+-H probabilities agree with the H^+ - H probabilities, at all impact parameters except the smallest, where the differences still persist. It is possible that these are due to the fact that the programs were originally written for much higher collisions energies and the low energy calculations have exposed the limitations of the algorithms. These problems were only associated with certain H^+ - H results and do not affect the conclusions reached regarding velocity scaling, but further exploration is obviously necessary.

6.8 Discussion

From the results presented, it appears that velocity scaling can be used for all energies when considering total charge exchange cross-sections and charge exchange to 1s. For individual final states, the cross-sections agree qualitatively and are of the same order of magnitude, the exceptions being where a Coulomb potential is used at the lowest energies. It is possible that here the cross-sections could be underestimated because of the small mass of the muon. Where detailed cross-sections are required, velocity scaling is not accurate for muon impact energies of less than 350 eV, for final states other than charge exchange to 1s. This is especially true of cross-sections to individual 2p states.

Semiclassical low energy studies of proton hydrogen collisions using non-linear trajectories (Gaussorgues et al, 1975b, Schinke and Kruger,1976) have tended to look at differential cross-sections. Further work on μ^+-H collisions to consider velocity scaling in differential cross-sections, and the effect of using curved trajectories on these, would be worthwhile.

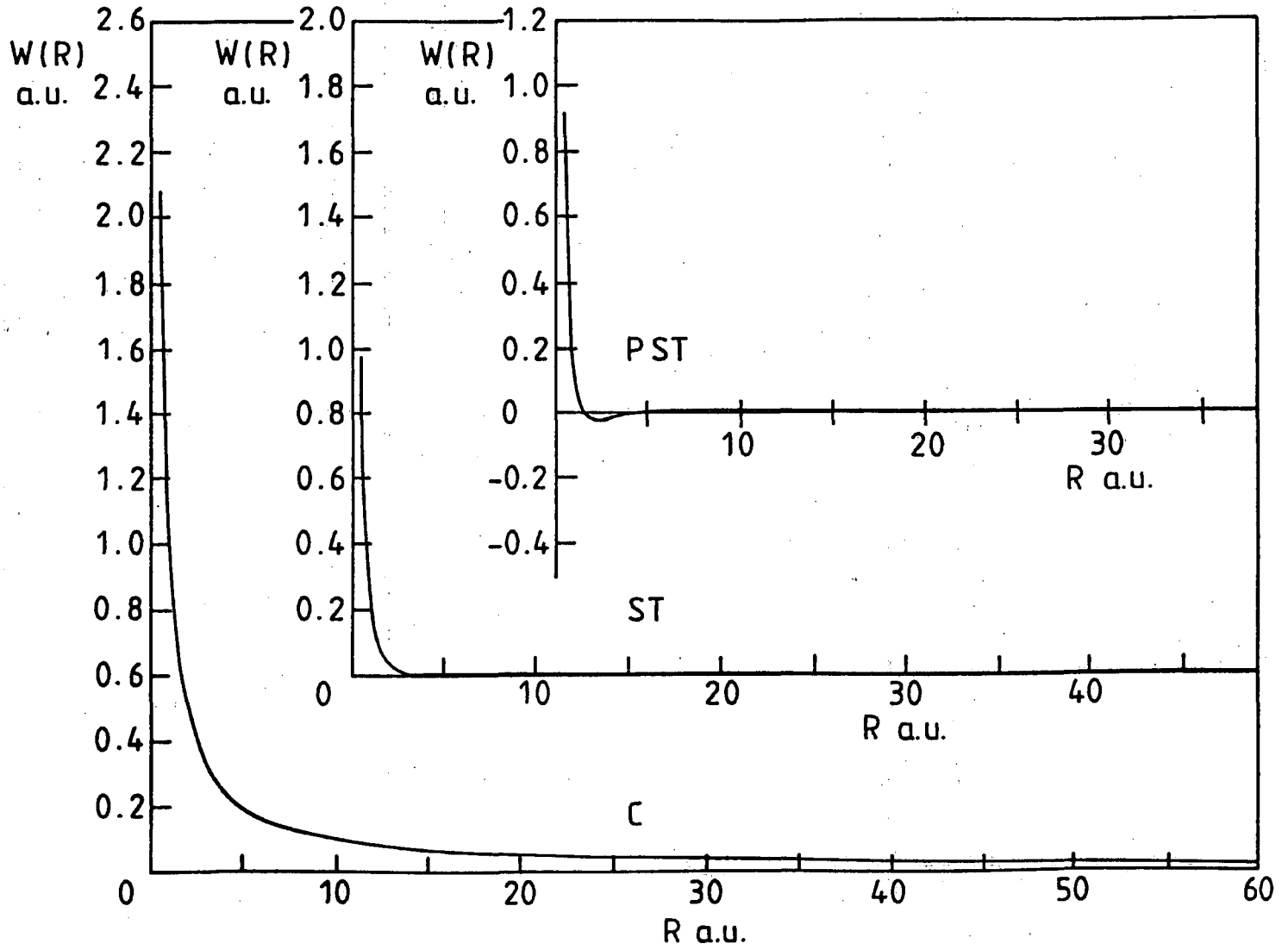

Figure 6.1 Internuclear Potentials for μ^+ and H Collisions. E^{μ}_{lab} = 0.1 keV and b = 0.48 a.u.

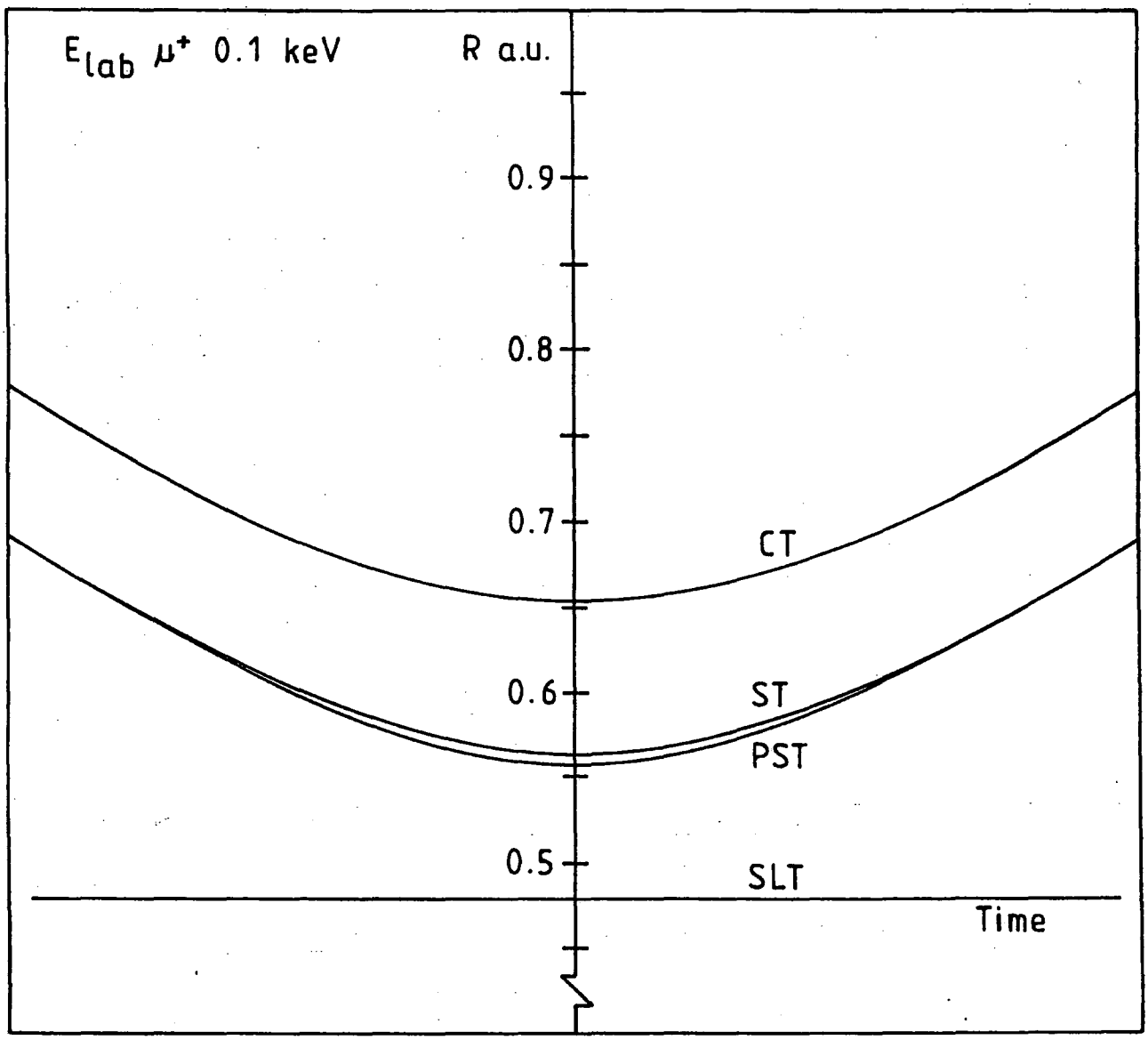

Figure 6.2 Trajectories produced by the Internuclear Potentials W(R). $E^{\mu}_{lab} = 0.1$ keV and b = 0.48 a.u.

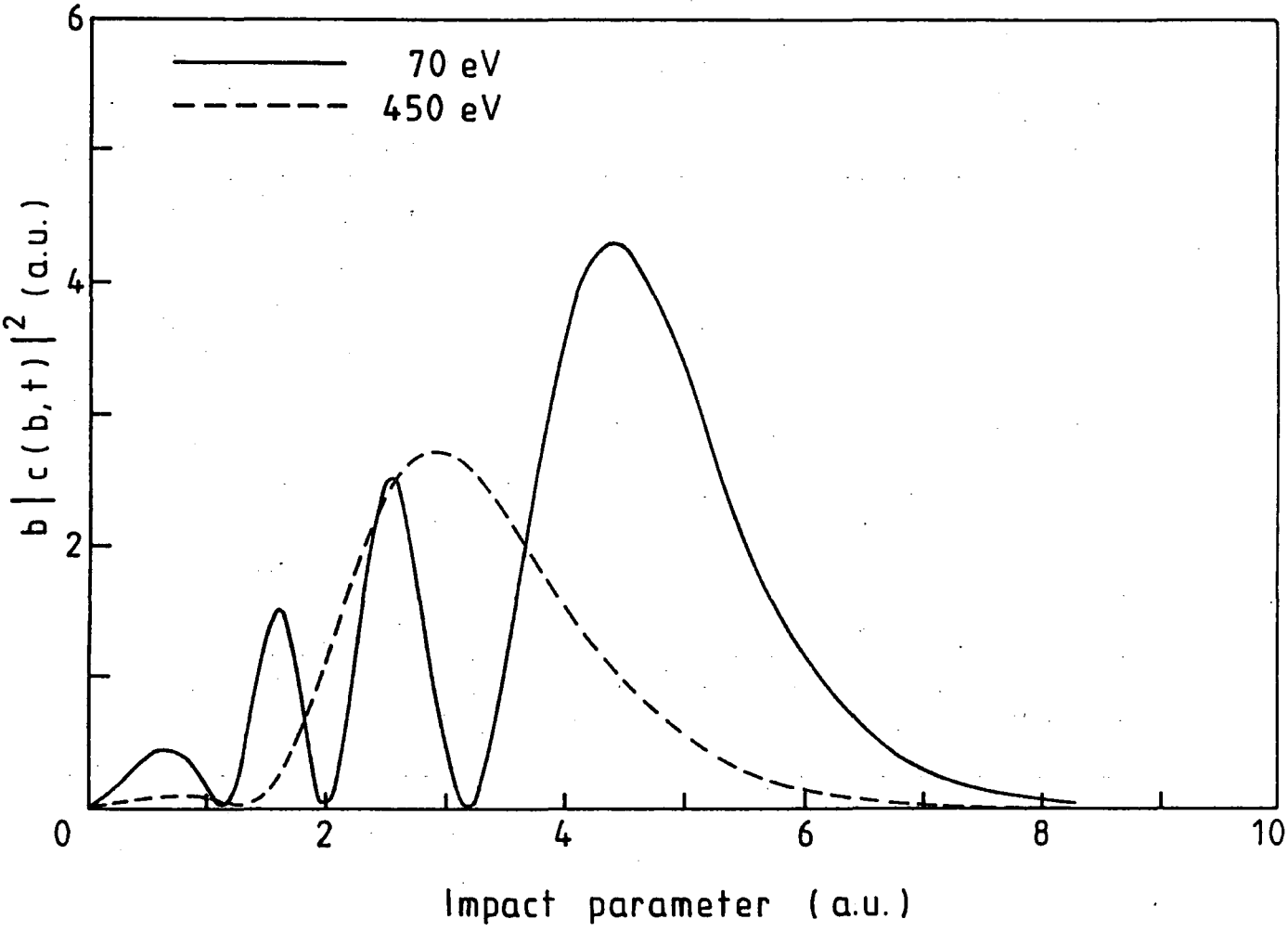

Figure 6.4 μ^+ **and H Collisions: The variation of b | c(b,t) |² with Impact Parameter for Charge Exchange to Mu(2s) - H^+ at Two** μ^+ **Laboratory Energies.**

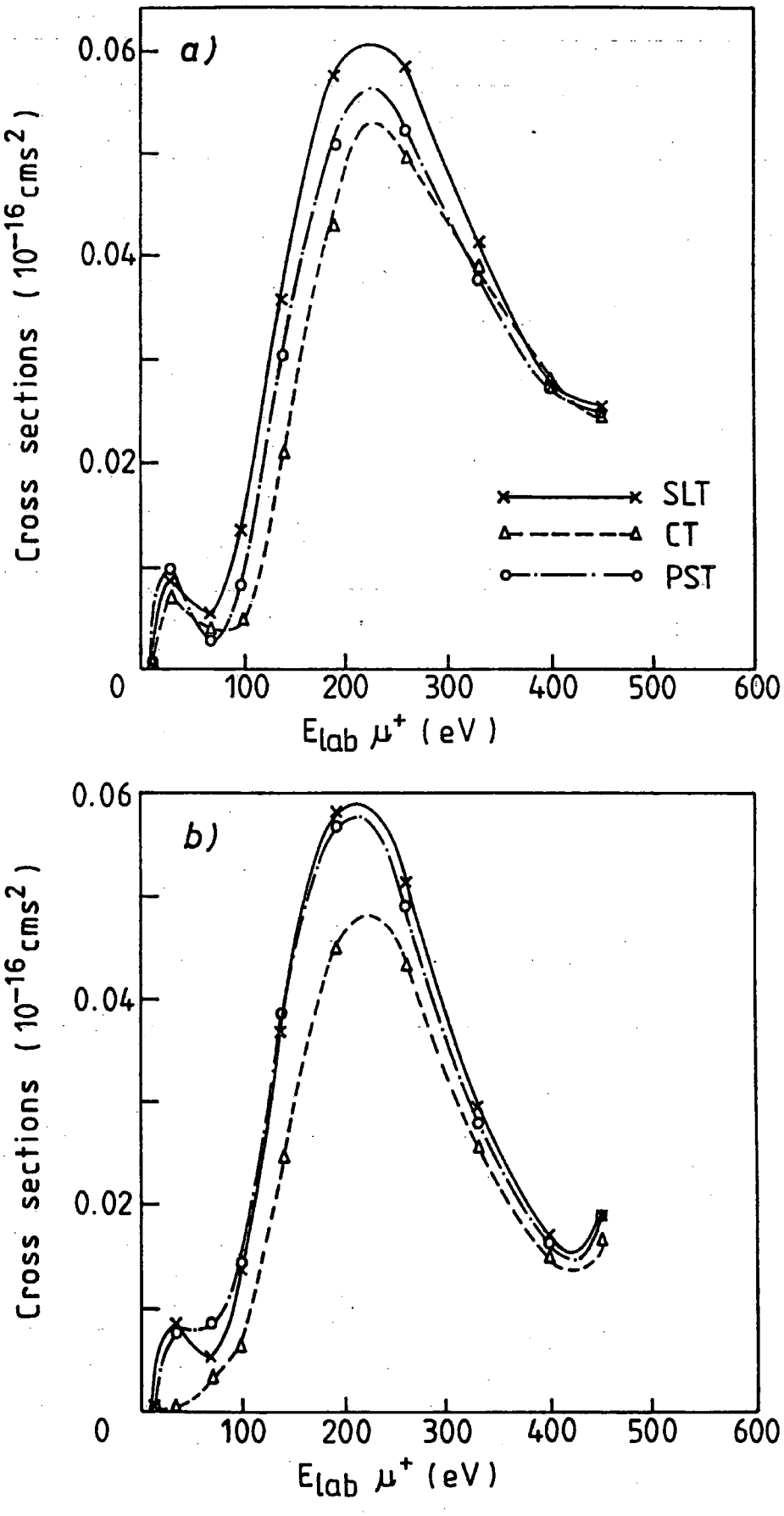

Figure 6.5 μ^+ and H Collisions: Cross-sections for:- (a) Direct Excitation to μ^+ - H(2s). (b) Charge exchange to Mu(2s) - H^+.

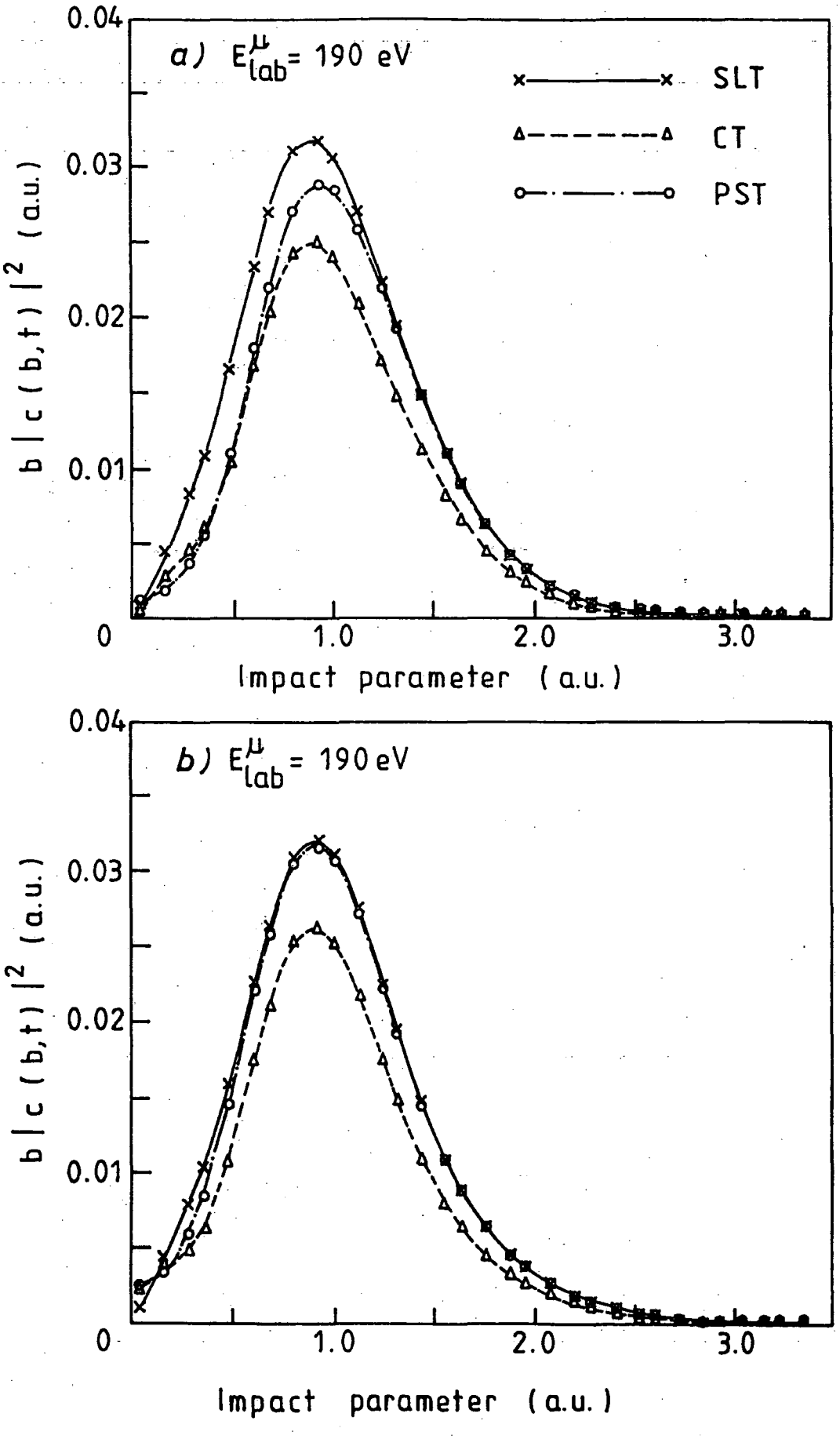

Figure 6.6 μ^+ **and H Collisions: The variation of b | c(b,t)|² with Impact parameter for:- (a) Direct Excitation to** μ^+ **- H(2s). (b) Charge exchange to Mu(2s) -** H^+.

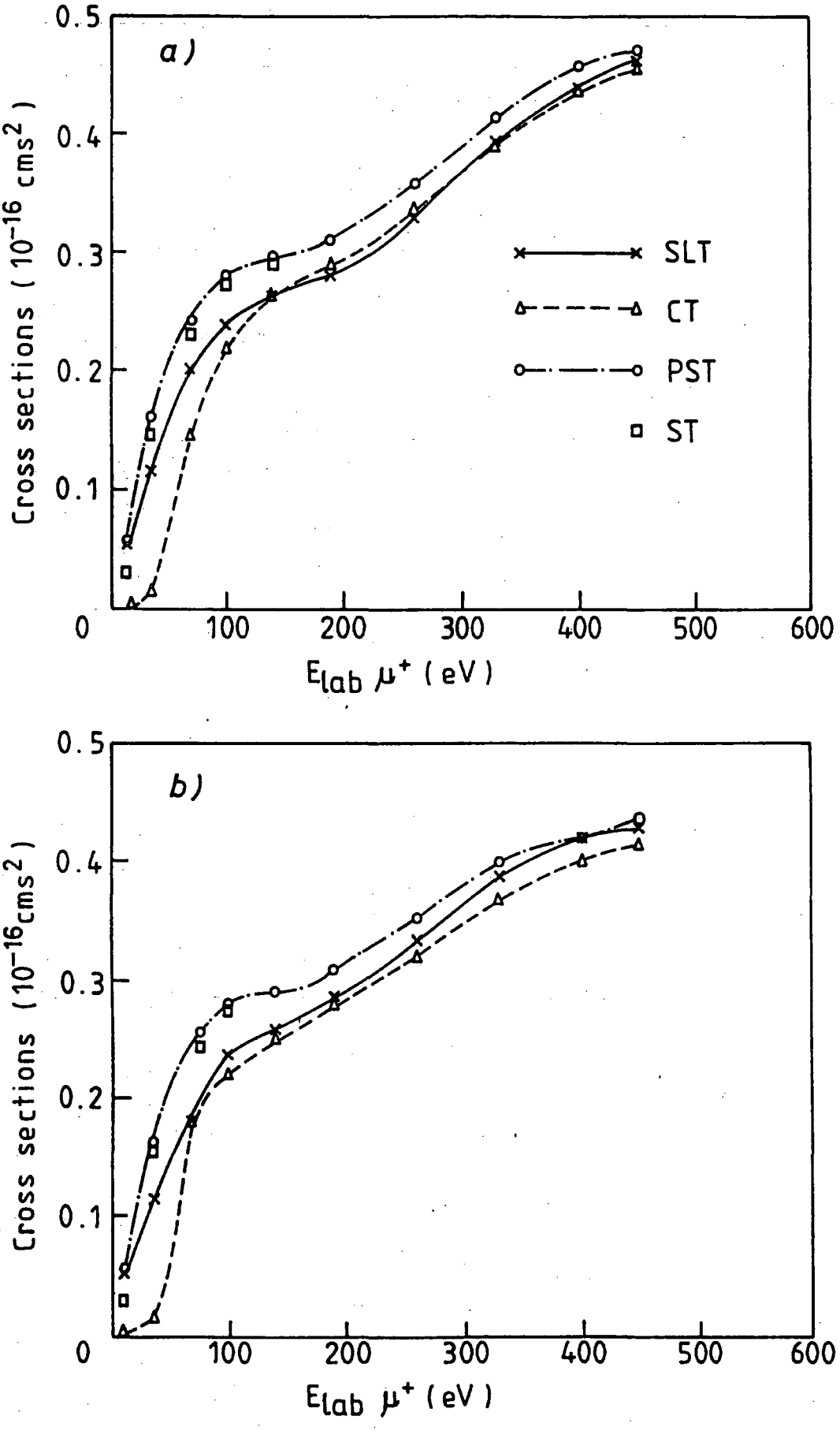

Figure 6.7 μ^+ and H Collisions: Cross-sections for:- (a) Direct Excitation to μ^+ - H(2p). (b) Charge Exchange to Mu(2p) - H^+.

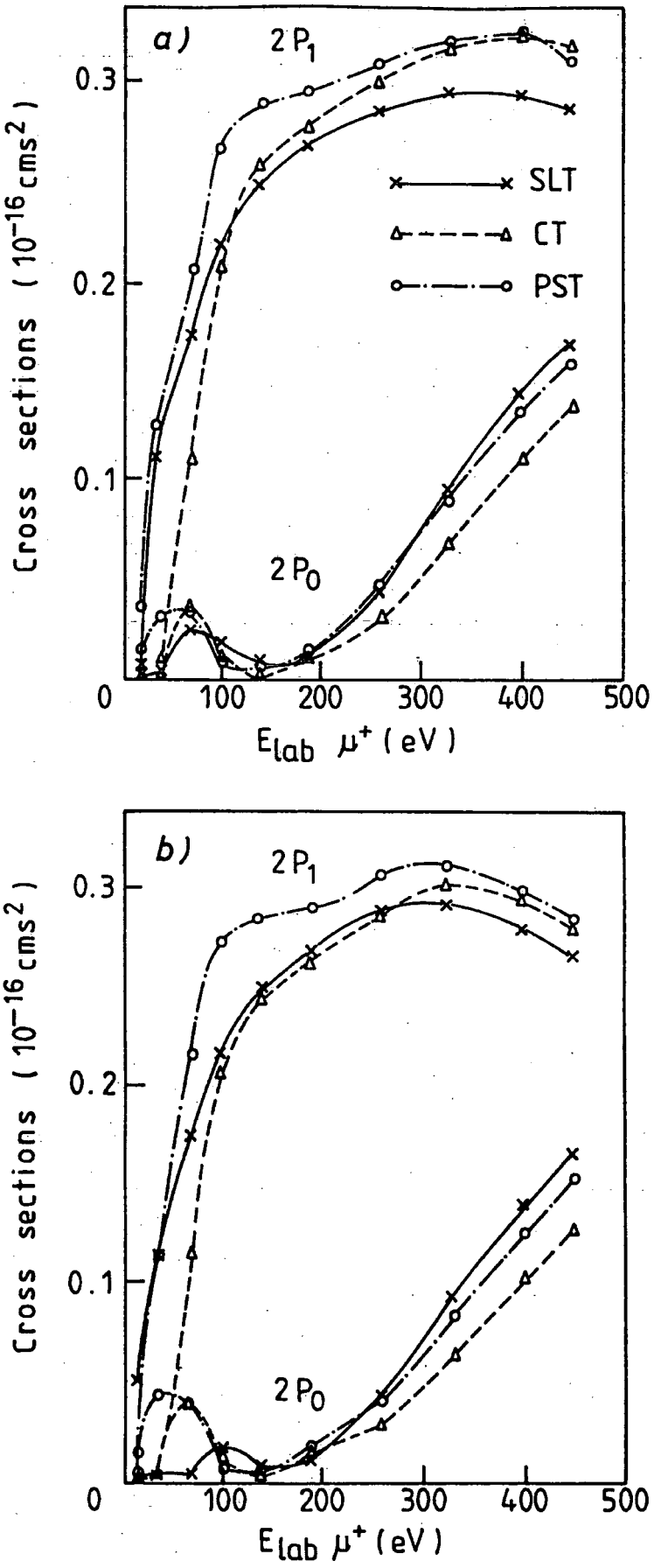

Figure 6.8 μ^+ and H Collisions: Cross-sections for:- (a) Direct Excitation to μ^+ - $H(2p_o)$ and μ^+ - $H(2p_1)$. (b) Charge Exchange to $Mu(2p_o)$ - H^+ and $Mu(2p_1)$ - H^+.

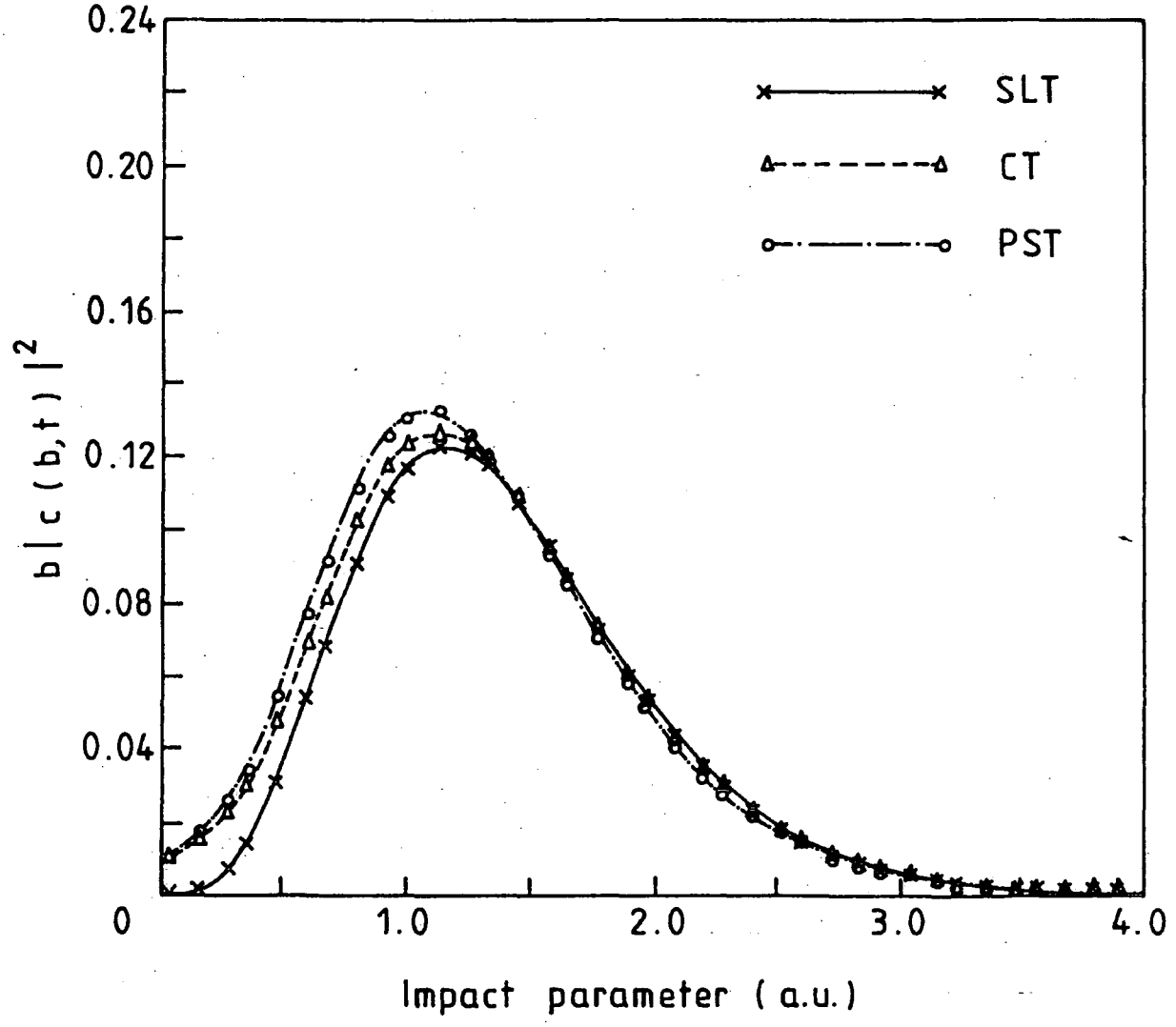

Figure 6.9 μ^+ **and H Collisions: The Variation of b|c(b,t)|² with b for Direct Excitation to** μ^+ **- H(2p$_1$) at** $E^{\mu}_{lab} = 0.400$ **keV.**

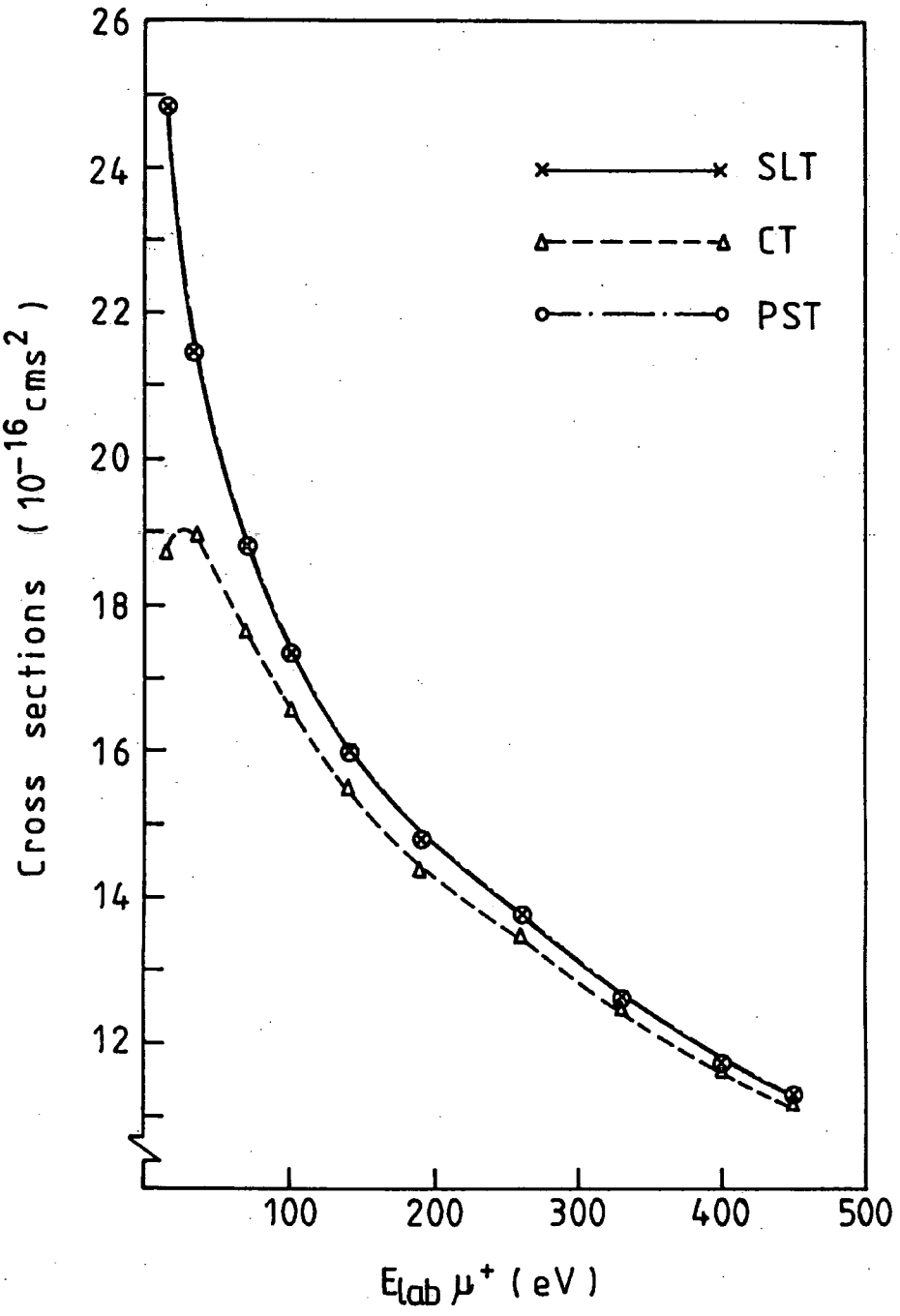

Figure 6.10 μ^+ and H Collisions: Total Charge Exchange Cross-sections.

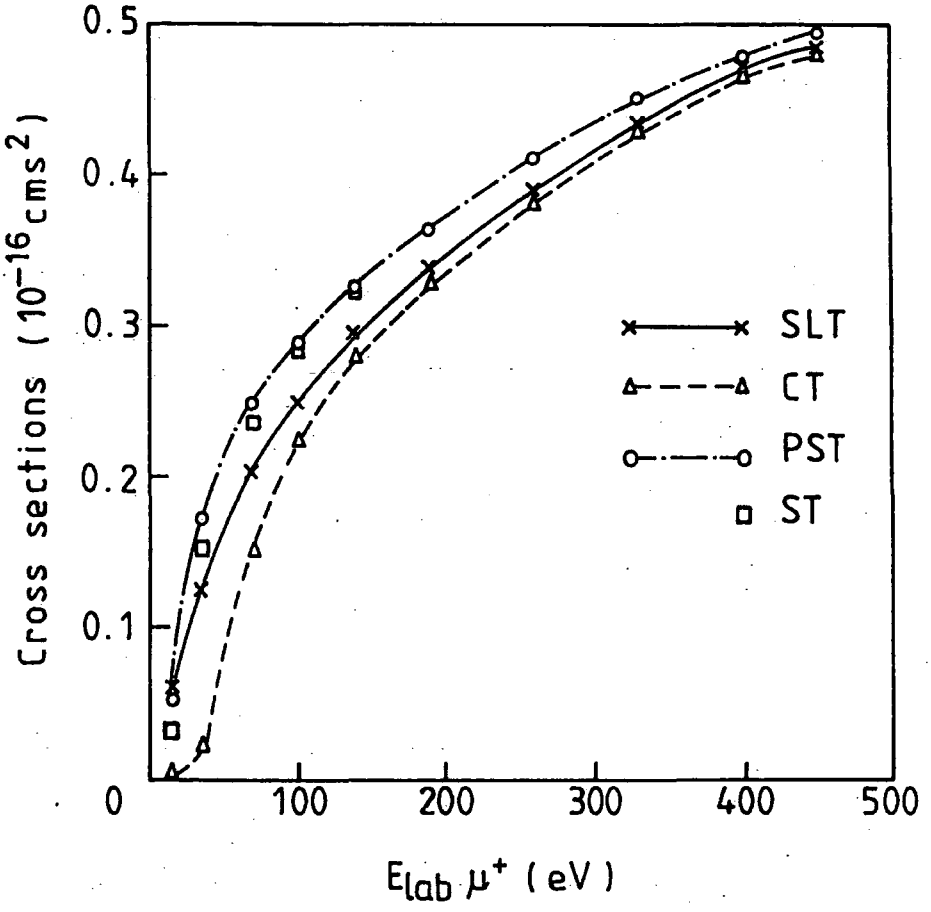

Figure 6.11 μ^+ **and H Collisions: Total Direct Excitation Cross-sections.**

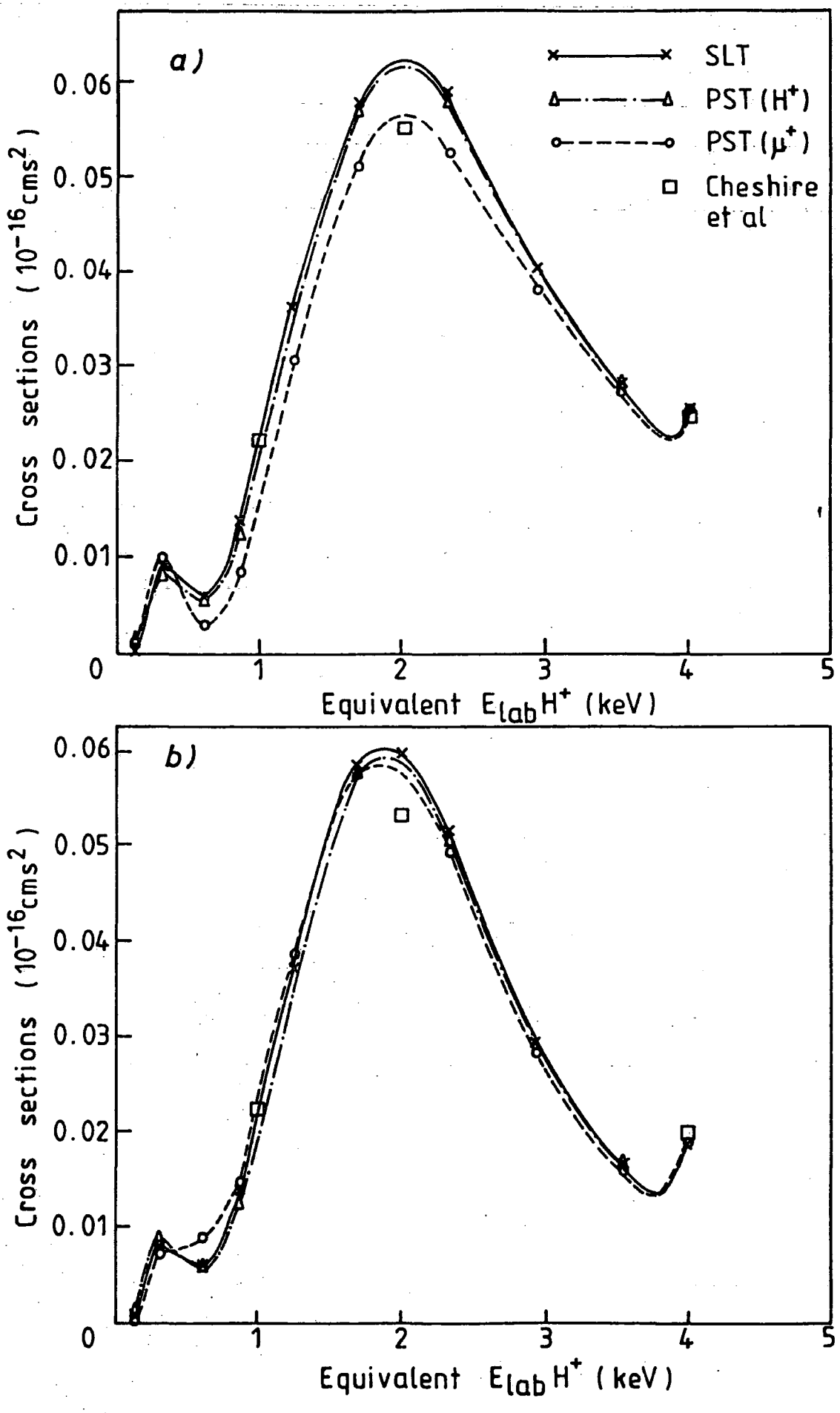

Figure 6.12 Comparison of μ^+ - H and H^+ - H Collisions at the Same Relative Velocity. Cross-sections for:- (a) Direct Excitation to H(2s). (b) Charge Exchange to either Mu(2s) or H(2s).

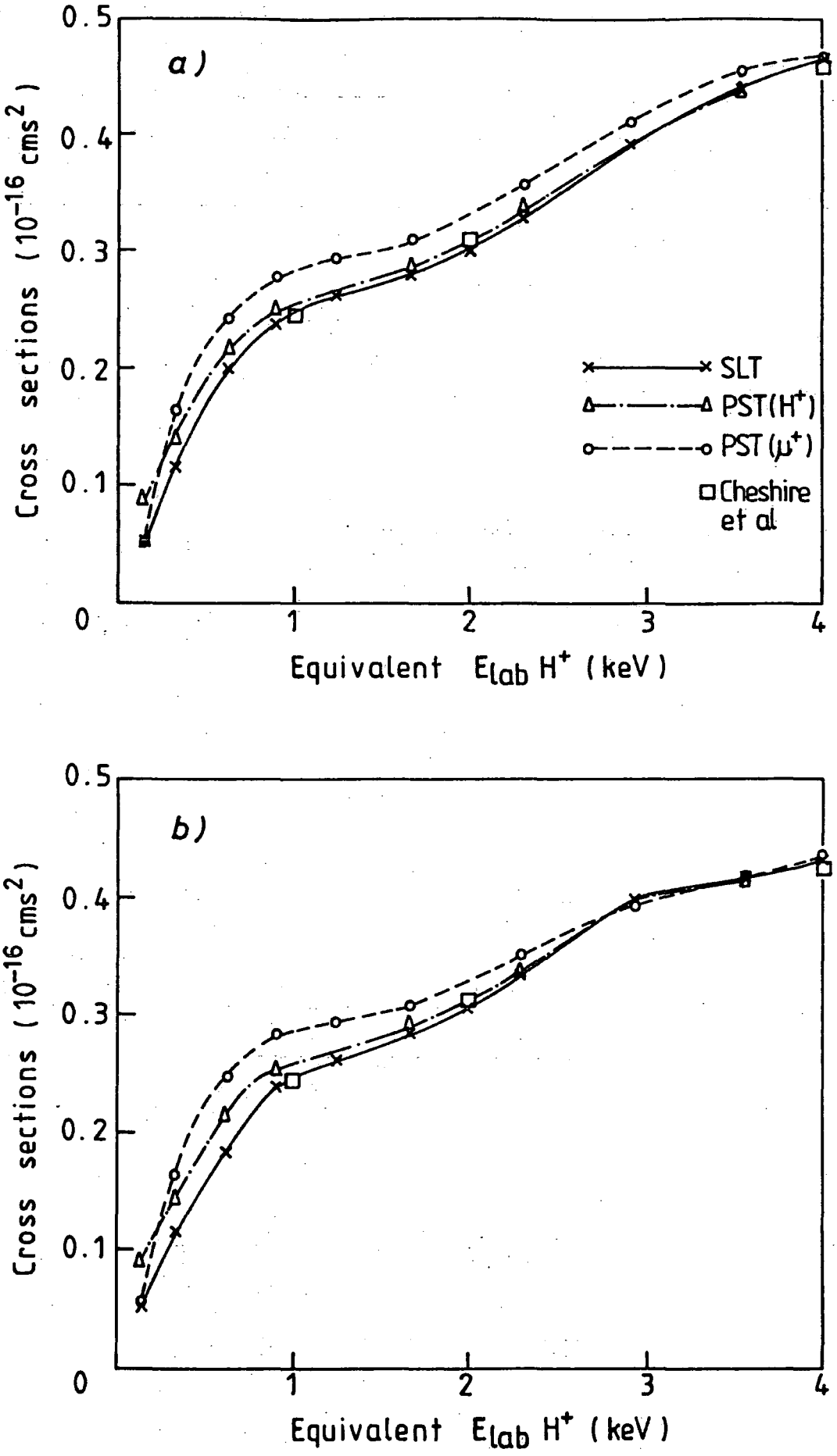

Figure 6.13 Comparison of μ^+ - H Collisions with H^+-H Collisions at the Same Relative Velocity. Cross-sections for:- (a) Direct Excitation to H(2p). (b) Charge Exchange to either Mu(2p) or H(2p).

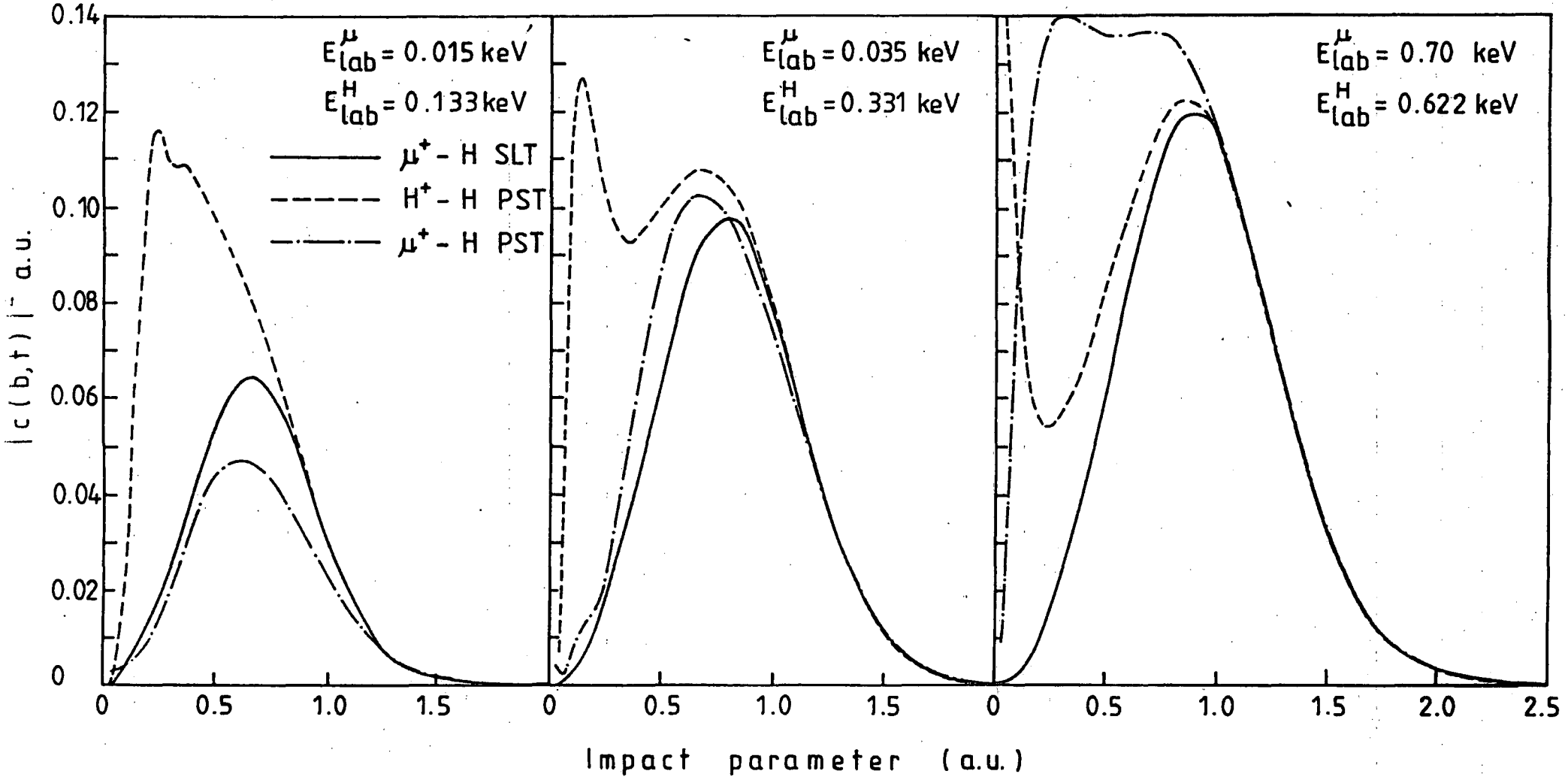

Figure 6.14 Comparison of μ^+ - H Collisions with H^+ - H at the Same Relative Velocities. Probabilities for Charge Exchange to $Mu(2p_1)$.

	Cross Sections (10^{-16} cms^2)		
E(eV)	SLT	PST	CT
15	24.189	24.24	
35	20.823	20.819	18.410
1405	15.6730	15.593	15.0332
2818	2.7575	2.7627	

Table 6.1: Comparison of Two state results: Charge transfer to 1s

E_{lab}(eV)	SLT	CT	PST	ST
15	24.793	18.714	24.785	24.785
35	21.428	19.005	21.469	24.456
70	18.823	17.626	18.740	18.752
100	17.343	16.596	17.410	17.395
140.5	16.041	15.554	16.002	16.016
190	14.826	14.469	14.879	14.868
260	13.811	13.502	13.770	13.773
330	12.652	12.499	12.624	12.635
400	11.757	11.644	11.756	11.764
450	11.311	11.198	11.325	11.321
1200	7.878		7.883	

Table 6.2: μ^+ - H Collisions : Total Charge exchange Cross-sections (10^{-16} cms^2)

E_{lab}	SLT	CT	PST	ST
15	24.739	18.713	24.727	24.552
35	21.303	18.989	21.299	21.304
70	18.618	17.463	18.477	18.499
100	17.092	16.369	17.114	17.107
140.5	15.745	15.278	15.670	15.690
190	14.487	14.150	14.514	14.509
260	13.425	13.139	13.370	13.378
330	12.234	12.106	12.198	12.213
400	11.321	11.230	13.314	11.324
450	10.862	10.760	10.866	10.872
1200	7.330		7.330	

Table 6.3: μ^+ - H Collisions : Charge exchange to 1s : Partial Cross- sections (10^{-16} cms^2)

Model	Distance of Closest Approach (R_o) a.u.	$W(R_o)$ a.u.
CT	1.0789	0.927
ST	1.0173	0.259
PST	1.0106	0.179

Table 6.4: Comparison of distances of closest approach

E_{lab}(eV)	SLT	CT	PST	ST
15	0.00059	0.3^{10-6}	0.00090	0.00045
35	0.0087	0.0072	0.0096	0.0076
70	0.0054	0.0042	0.0029	0.0028
100	0.0137	0.0048	0.0081	0.0074
140.5	0.0362	0.0211	0.0305	0.0290
190	0.0579	0.0428	0.0507	0.0496
260	0.0584	0.0496	0.0522	0.0520
330	0.0410	0.0393	0.0378	0.0381
400	0.0283	0.0281	0.0271	0.0272
450	0.0256	0.0246	0.0245	0.0245
1200	0.1036		0.1037	

Table 6.5: μ^+ - H Collisions: Excitation to 2s : Partial cross- sections (10^{-16} cms^2)

E_{lab}(eV)	SLT	CT	PST	ST
15	0.00060	0.34^{10-6}	0.00069	0.00030
35	0.0087	0.0002	0.0075	0.0062
70	0.0054	0.0036	0.0088	0.0086
100	0.0138	0.0064	0.0144	0.0142
140.5	0.0371	0.0247	0.0387	0.0380
190	0.0584	0.0449	0.0571	0.0561
260	0.0514	0.0431	0.0488	0.0482
330	0.0292	0.0257	0.0279	0.0276
400	0.0167	0.0148	0.0163	0.0163
450	0.0187	0.0164	0.0187	0.0188
1200	0.2865		0.2876	

Table 6.6: μ^+ - H Collisions : Charge exchange to 2s : Partial cross-sections (10^{-16} cms^2)

E_{lab}(eV)	SLT	CT	PST	ST
15	0.00085	0.15^{10-5}	0.01622	0.01131
35	0.00045	0.0072	0.0327	0.0208
70	0.0247	0.0380	0.0347	0.0342
100	0.0194	0.0114	0.0100	0.0098
140.5	0.0103	0.0033	0.0042	0.0042
190	0.0118	0.0114	0.0154	0.0148
260	0.0455	0.0324	0.0471	0.0451
330	0.0968	0.0686	0.0907	0.0877
400	0.1462	0.1122	0.1354	0.1321
450	0.1693	0.1385	0.1583	0.1553
1200	0.0809		0.0804	

Table 6.7: μ^+ - H collisions : Excitation to $2p_o$: Partial Cross- sections (10^{-16} cms^2)

E_{lab} (eV)	SLT	CT	PST	ST
15	0.00085	0.7^{10-6}	0.01600	0.01124
35	0.0045	0.0068	0.0455	0.0431
70	0.0054	0.0417	0.0392	0.0388
100	0.0194	0.0123	0.0090	0.0090
140.5	0.0104	0.0061	0.0074	0.0072
190	0.0120	0.0165	0.0180	0.0173
260	0.0453	0.0330	0.0440	0.0425
330	0.0968	0.0645	0.0846	0.0830
400	0.1398	0.1037	0.1266	0.1251
450	0.1652	0.1307	0.1541	0.1527
1200	0.1589		0.1607	

Table 6.8: μ^+ - H Collisions: Charge exchange to $2p_o$: Partial Cross-sections (10^{-16} cms^2)

E_{lab}(eV)	SLT	CT	PST	ST
15	0.0528	0.17^{10-6}	0.0374	0.0196
35	0.1124	0.0096	0.1297	0.1140
70	0.1750	0.1103	0.2072	0.1978
100	0.2176	0.2075	0.2696	0.2634
140.5	0.2491	0.2590	0.2901	0.2861
190	0.2683	0.2771	0.2959	0.2935
260	0.2855	0.3013	0.3101	0.3089
330	0.2940	0.3202	0.3213	0.3209
400	0.2935	0.3248	0.3203	0.3204
450	0.2871	0.3182	0.3113	0.3116
1200	0.1029		0.1043	

Table 6.9: μ^+ - H Collisions Excitation to $2p_1$: Partial Cross-sections (10^{-16} cms^2). 8 State Basis

E_{lab}(eV)	SLT	CT	PST	ST
15	0.0528	0.1^{10-6}	0.0402	0.0211
35	0.1123	0.0089	0.1170	0.1021
70	0.1750	0.1175	0.2160	0.2056
100	0.2175	0.2083	0.2728	0.2652
140.5	0.2487	0.2451	0.2858	0.2802
190	0.2687	0.2576	0.2902	0.2862
260	0.2891	0.2865	0.3072	0.3048
330	0.2926	0.3025	0.3130	0.3114
400	0.2796	0.2957	0.2994	0.2984
450	0.2646	0.2815	0.2824	0.2817
1200	0.1029		0.1043	

Table 6.10: μ^+ - H collisions. Charge exchange to $2p_1$: Partial Cross-sections (10^{-16} cms^2). 8 State Basis

E_{lab}(eV)	SLT	CT	PST	ST
15	0.0536	0.17^{10-5}	0.0536	0.0310
35	0.1996	0.1483	0.2420	0.2320
100	0.2370	0.2189	0.2795	0.2732
140.5	0.2624	0.2623	0.2942	0.2903
190	0.2802	0.2884	0.3113	0.2083
260	0.3310	0.3337	0.3572	0.3540
330	0.3909	0.3888	0.4120	0.4086
400	0.4397	0.4370	0.4557	0.3424
450	0.4563	0.4566	0.4696	0.4669
1200	0.1417		0.1418	

Table 6.11: μ^+ - H collisions. Excitation to 2p states of hydrogen : Partial cross sections (10^{-16} cms^2)

E_{lab}(eV)	SLT	CT	PST	ST
15	0.0536	0.8^{10-6}	0.0562	0.0323
35	0.1169	0.0157	0.1625	0.1453
70	0.1804	0.1592	0.2552	0.2445
100	0.2369	0.2207	0.2818	0.2741
140.5	0.2590	0.2512	0.2931	0.2874
190	0.2807	0.2741	0.3081	0.3036
260	0.3344	0.3195	0.3512	0.3473
330	0.3894	0.3670	0.3976	0.3944
400	0.4194	0.3994	0.4207	0.4235
450	0.4298	0.4123	0.4366	0.4344
1200	0.2618		0.2650	

Table 6.12: μ^+ - H collisions. Charge exchange to 2p states of Muonium : Partial Cross-sections (10^{-16} cms^2)

E_{lab} (eV)	SLT	CT	PST	ST
15	0.05957	0.2^{10-5}	0.0545	0.0314
35	0.1256	0.0197	0.1720	0.1525
70	0.2050	0.1526	0.2449	0.2348
100	0.2487	0.2238	0.2877	0.2816
140.5	0.2957	0.2834	0.3247	0.3193
190	0.3381	0.3312	0.3620	0.3579
260	0.4318	0.4281	0.4499	0.4467
330	0.4318	0.4281	0.4499	0.4467
400	0.4680	0.4651	0.4764	0.4797
450	0.4820	0.4812	0.4941	0.4914
1200	0.2453		0.2455	

Table 6.13: μ^+ - H Collisions : Total Excitation Cross-sections (10^{-16} cms^2)

E(eV)μ^+_{lab}	rel. vel (a.u.)	E(eV)H^+_{lab}
15.0	0.07298	133.054
35.0	0.11148	310.460
70.0	0.15765	620.920
100.0	0.18843	887.029
140.5	0.22335	1246.276
190.0	0.25973	1685.355
260.0	0.30384	2306.275
330.0	0.34230	2927.195
400.0	0.37686	3548.116
450.0	0.39972	3991.630

Table 6.14: μ^+ - H and H^+ - H Collisions : Comparison of laboratory energies at the same relative velocities

E_{lab}(eV)	E_{lab}(eV)	SLT	HPST	PST
15	133	0.0006	0.0023	0.0009
35	310	0.0087	0.0087	0.0096
70	620	0.0054	0.0055	0.0029
100	887	0.0137	0.0126	0.0080
190	1685.8	0.0579	0.0569	0.0507
	2000	0.0617		
260	2306	0.0584	0.0522	0.0522

Table 6.15: Comparison of μ^+ - H and H^+ - H Collisions: Excitation to 2s : Partial Cross-sections (10^{-16} cms^2)

E_{lab}(eV)	E_{lab}(eV)	SLT	HPST	PST
15	133	0.0006	0.0012	0.0007
35	310	0.0087	0.0087	0.0075
70	620	0.0054	0.0056	0.0088
100	887	0.0138	0.0127	0.0144
190	1686	0.0584	0.0572	0.0571
	2000	0.0597		
260	2306	0.0514	0.0505	0.0488

Table 6.16: Comparison of μ^+ - H and H^+ - H Collisions. Charge exchange to 2s : Partial Cross-sections (10^{-16} cms^2)

E_{lab}(ev)	E_{lab}(eV)	SLT	H PST	PST
15	133	0.0536	0.0868	0.01712
35	310	0.1169	0.1430	0.1624
70	620	0.1996	0.2140	0.2419
100	887	0.2370	0.2479	0.2795
190	1686	0.2802	0.2865	0.3113
260	2301	0.3310	0.3352	0.3572
400	3548	0.4397	0.4415	0.4557

Table 6.17: μ^+ - H and H^+ - H Collisions : Partial Cross-sections (10^{-16} cms^2). Excitation to 2p

E_{lab}(eV)	E_{lab}(eV)	SLT	H PST	PST
15	133	0.0536	0.0863	0.0562
35	310	0.1169	0.1433	0.1625
70	620	0.1804	0.2146	0.2552
100	887	0.2369	0.2483	0.2818
190	1686	0.2807	0.2868	0.3081
260	2306	0.3344	0.3384	0.3512
400	3548	0.4194	0.4211	0.4207

Table 6.18: μ^+ - H and H^+ - H Collisions. Charge Exchange to 2p

Chapter 7

Final Discussion and Conclusions

The results presented in Chapters four, five and six have examined the effect of using curved trajectories, within the atomic orbital Impact Parameter method, on three atomic systems with different characteristics.

7.1 Straight line results

Straight line Results have also been produced in the course of the work so that trajectory effects could be assessed consistently. It has therefore been possible to compare these with other calculations which have employed straight line paths. The straight line atomic orbital results for Be^{++}-H are in reasonable agreement with the molecular results of Wetmore et al (1986) and Bates et al (1964). This confirms the earlier conclusion of Fritsch (1982) and Bransden and Noble (1982) that the atomic orbital method can be used at lower energies than had previously been thought feasible. The straight line μ^+ - H cross sections (identical to the H^+ -H cross sections at the same relative velocity), are generally in good agreement with the atomic orbital results of Cheshire et al (1969).

7.2 Curved Trajectories

At the energies under consideration, the major part of the total cross sections calculated have been made up of contributions from charge exchange to 1s, or, in the case of the Be^{++} ionic core, to the 2s state of Be^+. The largest probabilities for these states in all three systems arise from impact parameters in the range 3 a.u. $< b <$ 8 a.u. The primary factor in the reduction of the curved trajectory cross sections from their straight line levels is the repulsive interaction between the nuclei. The 1s cross sections produced by systems with small nuclear charges, such as μ^+ - H and H^+ - H, are least affected by the inclusion of an internuclear potential. Those trajectories deviate less from straight line paths than the $^4He^{++}$ - $^4He^+$ and Be^{++} - H collisions involving more highly charged nuclei. The charge exchange cross sections to 1s in μ^+ - H collisions were also relatively insensitive to the type of internuclear potential employed, compared to the other final states.

It was found that the use of a shorter range repulsive static potential produced smaller trajectory effects than including the longer range coulomb potential.

The highest probabilities for charge exchange to excited states in Be^{++} - H and μ^+ - H collisions occurred at much smaller impact parameters (in the range 0 a.u.< b < 3 a.u.) than those to the primary charge exchange channels. When the most important probability amplitudes come from small b, as in the p state cross sections in Be^{++} and H, the trajectories arising from these are more sensitive to the internuclear potential. This leads to pronounced trajectory effects in these states, for both the above systems. In Be^{++} - H collisions the results are analagous to those produced by the molecular models (Wetmore et al, 1986, Bates et al, 1964) in which larger probabilities result from rotational coupling of the states at small internuclear separations.

It was found that cross sections for excited states also differ from straight line results over a larger range of energies than the ground state charge exchange cross-sections. The inclusion of the internuclear potential results in reduced cross sections for all m = 0 states. It is not possible to generalize the trajectory effects on the cross sections to $2p_1$ states, which are analogous to the $2p_\pi$ states. For instance, the cross-sections obtained for charge exchange to $Be^+(2p_1)$ were reduced when the internuclear potential was included. This was consistent with the results obtained for the other states of Be^+. However, the inclusion of the internuclear potential in μ^+ - H and H^+ - H collisions produced higher cross sections to $2p_1$ than the straight line model, except at the very lowest energies. This was more pronounced when a shorter range static potential was employed and when polarization effects were included. The latter effect was minor compared to that produced by the static potential. Gaussorgues et al (1975b) have also produced curved trajectory probabilities for the $2p_\pi$ states of H which are higher than for a straight line model at small impact parameters. It seems that the repulsion which keeps the ions apart, increases the chances of charge exchange to $2p_1$ states. Why the same effect does not occur in Be^{++} and H is not known.

When curved trajectory results for $^4He^{++}$ and $^4He^+$ collisions are compared with similar non-linear path molecular calculations, the atomic orbital results at the lowest energies are consistently below their molecular counterparts. It is likely that the molecular results at these energies are more realistic because of the assumption that the electron is shared between the two ions at small internuclear distances. This then results in slightly larger cross sections. Previously, where discrepancies existed between straight line molecular and atomic basis results, the atomic cross sections have been improved by the addition of continuum states of the electron, or pseudostates, as in the work of Cheshire et al (1969), Wilets and Gallaher (1966), and Fritsch and Lin (1982). These pseudostates give a more molecular character to the collisions. The present work has not considered the use of pseudostates, within a curved trajectory context, but further work on using suitably modified atomic orbital expansions might be valuable.

7.3 Velocity Scaling

The μ^+ - H results from Chapter six have confirmed that velocity scaling with H^+ - H gives accurate results for all energies when straight line paths are used. The results also confirm that the method is accurate enough for all n=2 states when a qualitative order of magnitude estimate is required. However the method is unreliable for predicting accurate low energy cross-sections for direct excitation and excited charge transfer states, when classical trajectories are employed. This is because the effect of the internuclear potential is more pronounced in μ^+ - H collisions due to the relatively light mass of the muon compared to hydrogen.

7.4 Differential Cross sections

From the results presented, differential cross sections are very sensitive to the inclusion of an internuclear potential, and the trajectory effects produced are more pronounced at larger angles in the range $0^o < \theta < 13^o$. The small angle approximation is more suitable for final channels in which the most important probabilities arise at larger impact parameters. This is true for $^4He^{++}$ and $^4He^+$ collisions and for charge transfer to 2s in Be^{++} and H collisions. These are also the cross sections which agree less well at lower energies with the first order approximation 1.114. The angular distributions calculated for charge exchange to $Be^+(2p)$ states are in better agreement with the first order approximations because the largest probabilities for these states are more sensitive to the classical nature of the trajectories.

7.5 Conclusion and Possibilities for Further Work

Due to pressure of time it has not been possible to explore the problems associated with the elastic differential cross sections. One way to proceed with this might be to calculate the elastic probability amplitudes for very large b by using an analytic form of 4.5 for the elastic channel. A long range correction to the probability amplitudes has been tried by Allan (1989), with limited success, but further work along these lines might be profitable.

A limitation to the work carried out for this thesis has been the amount of CPU time necessary to calculate each matrix element separately for every R, b and energy, in order to define the variation of the probabilities with b correctly. One way in which these calculations could be expedited would be to use parallel processing techniques. A two electron code developed by Slim (1990) from the same basic programs is in the process of being adapted for parallelism and similar work might be useful on the one electron code adapted for curved trajectories.

It appears that the atomic orbital method can be adapted successfully for low energy calculations by incorporating curved trajectories. The results obtained are comparable with molecular calculations and further work could include more

sophisticated basis sets and internuclear potentials.

Appendix A
A Derivation of the Eikonal Scattering Amplitude

The reader is referred to Nikitin and Umanskii 1984.

The expression for the scattering amplitude from Messiah (1962) is

$$f_{n'\ell'm'n\ell m} = \frac{-\mu}{2\pi}\int d^3R \exp(i(\vec{k}_i - \vec{k}_{n'}).\vec{R}) < \phi_{n'\ell'm'} \mid V_{AB} \mid \Phi > \qquad \text{(A.1)}$$

where V_{AB} is the internuclear potential. Φ is a wave function of the form 1.55 and $\phi_{n'\ell'm'}$ is the eigenfunction of the state labelled by the quantum numbers $n'\ell'm'$.

The co-ordinate system $\bar{x}, \bar{y}, \bar{z}$ in which the relative motion takes place is shown below

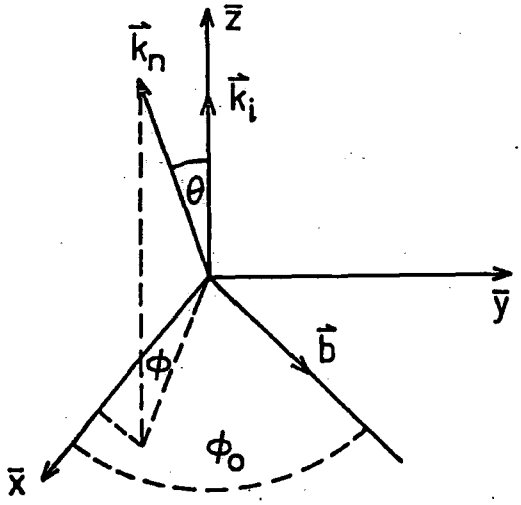

The initial wave vector $\vec{k}_i$ is along the $\bar{z}$ axis, the final wave vector is $\vec{k}_{n'}$ and the impact parameter vector $\vec{b}$ is orthogonal to $\bar{z}$. The equations for a straight line trajectory are:-

$$\vec{R}\,(t) = \vec{b} + \vec{r}\,t;\ \ \bar{z} = \vec{v}\,t \text{ and } \vec{v}\,.\vec{b} = 0 \qquad \text{(A.2)}$$

For small angled scattering $\vec{k}_i$ is not expected to differ from $\vec{k}_n$, appreciably and therefore

$$|\vec{k}_i| \simeq |\vec{k}_{n'}| \simeq k \tag{A.3}$$

Using the relationships above,

$$i(\vec{k}_i - \vec{k}_{n'}).\ \vec{R} = (\vec{k}_i - \vec{k}_{n'}).\ \vec{b} + (\vec{k}_i - \vec{k}_{n'})\ \vec{z}$$

$\vec{k}_i - \vec{k}_{n'} = \frac{\epsilon z}{v}$. The scalar product $\vec{k}_i \cdot \vec{b}$ is zero because $\vec{k}_i$ is along the $\bar{z}$ axis. $-\vec{k}_{n'} \cdot \vec{b} = (k_{n'x} b_x + k_{n'y} b_y)$ and the vector $\vec{b}$ can be expressed in terms of its azimuthal angle ϕ_o.

$$b_x = b\cos\phi_o b_y = b\sin\phi_o,$$
$$k_{n'x} = k\sin\theta\cos\phi \text{ and}$$
$$k_{n'y} = k\sin\theta\sin\phi = kb\sin\theta\cos(\phi - \phi_o).$$

For small angles $\sin\theta \approx \theta$ and so

$$i(\vec{k}_i - \vec{k}_{n'}).\ \vec{R} = \frac{\epsilon_{n'} z}{v} - kb\theta\cos(\phi - \phi_o) \tag{A.4}$$

The integral over d^3R is transformed as follows

$$d^3\vec{R} = \int dx \int dy \int dz$$
$$\text{where } \bar{x} = b\cos\phi_o\ \bar{y} = b\sin\phi_o,$$

which leads to the Jacobian

$$\begin{bmatrix} \cos\phi_o & -b\sin\phi_o \\ \sin\phi_o & b\cos\phi_o \end{bmatrix} dbd\phi_o = bdbd\phi_o$$

$$\int d^3\vec{r} = \int d\phi_o \int bdb \int vdt$$
$$\Phi = \sum_{n\ell m} c^{eik}_{n\ell m} \exp(-\epsilon_n t)\phi_{n\ell m}$$

where the $c^{eik}_{n\ell m}$ are eikonal probability amplitudes.

Substituting all these expressions into A1, the scattering amplitude becomes

$$f_{n'\ell'm'n\ell m} = -\mu v \int_o^\infty bdb \frac{1}{2\pi} \int_o^{2\pi} d\phi_o \exp[-ikb\theta\cos(\phi - \phi_o) \times$$
$$\int_{-\infty}^{\infty} dt \sum_{n\ell m} \exp[i(\epsilon_{n'} - \epsilon_n)t] < \phi_{n'\ell'm'} \mid V_{AB} \mid \phi_{n\ell m} > c^{eik}_{n\ell m}$$

Using 1.57, the time integration becomes

$$-i(\delta_{n'\ell'm'n\ell m} - S^{eik}_{n'\ell'm'n\ell m})$$

where $S^{eik}_{n'\ell'm'n\ell m}$ is the eikonal scattering matrix

$$S^{eik}_{n'\ell'm'n\ell m} = c^{eik}_{n'\ell'm'n\ell m}(+\infty)$$

The space fixed scattering matrix $S^{SF}_{n'\ell'm'n\ell m}$ is recovered by rotating the $\overline{xyz}$ frame through the Euler angles $\alpha = \phi_o - \frac{\pi}{2}$, $\beta + 0$, $\gamma = 0$ and

$$S^{eik}_{n'l'm'nlm} = \exp[i(m-m')(\phi_o - \frac{\pi}{2})]S^{SF}_{n'l'm'nlm}$$

$$f_{n'l'm'nlm} = i\mu v \int_o^\infty bdb \frac{1}{2\pi} \int_o^{2\pi} \exp[-ikb\theta\cos(\phi-\phi_o) + i(m-m')(\phi_o - \frac{\pi}{2})]d\phi_o \times(\delta_{n'e'm'} - S^{SF}_{n'l'm'nlm})$$

Let $\phi_o = \alpha + \phi$ and let

$$I_1 = \int_o^{2\pi} \exp[-ib\theta\cos(\phi-\phi_o) + i(m-m')(\phi_o - \frac{\pi}{2})]d\phi_o$$
$$= \int_o^{2\pi} \exp[-ikb\theta\cos(\phi-\phi-\alpha) + i(m-m')(\alpha+\phi-\frac{\pi}{2})]d\alpha$$
$$= \exp[i(m-m')(\phi-\frac{\pi}{2})]\int_o^{2\pi} \exp[-ikb\theta\cos(-\alpha) + i(m-m')\alpha]d\alpha$$
$$= \exp[i(m-m')(\phi-\frac{\pi}{2})]I_2$$
$$I_2 = \int_o^{2\pi} exp[-ikb\theta\cos\alpha + i(m-m')\alpha]d\alpha$$

Let $\alpha = \beta - \frac{\pi}{2}$

$$I_2 = \int \exp[-ikb\theta\sin\beta + i(m-m')\beta - i\frac{\pi}{2}(m-m')]d\beta$$
$$= \exp[-i\frac{\pi}{2}(m-m')]\int_o^{2\pi} \exp[-ikb\theta\sin\beta + i(m-m')\beta]d\beta$$
$$= \exp[-i\frac{\pi}{2}(m-m')]I_3$$
$$I_3 = \int_o^{2\pi} \exp[-ikb\theta\sin\beta + i(m-m')\beta]d\beta$$
$$= \int_o^{2\pi} \cos\{(m-m')\beta - kb\theta\sin\beta\}d\beta + i\int_o^{2\pi} \sin\{(m-m')\beta - kb\theta\sin\beta\}d\beta$$
$$= 2\pi J_{(m-m')}(kb\theta) \text{ from Watson (1966)}$$

Therefore

$$I_1 = \exp[i(m-m')\phi]\exp[-i(m-m')\frac{\pi}{2}]\exp[-i(m-m')\frac{\pi}{2}]2\pi J_{(m-m')}(kb\theta)$$
$$= \exp[i(m-m')\phi](-1)^{m-m'}2\pi J_{m-m'}(kb\theta)$$
$$= 2\pi\exp[i(m-m')\phi]J_{(m'-m)(kb\theta)}$$

and the Eikonal scattering amplitude is

$$f_{n'\ell'm'n\ell m} = i\mu v\exp[i(m-m_i)\phi]\int bdb(\delta_{n'\ell'm'n\ell m} - S^{SF}_{n'\ell'm'n\ell m})$$
$$\times J_{(m'-m)}(kb\theta)$$

Appendix B
The Stationary Phase approximation

The partial wave expression for the scattering amplitude f(θ) is

$$f(\theta) = \frac{1}{2ik}\sum_{l=0}(2l+1)e^{2i\eta_l}P_l(\cos\theta) \tag{B.1}$$

$$= -\frac{i}{2k}\sum_{l=0}2(l+\frac{1}{2})e^{2i\eta_l}P_l(\cos\theta) \tag{B.2}$$

In the limit of large l $P_l(\cos\theta)$ can be approximated by

$$P_l(\cos\theta) = \left[\frac{2}{\pi l\sin\theta}\right]^{\frac{1}{2}}\cos(e+\frac{1}{2})\theta - \frac{\pi}{4}$$

$$= \frac{1}{2}\left[\frac{2}{\pi l\sin\theta}\right]^{\frac{1}{2}}\left[exp\{i[(l+\frac{1}{2})\theta - \frac{\pi}{4}]\} + exp\{-i[(l+\frac{1}{2})\theta - \frac{\pi}{4}]\}\right]$$

In B.2 l + $\frac{1}{2} \approx$ l' in the limit of large l, and the summation can be changed to an integral

$$f(\theta) \approx -\frac{i}{2k}\int ldle^{2i\eta_l}\left[\frac{2}{\pi l\sin\theta}\right]^{\frac{1}{2}}\left[exp[i(l\theta - \frac{\pi}{4})] + exp[-i(l\theta - \frac{\pi}{4})]\right]$$

Removing the factor of -i by using

$$\cos\frac{\pi}{2} - i\sin\frac{\pi}{2} = exp(-i\frac{\pi}{2})$$

$$f(\theta) = \frac{1}{k(2\pi\sin\theta)^{\frac{1}{2}}}\int l^{\frac{1}{2}}dl[exp(i\phi^+) + exp(i\phi^-)]$$

where

$$\phi^{\pm} = 2\eta_l - \frac{\pi}{2} \pm (l\theta - \frac{\pi}{4})$$

and

$$\frac{\partial \phi -}{\partial l} = 2\frac{\partial \eta_l}{\partial l} - \theta$$

Using the JWKB classical phase shift η_l, the classical deflection function Θ is retrieved from $\Theta = 2\frac{\partial \eta}{\partial l}$

The ϕ_- can be expanded about the point $l = l_\theta$ giving

$$\phi_-(l) \approx \phi_-(l_\theta) + \frac{1}{2}\phi_-^{"}(l_\theta)(l - l_\theta)^2$$

$$\phi_-^{"}(l_\theta) = -\frac{\partial \Theta}{\partial l} \mid_{l=l_\theta}$$

$$f(\theta) \approx \frac{l_\theta^{\frac{1}{2}}}{k(2\pi \sin\theta)^{\frac{1}{2}}} exp(i\phi_-(l_\theta)) \int exp(-\frac{i\partial \Theta}{2\partial l}(l - l_\theta)^2) dl$$

$$exp(i\frac{\partial \Theta}{\partial l}(l - l_\theta)^2) \simeq exp(i\frac{\partial \Theta}{\partial l} l^2)$$

$$f(\theta) \approx \frac{l_\theta^{\frac{1}{2}}}{k(\pi \sin\theta)^{\frac{1}{2}}} \left[\frac{\pi}{\mid \frac{\partial \theta}{\partial l} \mid}\right]^{\frac{1}{2}} exp(\frac{i\pi}{4}) \exp(i\phi_-(l_\theta))$$

where the integral

$$\int_{-\infty}^{\infty} exp(-iax^2) dx = \left[\frac{\pi}{a}\right]^{\frac{1}{2}} \exp(-\frac{i\pi}{4})$$

has been used.

The scattering amplitude in the Stationary Phase approximation is therefore

$$f(\theta) \approx \frac{l_\theta^{\frac{1}{2}}}{k(\mid \frac{d\theta}{dl} \mid \sin\theta)^{\frac{1}{2}}} \times \exp(i(\phi_-(l_\theta) - \frac{\pi}{4}))$$

$$f(\theta) \approx \left[\frac{b}{\sin\theta \mid \frac{d\theta}{db} \mid}\right]^{\frac{1}{2}} exp(i(2\eta_{l_\theta} - l_\theta\theta - \frac{\pi}{2}))$$

Appendix C
An Expression for the Internuclear Phase.

The classical trajectory in the centre of mass frame is shown below.

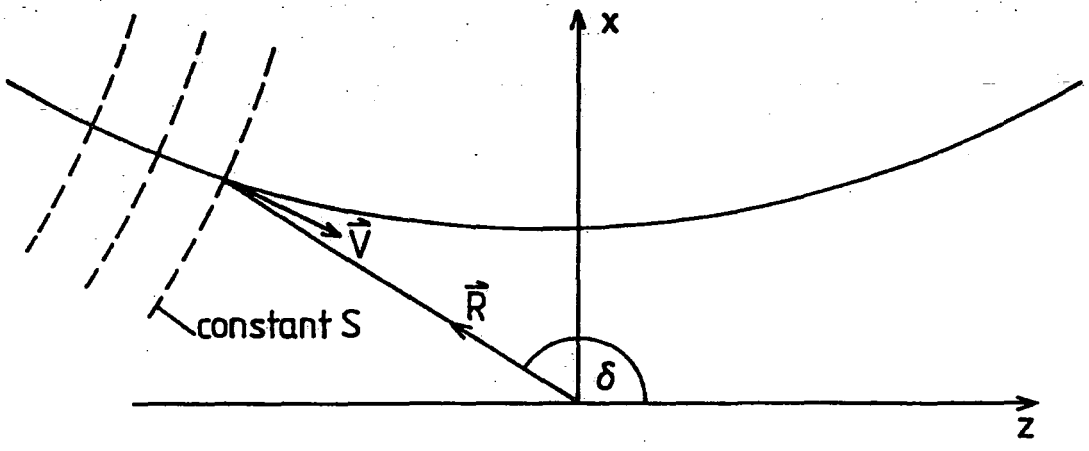

From Goldstein (1980), $\vec{\nabla}_R$ S is parallel to the normal to the surface at which S is constant.

From 2.32

$$\vec{\nabla}_R S(\vec{R}) = \{2\mu[E_{cm} - W(R)]\}^{\frac{1}{2}} \tag{C.1}$$

and

$$S(\vec{R}) = \int \vec{\nabla}_R S(\vec{R}).d\vec{s} \tag{C.2}$$

$S(\vec{R})$ is parallel to the velocity $\vec{v}$ along the trajectory, and so

$$\int \vec{\nabla}_R S(\vec{R}).d\vec{s} = \int |\vec{\nabla}_R S(\vec{R})|\,\hat{v}.d\vec{s} \tag{C.3}$$

The RHS of C3 can be expressed in terms of the cartesian coordinates x and z.

$$\hat{v} = \frac{1}{|\vec{v}|}\left(\frac{d\vec{x}}{dt} + \frac{d\vec{z}}{dt}\right) \text{ and } d\vec{s} = d\vec{x} + d\vec{z}$$

therefore

$$\vec{v}\ .d\ \vec{s} = \frac{1}{|\vec{v}|}[\frac{dx}{dt}dx + \frac{dz}{dt}dz]$$

The cartesian coordinates x and z are expressed in terms of R and δ

$$\begin{aligned}
x &= Rsin\delta; \quad z = Rcos\delta; \\
dx &= sin\delta dR \quad +Rcos\delta d\delta; \\
dz &= cos\delta dR \quad -Rsin\delta d\delta; \\
\frac{dx}{dt} &= \dot{R}sin\delta \quad +Rcos\delta\dot{\delta}; \\
\frac{dz}{dt} &= \dot{R}cos\delta \quad -Rsin\delta\dot{\delta};
\end{aligned}$$

and

$$\begin{aligned}
\frac{dx}{dt}dx + \frac{dz}{dt}dz == (sin\delta dR + Rcos\delta d\delta)(\dot{R}sin\delta + Rcos\delta\dot{\delta} + \\
+(cos\delta dR - Rsin\delta d\delta)(\dot{R}cos\delta - Rsin\delta\dot{\delta}) \\
= \dot{R}dR + R^2\dot{\delta}d\delta \\
= \dot{R}dR + R^2\tilde{\delta}\frac{d\delta}{dR}dR \\
|\vec{v}| = \{\left(\frac{dx}{dt}\right)^2 + \left(\frac{dz}{dt}\right)^2\}^{\frac{1}{2}} \\
= [(\dot{R}sin\delta + Rcos\delta\dot{\delta})^2 + (\dot{R}cos - \delta Rsin\delta\dot{\delta})^2]^{\frac{1}{2}} \\
= (\dot{R}^2sin^2\delta + R^2cos^2\delta\dot{\delta}^2 + 2R\dot{R}sin\delta cos\delta\dot{\delta} + \dot{R}^2cos^2\delta \\
+R^2sin^2\delta\dot{\delta}^2 - 2R\dot{R}sin\delta cos\delta\dot{\delta})^{\frac{1}{2}} \\
= (\dot{R}^2 + R^2\delta^2)^{\frac{1}{2}} \\
= \dot{R}[1 + R^2\dot{\delta}^2\{\frac{dt}{dR}\}^2]^{\frac{1}{2}} \\
= \dot{R}[1 + R^2\{\frac{d\delta}{dR}\}^2]^{\frac{1}{2}} \\
\vec{v}\ .d\ \vec{s} = \frac{(\dot{R} + R^2\delta\frac{d\delta}{dR})dR}{\dot{R}(1 + R^2\{\frac{d\delta}{dR}\}^2)^{\frac{1}{2}}} \\
= \frac{\dot{R}(1 + R^2\frac{d\delta}{dt}\frac{dt}{dR}\frac{d\delta}{dR})dR}{\dot{R}(1 + R^2\{\frac{d\delta}{dR}\}^2)^{\frac{1}{2}}} \\
= \frac{(1 + R^2(\frac{d\delta}{dR})^2)dR}{(1 + R^2(\frac{d\delta}{dR})^2)^{\frac{1}{2}}} \\
= (1 + R^2\{\frac{d\delta}{dR}\}^2)^{\frac{1}{2}}dR
\end{aligned}$$

which from 2.18 is $\frac{ds}{dR}$.

Returning to C1 and substituting for $\vec{v}\ .d\ \vec{s}$

$$\int \vec{\nabla}_R\, S(\vec{R}).d\ \vec{s} = \int |\vec{\nabla}_R\, (S(R))\, |\vec{v}\ .d\ \vec{s}$$

$$= \int [2\mu(E_{cm} - W(R))]^{\frac{1}{2}} \frac{ds}{dR} dR$$

$$\vec{\nabla}_R\, S(\vec{R}) ds = [2\mu(E_{cm} - W(R))]^{\frac{1}{2}} ds$$

which is expression 2.33.

$$S(\vec{R}) = [2\mu E_{cm}]^{\frac{1}{2}} (1 - \frac{W(R)}{E_{cm}})^{\frac{1}{2}}$$

Appendix D
Derivation of the Relationships 2.67, 2.68 and 2.69

To show that

$$\vec{\nabla}_{r_g} \gamma_n^B = \vec{v}_B; \ \nabla_{r_g}^2 \gamma_n^B = 0 \tag{D.1}$$

The electron bound to B has translation phase factors of the form $e^{i\gamma B_n}$ where

$$\gamma_n^B = \vec{v}_B \cdot \vec{r}_g - \int_o^t dt(\epsilon_n + \frac{v_B^2}{2}) \tag{D.2}$$

Considering the L.H.S. of D.1

$$\vec{\nabla}_{r_g} \gamma_n^B = \vec{\nabla}_{r_g} \vec{v}_B \cdot \vec{r}_g + \vec{v}_B \cdot \vec{\nabla}_{r_g} \cdot r_g - 0$$

$\vec{\nabla}_{r_g} \vec{v}_B = 0$ as $\vec{v}_B$ is constant with respect to $\vec{r}_g$ during the integration of the matrix elements.

$\vec{\nabla}_{r_g} \cdot \vec{r}_g = 1$ and

$$\vec{\nabla}_{r_g} \gamma_n^B = \vec{v}_B \quad \nabla_{r_g}^2 \gamma_n^B = 0 \tag{D.3}$$

To show that

$$\frac{\partial}{\partial t} |_{r_g} \phi = - \vec{v}_B \cdot \vec{\nabla}_{r_g} \phi \tag{D.4}$$

The L.H.S. of D.4 can be expressed as a product of partial fractions

$$\frac{\partial}{\partial t} |_{r_g} \phi = \frac{\partial \vec{R}}{\partial t} \times \frac{\partial \vec{r}_g}{\partial R} \times \frac{\partial \phi_n}{\partial r_g}$$

from the relationship

$$\vec{r}_g = \vec{r}_B + q\,\vec{R}$$

$$\frac{\partial \vec{r}_g}{\partial R} = q$$

$$\frac{\partial}{\partial t}\,|_{r_g}\,\phi = q\frac{\partial \vec{R}}{\partial t}\frac{\partial \phi_n}{\partial r_g}$$

$$= -\,\vec{v}_B\,.\,\vec{\nabla}_{r_g}\,\phi \qquad \text{(D.5)}$$

Considering

$$\dot{\gamma}_n^B = \frac{\partial}{\partial t}\,\vec{v}_B\,.\,\vec{r}_g + \vec{v}_B\,.\frac{\partial}{\partial t}\,\vec{r}_g - \epsilon_n - \frac{v_B^2}{2} \qquad \text{(D.6)}$$

The second expression $\vec{v}_B\,.\frac{\partial}{\partial t}\,\vec{r}_g$ is zero and $\dot{\gamma}_n^B = \vec{v}_B\,.\,\vec{r}_g - \epsilon_n - \frac{v_B^2}{2}$.
Expression 2.66 is

$$[H_{el} - \frac{i\partial}{\partial t}]exp(i\gamma_n^B)\phi =$$

$$exp(i\gamma_n^B)[H_{el} - i\,\vec{\nabla}_{r_g}\,\gamma_n^B.\,\vec{\nabla}_{r_g} - \frac{1}{2}\nabla_{r_g}^2(i\gamma)$$

$$-i\frac{\partial}{\partial t} + \dot{\gamma}_n^B]\phi$$

When the above expressions are substituted into 2.66 the expression becomes

$$exp(i\gamma_n^B[H_{el} + \frac{\partial}{\partial t}\,|_{r_g} + \frac{v_B^2}{2} - \frac{i\partial}{\partial t}\,|_{r_g} - \epsilon_n + \dot{\vec{v}}_B.\,\vec{r}_g$$

$$-\frac{v_B^2}{2}]\phi$$

$$= exp(i\gamma_n^B)[H_{el} - \epsilon_n + \dot{\vec{v}}_B.\,\vec{r}_g]\phi \qquad \text{(D.7)}$$

Bibliography

[1] Abramowitz M. and Stegun I. A. (1964) Handbook of Mathematical Functions. Dover Publications.

[2] Allan R. J. (1986) J. Phys. B 19 321.

[3] Allan R. J. (1988) Private Communication.

[4] Allan R. J. (1989) Private Communicatiojn.

[5] Allan R. J., Shingal R. and Flower D. R. (1986) J. Phys. B. 19 L251.

[6] Anderson C.J., Howald A.M. and Anderson L.W. (1979) Nucl. Instrum. Meths. 165 583.

[7] Bardsley J. N. (1974) Case Studies in Atomic Physics V4: Ed. E.W. McDaniel (North Holland, Amsterdam) p302.

[8] Bates D.R. (1960) Proc. Roy. Soc. A 257 22.

[9] Bates D. R. and Boyd A. H. (1962a) Proc. Phys. Soc. 79 710.

[10] Bates D. R. and Boyd A. H. (1962b) Proc. Phys. Soc. 80 1301.

[11] Bates D. R. and Crothers D. S. F. (1970) Proc. Roy. Soc. Lond. A 315 465-478.

[12] Bates D. R., Johnston H. C. and Stewart I. (1964) Proc. Phys. Soc. V84 517.

[13] Bates D. R., Massey H. S. W. and Stewart A. L. (1953) Proc. Roy. Soc. Lond. Ser. A 216 437.

[14] Bates D. R. and McCarroll R. (1958) Proc. Roy. Soc. Lond. A 245 175.

[15] Bates D.R. and Moiseiwitsch B. L. (1954) Proc. Phys. Soc. A67 805.

[16] Bates D. R. and Sprevak D. (1970) J. Phys. B 3 1483.

[17] Bates D. R. and Williams D. A. (1964)Proc. Phys. Soc. 83 425.

[18] Bethe H. A. and Salpetre E.E. (1957) Quantum Mechanics of one and Two Electron Atoms. Springer Verlag.

[19] Bottcher C. and Dalgarno A. (1974) Proc. Roy. Soc. Lond. A340. 187.

[20] Bransden B.H. (1969) Case Studies At. Physics 1 171.

[21] Bransden B. H. (1972) The Theory of Charge Exchange. Rep. Prog. Phys. 35 949-1005.

[22] Bransden B. H. (1983) Atomic Collision Theory: Second Edition. Benjamin/Cummings

[23] Bransden B. H. (1988) Unpublished Notes.

[24] Bransden B. H., Ermoleov A. M. and Shingal R. (1984) J. Phys. B 17 4515.

[25] Bransden B. H. and Forster C. (1990) J. Phys. B.23 115.

[26] Bransden B. H. and Joachain C.J. (1983) Physics of Atoms and Molecules.

[27] Bransden B. H. and Noble C. J. (1981) J. Phys. B. 14, 1849.

[28] Bransden B. H. and Noble C. J. (1982) J. Phys. B. 15, 451.

[29] Bransden B. H., Noble C. J. and Chandler J. (1983) J. Phys. B. 16. 4191.

[30] Briggs J. S. (1976) Rep. Prog. Phys. 39 217-289.

[31] Broglia R. A., Landowne S., Malfliet R. A., Rostokin V. and Winter A. (1974) Phys. Rep.11 1-28.

[32] Burns W. D. and Crothers D. S. F. (1976) J. Phys. B Vol. 9 No.14 2479.

[33] Chen J. C. Y. and Watson K. M. (1969) Phys. Rev. 188 236

[34] Cheshire I. M., Gallaher D. F., Taylor A. J. (1969) J. Phys. B Vol.3 813.

[35] Chidichimo-Frank M. C., Piacentini R. D. (1974) J. Phys. B Vol.7 No.5 548.

[36] Child M. S. (1974) Quantum Collision Theory. Academic Press Inc.

[37] Clenshaw C. W. and Curtis A. R. (1960) Numerische Mathematik V2 197.

[38] Coleman J. P. (1980) Computer Physics Communications 21 109

[39] Connor J. N. L. (1979) Semiclassical Methods in Molecular scattering and Spectroscopy. Chapter 2. NATO ASI.

[40] Connor J. N. L. and Marcus R. A. (1971) J. Chem. Phys. 55 5636.

[41] Corrigall B. and Wallace R. (1971) J. Phys. B Vol.4 1013.

[42] Crothers D. S. F.(1978) J. Phys. B 11 1025.

[43] Crothers D. S. F. and Hughes J. G. (1978) Proc. Roy. Soc. Lond. A 359 345.

[44] Crothers D. S. F. and Hughes J. G. (1979) Proc. Phil. Trans. Roy. Soc. 292 539.

[45] Crothers D. S. F. and Todd N. R. (1978) J. Phys. B. Vol 11 No. 21 L663.

[46] Crothers D. S. F. and Todd N. R. (1981) J. Phys. B 14 2233

[47] Crothers D. S. F. and Todd N. R. (1981) J.Phys. B 14 2251

[48] Dalgarno A. (1962) Advances in Physics 11 281.

[49] Daniele R. (1979) J. Chem. Phys. 70 (7) 3462.

[50] Delos J.B., Thorson W. R. and Knudson S. K.(1972) Phys. Rev A 6 709.

[51] Dickinson A. S. (1981) J. Phys.B 14 3685.

[52] Dickinson A. S. and Hardie D. J. W. (1979) J. Phys. B.12 4147.

[53] Falcon C. A. (1983) J. Phys. B 16 1793.

[54] Ferguson A. F. (1961) Proc. Roy. Soc. A264 540.

[55] Feynmann R. P. and Hibbs A. R. (1965) Quantum Mechanics and Path Integrals : McGraw-Hill.

[56] Fleming D. G. and Senba M. (1987) Nato Advanced Workshop on Atomic Physics with Positrons, Part 2.

[57] Flower D.R. (1983) Review of Atomic Physics as applied to the Diffuse Interstellar Medium. From Diffuse Matter in Galaxies, ed. J. Audouze et al. 239 : D. Reidel.

[58] Forster C., Shingal R.,Flower D. R., Bransden B. H. and Dickinson A. S. (1988) J. Phys. B 21 3941.

[59] Fritsch W. (1982) J. Phys. B 15 L389.

[60] Fritsch W. and Lin C. D. (1982a) J. Phys. B 15 L281.

[61] Fritsch W. and Lin C. D. (1982b) J. Phys. B 15 1255.

[62] Fritsch W. (1984) Phys. Rev A 30 1135.

[63] Froman N and Froman P.O. (1965) JWKB Approximation. (Amsterdam, North Holland).

[64] Froese Fisher C. (1977) The Hartree Fock Method for atoms. Wiley, New York.

[65] Gallaher D. F. and Wilets L. (1968) Phys. Rev. 169 139.

[66] Gaussorgues C., Le Sech C., Masnou-Seeuws F.,McCarroll R., Riera A. (1975a) J. Phys. B 8 No.2 239.

[67] Gaussorgues C., Le Sech C., Masnou-Seeuws F.,McCarroll R., Riera A. (1975b) J. Phys. B 8 No.2 253.

[68] Goldstein H. (1980) Classical Mechanics. Addison Wesley Series in Physics.

[69] Gradshteyn I. S. and Ryzhik I. M. (1980) Tables of Integrals, Series and Products. Academic Press.

[70] Green T. A. (1965) Proc. Phys. Soc. 86 1017-29.

[71] Green T.A., Shipsey E.J. and Browne J.C. (1981) Phys. Rev. A23 546.

[72] Greenland P. T. (1981) J. Phys. B 19 3707.

[73] Hardie D. J. W. (1981) Ph.D. Thesis Unpublished.

[74] Harshman D.R. (1987). Atomic Physics with Positrons. Ed. Humberstone. J. Armour P367.

[75] Hatton G. J., Lane N.F. and Winter T. G. (1979), J. Phys. B 12 L571.

[76] Helbig H. F. and Everhart E. (1965) Phys. Rev. 1 140 715.

[77] Houver J. C., Fayeton J. and Barad M. (1974) J. Phys. B V7 11 1358.

[78] Humberstone J.W. and McDowell M.R.C. (1983) Atomic Physics with Positrons.

[79] Humberston J. W. (1984) J. Phys. B 17 No. 11 2353.

[80] Jognaux A., Brouillard B. and Szucs S. (1978) J. Phys. B 11 No.21 L.669.

[81] Kimura M. and Thorson W. R. (1981) Phys. Rev. A Vol. 24 No.4 1780.

[82] Knudson S. K. and Thorson W. R. (1970) Can. J. Phys. 48 313.

[83] Landau L. D. and Lifshitz E. M. (1976) Mechanics : Course in Theoretical Physics. 3rd. Edition : Pergammon.

[84] Laughlin C. and Victor G. A. (1988) Adv. At. Mol. Phys. V 25. 163.

[85] Levy H. and Thorson W.R. (1969) Phys. Rev. 181 244.

[86] Lockwood G. J. and Everhart E. (1962) Phys. Rev 125 567

[87] McCarroll R. (1961) Proc. Roy Soc. A 264 547.

[88] McCarroll R. (1974) Atoms Molecules And Lasers; International Atomic energy Agency: Vienna 1974.

[89] McCarroll R. (1980) Atomic and Molecular Collision Theory: Ed Gianturco F. A. : Plenum.

[90] McCarroll R. and Salin A.(1968) J. Phys. B Ser.2 1 163.

[91] McCarroll R. Piacentini R. D. and Salin A. (1970) J. Phys. B Vol.3 137.

[92] Marcus R. A. (1970) Chem. Phys. Lett. 7 649.

[93] Marcus R. A. (1972a) J. Chem. Phys. 56 311.

[94] Marcus R. A. (1972b) J. Chem. Phys. 56 3548.

[95] Messiah A. (1962) Quantum Mechanics V2 Page 802, North Holland Publishing.

[96] Miller W. A. (1970a) J. Chem. Phys, 53 1949.

[97] Miller W. A. (1970b) J. Chem. Phys. 53 3578.

[98] Morse F. A. and Bernstein R. B. (1962), J. Chem Phys. 37 2019.

[99] Mott N. F. (1931) Proc. Camb. Phil. Soc. 27 553.

[100] Mott N. F. and Massey H. S. W. (1965) Theory of Atomic Collisions. 3rd. Edition. Oxford Clarendon Press.

[101] Newby C. W. (1985) J. Phys. B. 18 1781.

[102] Newman J. H., Cogan J. D., Ziegler D. L., Nitz D. E., Rundel R. D., Smith K. A. and Stebbings R. F. (1982) Phys. Rev. A 25.

[103] Nikitin E. E. and Ya Umanskii S. (1984) Theory of Slow Atomic Collisions : Springer Verlag.

[104] Oliver J. (1972) Comp. Jour. 15 141.

[105] Patterson T.N.L. (1968) The Optimum Addition of Points to Quadrature Formulae. Math. Comp. 22 p847.

[106] Peach G. (1982) Comment At. Mol. Phys. 11 101

[107] Peart B. and Dolder K. (1979) J. Phys. B Vol 12 No.24 4155.

[108] Pechukas P. (1969a) Phys. Rev. 181 166.

[109] Pechukas P. (1969b) Phys. Rev. 181 174.

[110] Perrot (1970) J. Phys. B. 9 L103.

[111] Piacentini R. D. and Salin A. (1974) J. Phys. B Vol 7 No.13 1666.

[112] Piacentini R. D. and Salin A. (1977) Computer Physics Communications 13 57-62.

[113] Post D. R. (1983) Physics of Ion-Ion and Electron-Ion Collisions: Ed. Brouillard F and McGowan J.W. NATO ASI V83 p 37.

[114] Rankin J. and Thorson W.R. (1978) Phys. Rev. A18 1990.

[115] Richards D. (1981) J. Phys. B 14 1465.

[116] Riera A. and Salin A. (1976) J. Phys. B 9 No.16 2877.

[117] Riera A. (1984) Phys. rev. A. V30, No. 5 2304.

[118] Rille E., Olson R. E., Peacher J. L., Blankenship D. M., Krale T. J., Redd E. and Park J. T. (1982) Phys. Rev. Letters 49 1819.

[119] Riley M. E. and Green T. A. (1971) Phys. Rev. A4 619.

[120] Rose M. E. (1957) Elementary Theory of Angular Momentum : Wiley.

[121] Ryufuku H. and Watanabe T. (1976) Journal of the Physical Society of Japan. Vol 41 No.3

[122] Schinke R. and Kruger H. (1976) J. Phys. B. V9 No. 14 2469.

[123] Schneiderman S. B. and Russek A. (1969) Phys. Rev. 181 311.

[124] Shakeshaft R. (1976) Phys. Rev. A 14 1626.

[125] Shampine L. F. and Gordon M. K. (1975) Computer Solutions of Ordinary Differential Equations: The Initial Value Problem. Freeman. San Francisco.

[126] Shingal R. (1985) Unpublished programs.

[127] Shingal R.(1986) Unpublished Results.

[128] Shingal R. (1988) J. Phys. B 21 2065,

[129] Shingal R., Bransden B. H., Ermoleov A. M., Flower D. R., Newby C. W. and Noble C. J. (1986) J. Phys B 19 309

[130] Shingal R., Bransden B. H. and Flower D. R. (1987) J. Phys. B 20 L477.

[131] Slater J. C. (1963) Quantum Theory of Molecules and Solids V1 : McGraw-Hill.

[132] Slim H. (1990) Private Communication.

[133] Thorson W.R. (1965) J. Chem. Phys. 42 3878.

[134] van Hemert M. C., van Dishoeck E. F., van der Hart J. A. and Koike F. (1985) Phys. Rev. A 31 No.4 2227.

[135] Watson G. N. (1966) Theory of Bessel Functions. Second edition. Cambridge University Press.

[136] Wetmore A. E., Cole H. R., and Olson R. E. (1986) J. Phys. B 19 1515.

[137] Winter T. G., Hatton G. J., Day A. R. and Lane N.F. (1987) Phys. Rev. A Vol. 36 No.2 625.

[138] Winter T. G. (1988) Phys. Rev. A, Vol.38 No.3 1612.

J. Phys. B: At. Mol. Opt. Phys. 21 (1988) 3941-3948. Printed in the UK

Total and differential cross sections for charge transfer in He^{2+}–He^{+} collisions: trajectory effects

C Forster†, R Shingal†, D R Flower†, B H Bransden† and A S Dickinson‡

† Physics Department, The University, Durham DH1 3LE, UK

‡ Physics Department, The University, Newcastle upon Tyne NE1 7RU, UK

Received 18 July 1988

Abstract. Cross sections have been computed for charge transfer in collisions between $^4He^+$ and $^4He^{2+}$ ions for centre-of-mass collision energies $0.21 \leq E \leq 2.50$ keV. The semi-classical impact parameter method was employed, with a basis of atomic orbitals modified by plane-wave translation factors. Both rectilinear and Coulomb trajectories were used, and the differential cross sections were found to be sensitive to the assumed form of trajectory. Comparison is made with molecular orbital calculations by Dickinson and Hardie.

1. Introduction

Charge transfer in collisions between ions and atoms has been intensively studied in view of its importance as a fundamental atomic process which occurs in both astrophysical and laboratory plasmas, including tokamak plasmas. To date the emphasis has been placed on measuring and computing integral charge transfer cross sections, with a greater or lesser degree of selection of the final state. Much less effort has been devoted to determining differential charge transfer cross sections, which provide more detailed information on the scattering process.

For centre-of-mass energies in excess of about 100 eV a classical description of the relative nuclear motion is appropriate. Straight-line paths are often supposed in practice, although the curvature of the trajectory becomes more significant as the collision energy decreases. Fritsch (1982) and van Hemert *et al* (1985) have studied nuclear trajectory effects in C^{6+}–H and He^{2+}–H scattering, respectively. In both cases it was found that the nuclear repulsion leads to a substantial reduction in the charge transfer cross sections with decreasing collision energy, E. For example, at $E = 100$ eV amu^{-1} the total cross section for charge transfer in C^{6+}–H scattering was smaller by a factor 0.63 when a Coulomb trajectory was assumed.

In the present paper, we investigate trajectory effects on both integral and differential cross sections for charge transfer in He^{2+}–He^{+} collisions. A symmetric, one-electron system was chosen because of the simplicity of the charge transfer process, which is dominated by resonant capture from the 1s ground state of the He^+ target. For this system, comparison may be made with the measurements by Jognaux *et al* (1978) and by Peart and Dolder (1979) of the process in which the nuclei are isotopically distinct, e.g.

$$^4He^+ + {}^3He^{2+} \rightarrow {}^4He^{2+} + {}^3He^+.$$

0953-4075/88/233941+08$02.50

The size of the acceptance angles of the detectors limited the angular resolution of the differential charge transfer cross section in these experiments. This angular resolution was taken into account by Dickinson and Hardie (1979), who compared their semiclassical calculations with the measurements.

Our own calculations of both integral and differential cross sections are described in § 2. The results are presented and discussed in § 3, followed by our concluding remarks in § 4.

2. Calculations

The semiclassical impact parameter method, with plane-wave translation factors, is an established technique for the theoretical study of excitation, ionisation and charge transfer in atomic collisions (see, for example, Bransden (1983)). In the implementation used here, the electronic wavefunction is expanded in terms of atomic orbitals located on each nucleus. A two-state expansion was adopted, incorporating the hydrogenic 1s states on each centre, which are Slater-type orbitals. The sufficiency of a two-state approximation was checked by comparing with the results of a twenty-state calculation (all distinct $n = 1, 2$ and 3 atomic orbitals on either nucleus) of the charge transfer cross section at $E = 0.5$ and 2.5 keV. The two-state and twenty-state calculations agreed to within about three per cent. Furthermore, the twenty-state calculation showed that the cross section technique for capture into the ground (1s) state was practically equal to the total charge transfer cross section, which is the quantity which has been determined experimentally.

The integrals over the electronic coordinates were evaluated in the body-fixed frame using prolate spheroidal coordinates and Gaussian quadrature schemes developed by one of us (Shingal 1984 unpublished). These matrix elements were then rotated into the space-fixed frame.

In our previous work it was assumed that the nuclei follow rectilinear trajectories, in which case their distance of closest approach is equal to the classical impact parameter. This restriction has since been removed in order that the effect on the trajectory, and hence the cross sections, of the Coulomb repulsion of the nuclei may be treated correctly. The calculation yields the transition amplitudes in the asymptotic region, $a_m(\rho, t \to \infty)$, as functions of the impact parameter, ρ. The corresponding integral cross section is obtained from

$$\sigma_m = 2\pi \int_0^\infty |a_m(\rho, t \to \infty)|^2 \rho \, d\rho. \tag{1}$$

Differential cross sections have been calculated with the aid of the program EIKON of Piacentini and Salin (1977). As the name suggests, this program is based on the eikonal approximation and is applicable to scattering through small angles. The original version of the program takes, as input, transition amplitudes evaluated on straight-line trajectories. In order to process, in a self-consistent manner, amplitudes generated on curved trajectories, it has been necessary to modify the expressions for the electronic and nuclear phases, as described below.

2.1. Internuclear phase

For the case of a straight-line path, the internuclear phase may be written (cf equation

(6) of Piacentini and Salin (1977)), in atomic units,

$$-(2Z_AZ_B/v)\int_0^\infty \frac{1}{R}\,dz$$

where v is the incident (relative) velocity, $z = vt$ is measured along the trajectory which is symmetric about $t = 0$, the point of closest approach, where the internuclear distance $R = \rho$ and Z_A and Z_B are the nuclear charges. For a curved trajectory the phase becomes

$$-(2Z_AZ_B/v)\int_0^\infty \frac{1}{R}\,ds$$

where s is measured along the trajectory from the point of closest approach where $R = R_0$ ($>\rho$ for $Z_A, Z_B > 0$). Denoting Z_AZ_B/E by α, where $E = \mu v^2/2$ is the incident energy in the centre-of-mass coordinate system and μ is the reduced mass, we have

$$ds = \pm dR\frac{[1-(\alpha/R)]^{1/2}}{[1-(\alpha/R)-(\rho^2/R^2)]^{1/2}}$$

and hence

$$-(2Z_AZ_B/v)\int_0^\infty \frac{1}{R}\,ds \approx -(2\mu E)^{1/2}\int_{R_0}^\infty \frac{\alpha}{(R^2-\alpha R-\rho^2)^{1/2}}\,dR \tag{2}$$

where terms of order α^2/R^2 and higher have been neglected, consistent with the assumption of scattering through small angles.

The integral in (2) is logarithmically divergent, but, as noted by Piacentini and Salin (1977), the divergent contribution is independent of the impact parameter, ρ, and the corresponding phase factor may be extracted from the integral (1) over ρ. As only the square of the modulus of the phase factor occurs in the expression for the cross section, the divergent contribution to the integral (2) vanishes. Performing the (standard) integral (2), we obtain the significant contribution to the phase,

$$(2\mu E)^{1/2}(\alpha/2)\ln[(\alpha/2)^2+\rho^2].$$

2.2. Electronic phases

As Gaussorgues *et al* (1975) pointed out, when evaluating *differential* cross sections the phase factor arising from the long-range Coulomb attraction between the electron and the incoming/outgoing nucleus must be taken into account. If the coupled differential equations for the transition amplitudes are integrated from $t = -t_{max}$ to $t = t_{max}$ and if $Z_A = Z_B = Z$, this additional phase may be written

$$2Z\int_{t_{max}}^\infty \frac{1}{R}\,dt = \frac{2Z}{v}\int_{R_{max}}^\infty \frac{dR}{(R^2-\alpha R-\rho^2)^{1/2}} \tag{3}$$

in which $R = R_{max}$ when $t = t_{max}$. Performing the integral and treating the divergent limit $R \to \infty$ as above, we obtain the significant contribution to the electronic phase

$$-\frac{2Z}{v}\ln\left[1-\frac{\alpha}{2R_{max}}+\left(1-\frac{\alpha}{R_{max}}-\frac{\rho^2}{R_{max}^2}\right)^{1/2}\right].$$

3. Results

In figure 1 is shown the integral charge transfer cross section as a function of the collision energy, E, in the centre-of-mass frame, for $0.21 \leqslant E \leqslant 2.5$ keV. Results obtained on assuming both rectilinear and curved trajectories are compared with the calculations of Dickinson and Hardie (1979). Following Bates and Boyd (1962), these authors used a two-state form of the perturbed stationary-state approximation, evaluating the difference in the non-Coulomb phaseshifts due to the gerade and ungerade scattering potentials by means of the JWKB approximation, in which the Coulomb repulsion of the nuclei was taken into account.

It may be seen from figure 1 that the nuclear repulsion leads to a reduction in the charge transfer cross section at low energies, where the results of Dickinson and Hardie fall between our rectilinear and Coulomb trajectory calculations. At high energies, the inclusion of translation factors ensures that our results lie below those of Dickinson and Hardie. All three determinations of the integral charge transfer cross section agree to within about 10 per cent, even at the lowest energies considered.

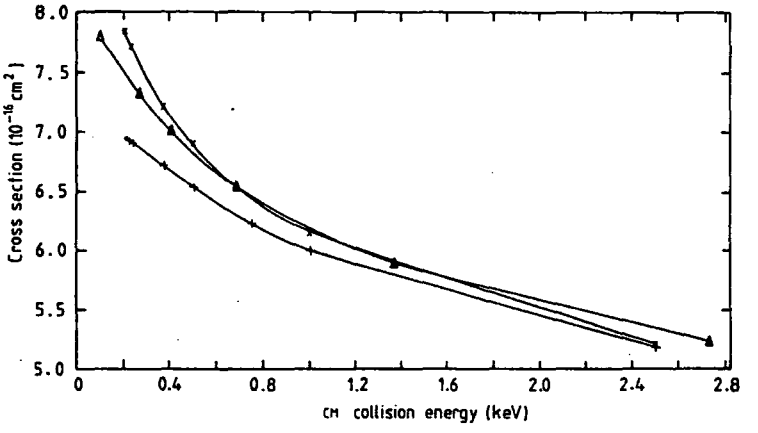

Figure 1. Integral charge transfer cross sections, in units of 10^{-16} cm^2, as functions of the centre-of-mass collision energy, in keV: +++ curved trajectory, present results; ××× straight-line trajectory, present results; ΔΔΔ Dickinson and Hardie (1979).

The integrand, $\rho|a(\rho, t \to \infty)|^2$ of equation (1) for the charge transfer cross section is plotted in figure 2 as a function of the impact parameter, ρ, for the centre-of-mass collision energy $E = 0.21$ keV. As noted by Dickinson and Hardie (1979), the integrand may also be written as $\rho \sin^2 \xi(\rho)$, where $\xi(\rho)$ is the difference between the non-Coulomb phaseshifts due to the scattering potentials arising from the lowest gerade and ungerade molecular states. The oscillatory structure which arises from the variation of ξ with ρ is clearly visible in figure 2.

The oscillatory structure in the variation of the integrand with ρ is reflected in the dependence of the differential cross section, $d\sigma/d\Omega$, on the scattering angle, θ, where $d\Omega = 2\pi \sin\theta \, d\theta$. An accurate determination of the differential cross section requires the transition amplitude, $a(\rho, t \to \infty)$, to be computed at a large number of values of ρ. Convergence tests with respect to this parameter were carried out, in the light of which $d\sigma/d\Omega$ was computed from a grid of 330 values of ρ at the lowest energy

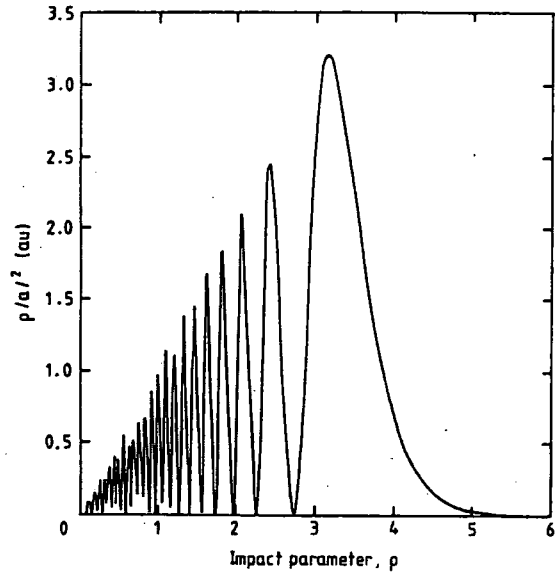

Figure 2. Plot of $\rho|a|^2$, in atomic units, against ρ, where ρ is the impact parameter and a is the amplitude for charge transfer. The centre-of-mass collision energy is 0.21 keV.

($E = 0.21$ keV) and of 210 values at the higher energies considered; this grid served as a basis for interpolation.

The differential cross section for charge transfer, derived assuming Coulomb trajectories, is plotted in figure 3 for $E = 0.21$, 0.50 and 2.50 keV. As expected, the cross section peaks at smaller scattering angles as the energy increases. At a given energy, elastic scattering dominates in the direction of forward scattering. As θ increases the importance of the elastic and charge transfer processes becomes comparable, resulting in interference and the oscillatory structure which is apparent in figure 3. We have

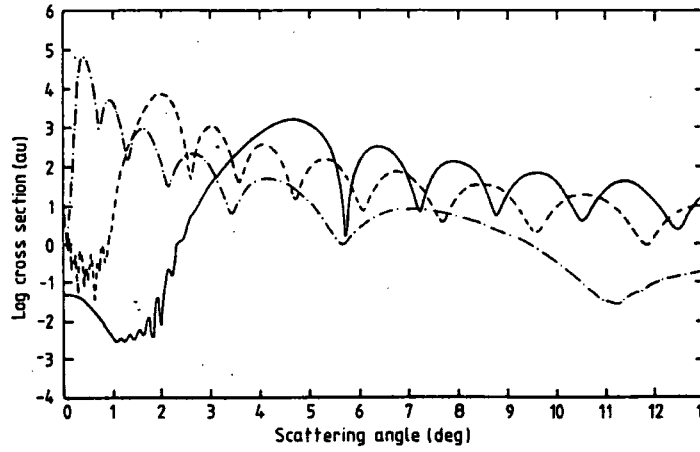

Figure 3. The logarithm (base 10) of the differential cross section (atomic units) for charge transfer as a function of the scattering angle (degrees) in the centre-of-mass system. Full curve, $E = 0.21$ keV; broken curve, $E = 0.50$ keV: chain curve, $E = 2.50$ keV.

noted above that these oscillations may also be interpreted in terms of the interference between scattering in the gerade and ungerade molecular states, which arise owing to the identity of the nuclear charges.

The effects on the differential cross section for charge transfer of introducing a Coulomb trajectory may be seen in figure 4. The main influence of the curvature of the trajectory is to shift $d\sigma/d\Omega$ to larger values of the scattering angle, θ, as might have been expected. The results presented in this figure confirm the anticipation that the differential cross section is a more sensitive probe of the scattering process than the integral cross section. The differences between the straight-line path and curved trajectory calculations of $d\sigma/d\Omega$ may be seen to attain between one and two orders of magnitude at certain values of θ.

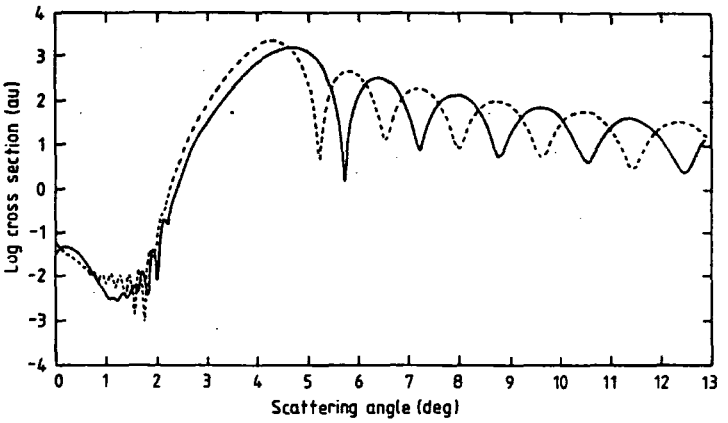

Figure 4. The logarithm (base 10) of the differential cross section (atomic units) for charge transfer, plotted against the centre-of-mass scattering angle (degrees). Full curve, curved trajectory; broken curve, straight-line trajectory. The collision energy is 0.21 keV.

Dickinson and Hardie (1979) compared their calculations of the cross section for charge transfer in collisions between $^4He^+$ and $^3He^{2+}$ with the measurements of Peart and Dolder (1979) and Jognaux *et al* (1978) by integrating the differential cross section over the instrumental acceptance angles. The theoretical results agreed significantly better with the measurements of Peart and Dolder than with the corresponding measurements of Jognaux *et al*. With this discrepancy in mind, it is instructive to compare our calculations, integrated over the acceptance angles, with results obtained using the same approach as Dickinson and Hardie.

The computed differential cross sections for charge transfer in collisions between $^4He^+$ and $^4He^{2+}$ ions are compared in figure 5 at a centre-of-mass collision energy of 0.5 keV. The computations may be seen to be very similar in magnitude but to be out of phase, with the result that the values of $d\sigma/d\Omega$ at particular values of θ can differ by an order of magnitude. When the differential cross sections are integrated over the instrumental acceptance angles, however, these differences are effectively 'washed out'. Thus, at the lowest energy considered (0.21 keV), the integrals agree to approximately ten per cent and to within one per cent at the highest energy (2.50 keV). We conclude that our (independent) calculations confirm the earlier theoretical work of Dickinson and Hardie (1979), casting further doubt on the specifications of the energy and acceptance angles in the experiments of Jognaux *et al* (1978). A similar conclusion

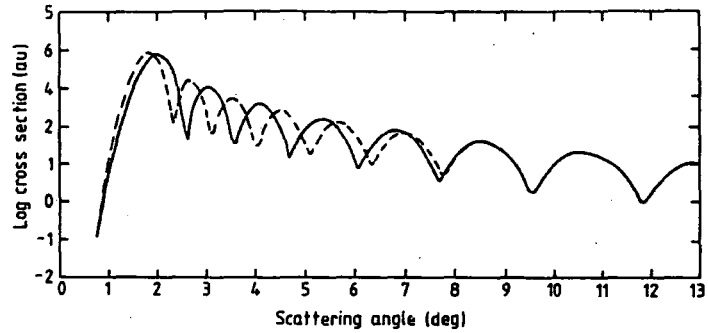

Figure 5. The logarithm (base 10) of the differential cross section (atomic units) for charge transfer, plotted against centre-of-mass scattering angle (degrees). Full curve, present curved trajectory calculations; broken curve, results obtained using the approach of Dickinson and Hardie (1979). The collision energy is 0.50 keV.

was reached by Falcon (1983), who performed quantal calculations of the differential cross sections for collision energies $E \leqslant 100$ eV in the centre-of-mass system. It is clear that measurements with finer angular resolution will be required to probe the charge transfer process in more detail.

4. Concluding remarks

We have investigated the importance of (Coulomb) trajectory effects on the cross section for charge transfer in collisions between He^{+} and He^{2+} ions, in the range of centre-of-mass energies $0.21 \leqslant E \leqslant 2.5$ keV. The integral cross section was found to be significantly reduced by the curvature of the trajectory at the lower energies considered. The differential cross section was much more sensitive to the relative nuclear trajectory, the cross sections for the straight-line and Coulomb cases differing by one to two orders of magnitude at given values of the scattering angle.

Comparison was made with calculations based upon the perturbed stationary-state approximation, as implemented by Dickinson and Hardie (1979). Their calculations were in satisfactory accord with the measurements of Peart and Dolder (1979), when the computed differential cross sections had been integrated over the acceptance angle of the detector. Whilst the variation with scattering angle of our differential cross sections differs appreciably from the perturbed stationary-state results, the integration over the acceptance angle brings the two calculations into close agreement. Experiments with finer angular resolution would lead to a more complete understanding of the charge transfer process.

Acknowledgments

The calculations were performed on NUMAC facilities at Durham and Newcastle. We have benefited from several discussions with Dr Christine Courbin-Gaussorgues. This work has been supported, in part, by a grant from the SERC. One of us (CF) acknowledges the receipt of a research studentship from the SERC.

References

Bates D R and Boyd A H 1962 *Proc. Phys. Soc.* **80** 1301
Bransden B H 1983 *Atomic Collision theory* 2nd edn (Reading, MA: Benjamin-Cumming)
Dickinson A S and Hardie D J W 1979 *J. Phys. B: At. Mol. Phys.* **12** 4147
Falcon C A 1983 *J. Phys. B: At. Mol. Phys.* **16** 1793
Fritsch W 1982 *J. Phys. B: At. Mol. Phys.* **15** L389
Gaussorgues C, Piacentini R D and Salin A 1975 *Comput. Phys. Commun.* **10** 223
Jognaux A, Brouillard F and Szucs S 1978 *J. Phys. B: At. Mol. Phys.* **11** L669
Peart B and Dolder K 1979 *J. Phys. B: At. Mol. Phys.* **12** 4155
Piacentini R D and Salin A 1977 *Comput. Phys. Commun.* **13** 57
van Hemert M C, van Dishoeck E F and van der Hart J A 1985 *Phys. Rev.* A **31** 2227

J. Phys. B: At. Mol. Opt. Phys. 23 (1990) 115-119. Printed in the UK

The interaction of positively charged muons with atomic hydrogen at low energies

B H Bransden and C Forster

Department of Physics, University of Durham, UK

Received 27 June 1989

Abstract. The concept of velocity scaling by which cross sections for electron capture and excitation initiated by positively charged muons are deduced from a knowledge of the corresponding proton induced cross sections is tested. It is found that velocity scaling holds to better than 1% for the 1s capture and total capture cross sections down to muon energies of the order of 15 eV, but for capture into excited states and for excitation velocity scaling becomes progressively inaccurate at energies less than about 300 eV.

1. Introduction

The possibility of forming beams of slow positively charged muons (μ^+) and also of slow muonium (μ^+e^-) and slow negative muonium ions $Mu^-(\mu^+e^-e^-)$, has been discussed recently (Harshman 1987). Associated preliminary work on the slowing in gaseous targets of 4.1 MeV muons produced at the TRIUMPH cyclotron has been reported by Fleming and Senba (1987). The dominant energy loss mechanism at keV energies and above is ionisation, but at lower energies electron capture, in which muonium is formed through the reaction

$$\mu^+ + A \rightarrow (\mu^+e^-) + A^+ \tag{1}$$

becomes increasingly important. In computational studies of the interaction of μ^+ mesons with noble gases (Fleming and Senba 1987, Senba 1988), it has been assumed that the cross sections for charge exchange and ionisation are the same for both H^+ and μ^+ interactions with atoms at the same relative v. This is known as velocity scaling. The ratio of the proton to the muon mass is

$$m = \frac{M_P}{M_\mu} = 8.87. \tag{2}$$

It follows that velocity scaling is satisfied provided

$$\sigma_\mu(E_L^\mu) = \sigma_H(E_L^H/8.87) \tag{3}$$

where E_L^μ and E_L^H are the energies of the muons and protons, respectively, in the laboratory system in which the target atom is at rest. The purpose of this paper is to test the assumption of velocity scaling by comparing cross sections for charge exchange and excitation in the $H^+ + H$ system, computed in a standard model, with those for the $\mu^+ + H$ system computed in the same way.

0953-4075/90/010115+05$03.50

2. The theoretical model

We shall be concerned with a range of relative velocities from 0.073 to 0.65 au, corresponding to proton energies, E_L^H, in the laboratory system, from 133 to 10 560 eV and muon energies, E_L^μ, also in the laboratory system, from 15 to 1200 eV. Over this velocity range it is known that a reasonable description of the $H^+ + H$ system is given by the impact parameter model in which the relative motion of the heavy particles is determined classically. It is assumed that an effective potential acts between the colliding ions and from this the classical trajectory

$$\boldsymbol{R} = \boldsymbol{R}(\boldsymbol{b}, \boldsymbol{v}, t)$$

is computed which determines the internuclear position vector in terms of the time, for given values of the impact parameter b and the velocity v. The electronic wavefunction then satisfies a time-dependent Schrödinger equation which is solved approximately by expanding the wavefunction in a suitable basis. This model has been described many times before, for example by Bransden (1983), and it is unnecessary to repeat the details here. Since we are not concerned with high absolute accuracy we have employed a small basis set, consisting of eight travelling atomic orbitals consisting of 1s, 2s, $2p_0$ and $2p_{\pm 1}$ hydrogenic wavefunctions on each heavy particle centre. Exactly the same model has been used to calculate cross sections for the $H^+ + H$ system, using a straight-line trajectory, for certain velocities in our range of interest by Cheshire *et al* (1969), and our numerical calculations agree with theirs at these velocities.

In the case of muon impact, the reduced mass of the heavy particles, although smaller than for the $H^+ + H$ system, remains large enough for the basic impact parameter model to be valid. However, because of the smaller reduced mass the classical trajectory for the $\mu^+ + H$ system may show significantly more curvature than does the trajectory for the $H^+ + H$ case at the same velocity. To the extent that the cross sections calculated using the non-linear trajectories agree with the straight-line case velocity scaling will hold, and this has been tested by making reasonable assumptions about the appropriate effective potential between the μ^+ (or H^+) particles and the hydrogen atom. The trajectory effect will be most pronounced for reactions which take place at small values of the impact parameter and negligible for those taking place at large values of b. Three choices of potential $W(R)$ have been investigated.

(i) $$W = W_S = (1 + 1/R)\exp(-2R).$$

This is the static potential between ground-state hydrogen and a proton or μ^+.

(ii) $$W = W_S + W_P$$

where

$$W_P = -(9/4R^4)\{1 - \tfrac{1}{3}e^{-2R}(1 + 2R + 6R^2 + \tfrac{20}{3}R^3 + \tfrac{4}{3}R^4) - \tfrac{2}{3}(1 + R)^4 e^{-4R}\}.$$

This is a combination of the repulsive static potential W_S and the long-range dipole attraction W_P due to the polarisability of atomic hydrogen (Bethe and Salpeter 1957).

(iii) $$W = W_C = 1/R.$$

This is the repulsive Coulomb potential between the heavy particles.

Of these three interactions (ii) is the most realistic, although it is known that W_P overestimates the long-range attraction (see a discussion in Bransden 1969). In ion-atom collisions it is known that it is often sufficient to use the unscreened Coulomb

potential between the heavy particles (iii). This is not the case with lighter systems, and as we shall see below there can be substantial differences between cross sections produced using the Coulomb potential (iii) and the potentials (i) and (ii).

3. Numerical results and conclusions

Cross sections for capture into the 1s, 2s, $2p_0$ and $2p_{\pm1}$ levels of muonium, and for excitation to the 2s, $2p_0$ and $2p_{\pm1}$ levels of hydrogen have been computed for a straight-line trajectory and for each of the three non-linear trajectories, for eleven energies with the interval $15 \leqslant E_L^{\mu} \leqslant 1200$ eV. A summary of the numerical results is given in tables 1 and 2, for the energies $E_L^{\mu} = 15$, 35, 100, 260 and 330 eV. Cross sections for the remaining energies (70, 140, 190, 400, 450 and 1200 eV) are available on request.

Table 1. Electron capture cross sections for $\mu^+ + H(1s) \rightarrow Mu(nl) + H^+$. SLT is the straight-line trajectory; (i) is the trajectory computed with $W = W_S$; (ii) is the trajectory computed with $W = W_S + W_P$; (iii) is the trajectory computed with $W = W_C$. The numbers in brackets refer to proton scattering at the same velocity.

		Cross sections (10^{-16} cm^2)			
E_L^{μ} (eV)†		SLT	(i)	(ii)	(iii)
15	1s	24.7	24.8	24.7 (24.7)	18.7
	2s	0.60×10^{-3}	0.30×10^{-3}	0.69×10^{-3} (1.20×10^{-3})	0.34×10^{-6}
	2p	0.54×10^{-1}	0.33×10^{-1}	0.56×10^{-1} (0.86×10^{-1})	8×10^{-6}
35	1s	21.3	21.3	21.3 (21.3)	19.0
	2s	0.87×10^{-2}	0.62×10^{-2}	0.75×10^{-2} (0.87×10^{-2})	0.20×10^{-3}
	2p	0.116	0.145	0.162 (0.143)	0.156
100	1s	17.09	17.11	17.11 (17.10)	16.36
	2s	0.138×10^{-1}	0.142×10^{-1}	0.144×10^{-1} (0.127×10^{-1})	0.64×10^{-2}
	2p	0.237	0.275	0.282 (0.248)	0.221
260	1s	13.43	13.38	13.37 (13.37)	13.14
	2s	0.51×10^{-1}	0.48×10^{-1}	0.49×10^{-1} (0.51×10^{-1})	0.43×10^{-1}
	2p	0.334	0.347	0.351 (0.338)	0.319
330	1s	12.2	12.2	12.2	12.1
	2s	0.29×10^{-1}	0.28×10^{-1}	0.28×10^{-1}	0.26×10^{-1}
	2p	0.389	0.394	0.398	0.368

† Muon energy in the laboratory system.

Turning to table 1, it can be seen immediately that for capture into the 1s ground state the results of a straight-line trajectory calculation agree completely with those for the trajectories computed with the screened potentials (i) and (ii). The fact that the capture cross sections computed with the Coulomb trajectory (iii) differs from the results of trajectories (i) and (ii), at the lower energies, illustrates that it is not adequate to use the unscreened potential for muon scattering. Since the 1s capture cross section dominates charge exchange, we see that velocity scaling holds accurately for the total charge exchange cross section. This is not the case for capture into the 2s and 2p levels. Particularly for the 2p level there are substantial differences between the

Table 2. Excitation cross sections for $\mu^+ + H(1s) \rightarrow \mu^+ + H(nl)$. E_L^*, SLT, (i), (ii), (iii) as in table 1. The numbers in brackets refer to proton scattering at the same velocity.

		Cross sections (10^{-16} cm^2)			
E_L^* (eV)		SLT	(i)	(ii)	(iii)
15	2s	0.59×10^{-3}	0.45×10^{-3}	0.90×10^{-3} (1.10×10^{-2})	0.3×10^{-6}
	2p	0.54×10^{-1}	0.31×10^{-1}	0.54×10^{-1} (0.87×10^{-1})	0.18×10^{-5}
35	2s	0.87×10^{-2}	0.76×10^{-2}	0.96×10^{-2} (0.87×10^{-2})	0.72×10^{-2}
	2p	0.117	0.145	0.162 (0.143)	0.17×10^{-1}
100	2s	0.137×10^{-1}	0.74×10^{-2}	0.81×10^{-2} (0.126×10^{-1})	0.48×10^{-2}
	2p	0.237	0.273	0.280 (0.214)	0.219
260	2s	0.58×10^{-1}	0.52×10^{-1}	0.52×10^{-1} (0.57×10^{-1})	0.50×10^{-1}
	2p	0.331	0.354	0.357 (0.335)	0.334
330	2s	0.41×10^{-1}	0.38×10^{-1}	0.38×10^{-1}	0.39×10^{-1}
	2p	0.391	0.408	0.412	0.389

straight-line trajectory case and the results with trajectories (i) and (ii), at energies below about 300 eV. The influence of the polarisation potential which is taken into account in trajectory (ii) is marked below about 150 eV. We conclude that velocity scaling cannot be used for capture into levels other than the ground state at energies below about 200 eV if high accuracy is required. The order of magnitude of the cross sections is, however, unaffected and velocity scaling remains useful if that is all that is required. In the case of the unscreened Coulomb trajectory even the order of magnitude of the capture cross sections (apart from the 1s case) is altered at the two lowest energies, but this just confirms that Coulomb trajectories, while adequate for ion–atom scattering, should not be employed for a particle as light as the muon.

Referring to table 2, we see that there is a marked trajectory effect for excitation of the 2s and 2p levels below about 150 eV, but by 330 eV the effect is very small. We conclude that velocity scaling is not accurate for excitation below about 350 eV, although the order of magnitude of the cross section is correctly given by this procedure.

Below about 2.0 keV (equivalent to a muon energy of 225 eV), the proton trajectories are sufficiently curved to have some effect on the cross section for excitation or capture into excited states. For this reason cross sections for proton-induced reactions have been included in tables 1 and 2 for certain velocities. It should be noted that for excitation and capture into excited states the muon cross section at some energies is closer to the straight-line results than are the corresponding proton cross sections and this is due to the detailed structure of the probability curves as a function of impact parameter. Agreement between the muon- and proton-induced cross sections at the same velocity is slightly improved in some cases when allowance is made for the non-linear proton trajectory, but our general conclusions as to velocity scaling are unaffected.

Acknowledgments

It is a pleasure to record useful conversations with Professor C J Joachain and Dr D R Flower. This project was supported, in part, by grants from the Science and Engineering Research Council and by the British Council.

References

Bethe H A and Salpeter E E 1957 *Quantum Mechanics of One- and Two-Electron Atoms* (Berlin: Springer)
Bransden B H 1969 *Case Studies At. Phys.* 1 171–245
—— 1983 *Atomic Collision Theory* 2nd edn (Reading, MA: Benjamin-Cummings)
Cheshire I M, Gallaher D F and Taylor A J 1969 *J. Phys. B: At. Mol. Phys.* 3 813
Dalgarno A and Lynn N 1957 *Proc. Phys. Soc.* A 70 22
Fleming D G and Senba M 1987 *Atomic Physics with Positrons* ed J W Humberston and E A G Armour (London: Plenum) p 343
Harshman D R 1987 *Atomic Physics with Positrons* ed J W Humberston and E A G Armour (London: Plenum) p 367
Senba M 1988 *J. Phys. B: At. Mol. Opt. Phys.* 21 3093